Membrane Separation Technique for the Treatment of Humic Acids Solution, Paper and Tea Factory Wastes

A Thesis Submitted for the Award of the Degree

of

DOCTOR OF PHILOSOPHY

by

Suman Saha

Department of Chemical Engineering

Indian Institute of Technology Guwahati

Guwahati-781 039, India

June 2018

Membrane Separation Technique for the Treatment of Humic Acids Solution, Paper and Tea Factory Wastes

A Thesis Submitted for the Award of the Degree

of

DOCTOR OF PHILOSOPHY

by

Suman Saha

(Roll No. 126107005)

Department of Chemical Engineering

Indian Institute of Technology Guwahati

Guwahati-781 039, India

June 2018

Department of Chemical Engineering

Indian Institute of Technology Guwahati, Guwahati, India

STATEMENT

I hereby declare that the matter embodied in this thesis is the result of investigations carried out by me in the Department of Chemical Engineering, Indian Institute of Technology Guwahati, Assam, India under the supervision of **Dr. Chandan Das.**

In keeping with the general practice of reporting scientific observations, due acknowledgement has been made wherever the work described is based on the findings of other investigations.

Guwahati — Suman Saha

June 2018

Department of Chemical Engineering

Indian Institute of Technology Guwahati, Guwahati, India

CERTIFICATE

It is certified that the work contained in this thesis entitled "**Membrane Separation Technique for the Treatment of Humic Acids Solution, Paper and Tea Factory Wastes**", by Mr. Suman Saha (Roll No. 126107005) for the award of Ph.D. degree, is a record of bonafide research carried out by him at the Department of Chemical Engineering, Indian Institute of technology Guwahati, under my guidance and supervision. The work embodied in this thesis has not been submitted to any other University or Institute for the award of any other degree or diploma.

Date:

Dr. Chandan Das
Associate Professor
Department of Chemical Engineering
Indian Institute of Technology Guwahati

ACKNOWLEDGEMENTS

It is my great privilege to sincerely thank several people who have supported me to complete my Doctoral Dissertation.

First and foremost, I take this opportunity to express my deep sense of respect and gratitude to my thesis supervisor, **Dr. Chandan Das**, for providing inspiration and valuable guidance throughout the course of this investigation. I am also indebted to him for his constant suggestions and encouragement. The experience of working with him, I strongly believe, will have far reaching influence in my future life. It has really been a remarkable experience working with him.

I would like to acknowledge my sincere gratitude to my doctoral committee members, **Prof. Mihir K. Purkait** and **Dr. Tapas K. Mandal**, Department of Chemical Engineering and **Dr. Bulu Pradhan**, Department of Civil engineering. Their intuitive revision of my work, valuable advice, and constructive suggestions during my research progress kept the flow of my research work in the right direction.

I would like to acknowledge my sincere gratitude to **Dr. Animes Kr. Golder** for his valuable suggestions and continuous encouragement during my research work.

I am indebted to **Prof. Aloke Kumar Ghoshal, Prof. Kaustubha Mohanty, Dr. Mahuya De, and Dr. Prakash Kotecha** for their research oriented teaching during my course of work. I also thank **Prof. Bishnupada Mandal**, Head, and Department of Chemical Engineering for his administrative support. Furthermore, I would like to thank all the other Faculties and Staff members of the Department of Chemical Engineering for their invaluable support during my research.

I express my sincere gratitude and acknowledgment to IIT Guwahati for all the facilities that were made available to me. I am grateful to the Analytical Laboratory of the **Department of Chemical Engineering** and **Central Instruments Facility**, **IIT Guwahati** for providing me with the necessary support for sample analysis.

I would sincerely like to thank **M/s. Nagaon Paper Mill, Jagi Road, Assam, India and M/s. Sindhu Tea Pvt. Ltd. situated in Golaghat district of Assam, India** from where all the effluents were collected during research work.

I wish to thank our lab alumina **Dr. Mahesh Kumar Gagrai**, **Dr. Vijay Singh**, **Dr. Arijit Das**, **Dr. Sujoy Bose, and Dr. Kibrom Alebel Gebru** for lending their hands of support whenever needed. I thank all my lab members **Mr. Amit Baran Das**, **Mr. Abhradip Pal, Mr. Abhishek Shukla, Mr. Kulbhushan Samal, Ms. Sushma**

Chakraborty, Ms. Aritra Das, Mr. Anudeep Venkata Durga Yedla, Mr. Pranav Sreenivasa Akella, Mr. Tapan Hazarika, Mr. Dunna Shyam, Mr. Vishal Kumar Sandhwar, Mr. Sandup Tshering Bhutia, Mr. Rishiket Kundu, Ms. Rijumoni Boro, Ms. Mounika Chevula, Ms.Shyamoli Hazarika, Ms. Devipriya Gogoi, Mr. Raj Kumar Das, Mr. Venkatnarasimha Rao Chelli, Mr. Atul Kumar Singh, and Ms. Meenal Vijay Wahane for providing a co-operative research environment.

My sincere thanks to IIT Guwahati friends **Mr. Randeep Singh, Dr. Himadri Sahu, Mr. Saptak Rarotra, Ms. Geeta Kumari, Ms. Basudhrity Banerjee, Mr. Abhik Bhattacharjee, Mr. Rahul Patwa, Mr. Supriyo Kumar Mondal, Dr. Rahul Ramteke, Dr. Sunny Kumar, Mr. Kuldeep Roy**, **Mr. Nirmal Mullick**, **Mr. Prince Kr. Baranwal, Mr. Rupam Sinha, Mr. Bitang Kwrung Tripura, Ms. Barnali Bhui, Mr. Ritesh Prakash, Ms. Ruby Kumari** for all the laughs, joyful moments, support and suggestions. I am thankful to the other research scholars of Chemical Engineering Department and all my IITG friends, who have shared their thoughts and views with me.

Words of motivation and encouragement from some of my friends and relatives were only a call away. They always appreciated my efforts and outcomes of my research work. My friends who always stood beside me, giving me hope and courage **Mrs. Manidipta De, Dr. Jayato Nayak, Ms. Zunipa Roy, Mrs. Ahana Bhaduri, Mr. Avik Chatterjee, Mr. Biswadeep Ghosh, Mr. Sachin Karmakar, Mrs. Somali Mondal** and many more. And I would like to take this opportunity to thanks each and every relatives of mine for their constant encouragement.

Finally, my whole hearted gratitude goes to my parents, **Mr. Raghunath Saha** and **Mrs. Tapasi Saha,** and my younger brother **Mr. Swagatam Saha** whose blessings, love, wise advice and boundless patience kept my morale high during the course of study.

Sincerely,

Suman Saha

TABLE OF CONTENTS

Nomenclature

A_1,B_1,C_1, D_1	Model terms for alum dosage (mg L^{-1}), initial pH, stirring speed (rad s^{-1}) and stirring time (min) respectively in the response surface methodology for the optimization study of alum coagulation process
A_2,B_2,C_2	Model terms for TMP drop (kPa), rotational speed (rad s^{-1}), and retentate flow rate (L min^{-1}), respectively in the response surface methodology for optimization of process parameters during treatment of paper industrial effluents
A_3,B_3,C_3	Model terms for solid weight (g), time (min), and temp (°C), respectively in the response surface methodology to optimize the total polyphenols leaching
A_m, A_0	Membrane active area and total surface area, respectively (m^2)
a	Solute particle radius (m)
a_0	The unsteady diffusion coefficient (L)
a_1	The film theory leaching coefficient (min^{-1})
a_2	The leaching coefficient for the Ponomaryov kinetic (min^{-1})
a_3	The parabolic leaching coefficient ($min^{-0.5}$)
a_4	The rate constant for the parabolic model ($min^{-0.5}$)
a_5	The parameter for the power law model (min^{-n})
a_6	The leaching coefficient for the hyperbolic diffusion model (min^{-1})
a_7	The diffusion parameter for the hyperbolic diffusion model (min^{-1})
a_8	The diffusion shape parameter for the Weibull's model (L)
a_9	The leaching coefficient for the Weibull's model (min^{a_8})
C_{os}, C_{ms}, C_{ps}	Solute concentration in the bulk, on the membrane active surface, and in the permeate side, respectively (mg L^{-1})
c_e	Concentration of water soluble polyphenols at saturation or equilibrium state
D_i	Desirability function for the optimization of process parameters
D_b, D_r, D_s	Brownian, rotational, shear-induced diffusivity, respectively (m^2 s^{-1})
d_i	Partial desirability function for specific response in RSM
d_e	Equivalent diameter (m)
E_{clean} (%)	Cleaning efficiency
J_0, $J_{effluent}$, J_{sp}, J_{HAs}	Pure water flux, permeate flux, the steady state permeate flux, and Humic acids permeate flux, respectively (L m^{-2} h^{-1})
K	Boltzmann constant (J K^{-1})
k	Mass transfer coefficient (m s^{-1})
k_A	Membrane surface blocked per unit of total volume permeated (m^{-1})

k_f, k_s, k_{cf}, k_{cl}	CPBM constant (s^{-1}), SPBM constant ($m^{-1/2}\ s^{-1/2}$), IPBM constant (m^{-1}), and CFM constant ($m^{-2}\ s$), respectively
k_B	Decrease of cross sectional area of the membrane pores per unit of the total volume permeated through the membrane (m^{-1}).
k_D	Cake layer area per unit of the total volume permeated through the membrane (m^{-1})
k_1	The pseudo first-order leaching rate constant (min^{-1})
k_2	The pseudo second-order leaching rate constant ($L\ mg^{-1}\ min^{-1}$)
k_3	The unsteady diffusion rate constant (min^{-1})
k_4	The film theory model rate constant (min^{-1})
k_5	The Ponomaryov empirical equation rate constant (min^{-1})
L_p	Hydraulic permeability ($m\ Pa^{-1}\ s^{-1}$)
N, n, n_c	Number of responses, number of axial runs, and number of central runs for RSM design, respectively
$P_{sep}, P_p, P_m,$ $P_{clean}, P_b, U_p,$ P_{tot}	Net power consumption for filtration, power generated by feed pump, power produced by induction motor, power consumed during cleaning process, power supply during back rotation, power supplied by ultrasonic bath, and total power used in entire process (filtration and cleaning), respectively (kW)
Q_{feed}	Feed flow rate ($m^3\ s^{-1}$)
R	Universal gas constant ($8.314\ J\ mol^{-1}\ K^{-1}$)
$R_{c_{SBM}}$, $R_{t_{SBM}}$, $R_{f_{SBM}}$, $R_{m_{SBM}}$, $R_{cl_{SBM}}$	Cake layer, net membrane, fouled membrane, fresh membrane, and clean membrane resistances, respectively (m^{-1})
r	Radius of the stirrer cell (m)
r_i	Significance of particular response in RSM
Re, Sc, Sh	Reynolds, Schmidt, and Sherwood number, respectively
R_1, R_2, R_3	Response model term for the permeate flux ($L\ m^{-2}\ h^{-1}$), ionic conductivity decreasing ($S\ m^{-1}$), and the percentage removal of TDS (%), respectively
R^2	Regression coefficient
T	Temperature (K)
u	Feed velocity ($m\ s^{-1}$)
Y, X_i	Predicted response and independent variables, respectively

Greek letters

$\beta_0, \beta_i, \beta_{ii}, \beta_{ij}$	Constant, linear, quadratic, and interaction coefficient, respectively
ω	Angular velocity (rad s^{-1})
τ	Applied torque (Watt s)
$\mu_{effluent}$	Viscosity of effluent (Kg m^{-1} s^{-1})
ε	Membrane surface porosity
ν	Kinematic viscosity (m^2 s)
η_f	Pump efficiency (%)
$\Delta\pi$	Osmotic pressure difference
$\rho_{effluent}$	Effluent density (kg m^{-3})
δ	Film thickness (m)
ΔP	Transmembrane pressure drop (k Pa)
σ	Standard error

Abbreviations

SBM	Spinning basket membrane module
RSM	Response surface methodology
MWCO	Molecular weight cutoff (kDa)
TSS	Total suspended solids (mg L^{-1})
TDS	Total dissolved solids (mg L^{-1})
COD	Chemical oxygen demand (mg L^{-1})
BOD	Biological oxygen demand (mg L^{-1})
Abs	Optical absorbance
CPBM	Complete pore blocking model
SPBM	Standard pore blocking model
IPBM	Intermediate pore blocking model
CFM	Cake filtration model
MSE	Mean square error

List of Figures

List of Tables

ABSTRACT

The work stated in this thesis is the treatment of Humic acids like natural organic materials, paper industrial waste effluents, and tea factory liquid and solid waste materials using various separation processes, like, unstirred batch cell and spinning basket membrane module ultrafiltration, alum coagulation and membrane ultrafiltration combined process, solvent leaching techniques with fruitful outputs. Several conventional methods, like, electrochemical, photocatalytic, and advanced oxidation process are reported previously to treat various industrial effluents and to recover natural organic products from the wastes. The severe chemical consumption and high operating cost are the major demerits for these conservative processes. However, membrane ultrafiltration offers large number of advantages as compared these conventional methods. Membrane processes are potentially better for the environmental science since the membrane approach requires the use of relatively simple and non-harmful materials.

In the first study, recovery of Humic acids synthetic solution is done using spinning basket membrane ultrafiltration. The permeate flux behavior, irreversible membrane pore clogging, the volume reduction factor (VRF) and the permeate quality are compared with an unstirred batch cell ultrafiltration successfully. This study has been explored at different transmembrane pressure (TMP) drops (207, 276, 345 and 414 kPa) and different concentration of HAs (50, 150, and 250 mg L^{-1}) for both the modules. To observe the effects of rotational speeds on recovery of Humic acids water solution, spinning basket module has been varied at different rotations such as, 10.47 to 73.30 rad s^{-1}. The internal pore blocking characteristics was investigated using modified Hermia's pore clogging models, like, complete, standard, intermediate pore blocking, and the cake filtration model. Concerning the cleaning process, the membrane turbulence was not enough to eliminate small particles from the active membrane pore walls. Thus, the only back rotation (10.47 to 52.36 rad s^{-1}) was not efficient to recover hydraulic flux after cleaning. Therefore, the application of ultrasonication (ultrasound power: 120 W, frequency: 50 kHz, sonication time: 5 to 25 min) for the fouled membrane cleaning purposes has been presented in this study with the fruitful productivities.

In the second study, the detailed explanations are reported for the treatment of paper (collected from M/s. Nagaon Paper Mill, Assam, India) and tea industrial effluents (collected from M/s. Sindhu Tea Pvt. Ltd. Golaghat, Assam, India) using spinning basket membrane ultrafiltration. The particular use of spinning basket module membrane

(SBMM) for the treatment of industrial effluents is novel, compact, energy-saving, and environment-friendly. To improve the performances of membranes, pretreatment of wastewater was done for the removal of suspended particles present in the effluents using vacuum filtration for paper industry wastewater and alum coagulation for tea factory effluent. Being the most popular pre-treatment method for membrane separation processes, alum coagulation has proved to be a simple and efficient method for reducing membrane fouling and hence aids in improving flux. Research endeavors are really scanty using such coagulation-spinning basket membrane ultrafiltration integrated technology exploiting alum for coagulation (pre-treatment) and a spinning basket module for membrane filtration (final treatment). For the coagulation process alum ($Al_2(SO_4)_3.18H_2O$) was used to remove suspended materials mainly from the tea factory effluent by varying four different process parameters such as, alum dosage (50-300 mg L^{-1}), pH (4-10), stirring speed (10.47-62.83 rad s^{-1}) and stirring time (30-180 min). Response surface methodology was studied to optimize these parametric conditions to remove suspended matters from the wastewater. Finally, spinning basket membrane ultrafiltration was performed under different parametric conditions like, applied transmembrane pressure drop (207, 276, 345 and 414 kPa), rotational speed (10.47 to 73.30 rad s^{-1}) and various MWCOs (5, 10, 30 and 50 kDa) to identify the flux decline behavior and get good quality of permeate for both the effluents like paper and tea industry wastewater. The rotational speed induces turbulence and shear force on the active membrane surfaces reduces the deposition of rejected particles thereby increasing the permeate flux. Various fouling characteristics have been studied using modified Hermia's pore blocking law. Brownian, rotational and shear-induced diffusion models were applied to evaluate the theoretical flux behavior. Response surface methodology (RSM) has been studied to optimize the filtration process. Optimum permeate quality has been obtained when initial TMP drop, rotational speed, and retentate flow rate were 350.61 kPa, 62.83 rad s^{-1}, and 2 L min^{-1}, respectively.

The eco-friendly management of solid waste materials after fruitful leaching of polyphenols like value added products has been performed successfully in the final study. The particular use of tea factory solid waste to extract the total polyphenols towards solid waste management is a novel and innovative approach. The present work uses the existing science to explore the different solvent leaching and diffusion of total polyphenols from the tea industry solid waste materials. The objectives of this current work are categorized into following segments: (i) selection of extractive solvent, (ii) optimization of process parameters to recover total polyphenols and finally, (iii) finding out the suitable leaching

and diffusion rate kinetic model, (iv) recovery of used green solvent and concentrate the phenolic components using spinning basket membrane module. Five solvents, namely, ethanol, methanol, acetone, ethyl acetate and de-ionized water, were used to extract the maximum total polyphenols from tea factory solid waste. The influence of temperature (30-90°C) during water leaching of total polyphenols was also explored. The effects of different solid waste content in water (0.5 to 2.5 g) at a various contact time of 10 to 90 min on the leaching of polyphenols from tea factory solid waste were verified. To optimize the leaching parameters such as solid content (g), leaching process time (min) and temperature ($^{\circ}$C), response surface methodology (RSM) were studied to achieve the optimum leaching of total polyphenols. Furthermore, the leaching and diffusion rate were determined and compared using different rate kinetic models, like pseudo first order, second order, the Elovich rate kinetic models, the unsteady diffusion, the film theory, the Ponomaryov equation, parabolic, power law, hyperbolic and the Weibull's models. Finally, spinning basket membrane ultrafiltration was performed using different MWCO membrane such as, 50 and 30 kDa and in the presence of various rotational speeds, like, 10.47 and 52.31 rad s^{-1} to recover and concentrate the extracted polyphenols. Simultaneously, the recovery of the green solvent such as, water has also been successfully carried out using the ultrafiltration process.

Keywords: Humic acids solution, unstirred batch cell, spinning basket module, ultrafiltration, modified Hermia's pore blocking model, ultrasonication, paper and tea industry wastewater, rotational speed, diffusion model, RSM, alum coagulation, tea factory solid waste, total polyphenols, solvent leaching, pseudo second-order kinetics, unsteady diffusion, optimization.

CHAPTER 1

INTRODUCTION, AIMS AND OBJECTIVES

In this chapter, a brief summary on the environmental pollution, various sources of the water pollution, the properties of the natural organic components, namely, Humic acids and treatment technologies of the Humic acids, different treatment methods of the paper and tea factory wastes are presented. Most of the industries, like, paper and tea industry use fresh water for a variety of purposes and produce wastewater. To avoid any health hazards affected by discharging untreated effluents into the environment, the effluents must be treated. The treatment of paper and tea industry waste effluent using several separation processes is described and compared with advanced membrane filtration technology. The detailed literature review on the treatment of paper industrial effluent, tea factory solid and liquid waste is deliberated subsequently throughout this chapter. The aims and objectives of this thesis work are also discussed in this chapter.

1. Introduction:

1.1. Environmental pollution:

Environmental pollution is the overview of impurities in a healthy and natural environment which is the reason of uncertainty, syndrome, damage or discomfort to the ecology for both the cases physical and living society (Margaritis and Kang, 2017, Franklin and Fruin, 2017). Contamination of soil, air, ground and surface water with various hazardous, toxic chemicals, and solid wastes due to the industrialization and human activities are the major problem which is increasing rapidly (Khan et al., 2017; Wang and Yang, 2016; Sarkar et al., 2017). Environmental Pollution became a prevalent issue after the World War II, for the radioactive effect from atomic fighting and testing. Not only that, a non-nuclear happening, *The Great Smog of 1952 in London*, killed a massive number of people. However, *The Great Smog of Delhi, 2017* is also a serious environmental pollution event that affected the entire National Capital of India due to the various sources of smoke such as production and manufacturing factories, vehicles, power plants, garbage burning, road dust, etc. Serious action must be taken against environmental pollution, as it has an adverse effect on the earth mainly, air and water. Environmental pollution began to pull a major and serious public devotion, after passing the *Clean Air Act* (Effective from 1963), the

National Environmental Policy Act (Effective from 1970), the *Clean Water Act* (Effective from 1972), and the *Noise Control Act* (Effective from 1972) (Raptis et al., 2017; Kirillin et al., 2013; Titelboim et al., 2017).

1.1.2. Parameters of contamination:

For industrial stream estimation and study of wastewater treatment, the properties or parameters of contaminants are enlisted here.

a) Color:

Natural organic components are the main responsible for the changing of color of natural water. The industrial wastewater contains a huge amount of organic materials including various dye reagents that are potentially harmful after leaching of this compounds into the groundwater or surface water which can change the color of natural water. Not only that, color of water is a vital index to measure dissolved humic substances in water body (Hongve and Akesson, 1996; Turner and Renegar, 2017).

b) Odor:

The chlorination of water results in the formation of severe halogenated components which are the reason for the change of quality of water. When the active chlorine compounds react with organic matters present in the water the disinfected halogen compounds formed. The musty odor is one of the major parameter to control the purity of drinking water (Taha et al., 2017; Yuan et al., 2017). It is generated degradation of organic components in soil by fungi, cyanobacteria, blue-green algae, actinomycete bacteria. The determination of musty odor is a difficult task. The high selective and sensitive technique is needed to analyze the musty-off aroma in water (Callejon et al., 2016).

c) pH:

The pH level of soil and water is an important parameter to balance the environmental ecosystem. Due to toxicity of chemicals and heavy metals the level of pH in the water and soil is changing gradually which has an adverse effect in aquatic life. Acid rain due to the nitrogen oxides, sulfur oxides present in the polluted air is the perfect examples of man-made influence on the pH of water (Jie et al., 2017; Tran et al., 2017).

d) Suspended matters:

Suspended matters are some toxic pollutants which are larger than 2 μm in size and do not dissolve in the water. The toxic suspended particles in water are dangerous for the existence of marine life. It can cause severe problems in ground and surface water by increasing the microbial activities (Wang and Yang, 2016).

e) Dissolved organic matters:

The remediation and control of dissolved organic materials from drink water and industrial effluents are the high interest to protect the environment from pollution. Due to the presence of dissolved materials the organoleptic properties, like, taste, color, odor of drinking water is affected. The appearance of organic matters in fresh water is described to rise the anthropogenic compounds in natural water. The solubility of the various components may be increased in the presence of dissolved organic materials in the ground water. Not only that, it causes fouling of membranes during treatment of wastewater. the origin of dissolved organic matters in water is the microbial degradation of chemicals that present in the soil and water due to the industrial activities (Levchuk et al., 2018; Jain et al., 2011).

f) Dissolved oxygen:

One of the most important parameters in aqueous studies is measurement of dissolved oxygen. For the good water quality adequate amount of dissolved oxygen is required. The oxygen level in water is approximately 5 mg L^{-1}. Due to the industrial activity the level of dissolved oxygen changes currently which affects the aquatic culture (Mader et al., 2017).

g) Turbidity:

Turbidity is a significant and crucial characteristics of water. The increasing of turbidity indicates the presence of excessive amount of inorganic and suspended materials, dissolved organic materials, colored components, and microorganisms. The high turbidity in drinking water can cause a health concern due to the growth of pathogens (Aboubaraka et al., 2017).

h) Heavy metals:

Water pollution due to the high concentration of heavy metals is a universal anxiety and required a worldwide care. Effluents coming from the mining, battery manufacturing factories, tanneries, and metallurgical industries are the responsible for the leaching of different kind of heavy metals, like, cadmium, cerium, chromium, antimony, arsenic, lead,

mercury etc. (Fang et al., 2018). The determination of metallic concentration in water is a major concern to protect the water pollution. Heavy metals containing wastewater should be treated significant and properly. Untreated water can lead to severe injury to the ecosystem resulting in a long-term effect on the environment (Tran et al., 2017).

i) Chloride content:

Petroleum, pulp and paper mills, pharmaceutical, and tannery industries generate high saline effluents in a large quantity containing the huge concentration of chlorides. The increase of chloride content in water would lead to major damage to groundwater, surface water, soil etc. The presence of chlorides in drinking water is highly detrimental. Regarding the sustainability of the freshwater, the determination and treatment of chloride content in the industrial effluents have to become a vital concern to protect the environment (Yan et al., 2016). In addition, various compounds such as humic substances can react with chlorides present in natural water and form strong toxic and carcinogenic complexes, like, aliphatic halogenated trihalomethanes. Thus, under such conditions, the determination of color, taste, odor, pH, suspended and dissolved organic matters, dissolved oxygen, turbidity heavy metals, and chlorides compounds is becoming a dynamic task for the treatment of liquid effluents to get highly purified and efficient water and protect the ecosystem from severe environmental pollution.

1.2. Water pollution - a threat to life:

Water contamination is a severe universal problem which needs ongoing estimation and review of water resource policy at all stages (Sanchez et al., 2016). Water pollution has been recommended as the leading international cause of deaths and diseases. Water is stereotypically considered to as polluted when the anthropogenic contaminants impaired into freshwater. Water pollution occurs from a number of different sources.

Direct disposal of waste materials from different industries, like, pulp and paper, textile and dye industries into the natural waterways cause waste to build up within the freshwater (Noorhosseini et al., 2017). Not only that the emission of hazardous fumes into the fresh air causes acid rain. When the acid rain sprays, it pollutes the local natural water lines including rivers, lakes, and streams. Not only that, the thermal pollution happens when water is basically used to cool the hot instruments in the factories and is released into

waterbodies. As a result, the temperature of the freshwater is highly increased (Titelboim et al., 2017).

This temperature change can cause aquatic life to die. If the pollution arises from one source, like, oil spill, it is named as point-source pollution. If the contamination comes from a number of sources, then it is named as nonpoint-source water pollution. **Figs. 1.1. (a)-(b)** describe the requirement of freshwater for the ecosystems on a worldwide scale in 2003 and 2015, respectively which indicates that the inadequacy of water is rapidly increasing due to the consumption of fresh water. India is also considered as a water-stressed country due to the rapid growth of civilization (World Resources Institute).

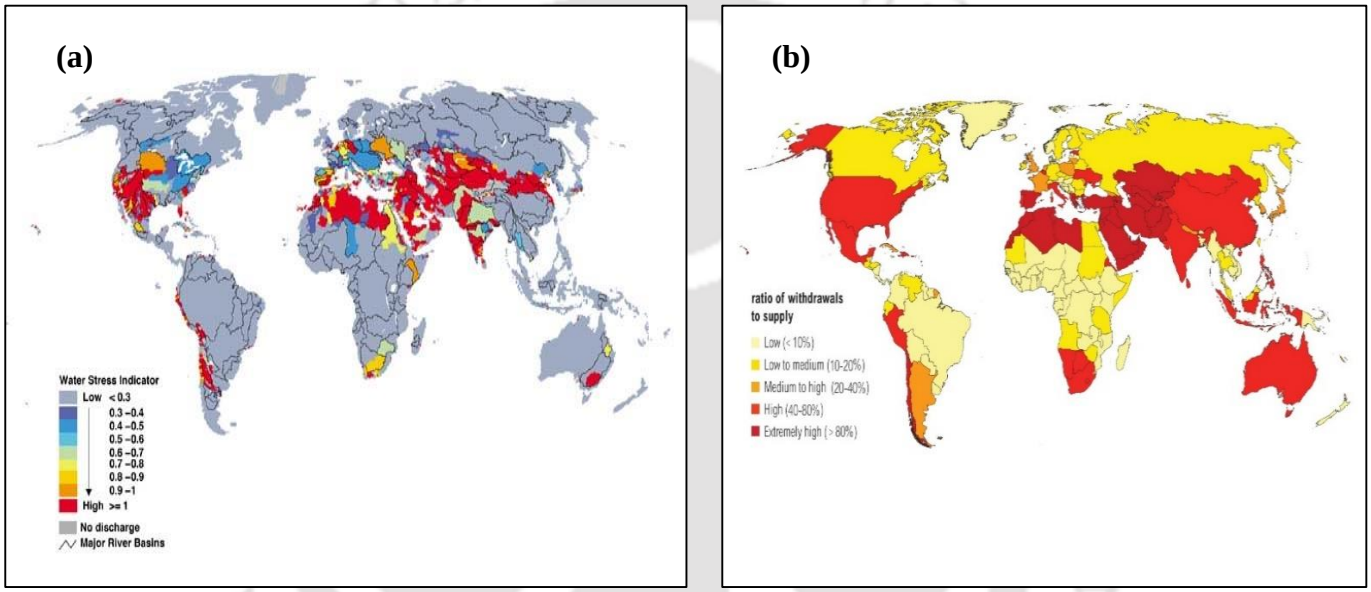

Fig. 1.1. (a) The global scenario of the water scarcity in the environment in the 2003, **(b)** the insufficiency of water on the universal scale in 2015 according to the World Resources Institute

1.2.1. The different industries involved in water pollution:

Many causes are involved to pollute water bodies. The direct sources, like, effluents discharge from various industries are one of the important contributors to freshwater pollution. Industrial activities produce a huge variety of waste products. Paper and pulp, textile, petrochemical refineries, food processing, metal working, tea, and dye factories are the major industries which generate a wide range of waste effluents.

Textile industry:

The effluents generated from textile industries have a high demand for chemical oxygen demand due to the large number of suspended solids, acidity, and other soluble materials. The contaminant features of textile wastes vary extensively among numerous organic ingredients, like, chromium ions, pigments, starches, and detergents in waste undergo biological and chemical variation which consume dissolved oxygen from the freshwater bodies and abolish aquatic life (Jain et. al., 2014).

Tanning industry:

The tanning industry is generally considered as pollutants produced industries which generate a huge amount of toxic chemicals. During the different unit operations, like, soaking, liming, de-liming, tanning, etc. a huge amount of wastewater is generated which consist of dissolved fats, bones, sodium chloride, sulfate, sulfide, chromium salts, keratin etc. Due to the difference in raw materials, various organic and inorganic ingredients the chemical and biological oxygen demand are changed to very high after discharging the tannery effluents into the fresh water (Tran et al., 2017).

Food processing industry:

Food processing industries produce waste effluent, like, liquor from yeast culture system, spent grain water, wastewater from a cooling tower, oil sludge etc. Food industry wastewater contains a few amounts of hazardous materials which can be categorized as nontoxic. In the dairy industry, a huge amount of freshwater is regularly used during cheese making process and produced wastewater which contains inorganic and organic materials (Frappart et al., 2008).

Petrochemicals and oil refining industries:

Petrochemicals and oil refining industries contain a high level of pollutants, like, oil products, hydrocarbons, phenolic compounds, heavy metals which are tough to degrade (Sarkar et al., 2017).

Metal industry:

Metal industries generally discharge wastewater containing heavy metals, like, chromium, lead, cadmium, and other metals such as zinc, nickel, copper, aluminum etc. With the rapid development of industries, heavy metal pollution is increasing now a day due to the

discharge of heavy metal-laden wastewater from these industries to the environment without any proper treatment (Yuan et al., 2017).

Radioactive industry:

Radioactive waste components are also the important source of water pollution. The radioactive wastes are mainly generated due to the various activities of Uranium mining processing, Nuclear fuel production, and radioisotope production for the medicine preparation and research purposes (Trznadel, 2017). The major wastes arising in a radioactive industry are the active solids, like, stainless steel containing cobalt and nickel, ion exchange resins, used uranium, radioactive liquids which can result in severe water pollution (Trznadel, 2017).

Mining operation:

Mining operation can cause different kind of metal leaching into acidic effluents. These effluents can increase the metal load in rivers, lakes, and groundwater (Ni et al., 2016). Therefore, freshwater contamination due to the leaching of heavy metals during mining operation has become a major environmental problem.

Agricultural industry:

The effluents generated agricultural industry are containing mainly farm and animal wastes, fertilizers, suspended materials, insecticides, and pesticides etc. The highly toxic chemicals can enter the groundwater by leaching and cause diarrhea, jaundice, dysentery, and typhoid-like waterborne infections (Chen et al., 2015).

Tea processing industry:

Waste management is an abundant challenge towards tea processing industries in the world. The raw materials, energy, water are the major inputs in tea factories which produces solid and liquid wastes containing phenolic components. There is a lack of inclusive review towards tea waste management systems. Highly colored wastewater containing polyphenols from tea factories is released in to freshwater stream during the cleaning purposes of production equipment. As a result, it changes the oxygen-containing capacity of freshwater bodies (Uzun et al., 2010; Goswami et al., 2014).

Paper and pulp industries:

With rising the use of papers in our daily life, the level of water pollution due to the paper industries is a novel highlight. The paper and pulp industries consume a large quantity of fresh water and generate highly contaminated wastewater. This effluent is renowned as a severe ecological threat due to the highly toxic chemicals discharged including high organic load, high salinity, suspended materials, inorganic components, and various metals content. On the other side, solids and gaseous pollutants are also discharged into the environment from paper and pulp industries. The effluents generated from paper and pulp industries contain a huge number of lignin derivative organic components, like, Humic substances. However, wood chips, bits of bark, cellulose, sulphur, and chlorine compounds and dissolved lignin a complex mixture of various chemicals are also the important impurities. All the contaminated materials produce a sludge which destroys certain types of marine life and environment as well (Wong et al., 2006). With rising consciousness of environmental protection, the significant and proper management of pulp and paper industry wastewater has become an important public issue which should be increased strictly (Guan et al., 2017).

Not only that, the paper industry wastewater contains a large number of natural organic materials. Natural organic components many times replicate the action of an important element in the living body, interfering with the metabolic system to cause severe sickness. Many organic components, particularly colored components are toxic, but some are vital for fertilization, like, Humic acids (HAs).

1.2.2. Generation, properties, benefits, and application of natural organic components, like, Humic acids found from different sources:

Natural organic components are the elemental carbonaceous substances found in mainly soil, sediment, and industrial effluents (pulp and paper industries). These materials mainly known as environmental black carbon such as Humic acids have a significant affinity for other organic and inorganic components (Radwan et al., 1997). Depending on their limited abundance, it is an important issue to quantify and characterize the Humic acids, like, natural substances which can play a major role as a natural pollutant in the environmental system (Roipel et al., 2016).

***The properties of Humic acids*:**

Humic substances are recognized as one of the major essential component in the environment (Ghabbour and Davies, 2001). Humic acids, natural heterogeneous molecules comprise an extraordinarily complex, polyfunctional polymers, formed during early diagenesis of bio matters and occur in soils, sediments, industrial effluents (pulp and paper factory), and natural water (Radwan et al., 1997). The hypothetical structure of Humic acids has been represented in the **Fig. 1.2**. The dominating functional groups of the naturally occurring humic acids are amino acids, ester, amide, benzene rings, aliphatic moieties, and carboxyl, ether groups, hydroxyl, amine groups, etc. (Ghabbour and Davies, 2001). These substances contain a huge number of organic compounds, higher hydrogen to oxygen (H/O) molar ratio, higher surface activity, more nitrogen content, more lipids, higher nitrogen to carbon ratio, a huge number of molecular weight distribution starting from 2 kDa up to over 500 kDa than commercial Humic acids (Shao et al., 2011). These substances are the most chemically active materials in the soil with the cation exchange abilities. They can interact with different kind of toxic organic substances, like, pesticides, herbicides, insecticides.

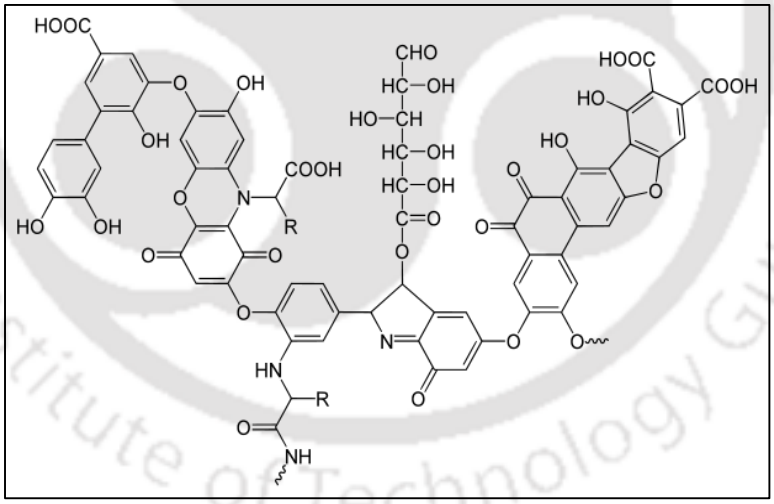

Fig. 1.2. Model hypothetical structure of Humic acids (Stevenson, 1994)

***The hypothetical theory of the generation of Humic acids*:**

The formation of humic substances occurs during lignin decomposition. The generation of humic substances may vary from one environment to another. Various techniques have been recommended to explain the formation of humic materials during the deterioration of

plant cells such as lignin in the soil and the pulp and paper industrial wastewater. The dead plant's residue and lignin components are transformed into dark-colored compounds by microbiological mechanisms. During the lignin decomposition, the carbon compounds are utilized by microorganisms and the residual portion accumulates as humic substances which can be fragmented into smaller materials, like, Humic acids during further microbial decomposition (Ghabbour and Davies, 2001). However, the lignin and cellulose are decomposed to phenolic acids during microbial degradation and then enzymatically oxidized to quinones (amino compounds) and produced Humic acids, like, compounds. In addition to the other possibilities, the pulp and paper industry is the major pathway to generate a significant amount of Humic acids in their waste effluents as the major waste materials of wood processing mechanism in the paper industry is lignin-derived compounds, cellulose, sugar etc. (Mendez et al., 2005).

1.2.3. Benefits of Humic acids:

Current scientific researchers explore that the productiveness of soil depends on the content of Humic acids. Humic substances are recognized to yield three types of benefits which have been pointed out in the next paragraph (Mendez et al., 2005).

Physical effects:

- Improve the soil structure and fertility
- Prevent the high water content and nutrient losses in productive soils
- Soil cracking and erosion prevention
- The rise of water holding volume of the soil
- Darken the color of the soil and thus help absorption of the sun energy
- Increase the aeration of soil

Chemical benefits:

- Normalize the pH value of soils
- Increase the uptake of nutrients and water by plants
- Reduce the leaching of toxic inorganic materials in the root zone of plants.
- Enhance the metal ions chelating capacities of soil.
- Improve the transformation of essential nutrient elements, like, nitrogen, phosphate, iron, zinc, potassium into forms available to plants.

Biological effects:

- Improve the stimulation capacity of plant enzymes and increase their production
- Act as an organic catalyst in many biochemical processes.
- Stimulate the growth of desirable micro-organisms in soil.
- Increase the amount of amino acids, chlorophyll content, sugars in plant cells and help in the photosynthesis process.
- The significant increment of vitamins and minerals content of plants.
- Improve the thickness of fruits cell walls.

1.2.4. Applications of Humic acids in different areas:

Humic substances, like, Humic acids are the natural plant growth promoter. Not only that, in the modern years the interest for natural Humic acids in medicine and cosmetics preparation purposes has been improved due to the high chemical activities such antioxidant properties. They have numerous biologic activities, like, antibacterial, antifungal, immunomodulatory and photo protecting functions (Mendez et al., 2005). The applications of Humic substances have been listed here.

Agricultural application:

- Natural organic fertilizer for plants
- Nitrate leaking reduction into the groundwater
- Stimulator for the plant growth and increase the yield of crops production
- Reduce the harmful effects of inorganic fertilizer.

Environmental prospects:

- Environmental contamination reduction
- Anti-collapse agent for petroleum drilling fluid
- Reduce the leaching of toxic materials such as heavy metals, organic matters from the soil

Industrial purposes:

- Natural dye production purposes
- As a natural additive to prevent seepage from large lagoons areas
- Use in the oil and gas drilling industry as additive materials to prevent collapse.

Medicine purposes:

- Veterinary medicine purposes
- Anti-viral and anti-inflammatory, anti-allergic, estrogenic, hyperemic medicine preparation
- Blood coagulation purposes
- Effective in contradiction of pathogenic bacteria

Cosmetic preparation purposes:

- Production of shower gels, creams, ointments due to the antioxidant properties
- Active against skin diseases, like, atopic dermatitis, psoriasis, and mild focal hyperhidrosis.
- Active against chronic hand dermatitis

1.2.5. Separation of Humic acids substances from various processes:

The wastewater generated from food, paper and pulp industries contain a huge amount of humic substances due to the decomposition of lignin, like, materials over years. According to authors, the major groups were found in humic substances are, like, carboxyl, aliphatic, amine, ester, phenols, amino acids etc. (Ghabbour and Davies, 2001). Few studies have been found to separate and purify these highly polydispersed materials towards fertilization.

1.2.5.1. Acid and alkaline extraction of Humic acids:

The alkaline extraction of Humic acids from peat sample using sodium hydroxide (NaOH) and sodium carbonate (Na_2CO_3) has already been explored to prepare an organic mineral based natural fertilizer. The efficiency of alkaline extraction of Humic acids was found to be inversely associated with the amount of alkaline solution added during extraction. The undesirable contamination of the extracted Humic acids was happened due to the presence of unwanted fibers and inorganic materials, like, clay and sands which were found to interfere during alkaline extraction process (Saito and Seckler, 2014).

Repetitive base extraction of peat sample was also carried out to obtain fractionated Humic acids component. The extraction process was performed for the eight times with the same peat sample until Humic acids was exhaustedly recovered. To identify the differences in molecular and chemical properties among different humic substances obtained from

different extraction cycles and to explore the possible factors causing in single cycle alkaline extraction were the two major objectives of this process. Due to the differences in solubility humic substances materials with a lower affinity for solid surfaces and having higher solubility were extracted during the earlier cycle and therefore, the large molecular weight and low polarity substances having less solubility were obtained after repetitive alkaline extraction (Li et al., 2003).

Humic and fulvic acid, like, materials were recovered from maize plant as the plant or vegetable residues are the important sources of carbon, nitrogen for the fertilizer purposes. The compost of maize plant residues was demonstrated to fractionate alkali soluble and unhydrolyzed-alkali soluble humic acid materials using benzene and ethanol mixture (2:1 v/v) and thereafter hot and cold sulfuric acid (H_2SO_4) to obtain solubilized lipids, waxes, hemicellulose, and cellulose, respectively to get more compact formation of lingo humic complex matrix which was further extracted according to alkaline process using NaOH and tetrasodium pyrophosphate ($Na_4P_2O_7$). The high chemical cost and low recovery were the major drawbacks during hot H_2SO_4 extraction of plant residue for the recovery of Humic acids, like, substances (Adani and Ricca, 2004).

1.2.5.2. Supercritical fluid CO_2 extraction of Humic acid from brown algae:

The supercritical fluid extraction of humic substances has a significant advantage over conventional extraction with acetone, ether, dioxane, and ethanol that it extracts humic materials within very short time period instead of the days needed for consecutive extraction. Brown algae namely, *Pilayella littoralis* (Phaeophyta) was already used to recover humic, like, substances efficiently using supercritical fluid CO_2 extraction process. However, it was reported that the extracted and isolated Humic acids sample had lower carbon and nitrogen content than the samples extracted from conventional organic solvent extraction due to the less removal of non-humic substances present in the extractive solution. Though this process demands the shorter time of extraction, the high operating cost and the less efficiency of removal of impurities are the major drawbacks factor for the supercritical fluid extraction to obtain the essential quantities of purified Humic acids (Radwan et al., 1997).

1.2.5.3. Application of ultrasonic vibration on the extraction of Humic acids:

Ultrasonic extraction of Humic acids from a brown soil was fruitfully reported earlier to obtain a significant amount of yields and to avoid the contamination and modification of

the components which were the main demerits of alkaline extraction of humic materials. However, it was stated that the elemental composition of humic substances was different from the classical extraction of Humic acids using acid-alkali titration. The high ash content and low content of carboxyl (-COOH) and phenolic groups (-OH) were reported while extraction of Humic acids using ultrasonication. It was stated that the application of sonolysis on extraction of Humic acids using pyrophosphate as extractor can only be reduced the time requirement from other rigorous processes though it can cause differences in the chemical and physical properties of the substances (Humic acids) which is not favorable towards use of Humic acids as a fertilizer (Ramunni and Palmieri, 1985).

1.2.5.4. Coacervate extraction method:

The coacervate extraction process was also applied for Humic acids extraction from aqueous solution maintaining the micellar solubilization phenomenon and cloud point polyethoxylated alcohols. Compare to the conventional extraction process of humic substances this technique has delivered high extraction efficiency, however, this process needs a huge amount of organic solvents, like, polyethoxylated alcohols for the continuous process of extraction of Humic acids (Ghouas et al., 2012).

1.2.5.5. Electromagnetic and electrocoagulation process:

The electromagnetic and electrocoagulation separation was explored to treat Humic acids content synthetic solution. The pH played an important role to enhance the removal efficiency of Humic acids from aqueous solution. It was reported that the batch electro coagulation process revealed the significant removal efficiency of more than 96% at pH 7 and 90 % at pH 3. Whereas, the reactivity of higher molecular weight parts of Humic acids before removal was raised effectively after introducing the electromagnetic effect during the separation process. However, the electromagnetic process in a continuous mode revealed a lower effect on the removal of Humic acids from the synthetic aqueous solution (Ghernaout et al., 2009).

1.2.5.6. Biological process to separate humic substances:

Aside from chemical processes, biological technology from food residue and green wastes remain a major desirable method for the separation of humic substances. Composting of vegetable residue for the separation of Humic acids has been reported with significant results. Food and green residue were sent to the composting chamber to complete the two

phase of composting process, like, active and curing phases. The composted materials were subjected to treat with NaOH and thereafter acidified with sulfuric acid to fractionate the composted materials into humic substances. It was reported that the oxygen to carbon ratio and total acidity of Humic acids in this process were found higher than other sources, like, peat and soil. Though the long duration of this biological process was the major demerit towards the isolation of Humic acids from food and green wastes (Adani et al., 2001; Quagliotto et al., 2006).

***1.2.5.7. Microwave assisted soxhlet method*:**

The different sewage sludges collected from different wastewater were used to extract Humic acids substances with a solvent mixture of methanol and dichloromethane (1:7) in a microwave assisted soxhlet system. The main difference between the soil and sludge extracted humic compounds has been reported about the distribution of elemental components, like, hydrogen, carbon, nitrogen, and oxygen. High degree of aliphaticity due to the high hydrogen and carbon ratio content has also been reported. Besides the high organic compounds, it was stated that the enrichment of lipids in the humic acids sample was difficult to determine during the methanol and dichloromethane solvents extraction process. The extraction and isolation of lipid components from the humic substances matrix was challenging which can be further improvised (Reveille et al., 2003).

***1.2.5.8. Fenton oxidation process*:**

The chemical oxidation processes, like, Fenton reaction and its modified version such as ozone and hydrogen peroxide combination have been the matter of a substantial attention for the recovery of natural organic components, like, humic substances from contaminated water and soil materials. The treatment process of humic substances content wastewater was carried out with the Fenton reagent, prepared by different ratios of ferrous sulphate ($FeSO_4$, 10%) and hydrogen peroxide (H_2O_2, 35%). However, the use of H_2O_2 reagent was the major cost of this treatment and it was becoming an important concern to design the process in a way where a significant recovery could be performed using a minimum amount of H_2O_2. The need of many reactive chemicals, high operating charge are also the important disadvantages during the oxidation process. Apart from this, the oxidation process can bound the reuse of Humic materials as fertilizer in the agricultural purposes due to the reduction of hydrogen/ carbon (H/C) ratio and nitrogen content (Kochany and Kochany, 2008).

1.2.5.9. Nitric acid oxidation process:

The conventional biological and acid-alkaline processes are usually insufficient to recover purified Humic acids substances for the agricultural purposes. It is well known that peat coal samples have an effective amount of humic substances which can be further chemically oxidized to achieve a huge yield of Humic acids. In view of that, the wet oxidation process using a different concentration of the nitric acid solution (1 g coal sample with 5 mL of 5%, 10%, and 15% nitric acid) has been developed to chemically extract humic substances from coal samples. It was reported that the reuse of nitric acid was also carried out during this oxidation process. The maximum purity was achieved using a low concentration of the nitric acid solution (5%) whereas, the recovery efficiency was not effective for the use of agricultural purposes. Nevertheless, the expensive chemical cost and the generation of toxic gas (NO_x) are not in favor of the use of wet oxidation process industrially (Cho and Lwin, 2012).

1.2.5.10. Ferric chloride coagulation process:

Though the ferric chloride coagulation process was investigated earlier in the field of effluent treatment and water supply, the recovery of humic materials from the dewatering wastewater of thermally treated sludges towards organic fertilizer was introduced using ferric coagulation technique. Approximately, 70% of humic substances were recovered using hydrolyzed ferric ions at the pH level of 4.5 (Yang and Li, 2016).

1.2.5.11. Membrane electrolysis and electrocoagulation process:

When the biological process takes a long time interval for the recovery of humic substances membrane electrolysis promises significant results to treat industrial wastewater for the recovery of humic, like, substances. In the membrane electrolysis process polyethersulfone microfiltration membrane, anion exchange, and cation exchange membrane were chosen to perform the filtration process. Titanium oxide coated electrode and a stainless steel electrode were applied as anode and cathode, respectively to perform the membrane electrolysis process. Though the less generation of sludge materials, no needed for extra chemical reagents and the easy operating system were the major effective benefits for the use of membrane electrolysis, the recovery of humic, like, colored components and the reduction of chemical oxygen demand were very less efficient (up to 70%) after using high energy consumption of 3 kW h m^{-3} (Kliaugaite et al., 2013).

***1.2.5.12. Application of membrane ultrafiltration for the treatment of humic substances*:**

In recent decades, the membrane ultrafiltration has become an innovative separation technology to purify the effluents rather than conventional treatment process, like, carbon adsorption, oxidation etc. Chemical and mechanical treatment processes was used to treat natural organic matters which have already been discussed (Manttari et al., 2008). Recent studies have shown that Humic substances are recognized as major foulant during water treatment (Lowe and Hossain, 2008). Not a very significant removal rate of Humic acids has been reported (Galambos et al., 2004; Shao et al., 2011; Lowe and Hossain, 2008). The membrane separation techniques can deliver a huge number of merits as compared to the conventional methods. This various filtration process is becoming an important tool for the separation of a wide number of compounds ranging from natural organic components separation to sludge purification. Membrane separation techniques are potentially perfect techniques for the minimization of environmental contamination since the membrane filtration requires the use of comparatively simple and non-harmful materials. However, Humic acids substances can also be recovered using membrane process.

The separation of humic substances in the presence of mineral salts ions (Ca^{+2}) was investigated using ultrafiltration membrane made of regenerated cellulose. Considering the high amount of membrane permeability, the reduction of membrane fouling was tried to adjust the pH conditions of the aqueous solution from 4.6 to 7.0. The filtration pressure and the concentration of humic substances were maintained at 100 kPa and 20 mg L^{-3}. However, 90% retention of humic substances molecules was achieved when pH of the solution was 7.0. Whereas, it was reported that with increasing mineral salts concentration from 50 to 100 mg L^{-1} the rejection of natural organic substances was decreased. The presence of Ca^{+2} salts ions was not significant to improve the membrane fouling behavior of the regenerated cellulose membrane. Due to the high ionic strength of the increased Ca^{+2} concentration humic substances particles displayed an affinity to shrinking which could be increased the deposition of rejected materials on the active membrane surfaces. Thus, the separation process and the transport properties of the membrane cellulose membrane were deteriorated in the presence of Ca^{+2} ions (Korbutowicz et al., 1999).

The demand for the production and purification of the clean potable drinking water from any natural or industrial sources is ignited to improve the research extensively towards novel alternative processes. In this addition, the use of membrane ultrafiltration has sparked significantly for the production of potable drinking water and the treatment of industrial effluents as well. Regenerated cellulose membrane with the different molecular weight cut

off (3, 5, 10 kDa) and high surface area of 0.1 m^2 was applied to purify the tap water containing Humic acids components. Although the removal efficiency of Humic substances from the synthetic feed solution made of deionized water was approximately 90%, this process was affected due to the significant membrane surface fouling for the 3 and 5 kDa MWCO membranes. Whereas, with the help of high retentate flow rate and transmembrane pressure drop of 210 kPa, 10 kDa MWCO membrane provided a significantly high permeation of 140-180 L m^{-2} h^{-1} initially, within 10 min of operation it reduced up to 100 L m^{-2} h^{-1} due to the severe irreversible pore clogging. On the other side, the continuous decline of permeate flux from 100 to 60 L m^{-2} h^{-1} was observed within 20 min of ultrafiltration during the treatment of Humic acids from tap water due to the presence of ions and other impurities (Lowe and Hossain, 2008).

The flat sheet membranes made of polyethersulfone and polyaryletherketone were used in a cross-flow ultrafiltration module with the active surface area of 0.036 m^2 to treat Humic acids model solution (concentration of 10 mg L^{-1}) and high Humic acids content well water. The result revealed that the 83% of recovery of Humic acids molecules was achieved during ultrafiltration. Whereas, the performances of the above-said membranes were not significant during the treatment of Humic acids content well water due to the less rejection of the smaller molecular weight components present in the water. This phenomenon was responsible for the less effective ultrafiltration of humic substances containing well water (Galambos et al., 2004).

On the other side, one hollow-fiber module with nanofiltration membrane made of polyamide (MWCO of 0.3 to 0.4 kDa) was also performed and compared with cross-flow filtration with the same feed. It was reported that though the significant rejection was achieved during hollow-fiber nanofiltration, the severe decline of permeate flux was observed due to the irreversible membrane fouling and the operating cost was very high during nanofiltration as the applied pressure drop was around 20 bar (Galambos et al., 2004).

Humic substances, from the landfill leachate, was successfully recovered and utilized as a natural fertilizer using continuous spiral wound membrane ultrafiltration (MWCO of 2500 Da) until the significant concentration of humic substances was achieved in the retentate solution. it was reported that the efficiency of this process in terms of the purity of humic substances compounds was about only 50% after applying transmembrane pressure drop of 0.7 MPa. The fractional recovery of humic components was affected due to the presence of salts ions, like, Na^+, K^+, Mg^+, and Ca^+ (Yue et al., 2011).

Several studies have revealed that membrane ultrafiltration process had a significant rejection capacity of natural organic matters, however, fouling characteristic is the severe factor that limits its widespread industrial applications. The low-pressure ultrafiltration using polyvinyl chloride hollow-fiber membrane (MWCO of 50 kDa) was performed in a full scale potable and drinking water treatment purposes. The process was performed in a dead-end method. Before the membrane ultrafiltration, poly-ferric sulfate (PFS) was used as a coagulant (dosage was 10-15 mg L^{-1}) to remove the suspended materials from the source water. However, the severe flux decline was found due to the membrane fouling as humic substances, like, natural organic materials are already recognized as the major foulant for membrane ultrafiltration especially ultra-low pressure filtration of potable water. Enormous irreversible fouling may be occurred using hollow-fiber membrane ultrafiltration due to the adsorption of humic substances during filtration. However, this study focused on the investigation of organic foulant behavior on ultrafiltration using a hollow-fiber membrane, the remediation of fouling layer using various advanced processes were not addressed here (Xiao et al., 2012).

There are insufficient literatures have been found about the purification and recovery of valuable materials, like, Humic acids from the waste effluents using membrane ultrafiltration (Li et al., 2009). A hybrid method, like, alkaline treatment afterward membrane ultrafiltration was investigated to extract Humic acids components from waste activated sludge. After the centrifugation of the disintegrated sludge with NaOH, the supernatant was subjected to send in an ultrafiltration membrane unit to extract and concentrate Humic acids components. Based on the Humic acids molecular weight distribution, a porous ceramic tubular membrane device (mesh size of 0.45 μm) was used to perform the extraction of humic substances at a maximum pressure drop of 1.0 MPa. It was informed that the concentration of Humic acids in the retentate was reached at 30 g L^{-1} when the supernatant solution was concentrated about to 20 times during ultrafiltration. The adsorption of protein and the other metal ions, like, Na^+, and K^+ on the membrane active surface was the severe factor which made an impact over the permeation (Li et al., 2009).

1.3. Treatment of paper industrial wastewater and an approach to recycle the produced water:

The precious resource in the environment is water. Recycling of water from the factories and the industrial effluents can deliver considerable benefits towards living ecosystem. Thus, treatment of industrial wastewater is very significant activity now a day, rather than discharging untreated water to the surface water, rivers or oceans (Bhuiyan et al., 2016). The purpose of the treatment of effluents is nothing but water conservation and sustainability in our environment. Reuse of water is socially and environmentally feasible and economically viable (Ruiz-Rosa. et al., 2016) The reason for the water recycling is the reuse of treated wastewater for the favorable and valuable purposes, like, agricultural, industrial, landscape irrigation, cooling water for power plants, construction purposes, dust controlling, artificial lakes, processing water for various industries etc. Due to the reckless civilization and industrialization, the scantiness of water is increased continuously which will become scarce in our country and India can be considered as water stress country in the coming periods (Tiwari et al., 2016).

Paper industry is one of the important economically advanced industry among all industries present in the environment. The paper factory is categorized as a high water-intensive industry for the large consumption of freshwater during the different stages of papermaking purposes. According to the report, the pulp and paper industry consumes approximately 60 m^3 of water per ton of production of paper (Wong et al., 2006; Savant et al., 2006). It is observed that pulp and paper industry discharges huge volume of highly toxic and colored effluents regularly in the environment. It is found in literatures that various pulp processing stages, like, wood casting, pulping and washing, bleaching, screening, chemical pulping, papermaking and chemical recovery generate highly polluted effluents containing soluble and non-soluble wood derivative products (Chanworrawoot and Hunsom, 2012). This effluent contains high organic substances causing high chemical oxygen demand (COD) as well as biological oxygen demand (BOD) (Ghaly et al., 2011; Soloman et al., 2009). Apart from organic matters, suspended solids, metals, fatty and resins acids, tannins lignin derivative compounds are responsible for water pollution. Heavy metal ions, like, Pb, Cr, Hg, As can be present in this type of effluent (Latorre et al., 2003; Ali and Sreekrishnan, 2001; Thompson et al., 2001). The organic substances found in pulp and paper industry wastewater are mostly raw materials dependent and vary with location, environmental situation, and process parametric conditions. The discharge of inadequately treated

effluents into the river water can cause a severe problem for aquatic life, including air and land pollution. Thus, the primary, secondary or tertiary treatment of paper and pulp industrial waste effluent is needed regularly to minimize the environmental pollution (Andrews et al., 2014; Pokhrel and Viraraghavan, 2004). Several studies were performed to treat pulp and paper industrial waste effluents including conventional processes such as aerated lagoons, activated sludge treatment, sedimentation or flotation, etc.

1.3.1. Anaerobic digestion process:

Anaerobic digestion plant is the most collective wastewater treatment process which is used for the removal of dissolved organic materials in several countries (Meyer and Edwards, 2014; Kumar et al., 2014). This process has reported maximum amount of dechlorination of paper industrial wastewater (Savant et al., 2006). The coagulation followed by anaerobic acidification and aeration package reactor was designed to treat pulp and paper industrial effluents for the effective removal of adsorbable organic halides, chemical and biological oxygen demand. The significant amount of toxic materials was reduced through the coagulation process due to the acidification reaction in the anaerobic digester. However, up to 88.1% and 81% removal of COD and BOD, respectively indicated that the highly toxic organic halides were difficult to treat during the anaerobic biological process (Chen et al., 2003).

1.3.2. Application of flocculation process using polymeric flocculants:

In the recent period, the application of synthetic polyelectrolytes, like, polyacrylamide during flocculation has ignited the effective removal of suspended materials from the paper industrial waste effluents. The jar test experiments with different dosages of polyacrylamide (0.5 to 15 mg L^{-1}) were achieved 93% and 98% removal of chemical oxygen demand (COD) and total suspended solids (TDS), respectively, from the paper and pulp mill wastewater. Though the several merits of the polymeric flocculation are the no residual metal ions, and good settling characteristics with dense and strong flocks, the extensive industrial application of polymeric flocculation is still challenging due to the complex behavior of this process (Wong et al., 2006).

1.3.3. Consortium bacterial treatment of paper industry effluent:

The conventional processes have been carried out worldwide, it produces an adequate amount of untreated sludge which itself requires further treatment. Being low shock loading, low capacity to remove biodegradable toxic substances and the high cost of the common treatment processes, the biological approach was obtained as an environmentally friendly technology for the treatment of waste effluents. Researchers studied sequential batch reactor using *Klebsiella sp., Alcaligens sp. and Cronobacter sp*. bacterial consortium for the potential degradation of lingo-cellulosic compounds from the effluents of paper and pulp industry. It was reported that the consortium bacteria were capable to remove the lingo-cellulosic components after 16 to 18 h of incubation and up to 91% removal of BOD was achieved. Whereas, this process was less effective to remove colored components and chemical oxygen demand. 55% and 72.3% removal capacity of coloring compounds and COD were reported, respectively during bacterial treatment of paper industry effluents. Therefore, more advanced eco-friendly alternative techniques should be required to treat the pulp and paper mill wastewater appropriately and set the strict discharge limits for this type of industry (Kumar et al., 2014).

1.3.4. Electrocoagulation process:

Currently, the most studies on purification of waste effluents have been made with the electrochemical process. Previous reports demonstrated that the electrochemical method is more capable to remove chemical and biological oxygen demand from any industrial effluents. The pulp and paper industrial effluents cause a severe pollution to the fresh water after discharging untreated wastewater with a high level of COD, BOD, suspended solids, adsorbable chlorinated compounds, resins, lignin derivative humic substances, sulphur compounds, fatty acids compounds etc. Recently, electrochemical process, including electrocoagulation for the removal of organic components in the pulp and paper industry wastewater has been performed extensively. Two different electrodes made by aluminum (Al) and iron (Fe) were studied to degrade lignin and phenolic component and to reduce COD and BOD from the paper mill wastewater at the various current density and different electrolysis time. The removal efficiency of lignin and phenolic component was increased with increasing current density by creating metallic hydroxide flocks within the wastewater. There was a high probability of coagulation of smallest charged particles due

to the formation of the electric field by which small colloidal materials were removed. However, the removal capacities of this method using two different electrodes, like, Fe and Al in terms of COD (55% and 75%, respectively) and BOD (80% and 70%, respectively) removal were not significant due to the formation of the complex chemical structure of lignin during electrochemical treatment. The operating cost consumption is high for the hybrid continuous electrochemical process (Ugurlu et al., 2008).

1.3.5. Photocatalytic treatment of paper mill wastewater:

In the current years, the advanced oxidation process is developed for the effective treatment of industrial wastewater. Heterogeneous photocatalytic degradation of organic and toxic pollutants is a challenging technology from industrial wastewater. The photodegradation activates and surface properties of titanium dioxide (TiO_2) loaded activated carbon fibers (ACF) were investigated during the treatment of paper mill wastewater. It was observed that the maximum COD removal of 72% was occurred within 40 min of photocatalytic reaction and reached its equilibrium condition gradually. The untreated lignin-derived materials were the main responsible for the low removal of COD from the wastewater (Yuan et al., 2007).

The activity of nano titanium dioxide particle as a superior photo catalyst was evaluated to treat the paper industrial waste effluents under solar irradiation. The result showed that the removal efficiency of COD increased from 46.3 to 70.5% with increasing photo catalyst dosage from 0.25 to 0.75 g L^{-1}, and pH 6.5 to 10. The maximum percentage removal of COD at high TiO_2 loading was happened due to the significant photocatalytic degradation of organic pollutant present in wastewater. This process reduced the total suspended solid materials up to 80.4% from the effluent which was not effective. The recovery of TiO_2 materials is an essential issue during industrial application of this photocatalytic degradation process (Ghaly et al., 2011).

1.3.6. Membrane technology for the treatment of wastewater:

More experiments are going on to focus on environmental pleasant processes for the treatment of wastewater. To minimize the cost-effectiveness, membrane filtration suggests an attractive alternative process for the purification of waste effluents (Manttari et al.,

2006). For an illustration, ultrafiltration has been used effectively for the recovery of natural organic materials and also for the reuse of process waters from various industries (Galambos et al., 2004).

Ultrafiltration, nanofiltration, hybrid membrane filtration, and advanced membrane module are now applying apparently to purify and reuse the effluents from the pulp and paper industries. Few studies have been performed with advanced type membrane devices for wastewater treatment purposes. Membrane filtration delivers an effective alternative to purify paper industry effluent for reuse. The treatment of wastewater using membrane separation has a reputable influence on environmental science due to the huge advantages of membrane technology. The low operating cost of membrane filtration gives numerous opportunities to apply this technology to a wide range. However, an enormous decline of permeate flux is the critical restriction to remove organic substances using membrane ultrafiltration. Recent studies have shown that organic substances are recognized as major foulant during water treatment (Lowe and Hossain, 2008). The advanced separation of natural pollutants from wastewater are facing a vital problem due to the building up of gel or cake layer formation of rejected particles on the membrane surfaces during filtration (Mousa, 2007). To restrict the formation of concentration polarization at the time of cross-flow filtration, researchers had stated the enrichment of very high feed velocity. It has been delivered that the increase in feed flow-rate leads to boost the turbulence at membrane area, which tends to minimize the concentration polarization layer thickness (Deon et al., 2010; Deon et al., 2013). Researchers have pointed out about the shear-induced or dynamically enhanced membrane filtration processes to enhance permeate flux. As because, vibratory shear enhanced (VSEP) and rotating disk membrane (RDM) modules can be the alternatives to decrease the cake layer formation on the membrane active areas during separation (Jaffrin, 2012). Development of advanced membrane module to decrease the concentration polarization is a big encounter now a day. For the reduction of fouling, comprehensive studies have already been started over last two decades (Sarkar et al., 2012).

Few results are reported about the treatment of waste effluents from effluents using shear-induced separation. High shear rate and transmembrane pressure drop were performed to achieve high rejection of solutes to treat dairy wastewater using nanofiltration rotating disk membrane. According to the total power input, a high specific energy ingestion was found under extreme hydraulic conditions during the nanofiltration of dairy industry effluent using rotating disk module (Luo et al., 2010). Except rotating disk module, nearly 18.15

kW power consumption was stated during shear-induced reverse osmosis treatment of dairy process water (Frappart et al., 2008). Though the vibratory shear enhanced module is capable to produce a high amount of permeation, the increase of high energy ingesting due to module vibration is the important limitations for this module. To reduce concentration polarization and cleaning cost, shear enhanced spinning basket membrane module has already been designed and developed to recover polyethylene glycol (PEG) with fixed retentate flow of 10^{-4} m^3 s^{-1}. Inbuilt back rotation system of this novel module can save the operating cost. They have stated that higher permeate flux was found at a power consumption of 0.94 kW which was very marginal compared to the all existing membrane modules they have enlisted (Sarkar et al., 2012).

1.4. Application of advanced separation technology towards tea factory generated wastewater:

Tea production is an important component in the global food and beverage industry. In terms of global production, India is the second largest producer of tea processing in the world following China (Pasrija and Anandharamakrishnan, 2015). The geographic conditions favor the growth of tea in the north-eastern part of India. However, processing of fresh tea leaves from the garden to readymade market requires various industrial processes (Gadhkari et al., 2015). Wastes generated by tea industries are of both solid and liquid in nature. The liquid waste is produced in a tea factory during cleaning of equipment and factory sites. The amount of effluent generated during cleaning of equipment needs an immediate attention and proper waste management procedure. The tea factory effluent contains high levels of organic matter, high chemical oxygen demand (COD) and suspended materials as well as dissolved solids. The reddish color of the effluent indicates the presence of polyphenolic and other organic components, which need to be treated to reuse the water prior its discharge in the environment (Uzun et al., 2010; Goswami et al., 2014). Due to industrial reluctance to maintain the profit margins, sometimes such effluents are directly disposed into the river. In the recent decades, many of the research attempts were directed towards the effective abatement and minimization of water pollution (Bhuiyan et al., 2016). A number of methodologies have been incorporated to treat industrial wastewater, including chemical, biological processes (Andrews et al., 2014; Ali and Sreekrishnan, 2001; Meyer and Edwards, 2014). A few results are reported to remove

the organic and inorganic compounds from tea industry wastewater. To prevent quick fouling in membrane-based processes, a pre-treatment stage is often necessary to be integrated during the treatment of wastewater.

Previous studies have reported about the feasibility of cement kiln dust containing calcium oxide (CaO) and silicon dioxide (SiO_2) as a low-cost coagulant in the treatment of wastewater from tea industry. However, at the optimum dose of 2.5 g L^{-1} coagulant, it failed to reduce COD concentration in the treated effluent (only by 9.09%) because of the low removal efficiency of proteins, theaflavins, and thearubigins. It was suggested that the treatment of tea factory wastewater can be performed using membrane filtration specifically reverse osmosis for the potable water (Yadav and Kalaiyarasi, 2015).

For the treatment of instant tea powder factory effluent, a combination of the coagulation-membrane system was adopted. To reduce the reversible or irreversible fouling on the active membrane surfaces the coagulation-flocculation was performed as a new pretreatment technique. However, employing polyaluminum ferric chloride (PAFC) as the coagulating agent, at optimum conditions of pH at 5, the temperature at 20˚C and coagulant dose of 800 mg L^{-1}, coagulation as pre-treatment removed only 44.1, 32.6, 72.5, and 57% of turbidity, COD, TSS and TOC, respectively. It was suggested that when polyaluminum ferric chloride and the organic components react with each other, a part of the complex materials undergoes a charge reversal mechanism that causes the adverse repulsion between PAFC and organic components resulting weaker removal efficiency during treatment of tea factory wastewater (Chen et al., 2015).

The approach of combined advanced oxidation process with other technique, like, adsorption has expanded substantial attention in the treatment of wastewater. The application of a combined adsorption and advanced oxidation to purify tea factory effluent is possibly more operative than the conventional processes such as activated sludge methods, single adsorption process. Natural zeolite with a range of 50 to 200 mg L^{-1} was used as an adsorbent. The dose of oxidant reagent such as hydrogen peroxide (H_2O_2) was 0.1 to 0.4 mL. This process was successful in reducing color intensity by 88% when the adsorbent dose was 200 mg L^{-1}. In case of H_2O_2, only 68% color removal was observed with 0.4 mL oxidant dose due to the generation of intermediate products during oxidation (Otieno et al., 2014). This is where the membrane filtration steps in being a promising technology which is eco-friendly, modular designed and flexible process with reduced consumption of energy and materials (Manttari et al., 2006).

Being the most popular pre-treatment method for membrane separation processes, alum coagulation has proved to be a simple and efficient method for reducing membrane fouling and hence aids in improving flux. The efficiency of coagulation process is found to be dependent on factors, like, type of coagulant and its dosage, pH, mixing speed, mixing time (Konieczny et al., 2009). This research is directed towards integration of coagulation process followed by membrane-based processes, where it is absolutely necessary to optimize the parameters of coagulation to improve process efficiency. This study is focused on the development of a new green process that permits continuous treatment of tea industry wastewater by generating clean and reusable effluent in a small, compact, energy-saving, and environment-friendly system. Researchers are really scanty using such coagulation-spinning basket membrane ultrafiltration integrated technology exploiting alum for coagulation (pre-treatment) and a spinning basket module for membrane filtration (final treatment).

1.5. Utilization of tea factory solid wastes towards environmental management:

Waste management is a global concern that mainly brings emerging countries into the limelight. It requires suitable strategies, essential resources and healthy infrastructures for an organized and sustainable waste management system (Uzun et al., 2010). Though it is reported that tea industry does not pose any huge threat to the environment, a significant portion of solid waste is being treated and reused in some scientific ways (Malkoc and Nuhoglu, 2007). Tea solid waste is mainly the part of unwanted woody shoots. During harvesting, these unwanted parts are mixed with tea leaves. The lignin-based woody slices are not treated by the tea industry during the production and made into tea industry solid waste (Malkoc and Nuhoglu, 2006). Furthermore, solid wastes are again generated from the packaging, sorting area and the weighing section in the factories. The highest amount of solid waste is also generated from the withering stage due to spillage (Amarasinghe andWilliams, 2007). The solid tea waste is about 2.5% of the total production. Generally, these wastes are mainly returned to the field to deposit into the store area (Malkoc and Nuhoglu, 2005). In the matter of solid waste management, the products which can be produced from tea solid waste using extraction methods are mainly polyphenols, caffeine, pigments, foaming reagents (Yuan et al., 2008) or tea seed bio-oil (Uzun et al., 2010; Lin et al., 2015). Among those products, polyphenols mainly represent the most plentiful constituents in tea leaves as well as tea processing solid wastes (Todisco et al., 2002). Tea

polyphenols have antioxidant activities. The phenolic compound has a deep impact on pharmaceutical purposes, like, anti-carcinogenic, anti-ulcer, anti-mutagenic activities etc. (Nawaz et al., 2006; Halake and Lee, 2017). The natural phenolic compounds have also good effects in the field of corrosion inhibition (Prabakaran et al., 2016). These compounds can be used as a natural dye reagent also. It can be used to replace some of the phenol in phenol-formaldehyde resins to manufacture polymers as well. A numerous number of experiments have been performed towards the removal of heavy metals, like, Cu, Cd, Pb, Cr, Ni from various wastewater using low-cost tea solid waste as it contains a huge amount of cellulose, lignin, hemicellulose components with a large number of surface area (Malkoc and Nuhoglu, 2006; Amarasinghe and Williams, 2007; Malkoc and Nuhoglu, 2005; Yuan et al., 2008; Cay et al., 2004; Weng et al., 2014). According to literature, the efficiency of the adsorption of metals significantly depended on phenolic compounds which are present in the tea solid wastes (Malkoc and Nuhoglu, 2007; Malkoc and Nuhoglu, 2006). The usage of tea factory solid waste to extract the total polyphenols towards solid waste management is a novel and innovative approach. The present work uses the existing science to explore the different solvent leaching and diffusion of total polyphenols from the tea industry solid waste materials. The eco-friendly management of solid waste materials after fruitful leaching of polyphenols, like, value-added products has been performed successfully in the current study. No such result has been reported on the recovery of valuable phenolic compounds from tea industry solid waste previously. Most of the cases solid waste was used for metal removal purposes. In the literature, it is mentioned that before going to adsorption, de-colorization of solid waste is the important process of metals removal (Cay et al., 2004; Weng et al., 2014). No such results have been found about the recovery of polyphenols from the tea factory generated solid waste during the de-colorization process.

1.6. Knowledge gap and objectives of the project work:

The specific utilization of the spinning basket module membrane (SBMM) for the Humic acids ultrafiltration, treatment of paper and tea industry effluents is novel, compact, energy-saving, and environment-friendly. For the identification of the pattern of fluid flow in the membrane basket at various flow rates and basket rotational speeds to purify the synthetic wastewater at a fixed molecular weight cutoff (MWCO) membrane (50 kDa), spinning basket membrane module was used previously (Sarkar et al., 2012). Concerning the

cleaning process, the membrane turbulence was not enough to eliminate small particles from the active membrane pore walls (Sarkar et al., 2012). Thus, the only back rotation was not efficient to recover hydraulic flux after cleaning. Therefore, the application of ultrasonication for the fouled membrane cleaning purposes has been presented in this study as a way to handle the cleaning process. The mechanism of preliminary permeate flux decline due to the membrane irreversible pore blocking has found no evidence in the literature previously. The process parameters, such as transmembrane pressure drop (TMP), rotational speeds, and retentate flow rate are optimized using response surface methodology (RSM) during the treatment of industrial effluents to achieve the maximum level of removal of organic or inorganic compounds. An overview of rotational diffusion model is reported in the present study to evaluate the module performance. In addition, the current study proves that the shear-enhanced spinning basket membrane ultrafiltration can be used with low power consumption than other processes for continuous operation process during the industrial effluents treatment with be fruitful results. However, the use of tea factory solid waste for the recovery of the total polyphenols using solid-liquid extraction or leaching towards solid waste management is also an innovative approach. Research endeavors are really scanty using such leaching- membrane ultrafiltration integrated technology to explore the effects of various solvents during the leaching of total polyphenols and a spinning basket module to concentrate the phenolic compounds towards the eco-friendly management of solid waste materials. The present work uses the existing science to explore the different solvent leaching and diffusion of total polyphenols from the tea industry solid waste materials. No such result has been reported on the recovery of valuable phenolic compounds from tea industry solid waste previously. Most of the cases solid waste was used for metal removal purposes. In the literature, it is mentioned that before going to adsorption, de-colorization of solid waste is the important process of metals removal (Cay et al., 2004; Weng et al., 2014). Nobody has reported about the recovery of polyphenols from the tea factory generated solid waste during the de-colorization process. Thus, a significant recovery of polyphenols using batch leaching followed by spinning basket membrane ultrafiltration has been demonstrated in the present study.

The specific objectives are designed to carry out this project work.

Performance characterization study of spinning basket membrane module during Humic acids ultrafiltration

- To study permeate quality with variation of TMP drops and rotational speeds.
- To analyze the fouling characteristics using modified Hermia's pore blocking mechanism.
- To identify the effects of ultrasonication on irreversible fouling.
- To study energetic consideration

Treatment of paper industry and tea factory generated effluents using shear induced membrane ultrafiltration

- To evaluate the performance of spinning basket membrane for the treatment of paper industry wastewater.
- To study permeate quality with variation of TMP drops, rotational speeds and MWCO of membranes.
- To analyze the fouling characteristics using modified Hermia's pore blocking mechanism
- To optimize the process parameters using Response Surface Methodology (RSM).

Recovery of polyphenols from tea factory solid waste materials using a hybrid process of leaching-membrane filtration

- To extract the total polyphenols from tea factory solid waste by varying different parameters, like, various solvents (ethanol, methanol, acetone, ethyl acetate), Solid content, temperature, time
- To optimize the parametric conditions using RSM
- To study kinetics of leaching using different kinetics models
- To study spinning basket membrane filtration for polyphenols concentration

References:

A. U. Ramunni, F. Palmieri, Use of ultrasonic treatment for extraction of humic acid with inorganic reagents from soil, Org. Geochem. 8 (1985) 241-246.

A. Radwan, R. J. Willey, G. Davies, A. Fataftah, E. A. Ghabbour, S. A. Jansen, Supercritical fluid CO_2 extraction accelerates isolation of humic acid from live Pilayella littoralis (Phaeophyta), J. Appl. Phycol. 8 (1997) 545-551.

A. Latorre, A. Rigol, S. Lacorte, D. Barcelo, Comparison of gas chromatography–mass spectrometry and liquid chromatography–mass spectrometry for the determination of fatty and resin acids in paper mill process waters, J. Chromatogr. A. 991 (2003) 205-215.

A. A. Sanchez, A. Rico, M. Vighi, Effects of water scarcity and chemical pollution in aquatic ecosystems: State of the art, Sci. Tot. Env. 572 (2016) 390-403.

A. E. Aboubaraka, E. F. Aboelfetoh, E. Z. M. Ebeid, Coagulation effectiveness of graphene oxide for the removal of turbidity from raw surface water, Chemosphere 181 (2017) 738-746.

B. M. W. P. K. Amarasinghe, R. A. Williams, Tea waste as a low cost adsorbent for the removal of Cu and Pb from wastewater, Chem. Eng. J. 132 (2007) 299-309.

B. B. Uzun, E. A.Varol, F. Ates, N. Ozbay, A. E. Putun, Synthetic fuel production from tea waste: Characterisation of bio-oil and bio-char, Fuel 89 (2010) 176-184.

B. Chen, X. Xiong, Z. Yao, N. Yin, Z. X. Low, Z. Zhong, Integrated membrane process for wastewater treatment from production of instant tea powders, Desalination 355 (2015) 147-154.

B. Saito, M. M. Seckler, Alkaline Extraction of Humic Substances from Peat Applied to Organic-Mineral Fertilizer Production, Brazilian J. Chem. Eng. 31 (2014) 675-682.

C. H. Weng, Y. T. Lin, D. Y. Hong, Y. C. Sharma, S. C. Chen, K. Tripathi, Effective removal of copper ions from aqueous solution using base treated black tea waste, Ecologic. Eng. 67 (2014) 127-133.

C. E. Raptis, J. M. Boucher, S. Pfister, Assessing the environmental impacts of freshwater thermal pollution from global power generation in LCA, Sci. Tot. Environ. 580 (2017) 1014-1026.

D. Hongve, G. Akesson, Spectrophotometric Determination of Water Colour in Hazen Units, Water Res. 30 (1996) 2771-2775.

D. Pokhrel, T. Viraraghavan, Treatment of pulp and paper mill wastewater-a review, Sci. Total Environ. 333 (2004) 37-58.

D. V. Savant, R.A. Rahman, D.R. Ranade, Anaerobic degradation of absorbable organic halides (AOX) from pulp and paper industry wastewater, Bioresour. Technol. 97 (2006) 1092-1104.

D. Ghernaout, B. Ghernaout, A. Saiba, A. Boucherit, A. kellil, Removal of humic acids by continuous electromagnetic treatment followed by electrocoagulation in batch using aluminium electrodes, Desalination 239 (2009) 295-308.

D. Yue, B. Han, G. Qi, Y. Cheng, Recovery of humic substances from landfill leachate via 2500 Da ultrafiltration membrane, Water Res. Manage. 145 (2011) 737-746.

D. Sarkar, A. Sarkar, A. Roy, C. Bhattacharjee, Performance characterization and design evaluation of spinning basket membrane(SBM) module using computational fluid dynamics (CFD), Sep. Purif. Technol. 94 (2012) 23-33.

D. Kliaugaite, K. Yasadi, G. Euverink, M. F. M. Bijmans, V. Racys, Electrochemical removal and recovery of humic-like substances from wastewater, Sep. Purif. Technol. 108 (2013) 37-44.

D. O. Otieno, A. Kumar, M. S. Onyango, O. Aoyi, Treatment of Tea Industry Wastewater Using a Combined Adsorption and Advanced Oxidation Process, Proceedings of 2014 International Conference on Sustain. Res. Innov. 5 (2014) 100-103.

D. Pasrija, C. Anandharamakrishnan, Techniques for extraction of green tea polyphenols: A review, Food Bio. Technol. 8 (2015) 935-950.

D. Titelboim, A. A. Labin, B. Herut, M. Kucera, C. Schmidt, O. H. Kaphzan, O. Ovadia, S. Abramovich, Selective responses of benthic foraminifera to thermal pollution, Marine Pollut. Bullet. 105 (2017) 324-336.

E. A. Ghabbour, G. Davies, Humic Substances, Structures, Models and Functions. RSC Advances, (2001).

E. M. P. Mendez, J. Havel, J. Patocka, Humic substances- compounds of still unknown structure: applications in agriculture, industry, environment, and biomedicine, J. Appl. Biomed. 3 (2005) 13-24.

E. Malkoc, Y. Nuhoglu, Investigations of nickel(II) removal from aqueous solutions using tea factory waste, J. Hazard. Mater. B127 (2005) 120-128.

E. Malkoc, Y. Nuhoglu, Fixed bed studies for the sorption of chromium(VI) onto tea factory waste, Chem. Eng. Sci. 61 (2006) 4363-4372.

E. Malkoc, Y. Nuhoglu, Potential of tea factory waste for chromium(VI) removal from aqueous solutions: Thermodynamic and kinetic studies, Sep. Purif. Technol. 54 (2007) 291-298.

E. L. Kochany, J. Kochany, Effect of humic substances on the Fenton treatment of wastewater at acidic and neutral pH, Chemosphere 73 (2008) 745-750.

E. Margaritis, J Kang, Relationship between green space-related morphology and noise pollution, Eco. Indicat. 72 (2017) 921-933.

F. J. Stevenson, Humus Chemistry. Genesis, Composition, Reactions, 2nd ed., Wiley, New York, (1994).

F. Adani, P. Lozzi, P. Genevini, Determination of Biological Stability by Oxygen Uptake on Municipal Solid Waste and Derived Products, Compost Sci. Utiliz. 9 (2001) 163-178.

F. Adani, G. Ricca, The contribution of alkali soluble (humic acid-like) and unhydrolyzed-alkali soluble (core-humic acid-like fractions extracted from maize plant to the formation of soil humic acid, Chemosphere 56 (2004) 13-22.

G. Thompson, J. Swain, M. Kay, C.F. Forster, The treatment of pulp and paper mill effluent: a review, Bioresour. Technol. 77 (2001) 275-286.

G. Kirillin, T. Shatwell, P. Kasprzak, Consequences of thermal pollution from a nuclear plant on lake temperature and mixing regime, J. Hydrol. 496 (2013) 47-56.

G. Z. Trznadel, Advances in membrane technologies for the treatment of liquid radioactive waste, Desalination 321 (2013) 119-130.

G. Ni, S. Christel, P. Roman, Z. L. Wong, M. F. M. Bijmans, M. Dopson, Electricity generation from an inorganic sulfur compound containing mining wastewater by acidophilic microorganisms, Res. Microbio. 167 (2016) 568-575.

H. Nawaz, J. Shi, G. S. Mittal, Y. Kakuda, Extraction of polyphenols from grape seeds and concentration by ultrafiltration, Sep. Purif. Technol. 48 (2006) 176-181.

H.A. Mousa, Investigation of UF membranes fouling by humic acid, Desalination 217 (2007) 38-51.

H. Li, Y. Jin, Y. Nie, Application of alkaline treatment for sludge decrement and humic acid recovery. Bioresour. Technol. 100(2009) 6278-6283.

H. Ghouas, B. Haddou, M. Kameche, Z. Derriche, C. Gourdon, Extraction of humic acid by coacervate: Investigation of direct and back processes, J. Hazard. Mater. 205-206 (2012) 171-178.

http://www.peopleandtheplanet.com/images/waterscarcity%20map_wri.html (accessed on 15.06.18).

http://www.wri.org/blog/2015/08/ranking-world%E2%80%99s-most-water-stressed-countries-2040 (accessed on 15.06.18).

I. Levchuk, J. J. R. Marquez, M. Sillanpaa, Removal of natural organic matter (NOM) from water by ion exchange- A review, Chemosphere 192 (2018) 90-104.

I. Galambos, G. Vatai, E.B. Molnar, Membrane screening for Humic substances removal, Desalination 162 (2004) 111-116.

I. Ruiz-Rosa, F. J. Garcia-Rodriguez, J. Mendoza-Jimenez, Development and application of a cost management model for wastewater treatment and reuse processes, J. of Clean. Prod. 113 (2016) 299-310.

J. Lowe, Md.M. Hossain, Application of ultrafiltration membranes for removal of humic acid from drinking water, Desalination 218 (2008) 343-354.

J. Shao, J. Hou, H. Song, Comparison of humic acid rejection and flux decline during filtration with negatively charged and uncharged ultrafiltration membranes. Water Res. 45 (2011) 473-482.

J. Luo, L. Ding, Y. Wan, P. Paullier, M.Y. Jaffrin, Application of NF-RDM (nanofiltration rotating disk membrane) module under extreme hydraulic conditions for the treatment of dairy wastewater, Chem. Eng. J. 163 (2010) 307-316.

J. Andrews, A.M. Smit, S. Wijeyekoon, B. Mcdonald, S. Baroutian, D. Gapes, Application of hydrothermal treatment to affect the fermentability of Pinus radiata pulp mill effluent sludge, Bioresour. Technol. 170 (2014) 100-107.

K. T. Cho, M. Z. Lwin, Study on the Analysis of Nitrohumic Acids from Two Different Rank Myanmar Coal by Ultraviolet Spectroscopy, International Conference On Chemical Processes and Environmental Issues (ICCEEI'2012), Singapore, July15-16, (2012).

K. Konieczny, D. Sakol, J. Plonka, M. Rajca, M. Bodzek, Coagulation-ultrafiltration system for river water treatment, Desalination 240 (2009) 151-159.

K. Chanworrawoot, M. Hunsom, Treatment of wastewater from pulp and paper mill industry by electrochemical methods in membrane reactor, J. Environ. Manage. 113 (2012): 399-406.

K. Halake, J. Lee, Functional hyaluronic acid conjugates based on natural polyphenols exhibit antioxidant, adhesive, gelation, and self-healing properties, J. Ind. Eng. Chem. 54 (2017) 44-51.

K. Yuan, B. Chen, Q. Qing, S. Zou, X. Wang, T. Luan, Polycyclic aromatic hydrocarbons (PAHs) enrich their degrading genera and genes in human-impacted aquatic environments, Environ. Poll. 230 (2017) 936-944.

L. Li, W. Huang, P. Peng, G. Sheng, J. Fu, Chemical and Molecular Heterogeneity of Humic Acids Repetitively Extracted from a Peat, Soil Sci. Soc. Am. J. 67 (2003) 740-746.

L. Goswami, S. Sarkar, S. Mukherjee, S. Das, S. Barman, P. Raul, P. Bhattacharyya, N. C. Mandal, S. Bhattacharya, S. S. Bhattacharya, Vermicomposting of Tea Factory Coal Ash: metal accumulation and metallothionein response in *Eisenia fetida* (Savigny) and *Lampito mauritii* (Kinberg), Bioresour. Technol. 166 (2014) 96-102.

L. Z. Jie, L. L. Song, M. Jing-zhu, Y. Li, The characteristics changes of pH and EC of atmospheric precipitation and analysis on the source of acid rain in the source area of the Yangtze River from 2010 to 2015, Atmospher. Environ. 156 (2017) 61-69.

L. Fang, L. Li, Z. Qu, H. Xu, J. Xu, N. Yan, A novel method for the sequential removal and separation of multiple heavy metals from wastewater, J. Hazard. Mater. 342 (2018) 617-624.

M. K. Korbutowicz, K. M. Nowak, T. Winnicki, Analysis of membrane fouling in the treatment of water solutions containing humic acids and mineral salts, Desalination 126 (1999) 179-185.

M. Ali, T.R. Sreekrishnan, Aquatic toxicity from pulp and paper mill effluents: a review. Adv. Environ. Res. 5 (2001) 175-196.

M. Manttari, K. Viitikko, M. Nystrom, Nanofiltration of biologically treated effluents from the pulp and paper industry, J. Membr. Sci. 272 (2006) 152-160.

M. Frappart, M. Jaffrin, L.H. Ding, Reverse osmosis of diluted skim milk: Comparison of results obtained from vibratory and rotating disk modules, Sep. Purif. Technol. 60 (2008) 321-329.

M. Manttari, M. Kuosa, J. Kallas, M. Nystrom, Membrane filtration and ozone treatment of biologically treated effluents from the pulp and paper industry, J. Membr. Sci. 309 (2008) 112-119.

M. Ugurlu, A. Gurses, C. Dogar, M. Yalcin, The removal of lignin and phenol from paper mill effluents by electrocoagulation, J. Enviorn. Manag. 87 (2008) 420-428.

M. Y. Ghaly, T.S. Jamil, I.E. El-Seesy, E.R. Souaya, R.A. Nasr, Treatment of highly polluted paper mill wastewater by solar photocatalytic oxidation with synthesized nano TiO_2, Chem. Eng. J. 168 (2011) 446-454.

M. Y. Jaffrin, Dynamic filtration with rotating disks, and rotating and vibrating membranes: an update, Current Opinion in Chem. Eng. 1 (2012) 171-177.

M. Prabakaran, S. H. Kim, V. Hemapriya, I. M. Chung, Evaluation of polyphenol composition and anti-corrosion properties of *Cryptostegia grandiflora* plant extract on mild steel in acidic medium, J. Ind. Eng. Chem. 37 (2016) 47-56.

M. A. Khan, S. Khan, A. Khan, M. Alam, Soil contamination with cadmium, consequences and remediation using organic amendments, Sci. Tot. Env. 601-602 (2017) 1591-1605.

M. Franklin, S. Fruin, The role of traffic noise on the association between air pollution and children's lung function, Environ. Res. 157 (2017) 153-159.

M. Mader, C. Schmidt, R. Geldern, J. A. C. Barth, Dissolved oxygen in water and its stable isotope effects: A review, Chem. Geo. 473 (2017) 10-12.

M. Taha, E. Shahsavari, A. A. Medina, M. F. Foda, B. Clarke, F. Roddick, A. S. Ball, Bioremediation of biosolids with Phanerochaete chrysosporium culture filtrates enhances the degradation of polycyclic aromatic hydrocarbons (PAHs), App. Soil Eco. 2017. https://doi.org/10.1016/j.apsoil.2017.11.002.

N. R. Turner, D. A. Renegar, Petroleum hydrocarbon toxicity to corals: A review, Marine Poll. Bullet. 119 (2017) 1-16.

P. Quagliotto, E. Montoneri, F. Tambone, F. Adani, R. Gobetto, G. Viscardi, Chemicals from Wastes: Compost-Derived Humic Acid-like Matter as Surfactant, Environ. Sci. Technol. 40 (2006) 1686-1692.

P. A. Soloman, C.A. Basha, M. Velan, N. Balasubramanian, P. Marimuthu, Augmentation of biodegradability of pulp and paper industry wastewater by electrochemical pre-treatment and optimization by RSM, Sep. Purif. Technol. 69 (2009) 109-117.

P. Xiao, F. Xiao, D. Wang, T. Qin, S. He, Investigation of organic foulants behavior on hollow-fiber UF membranes in a drinking water treatment plant, Sep. Purif. Technol. 95 (2012) 109-117.

P. V. Gadhkari, M. Balarman, U. S. Kadimi, Polyphenols from fresh frozen tea leaves (*Camellia assamica* L.,) by supercritical carbon dioxide extraction with ethanol entrainer-application response surface methodology, J. Food Sci. Technol. 52 (2015) 720-730.

P. Sarkar, A. Roy, S. Pal, B. Mohapatra, S. K. Kazy, M. K. Maiti, P. Sar, Enrichment and characterization of hydrocarbon-degrading bacteria from petroleum refinery waste as potent bioaugmentation agent for *in situ* bioremediation, Bioresour. Technol. 242 (2017) 15-27.

Q. Wang, Z. Yang, Industrial water pollution, water environment treatment, and health risks in China, Environment. Pollut. 218 (2016) 358-365.

R. Yuan, R, Guan, P, Liu, J, Zheng, Photocatalytic treatment of wastewater from paper mill by TiO_2 loaded on activated carbon fibers, Colloids and Surfaces A: Physicochem. Eng. Aspect. 293 (2007) 80-86.

R. M. Jain, K. H. Mody, J. Keshri, B. Jha, Biological neutralization of chlor-alkali industry wastewater, Marine Poll. Bullet. 62 (2011) 2377-2383.

R. M. Jain, K. P. Mody, J. Keshri, B. Jha, Biological neutralization and biosorption of dyes of alkaline textile industry wastewater, Marine Poll. Bullet. 84 (2014) 83-89.

R. M. A. Bhuiyan, M. M. Rahman, A. Sahid, M. M. Bashar, M. A Khan, Scope of reusing and recycling the textile wastewater after treatment with gamma radiation, J. of Clean. Prod. 112 (2016) 3063-3071

R. M. Callejon, C. Ubeda, R. R. Reina, M. L. Morales, A. M. Troncoso, Recent developments in the analysis of musty odour compounds in water and wine: A review, J. Chromato. A 1428 (2016) 72-85.

R. Roipel, S. Siemann, F. Caron, Microbial Changes in the Fluorescence Character of Natural Organic Matter from a Wastewater Source, J. Water Res. Protect. 8 (2016) 873-883.

S. Todisco, P. Tallarico, B. B. Gupta, Mass transfer and polyphenols retention in the clarification of black tea with ceramic membranes. Innovative Food Sci. Emerg. Technol. 3 (2002) 255-262.

S. Cay, A. Uyanik, A. Ozasik, Single and binary component adsorption of copper (II) and cadmium (II) from aqueous solutions using tea-industry waste, Sep. Purif. Technol. 38 (2004) 273-280.

S. S. Wong, T.T. Teng, A.L. Ahmed, A. Zuhairi, G. Najafpour, Treatment of pulp and paper mill wastewater by polyacrylamide (PAM) in polymer induced flocculation. J. Hazard. Mater. 135 (2006) 378-388.

S. Deon, P. Dutournie, L. Limousy, P. Bourseau, The Two-Dimensional Pore and Polarization Transport Model to Describe Mixtures Separation by Nanofiltration: Model Validation, AIChE J. 57 (2010) 985-995.

S. Deon, P. Dutournie, P. Fievet, L. Limousy, P. Bourseau, Concentration polarization phenomenon during the nanofiltration of multi-ionic solutions: Influence of the filtrated solution and operating conditions, Water Res. 47 (2013) 2260-2272.

S. K. Yadav, R Kalaiyarasi, Feasibility analysis of industrial symbiosis between cement industry and tea industry, Inter. J. Environ. 4 (2015) 20-34.

S. Tiwari, C.R. Behera, B. Srinivasan, Simulation and experimental studies to enhance water reuse and reclamation in India's largest dairy industry, J. Environ. Chem. Eng. 4 (2016) 605-616.

S. A. Noorhosseini, M. S. Allahyari, C. A. Damalas, S. S. Moghaddam, Public environmental awareness of water pollution from urban growth: The case of Zarjub and Goharrud rivers in Rasht, Iran, Sci. Tot. Env. 599-600 (2017) 2019-2025.

T. Meyer, E.A. Edwards, Anaerobic digestion of pulp and paper mill wastewater and sludge, Water Res. 65 (2014) 321-349.

T. K. Tran, K. F. Chiu, C. Y. Lin, H. J. Leu, Electrochemical treatment of wastewater: Selectivity of the heavy metals removal process, Inter. J. Hydrogen Energy 42 (2017) 27741-27748.

V. Reveille, L. Mansuy, E. Jarde, E. G. Sillam, Characterisation of sewage sludge-derived organic matter: lipids and humic acids, Org. Geochem. 34 (2003) 615-627.

V. Kumar, P. Dhall, S. Naithani, A. Kumar, R. Kumar, Biological Approach for the Treatment of Pulp and Paper Industry Effluent in Sequence Batch Reactor, J. Bioremed. Biodeg. 5 (2014) 218-227.

X. Z. Yuan, Y. T. Meng, G. M. Zeng, Y. Y. Fang, J. G. Shi,. Evaluation of tea-derived biosurfactant on removing heavy metal ions from dilute wastewater by ion flotation, Colloid. Surf. A: Physicochem. Eng. Aspec. 317 (2008) 256-261.

X. Lin, Z. Chen, Y. Zhang, W. Luo, H. Tang, B. Deng, J. Deng, B. Li, Comparative characterisation of green tea and black tea cream: Physicochemical and phytochemical nature, Food Chem. 173 (2015) 432-440.

Y. Chen, H, Zhan, Z, Chen, S. Fu, Study on the treatment of the sulfite pulp CEH bleaching effluents with the coagulation–anaerobic acidification–aeration package reactor, Water Res. 37 (2003) 2106-2112.

Y. Yang, H. Li, Recovering humic substances from the dewatering effluent of thermally treated sludge and its performance as an organic fertilizer, Front. Environ. Sci. Eng. 10 (2016) 578-584.

Y. Guan, C. Chu, C. Shao, M. Ju, E. Dai, Study of integrated risk regionalisation method for soil contamination in industrial and mining area, Eco. Indicat. 83 (2017) 260-270.

Z. Q. Yan, L. M. Zeng, Q. Li, T. Y. Liu, H. Matsuyama, X. L. Wang, Selective separation of chloride and sulfate by nanofiltration for high saline wastewater recycling, Sep. Purif. Technol. 166 (2016) 135-141.

CHAPTER 2

MATERIALS, METHODOLOGY, AND THEORETICAL STUDY

In this chapter, detailed experimentation, procedures, use of different chemicals and reagents, operating conditions, and theoretical studies for the membrane ultrafiltration and the leaching of polyphenols throughout the project work has been discussed. It includes the estimation of physicochemical properties such as, chemical oxygen demand (COD), pH of the effluents, total dissolved (TDS) and suspended (TSS) materials, clarity, conductivity, metal ion concentration, functional group and elemental analyses, etc. of the industrial effluents, like, paper and tea factory wastewater along with total polyphenols estimation from the solid waste materials. The detailed experimentation for the optimization study of the process parameters using response surface methodology (RSM) has also been deliberated in this chapter.

2.1. Materials and experimentation:

2.1.1. Chemicals, membrane, and collection of raw effluents:

All the chemicals, like, commercial Humic acids (HAs), sulphuric acid (H_2SO_4), silver sulphate (Ag_2SO_4), potassium dichromate ($K_2Cr_2O_7$), hydrate ferrous ammonium sulphate ($Fe(NH_4)_2(SO_4)_2$), mercuric sulphate ($HgSO_4$), sodium nitrite ($NaNO_2$), Folin-Ciocalteu reagent, aluminum chloride ($AlCl_3$), Gallic acid, acetone, ethyl acetate, quercetin, epigallocatechin, procured from M/s. Loba Chemie Pvt. Ltd. (India), M/s. Merck Ltd. (India), M/s. Sisco Research Laboratories Pvt. Ltd. (India), M/s. Sigma Aldrich (India) were analytical grade. Whatman and syringe filter papers (0.45 μm) were purchased from M/s. Merck Ltd. (India). The chemicals were used without any further treatment. H_2SO_4, Ag_2SO_4, $K_2Cr_2O_7$, $Fe(NH_4)_2(SO_4)_2$, $HgSO_4$ were used to prepare reagents during the analysis of chemical oxygen demand of the samples. Folin-Ciocalteu reagent, aluminum chloride ($AlCl_3$), Gallic acid were used during the analysis of total polyphenols. The coagulant reagent such as, alum ($Al_2(SO_4)_3.18H_2O$) was obtained from the local grocery shop in Guwahati, Assam, India. 0.1N HCl and 0.1N NaOH buffer solutions were prepared to adjust the desired pH. Milli-Q water (Millipore Filtration Unit, Elix-3, USA) was used for the preparation of fresh reagents during the sample analysis process. All the glass and plastic wares made of polypropylene were mostly purchased from M/s. Borosil Glass

Works Ltd. (India) and M/s. Tarsons Products Pvt. Ltd. (India), respectively. The details of chemicals and reagents are enlisted in the **Table 2.1**.

Table 2.1. List of chemicals and reagents used for the project works

Reagents/chemicals	Grade	Purity (%)	CAS/ Catalogue no.	Manufacture
Humic acids	AR		68514-28-3	M/s. Loba Chemie Pvt. Ltd. (India)
Gallic acid ($C_7H_6O_5$)	AR	99.5	5995-86-8	
Sulphuric acid (H_2SO_4)	AR	98	7664-93-9	
Silver sulphate (Ag_2SO_4)	AR	99	10294-26-5	
Potassium dichromate ($K_2Cr_2O_7$)	AR	99	7778-50-9	
Ferrous ammonium sulphate (FAS) $[Fe(NH_4)_2(SO_4)_2]$	AR	98.5	7783-85-9	
Mercuric sulphate ($HgSO_4$)	AR	99	1.93620.0251	
Sodium chloride (NaCl)	AR	99.5	7647-14-5	
Potassium chloride (KCl)	AR	99.5	7447-40-7	M/s. Merck Ltd. (India)
Potassium bromide (KBr)	AR	99.5	03-02-7758	
Zinc sulphate ($ZnSO_4$)	AR	99.5	7446-20-0	
Nickel sulphate ($NiSO_4$)	AR	99.5	1.93650.0521	
Copper sulphate ($CuSO_4$, $5H_2O$)	AR	99	7758-98-7	
Acetone (C_3H_6O)	AR	99	67-64-1	
Ethyl acetate ($C_4H_8O_2$)	AR	99.7	1.09623.1000	
HCl	AR	37	1.93001.2521	
NaOH	AR	99	1310-73-2	
Sodium nitrite ($NaNO_2$)	AR	98	1.93654.0521	
Aluminum chloride ($AlCl_3$)	AR	98	7446-70-0	
Magnesium chloride ($MgCl_2$)	AR	99.5	10034-99-8	M/s. Titan Biotech Ltd. (India)
Epigallocatechin ($C_{22}H_{18}O_{11}$)	AR	99		M/s. Sigma Aldrich (India)
Folin & Ciocalteu's Phenol Reagent	AR	2.0 N	39520 (062015)	M/s. Sisco Research Laboratories Pvt. Ltd. (India)
Methanol (CH_4OH)	HPLC	99.8	67-56-1	
Acetonitrile (C_2H_3N)	HPLC	99.9	75-05-8	
Ethanol (C_2H_5OH)	AR	99.5	UN1170	M/s. Tedia High Purity Solvents (USA)

Membrane:

Commercial polyethersulfone membranes with different molecular weight cutoff such as, 50, 30, 10, and 5 kDa (a flat sheet and asymmetric) obtained from M/s. Permionics Membranes Pvt. Ltd., Vadodara (Pin code: 390016), Gujarat, India were used in this study. The typical operating pH range of this membrane is 2-14.

Paper industry wastewater:

Paper mill waste effluent was collected from the effluent treatment plant of M/s. Nagaon Paper Mill, Jagi Road, Assam, India (Latitude: 26.2078° N and Longitude: 92.406° E). Clean and sterilized containers were used to collect samples and stored in the refrigerator at 4°C.

Tea factory wastewater and the solid wastes:

Tea factory wastewater and solid waste materials were collected from M/s. Sindhu Tea Pvt. Ltd. situated in Golaghat district of Assam, India (Latitude: 26.2078° N and Longitude: 92.406° E). This industry has a good annual capacity to produce good quality of Assam tea. After collection, solid waste was washed with DI water and dried at 40°C for 12 h in a hot air oven. The effluent was stored in clean and sterilized containers at 4°C in the refrigerator.

2.1.2. Experimental setup:

2.1.2.1. Unstirred batch cell membrane module (U.S.B.C.M.M.):

An unstirred batch cell module was used for the feasibility study of the purification of Humic acids contained water. The schematic diagram is shown in **Fig. 2.1**. This filtration model was made of stainless steel with the feed capacity of 0.35 L. A cylindrical vessel (77.5×10^{-3} m, inner diameter) was attached to flanges. To uphold the mechanical support on the flat sheet membrane, a circular web like a grid made of aluminum metal was utilized as a base. A circular polyethersulfone membrane with 33.4×10^{-4} m^2 active surface area was placed over the metallic support. Two identical rubber gaskets were used to avoid leakage during ultrafiltration. Air compressor was utilized to generate transmembrane pressure drop (TMP drop) during separation through the filtration cell. On the other side,

permeate was collected from the bottom of the batch cell into the borosilicate measuring cylinder.

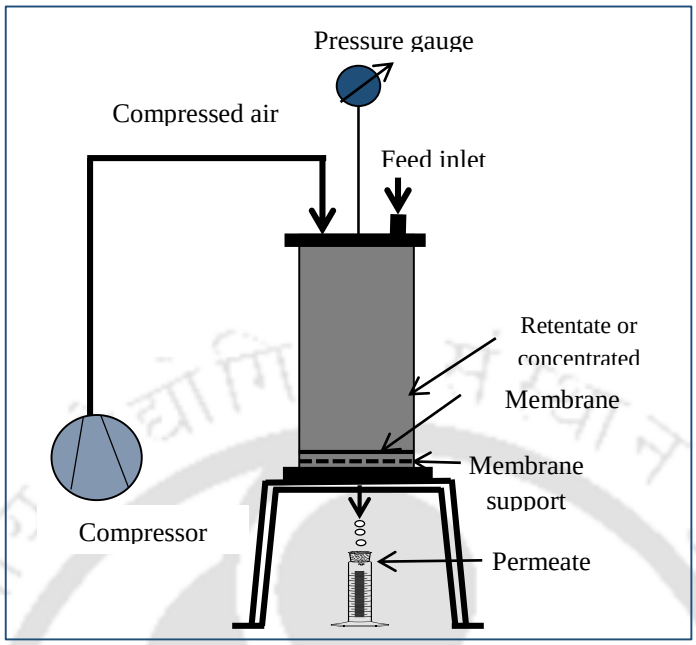

Fig. 2.1. Schematic diagram of unstirred membrane batch ultrafiltration module

2.1.2.2. Spinning basket membrane module (S.B.M.M.) description:

A model of a spinning basket membrane module (S.B.M.M.), fabricated by M/s. Gurpreet Engineering Works, Kanpur (Pin code: 208001), (India) is described in **Fig. 2.2**. Four radial arms made by stainless steel have been fitted with a single hollow shaft centrally. A three-phase induction motor was used to control the rotation of the membrane basket during filtration. The route of the rotational speed of the membrane basket is anti-clockwise. The induction motor has been connected with a V-belt with the central channel. As a result, during filtration, permeate can easily pass through the thin channel. A small distance between the steel plates and the cylindrical case gives significant and higher effective transmembrane pressure (TMP) during membrane filtration. The basket height and diameter were 0.115 and 0.25 m, respectively. Each steel plate was (0.08 ×0.09) m in size with 38.87×10^{-4} m^2 effective membrane area. The total membrane active area was 155.48×10^{-4} m^2. Rubber gasket (0.068×0.065 m^2) was placed on the membrane to protect the leakage during ultrafiltration. Polyethersulfone (PES) membrane material was attached to these steel plates during ultrafiltration. A cooling jacket was used to maintain the feed temperature at the temperature of 28± 2°C by circulating cold water. The snapshot of this

membrane module is shown in **Fig. 2.3**. Due to the vortex-like flow among the arms, the lesser amount of solutes can accumulate on the membrane surface causing less degree of concentration polarization (Sarkar et al., 2012). For the cleaning purposes, the main operational characteristic depends on basket rotational speed (ω). During the cleaning process, the basket rotates clockwise, means in the direction of the impermeable sides of steel plates. Due to the local vacuum on the membrane surfaces after releasing the applied TMP drop to the atmospheric pressure using the back pressure regulator (Sarkar et al., 2012), the accumulated solutes become swept away from membrane surfaces.

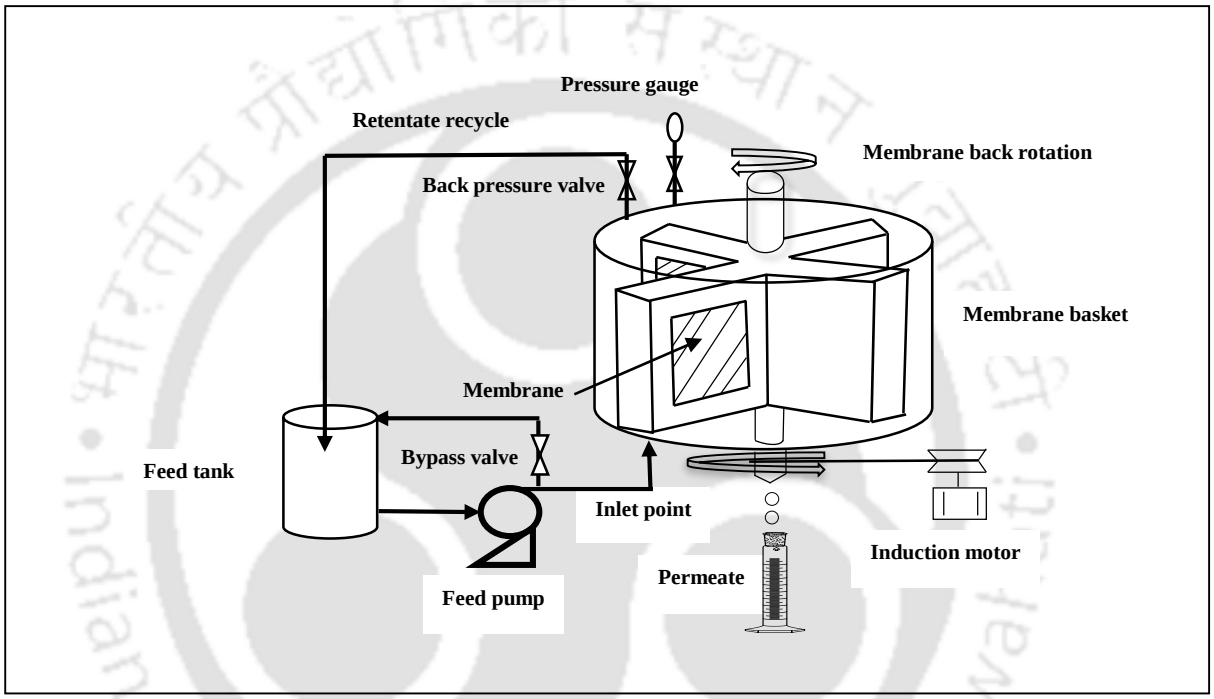

Fig. 2.2. Experimental representation of a lab scale spinning basket membrane module (SBMM)

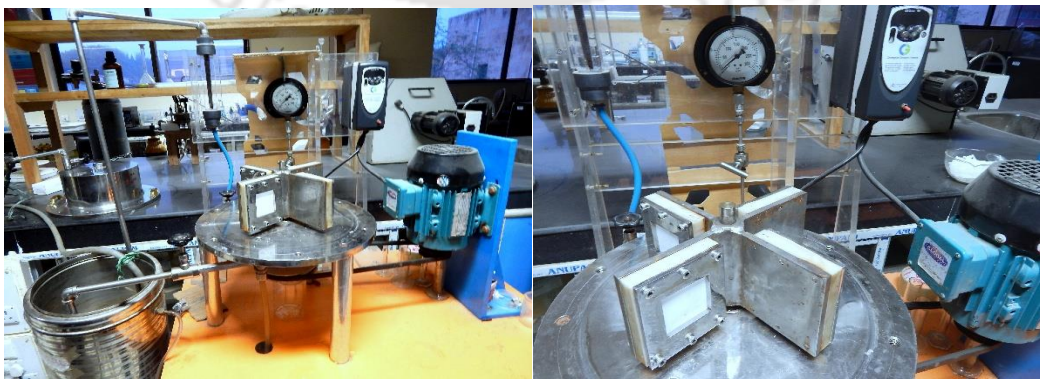

Fig. 2.3. Pictorial view of spinning basket membrane module (SBMM)

2.1.3. Experimental procedures:

2.1.3.1. Experimentation and operating condition for Humic acids ultrafiltration:

In the present study, ultrafiltration experiments were conducted using the unstirred batch cell filtration module with 33.4×10^{-4} m^2 membrane area. The batch set up was pressurized with deionized water for 2hr at 414 kPa applied transmembrane pressure (TMP) drop to overcome the compaction effect of the new membrane. The water flux was measured as a function of time until a steady value was obtained. Whereas, TMP drop (kPa), membrane basket rotation (rpm, rad s^{-1}) and feed concentration (mg L^{-1}) were varied as major parameters for the shear-enhanced ultrafiltration of Humic acids. To explore the effects of these principal parameters, like, applied TMP drops, rotational speed, the experiments were performed at different operating pressures (207, 276, 345 and 414 kPa) and various rotational speeds at 10.47, 20.93, 31.41, 52.36 and 73.30 rad s^{-1}. **Table A1** in the appendix describes the conversion value of rpm to rad s^{-1}. During filtration, the pressure was adjusted with the support of feed and retentate-line control valves. Whereas, the retentate flow rate was fixed arbitrarily at 5.0×10^{-5} m^3 s^{-1} using a back pressure regulator valve. The feed concentrations were varied from 50 to 250 mg L^{-1} for both the cases.

2.1.3.2. Pretreatment and ultrafiltration of paper industry wastewater:

The collected paper industry effluent is kept for two days to settle the macro particles gravimetrically. To decrease the total suspended solids (TSS) materials, the wastewater is subjected to vacuum filtration set up with 0.45 μm Whatman filter paper for better treatment during membrane ultrafiltration. The major objective is to illustrate the permeate flux decline behavior at four different MWCO membranes, such as 5, 10, 30 and 50 kDa at different operating conditions, like, transmembrane pressure (TMP) drops (207 to 414 kPa) and membrane basket rotations (10.47 to 73.30 rad s^{-1}) during the treatment of industrial effluent. After that, operating pressure was adjusted with the help of feed and retentate line control valves. Feed tank temperature was maintained at 28± 2° C with the help of cold water. After the ultrafiltration experiment, the rejected and concentrated sample was collected from the membrane surfaces and was analyzed for functional groups and material compositions. Prior to analysis, the concentrated residual sample was dried at 85± 5°C in a hot air oven (Make: M/s. Navyug Udyog, India; Model: NU-101) for overnight (12 h). After drying the sample was ground in a mortar and pestle and transferred in an airtight container for the consequent analyses.

2.1.3.3. Coagulation process (pre-treatment) and ultrafiltration technique (final treatment) for tea factory wastewater:

The coagulation experiments were conducted varying four different parameters, namely, alum dosage (mg L^{-1}), pH, stirring speed (rad s^{-1}) and stirring time (min). Response surface methodology (RSM) was performed to generate experimental design (Table 2.2) using minimum and maximum values of the different parameters. Design expert software (version 8.0.7.1, Stat-Ease, Inc., Minneapolis, USA) was used to optimize the coagulation parameters during the pretreatment process. The essential descriptions of all equations have been deliberated in our previous study. In the present study, the effects of alum salt (*A*, mg L^{-1}) on the removal of total dissolved solids, suspended materials, and turbidity were explored varying the salt content from 50 to 300 mg L^{-1}. The minimum and maximum ranges of the other parameters were like, pH (*B*), stirring speed (*C*, rad s^{-1}), and stirring speed (*D*, min) were, 4 and 10; 10.47 and 62.83 rad s^{-1}; and 30 and 180 min, respectively. The preferred stirring speed for the coagulation was controlled using magnetic stirrer (M/s. Tarsons India; model: Spinot). The desired responses were Percentage removal of total dissolved solids (%, TDS), percentage removal of total suspended solids (%, TSS) and the turbidity (NTU) of the samples. After designated alum dosage was added to the tea effluents, all the experiments were proceeded in the presence of different stirring speed and according to various stirring time which were tabulated in Table 2.2. Subsequently, the effluent and alum mixture was allowed to settle down at 1h to analyze the removal of suspended materials, dissolved solids, and turbidity. All the experiments were performed at room temperature (28±2°C). On the other side, final treatment was performed using the spinning basket membrane ultrafiltration by varying different MWCOs (5, 10, 30, and 50 kDa), applied TMP drops (207 to 414 kPa) and the different rotational speeds starting from 10.47 (100 rpm) to 73.30 (700 rpm) rad s^{-1}.

Choice of alum coagulation as a pretreatment method

Previously, for the treatment of various industrial effluents, aluminum-based coagulants reagents, mainly, alum [$Al_2(SO_4)_3$. nH_2O] showed significant results towards the separation of the suspended and dissolved materials present in the wastewater. Aluminum chloride, polyaluminum chloride are also considered to eliminate various contaminants from effluents. Although, the dissolved air flotation process resulted suitable removal of microorganisms and organic components present in the wastewater or sea water, the high energy cost is the major demerit for this intensive process (Loganathan et al., 2018). The

effects of polyaluminum chloride (PACl) to remove the organic components and to control the membrane fouling from the suspended materials were already investigated. In the presence of secondary coagulant reagent, like, chitosan, polyaluminum chloride (PACl) produced significant removal of pharmaceuticals and personal care products (PPCPs) from wastewater (Park et al., 2018). However, the formation of toxic compounds, such as, trihalomethanes (THMs) in the presence of chloride ions is the critical concern during use of polyaluminum chloride (PACl) as coagulant reagents (Lyon et al., 2014). Whereas, the effects of tannin-based coagulant agent, namely, Tanfloc were explored during the pretreatment of municipal wastewater. This natural organic coagulant reagent can enhance the performance of effluent clarification mainly in biological treatment units. However, to develop the ability to coagulate and flocculate the colloids, the chemical modification of the tannin-based reagent is required using various chemical mixtures, like, formaldehyde, quaternary Nitrogen (NH_4Cl), and hydrochloric acid (HCl). Thus, this modification process enhances the chemical cost of the entire process. Beside the cost effectiveness, this method takes time to produce the modified Tanfloc coagulant reagent (Hameed et al., 2018). As a result, alum salt, a classical metal coagulant reagent is selected in the present study for the pretreatment of organic compound loaded tea industry wastewater.

The organic materials present in the tea factory effluents was mainly polyphenolic compounds. The monomeric and polymeric hydrolyzed aluminum ions are formed after dissolving the alum salts in water. With increasing coagulant concentration, hydrolysis process occurs to form aluminum hydroxide [$Al(OH)_3$ (s)].

Alum has a robust affinity to generate insoluble complexes with the polar molecules, especially water (H_2O) and also hydroxyl, and carboxyl groups. The colored components, containing hydroxyl groups, are significantly destabilized and steadily develop into flocks in the presence of alum dosage which produces coordination complexes with the help of coordination reaction follows.

2.1.3.4. Leaching methodology to recover polyphenols using different solvents:

Different organic solvents to water ratio (1:4, 2:3, 3:2, 4:1, and 5:0 vol: vol) such as methanol, ethanol, acetone and ethyl acetate on the leaching of total polyphenols were prepared during leaching. The final volume of the solvent-water mixture was maintained at 50 mL. To investigate the impact of the leaching temperature on the recovery of

polyphenols, a fixed amount of dried solid waste was added in 50 mL of DI water and the leaching temperature was varied from 30 to 90°C. The temperature range was selected based on the common processing of total polyphenols using tea leaves and other tea beverage production. The desired temperature (30-90°C) during the leaching was controlled using magnetic stirrer hot plate (Make: M/s. Tarsons Products Pvt. Ltd., India; Model: Spinot Digital). To identify the effect of solid waste content in different solvents, a series of dried solid waste was fixed, like, 0.5, 1.0, 1.5, 2.0, 2.5 g in 50 mL and then extracted according to different parametric conditions. Leaching time was maintained from 10 to 90 min for all the cases. The stirring speed was fixed at 500 rpm (52.36 rad s^{-1}). Whereas, for the different organic solvents leaching, (methanol, ethanol, acetone and ethyl acetate), the temperature was maintained at 28± 2°C. All experiments were performed in triplicate (Das et al., 2015). After leaching, the solution was filtered with 0.45 μm Whatman filter paper.

2.1.3.4.1. Operating conditions for spinning basket membrane ultrafiltration for the concentration of phenolic compounds after leaching:

The spinning basket membrane module (SBMM) was performed to concentrate the total polyphenols and simultaneously to recover the water, a green solvent, after leaching of phenolic compounds from tea factory solid waste materials. The setup design of SBMM and experimentation were similar as reported in the setup design section. The commercial polyethersulfone flat sheet, asymmetric polymeric membrane of different MWCOs (30 and 50 kDa) were tested at various applied TMP drops (207, 276, 345, and 414 kPa). To investigate the effects of membrane basket rotation, the experiments were performed by the varying rotational speed at 10.47 (100 rpm) and 52.36 (500 rpm) rad s^{-1}. The experiments were performed according to the standard membrane ultrafiltration process. The cumulative permeate volumes for all samples were collected for the duration of 60 min approximately. The permeate flux was calculated according to the Darcy's law. Retentate samples were collected after the different time break for further analysis.

2.2. Cleaning study for fouled membrane using module back rotation and ultrasonication process:

To avoid the severe effects of chemical cleaning on membrane surfaces, the spinning basket module was cleaned with two different techniques: (i) using module back rotation and (ii) ultrasonication. After all the experiments, the basket was set to rotate in the reverse

direction at the impermeable side of the steel plate. Maximum operating time for the module back rotation was 45 min. As the membrane basket rotation is an important parameter to increase solvent flux, during back rotation speed was varied from 100 to 500 rpm. A low TMP drop at 140 kPa (Sarkar et al., 2012) was maintained during the cleaning performance. The applied pressure was minimized using the back pressure regulator to create a local vacuum on the membrane surfaces (Sarkar et al., 2012).

2.2.1. Fouled membrane cleaning process using ultrasound:

Application of ultrasound has been introduced in the field of membrane filtration as well as in cleaning study (Li et al., 2002). The effects of ultrasonication on the cleaning of a whey fouled membrane in a dairy industry has already been investigated and also optimized during the cross-flow ultrafiltration (Muthukumaran et al., 2004; Muthukumaran et al., 2005). To obtain the significant effects of ultrasound on the membrane cleaning, the assembled membrane module was placed in an ultrasonic bath. Research has suggested that ultrasound-assisted fouled membrane cleaning is a promising technique to clean the membrane pores at the industry level to reduce the chemical cost of the chemical cleaning process. Thus, the significant effect of ultrasonication of a fouled membrane with respect to time was investigated after spinning basket membrane ultrafiltration of Humic acids solution. For these experiments, temperature, ultrasound (US) power and, frequency were fixed at 25°C, 120 W, 50 kHz, respectively. If the power supply in the ultrasonic bath is increased from 120 W to higher range, there is a possibility of breakage of the membrane during cleaning. In the present study, the power of the ultrasound bath was fixed to 120 W to control the damaging of the membrane surface. Distilled water as liquid media was used for sonication. After module back rotation, membranes were removed from the spinning basket module and kept in a beaker, filled with distilled water. Then the beaker was placed in the ultrasound bath for better cleaning purposes. The temperature of the ultrasonic bath was kept constant at 25°C by recirculating the cold water in the ultrasonic bath during the cleaning process.

2.3. Samples analysis using different analytical techniques:

In the present study, different parameters, such as total suspended solids (TSS) compounds, pH, total dissolved solids (TDS) materials, ionic conductivity, the percentage of clarity (*T* %), chemical oxygen demand (COD), and biological oxygen demand (BOD) were analyzed

in our laboratory. The standard procedures were followed to study the physicochemical properties (Das et al., 2006). UV-vis spectroscopy with an optical path length of 1 cm (Make: M/s. Thermo Fisher Scientific, India; Model: UV 2300) at 254 nm (λ_{max}) was used to measure the initial and final concentration of Humic acids (Goslan et al., 2009). A series of standard solutions (0 to 40 mg L^{-1}) of pure Humic acids was prepared for the calibration. A linear relationship was found with a correlation coefficient of 0.99 (R^2). The ionic conductivity (S m^{-1}) and the total dissolved solid (TDS, mg L^{-1}) for all the samples were analyzed using a conductivity meter (Make: M/s. Thermo Fisher Scientific, Singapore; Model: Eutech Instrument-CON 700).

The clarity of all samples was examined as % $T = 100 \times 10^{-Abs}$, where, *Abs* is the optical absorbance at 660 nm using UV-vis Spectroscopy (Make: M/s. Thermo Fisher Scientific, India; Model: UV 2300) (Das et al., 2015).

The pH values of the samples were measured by a pH meter (Make: M/s. Thermo Fisher Scientific, Singapore; Model: Eutech Instrument-pH 700). The ionic conductivity (S m^{-1}) and TDS (mg L^{-1}) were measured by an auto-ranging conductivity meter (Make: M/s. Thermo Fisher Scientific, Singapore; Model: Eutech Instrument-CON 700). The viscosity of the sample was calculated using a rheometer (Make: M/s. Thermo Electron, Germany; Model: Rheostress RS 1).

Chemical oxygen demand (COD, mg of dissolved O_2 L^{-1}) was obtained using standard dichromate and ferrous ammonium sulphate titration method using closed reflux digester (Make: M/s. Hach Company, India; Model: DRB 200). The dichromate solution ($K_2Cr_2O_7$) was used as a digestion solution. A sample of 2.5 mL was added to 3 mL of the acid reagent (Ag_2SO_4 in H_2SO_4) followed by the dichromate solution ($K_2Cr_2O_7$). All the samples including the blank solution were placed in the COD digester vessel at 150°C for 120 min. After cool down to room temperature, solutions were titrated with the standard solution of ferrous ammonium sulphate (FAS) [$Fe(NH_4)_2(SO_4)_2$] as an indicator. The dissolved oxygen of the samples was measured using a digital DO meter (Make: M/s. HANNA Instruments, USA; Model: HI 2400).

The particle size of the effluent was examined using Delsa™ Nano particle size analyzer (Make: M/s. Beckman Coulter, Switzerland; Model: Delsa Nano C).

The elemental analysis of the concentrated materials of the paper industrial effluents was performed using Energy-dispersion X-ray spectroscopy equipped with field emission scanning electron microscopy (Make: M/s. Zeiss, Germany; Model: Sigma).

The mass loss behavior of the concentrated compounds of the paper industrial effluents were studied using thermal gravimetric analyses (Make: M/s. Netzsch, Germany; Model: TG 209 F1 Libra) under nitrogen (N_2) gas at a heating rate of 5°C. The amount of 8 mg sample was analyzed in the temperature range of 28 to 650°C.

The presence of various functional groups of different components found in the paper industry effluent was confirmed by the Fourier-transform infrared spectroscopy (Make: M/s. Shimadzu, Japan; Model: IRAffinity-1) using the KBr pellet method. The dried KBr salt to sample (99:1 w/w) was ground and transferred to the pellet casting die to make a thin pellet using 5 to 7 tons of pressure. The pure KBr pellet was used to make the background clear by scanning from 450 to 5000 cm^{-1} with the resolution of 4 cm^{-1}. For the liquid samples, a small drop of the permeate sample of the ultrafiltration was added to the thin KBr pellet using a syringe. The metal concentrations (mg L^{-1}), such as sodium (Na), zinc (Zn), nickel (Ni), potassium (K), iron (Fe), magnesium (Mg), manganese (Mn), and copper (Cu) were studied by Flame Atomic Absorption Spectrometer (Make: M/s. Varian, Netherland; Model: Spectra AA 220 FS). The specific metal hollow cathode lamps were used to determine the metal ion concentration during analysis.

To analyze the extracted compounds from the tea factory solid wastes using different analytical techniques, all the extracts were filtered with 0.45 μm membrane syringe filters at first. The total polyphenols (mg L^{-1} GAE) was determined by spectrophotometer using gallic acid as standard, according to the Folin-Ciocalteu method (Pearson's correlation coefficient: R^2 =0.987) (Rover and Brown, 2013; Karadirek et al., 2016; Li et al., 2012). The absorbance of the reaction mixture was read at 765 nm. In order to adjust the error, all the experiments were performed in the triplicate mode.

To determine the concentration of epigallocatechin in the extract and after ultrafiltration, C 18 HPLC column (length: 150 mm; diameter: 3.5 mm) equipped with a UV-visible detector (Make: M/s. Shimadzu, Singapore; Model: Prominence HPLC System) was used. This process was performed with the mobile phases consisting of 1% orthophosphoric acid (H_3PO_4) in DI water (Gottumukkala et al., 2014) and acetonitrile with a flow rate of 1 mL min^{-1} and wavelength of 280 nm. The UV-vis spectroscopic method was adapted to measure the total flavonoids components according to the quercetin standard curve (Sharma et al., 2016). 0.15 mL of 5% sodium nitrite ($NaNO_2$) aqueous solution was added to the extractive materials (2.5 mL) and vortexed. 0.15 mL of 10% aluminum chloride ($AlCl_3$) and 1 mL of 1M sodium hydroxide (NaOH) were added after 5 min of the vortex. After

mixing all the standards along with the extracted samples were measured against a blank prepared by 80% methanol at 510 nm (Zhishen et al., 1999).

2.4. Theoretical deliberation:

2.4.1. Theory of membrane ultrafiltration and cleaning study:

The performance of the spinning basket module for the treatment of Humic acids, industrial effluents was analyzed in terms of the permeate flux decline, the total membrane resistance ($R_{t_{SBMM}}$) and the net power consumption (P_{sep}).

Darcy's law (Eq. 2.1) has been applied to determine membrane hydraulic (L_p, m Pa^{-1} s^{-1}) and the Humic acids permeate flux (Das et al., 2006, Singh and Das, 2014, Facundo et al., 2013).

$$J_{HAs} = L_P \Delta P = \frac{dV}{A_m dt} = \frac{\Delta P}{\mu_{pHAs} R_{t_{SBM}}} \tag{2.1}$$

A_m, dV, ΔP, μ_{pHAs} and, $R_{t_{SBMM}}$ are the membrane active surface area (m^2), permeate volume (m^3), the applied TMP drop (kPa), the viscosity value (kg m^{-1} s^{-1}) of collected permeate and, the net membrane resistance (m^{-1}), respectively.

During the treatment of industrial waste effluent, a substantial osmotic pressure can be exerted due to high feed concentration. The permeate flux can be defined as follows (Singh et al., 2013):

$$J_{effluent} = L_p(\Delta P - \Delta\pi) \tag{2.2}$$

According to Van't Hoff equation $\Delta\pi$ can be expressed as:

$$\Delta\pi = RT(C_{ms} - C_{ps}) \tag{2.3}$$

$$J_{effluent} = L_p[\Delta P - RT(C_{ms} - C_{ps})] \tag{2.4}$$

whereas, C_{ms} is the solute concentration on the membrane surface. As the membrane ultrafiltration process is a pressure assisted operation, the concentration of suspended particles in the vicinity of the membrane (C_{ms}) cannot be determined analytically. The solutes will be diffused back to the bulk solution after the releasing of applied pressure during membrane filtration. As a result, C_{ms} can be considered as a theoretical parameter which could be further substituted in terms of feed or bulk concentration (C_{os}). According to film theory or concentration polarization model, the solute concentration on the membrane surface (C_{ms}) can be evaluated theoretically. Eq. 2.5 can be used to calculate the

value of solute concentration on the membrane surface (C_{ms}) during any membrane ultrafiltration process (De, Novel Separation Processes (Web) Module 3, 2012). C_{ps} is the solute concentration in the produced water (collected permeate). R is the ideal gas constant (8.314 J mol^{-1} K^{-1}). T is defined absolute temperature (K) (Singh et al., 2013).

Now according to concentration polarization model

$$\frac{C_{ms}-C_{ps}}{C_{os}-C_{ps}}=\exp(\frac{J_{effluent}}{k}) \tag{2.5}$$

Due to the high rejection using the spinning basket membrane module, the solute concentration in the permeate section could be considered absolutely negligible with respect to the solute concentration in the feed stream. As a result, C_{ps} can be considered as negligible as C_{ms} or C_{os} (Singh et al., 2013).

$$\frac{C_{ms}}{C_{os}}=\exp(\frac{J_{effluent}}{k})=(1+\frac{J_{effluent}}{k}) \tag{2.6}$$

where k is the mass transfer coefficient ($k=\frac{D}{\delta}$). D is the solute diffusivity and δ is the film thickness (Singh et al., 2013).

Now, using Eq. (2.4) and (2.6) we can get,

$$J_{effluent}=L_P\left[\Delta P-C_{os}\left(1+\frac{J_{effluent}}{k}\right)RT\right] \tag{2.7}$$

We know,

$$J_{effluent}=L_P\Delta P=\frac{\Delta P}{\mu_{effluent}R_{m_{SBMM}}} \tag{2.8}$$

$R_{m_{SBMM}}$ is the fresh membrane resistance (m^{-1}).

Putting the value of L_P in Eq. (2.7) we have,

$$J_{effluent}=\frac{1}{\mu_{effluent}R_{m_{SBMM}}}[\Delta P]-\frac{C_{os}RT}{\mu_{effluent}R_{m_{SBMM}}}\left(1+\frac{J_{effleunt}}{k}\right) \tag{2.9}$$

Now after arranging Eq. (2.9) we can get

$$J_{effluent}\left(1+\frac{C_{os}RT}{\mu_{effluent}R_{m_{SBMM}}k}\right)=\frac{1}{\mu_{effluent}R_{m_{SBMM}}}[\Delta P]-\frac{C_{os}RT}{\mu_{effluent}R_{m_{SBMM}}} \tag{2.10}$$

Finally, we have the following Eq. (2.11) to calculate the flux value.

$$J_{effluent} = \frac{(\Delta P - C_{os} RT)}{(\mu_{effluent} R_{mSBMM} + \frac{C_{os} RT}{k})} \tag{2.11}$$

Now, to identify the value of *k*, the suitable Sherwood number relation is used here. Spinning basket membrane modules act as a stirring cell. The applicable Sherwood number relation has been selected from the literature (De, Novel Separation Processes (Web) Module 3, 2012; Banerjee and De, 2012).

The description of Reynolds and Schmidt number:

$$\text{where, } \mathrm{Re} = \frac{\rho_{effluent} \omega r^2}{\mu_{effluent}} \tag{2.12}$$

Sc is Schmidt number

$$Sc = \frac{\mu_{effluent}}{\rho_{effluent} D} \tag{2.13}$$

where *r* is the radius (m) of the stirred cell, ω is the stirrer speed (rad s^{-1}) and *D* is the diffusivity (m^2 s^{-1}).

$$Sh = \frac{kr}{D} = 0.285(\mathrm{Re})^{0.55} (Sc)^{0.33} \tag{2.14}$$

The Brownian diffusion model:

$$D_b = \frac{KT}{6\pi\mu a} \tag{2.15}$$

where *K* is the Boltzmann constant (1.38×10^{-23}, J K^{-1}), *T* is temperature (301 K), and *a* is the particle radius.

Now, using Eq. (2.14) and Eq. (2.15) we have,

$$k = \frac{0.628\times10^{-19}}{a\times r} \left(\frac{\rho_{effluent} \omega r^2}{\mu_{effluent}}\right)^{0.55} \left(\frac{\mu_{effluent} \times a \times 10^{19}}{\rho_{effluent} \times 2.204}\right)^{0.33} \tag{2.16}$$

Now, we can easily evaluate the calculated flux with the help of Eq. (2.11) and Eq. (2.16).

The rotational diffusion model:

$$D_r = \frac{KT}{8\pi\nu a^3} \tag{2.17}$$

Rotational diffusion constant (D_r) has a unit of s^{-1}. So for the unit balance,

$$D_r \times r^2 = \frac{KTr^2}{8\pi\nu a^3} \tag{2.18}$$

where ($D_r \times r^2$) is the reformed rotational diffusion constant (m^2 s^{-1}).

To calculate mass transfer coefficient Eq. (2.14) and Eq. (2.18) can be used

$$k = \frac{0.325\times10^{-19}}{a\times r}\left(\frac{\rho_{effluent}\omega r^2}{\mu_{effluent}}\right)^{0.55}\left(\frac{\mu_{effluent}\times a\times10^{19}}{\rho_{effluent}\times1.14}\right)^{0.33} \quad (2.19)$$

Now, we can easily evaluate the calculated flux with the help of Eq. (2.11) and Eq. (2.19).

The shear-induced diffusion model:

The practical shear-induced diffusion model is presented in Eq. (2.20) (Singh et al., 2013).

$$D_s = 3.63\frac{ua^2}{d_e} \quad (2.20)$$

where u, and d_e are feed velocity (ms^{-1}) and equivalent diameter (m), respectively.

Now as said earlier, the spinning basket module is an example of a stirring cell. The equivalent diameter has been substituted with the rotating cell diameter ($d_e=d=r/2$) and u has been replaced by angular velocity ($\omega\, r$).

$$D_s = 7.26\frac{(\omega r)\times a^2}{r} \quad (2.21)$$

So, for the mass transfer coefficient (k)

$$k = \frac{D_s\times0.285}{r}\left(\frac{\rho_{effluent}\omega r^2}{\mu_{effluent}}\right)^{0.55}\left(\frac{\mu_{effluent}}{\rho_{effluent}\times D_s}\right)^{0.33} \quad (2.22)$$

Now, the theoretical permeate flux can be evaluated with the help of Eq. (2.11) and Eq. (2.22).

The total resistance calculation:

The following equation describes the total membrane resistance (Das et al., 2006; Singh and Das, 2014):

$$R_{t_{SBM}} = R_{c_{SBM}} + R_{f_{SBM}} + R_{m_{SBM}} \quad (2.23)$$

where, the cake layer resistance, the fouling membrane resistance and, the fresh membrane resistance (m^{-1}) are $R_{c_{SBM}}$.,$R_{f_{SBM}}$ and, $R_{m_{SBM}}$, respectively. The following equation is for the calculation of the fresh membrane resistance.

$$R_{m_{SBM}} = \frac{\Delta P}{\mu_w J_w} \quad (2.24)$$

where, μ_w indicates the pure water viscosity (Pa s). Finally, $R_{f_{SBMM}}$ (m^{-1}) can be evaluated using the following equation:

$$R_{f_{SBM}} = \frac{\Delta P}{\mu_w J_f} - R_{m_{SBM}} \quad (2.25)$$

where J_f is the pure water flux (L m^{-2} h^{-1}) after the ultrafiltration.

Now the resistance for the generated cake layer on the membranes can be evaluated (Singh and Das, 2014).

$$R_{c_{SBM}} = [R_{t_{SBM}} - (R_{f_{SBM}} + R_{m_{SBM}})] \quad (2.26)$$

Observed rejection $(R_{obs_{HAs}})$ during the ultrafiltration of Humic acids can be defined as follows (Singh et al., 2013):

$$R_{obs_{HAS}} = 1 - \frac{C_{p_{HAs}}}{C_{0_{HAs}}} \quad (2.27)$$

In this equation, $C_{0_{HAs}}$ and $C_{p_{HAs}}$ (mg L^{-1}) indicate the initial and the final Humic acids concentration in the bulk solution and permeate, respectively.

The calculation of volume reduction factor (VRF):

The VRF value was calculated using Eq. (2.28):

$$VRF = \frac{V_0}{V_{R_{HAs}}(t)} = \frac{V_0}{V_0 - V_{P_{HAs}}(t)} \quad (2.28)$$

where V_0 (mL) is the initial feed volume (mL). $V_{R_{HAs}}$ (mL) is the retentate final volume at particular time (t) period. $V_{P_{HAs}}$ (mL) is the collected permeate with respect to process time for both the modules (SBM and batch cell). VRF values differ from 1 to ∞. At the starting of the operation $V_{R_{HAs}}(t) = V_0$, means $VRF = 1$. When the entire feed sample passes through the membrane $V_{R_{HAs}}(t) = 0$, $VRF = \infty$ (Singh et al., 2013; Singh and Das, 2014).

The calculation of cleaning efficiency:

After cleaning experiments using deionized water and ultrasound, water flux was evaluated again. Cleaning efficiency (E_{clean}, %) has been calculated according to Eq (2.29):

$$E_{clean}(\%) = \frac{R_{f_{SBMM}} - R_{cl_{SBMM}}}{R_{f_{SBMM}} - R_{m_{SBMM}}} \times 100 \quad (2.29)$$

$R_{cl_{SBMM}}$ is the clean membrane resistance (m^{-1}). The water flux (J_{wcl}) was evaluated at the finish of each cleaning process (Facundo et al., 2013).

The power consumption calculation:

Total power consumption during the separation process (P_{sep}) has been obtained as the summation of the power supplied by the induction motor (P_m) and the piston pump (P_p) (Sarkar et al., 2012).

$$P_{sep} = P_P + P_m \tag{2.30}$$

During cleaning process, the net power consumed (P_{clean}) was the summation of the power consumed during back rotation (P_b) and the power supplied in an ultrasonic bath (U_p).

$$P_{clean} = P_b + U_p \tag{2.31}$$

Now the power supplied to the entire process (filtration and cleaning)

$$P_{tot} = P_{sep} + P_{clean} \tag{2.32}$$

Power supplied by the piston pump (Frappart et al., 2008) was expressed using Eq. (2.33).

$$P_p = \frac{Q_{feed}\Delta P}{\eta} \tag{2.33}$$

The feed flow rate is indicated by Q_{feed} ($m^3\ s^{-1}$), η is the pump effectiveness (%). One assumption has been incorporated that the pump head has been taken as equal to operating TMP drop (ΔP). For a three-phase induction motor, the net power intake is directly related to the membrane basket rotation or angular velocity (ω). In the present study, induction motor power consumption (P_m) has been calculated as:

$$P_m = \tau \times \omega \tag{2.34}$$

τ is proportionality constant. ω is applied rotational speed (rad s^{-1}). τ is defined as torque (Watt s) generated by a rotating shaft.

2.4.2. Characterization of irreversible fouling using modified Hermia's pore blocking model:

Membrane fouling happens due to the settle down of retained solute particles on the active membrane surfaces, pore mouths, and pore walls causing transient flux decline. In the current study, to define the fouling mechanisms, Hermia's pore blocking model has been studied. This model contains four various reversible and irreversible fouling models to analyze the mode of membrane fouling characteristics, such as (Vela et al., 2008; Das et al., 2015) the complete pore blocking model (CPBM), the standard pore blocking model (SPBM), the intermediate pore blocking model (IPBM), and the cake filtration model (CFM) (Field et al., 1995).

Definitions of various pore blocking mechanisms:

Complete pore blocking model (CPBM):

When the membrane pores are completely blocked by the comparatively large size of particles, this type of pore clogging is called as the complete pore blocking (CPBM).

Standard pore blocking model (SPBM):

When the solute adsorption onto the membrane pore wall occurs due to the presence of small particles in size, the standard pore blocking model (SPBM) gives the perfect model prediction for fouling study.

Intermediate pore blocking model (IPBM):

When the size of the membrane pore is almost similar to the size of the solutes, all the membrane active pores are blocked just to the arrival side of the feed, the intermediate pore blocking (IPBM) happens.

Cake filtration model (CFM):

The cake filtration model (CFM) predicts the perfect model fitting when the retained solute creates a gel or cake type layer on the active membrane surface (Vela et al., 2008).

Fig. 2.4 demonstrate the graphical presentation of various membrane fouling mechanisms. Eq. (2.35) delivers the Hermia's pore blocking model for the dead-end filtration mode.

$$\frac{d^2t}{dV^2} = K\left(\frac{dt}{dV}\right)^n \tag{2.35}$$

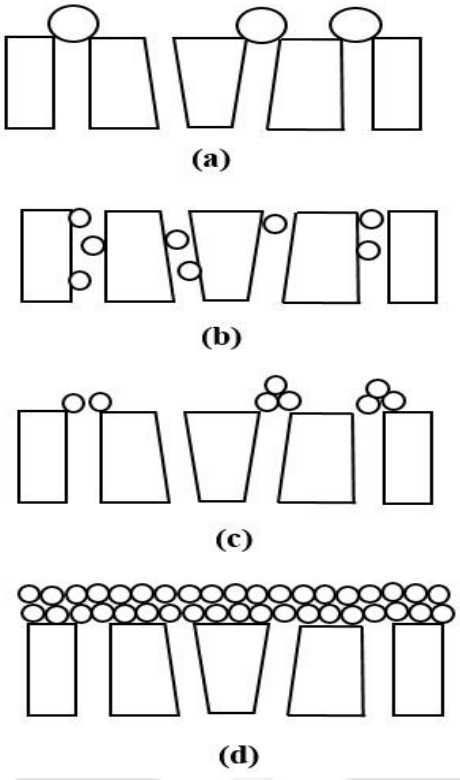

Fig. 2.4. Graphical illustration of membrane fouling mechanisms: (a) CPBM, (b) SPBM, (c) IPBM, and (d) CFM

The modified Hermia's pore-blocking model is presented as follows:

$$-\frac{dJ_{HAs}}{dt} = k(J_{HAs} - J_{sp})J_{HAs}^{(2-n)} \tag{2.36}$$

To analyze the various fouling modules, the parameter n has the different significant value such as (i) complete pore blocking: n=2 (ii) standard pore blocking: n=3/2, (iii) intermediate pore blocking: n=1, and (iv) cake filtration model: n=0 (Field and Wu, 2011). The linearized forms of above said models are tabulated in the **Table 2.2** (Briao and Tavares, 2012).

Table 2.2. Linearized forms and significances of different blocking mechanisms

Pore blocking mechanism	Linearized form (Briao and Tavares, 2012)	Physical significance	Model Constants (k) (Briao and Tavares, 2012)
CPBM	$J_{HAs} = J_{sp} + (J_0 - J_{sp})e^{(-k_f t)}$	Fouling occur at the membrane pore entrance	$k_f = J_0 k_A / \varepsilon$ (s^{-1})
SPBM	$\frac{1}{J_{HAs}^{1/2}} = \frac{1}{J_0^{1/2}} + k_s t$	Retentate particles deposition over the pore walls	$k_s = 2\frac{k_B}{A_0} A J_0^{1/2}$ ($m^{-1/2}\, s^{-1/2}$)
IPBM	$k_{cf} t = \frac{1}{J_{sp}} \ln\left(\frac{J_{HAs}(J_0 - J_{sp})}{J_0(J_{HAs} - J_{sp})}\right)$	Pore clogging with particle deposition on membrane surface	$k_{cf} = k_A$ (m^{-1})
CFM	$k_{gl_{HAs}} t = \frac{1}{J_{sp}^{\,2}}\left[\ln\left(\frac{J_0(J_0 - J_{sp})}{J_{HAs}(J_{HAs} - J_{sp})}\right)\right] - J_{sp}\left(\frac{1}{J_{HAs}} - \frac{1}{J_0}\right)$	Membrane surface deposition of the retentate particles and gel layer creation	$k_{gl_{HAs}} = \frac{2R_{c_{SBM}} k_D}{J_0 R_{m_{SBM}}}$ ($m^{-2}\, s^{-2}$)

2.4.3. Kinetics of total polyphenols leaching from the tea factory solid waste:

The mechanism of hot water leaching of total polyphenols from tea factory solid waste was confirmed to occur in two major stages, like, leaching and dissolution of polyphenols near the solid particle surfaces followed by the diffusion of polyphenols from the solid waste to the aqueous solution. The kinetics of the leaching of total polyphenols were studied using different rate models and compared. The pseudo first order, second order, and the Elovich kinetics model were applied to determine the theoretical prediction of total polyphenols leaching using aqueous solution. The rate of leaching is directly relative to the difference between the concentration of the water-soluble polyphenols at an equilibrium stage and the concentration at any time condition.

$$\frac{\Delta c}{\Delta t} = k_1 (c_e - c) \qquad (2.37)$$

Where, c (mg L^{-1} GAE), c_e (mg L^{-1} GAE), k_1 (min^{-1}) are, the concentration of total polyphenols at any time(t), at equilibrium or saturation state and the first order leaching rate constant, respectively **(**Oumarou et al., 2007).

Pseudo first order model:

The influence of different solid content (g) on the total polyphenols leaching has been analyzed theoretically using leaching first order kinetic model.

$$c = c_e(1-\mathrm{e}^{-k_1 t}) \tag{2.38}$$

The linearized form has been described here.

$$\ln(c_e - c) = \ln(c_e) - \frac{k_1 t}{2.303} \tag{2.39}$$

Pseudo second order model:

The second order rate kinetics can be expressed as follows:

$$\frac{\Delta c}{\Delta t} = k_2 \left(c_e - c\right)^2 \tag{2.40}$$

$$c = \frac{k_2 c_e^{\,2} t}{1 + k_2 c_e t} \tag{2.41}$$

Eq. (2.41) is the integrated form of the second order leaching rate model where boundary conditions are c=0 at t=0 and c=c_e at t=t. Eq. (2.42) can be rearranged to obtain the linearized form. Eq. (2.42) has been analyzed to identify the second order rate constant for this model in the present study **(**Oumarou et al., 2007).

$$\frac{t}{c} = \frac{1}{k_2 c_e^{\,2}} + \frac{t}{c_e} \tag{2.42}$$

Where, k_2 (L mg^{-1} min^{-1}) is the second order leaching rate constant.

Elovich kinetics model:

The Elovich kinetic equation to identify the leaching rate is expressed as follows:

$$\frac{\Delta c}{\Delta t} = \alpha e^{(-\zeta c)} \tag{2.43}$$

Where, α (L mg^{-1}) and ζ (mg L^{-1} min^{-1}) are the initial and final leaching rate constant, respectively. Eq. (2.43) can be integrated with the help of boundary conditions, c=0 at t=0 and c=c at t=t. Eq. (2.44) results the integrated linearized form of Elovich kinetic model (Kitanovic et al., 2008; Oumarou et al., 2007).

$$c = \frac{1}{\alpha}\ln(\alpha\zeta) + \frac{1}{\alpha}\ln t \tag{2.44}$$

Determination of the rate of diffusion and the leaching efficiency:

The diffusion rate of the total polyphenols at the different solid content in 50 mL has been evaluated using various models such as the unsteady diffusion, the film theory, and the Ponomaryov empirical equation.

The unsteady diffusion model:

The mass transfer of polyphenols from the tea factory solid waste materials into the solution occurs via diffusion. This conventional process has been described theoretically using the unsteady diffusion model. To identify the unsteady diffusion rate and the diffusion coefficient this model has been applied according to experimental data. Mostly, the unsteady diffusion model was used during the leaching of bioactive components from plant species (Velickovic et al., 2006). Here, this model was used to fit experimental data for the identification of the diffusion rate of the instantaneous leaching of polyphenols without any chemical reaction by means of leaching coefficient.

$$\frac{c}{c_e} = (1 - a_0)e^{-k_3 t} \tag{2.45}$$

Where, k_3 (min^{-1}) and a_0 (L) were the unsteady diffusion rate constant and the model parameter, respectively (Velickovic et al., 2006).

The linearized form of Eq. (2.45) is as following:

$$\ln\left(\frac{c}{c_e}\right) = \ln(1-a_0) - k_3 t \tag{2.46}$$

The film theory model:

It is known that the diffusion of polyphenols occurs due to the variation of concentration into the water. This concentration profile is presented by Eq. (2.47).

$$\frac{c}{c_e} = 1-(1-a_1)e^{-k_4 t} \tag{2.47}$$

where, k_4 (min^{-1}) and a_1 were the film theory rate constant, and the model parameter, respectively (Velickovic et al., 2006).

Eq. (2.48) describes the linearized form of this model.

$$\ln\left(1-\frac{c}{c_e}\right) = \ln(1-a_1) - k_4 t \tag{2.48}$$

Ponomaryov empirical equation:

The leaching of any organic materials from plant cells can be categorized into two different stages, namely, the dissolution of soluble particles and the diffusion process. The later stage is slower than the first stage. The mechanism of slower diffusion can be analyzed using a mathematical model, like, the Ponomaryov theoretical model. The slower diffusion rate constant is determined from this theoretically based model which is described in Eq. (2.49)

$$1-\frac{c}{c_e} = a_2 + k_5 t \tag{2.49}$$

Where, k_5 (min^{-1}) and a_2 were the Ponomaryov empirical equation diffusion rate and model constant, respectively (Velickovic et al., 2006).

Analysis of leaching coefficient using different empirical models:

The leaching efficiency has been determined evaluating the values of leaching coefficient according to the experimental data using different empirical models namely, parabolic, power law, hyperbolic, Weibull's models.

Parabolic diffusion model:

Parabolic diffusion is fitted to the leaching data during the total polyphenols leaching from the tea factory solid waste. The efficiency of the instantaneously leaching of polyphenols is analyzed using this model by means of leaching or washing coefficient. Eq. (2.50) represents the parabolic diffusion model for the recovery of polyphenols from solid waste (Kitanovic et al., 2008).

$$\frac{c}{c_e} = a_3 + a_4 t^{0.5} \tag{2.50}$$

Where, a_3 and a_4 ($min^{-0.5}$) were the parabolic leaching or washing coefficient and the model constant, respectively.

Power law model:

The power law model can be used to identify the theoretical mechanisms of the diffusion efficiency of the organic compounds in the aqueous solvent. The distribution of polyphenols within the solid waste particles is considered homogeneous here. Eq. (2.51) describes the power law model for the polyphenols leaching (Kitanovic et al., 2008).

$$\frac{c}{c_e} = a_5 t^n \tag{2.51}$$

Where, a_5 (min^{-n}) was the parameters for the power law model and the leaching exponent, respectively (Kitanovic et al., 2008).

The linearized form of this model is as follows:

$$\ln\left(\frac{c}{c_e}\right) = \ln a_5 + n \ln t \tag{2.52}$$

Hyperbolic diffusion model:

The hyperbolic empirical law is used to identify the leaching coefficient of the total polyphenols from the tea factory solid waste. Eq. (2.53) presents the hyperbolic diffusion model for the polyphenols recovery.

$$\frac{c}{c_e} = \frac{a_6 t}{1 + a_7 t} \tag{2.53}$$

Where, a_6 (min^{-1}) and a_7 (min^{-1}) were the parameters for the hyperbolic diffusion model (Kitanovic et al., 2008).

Eq. (2.54) reveals the linearized form of the hyperbolic model.

$$\frac{c_e}{c} = \frac{1}{a_6 t} + \frac{a_7}{a_6} \tag{2.54}$$

Weibull's diffusion model:

Weibull's empirical diffusion model has been used to determine the slow leaching coefficient during recovery of total polyphenols from solid waste materials. This model can de describe that the diffusion of polyphenols occurs only towards the outer surface of solid particles.

$$\frac{c}{c_e} = 1 - e^{\left(-\frac{t^{a_8}}{a_9}\right)} \tag{2.55}$$

Where, a_8 (L) and a_9 ($\min^{a_8}$) were the parameters for the Weibull's diffusion model (Kitanovic et al., 2008).

Eq. (2.56) reveals the linearized form of the Weibull's model.

$$\ln\left[-\ln\left(1-\frac{c}{c_e}\right)\right]=-\ln a_9+a_8\ln t \tag{2.56}$$

2.4.4. Response surface methodology for optimal conditions:

The performance of the spinning basket module (SBM) has been finally optimized using the optimization tool, namely, response surface methodology (RSM). The face centered design has been studied to optimize the effective process parameters with a minimum number of experiments (Kushwaha et al., 2014). RSM uses experimental data which has been obtained from particular experimental design to determine the optimum conditions. Mainly, three major steps involve to identify the optimum result such as, (i) To perform the statistically designed experimentation, (ii) to estimate the coefficient in a mathematical model and analyzing the responses and (iii) to determine the adequacy of the significant model (Bose and Das, 2015).

The empirical equations for the response surface methodology:

The relationship between output variables (Y) and input factors (X_i) as follows:

$$Y=f(X_1,X_2,X_3,...,X_n) \tag{2.57}$$

The central composite design (CCD) has been applied to optimize the effective parameters for the ultrafiltration process with a minimum number of experiments (Kushwaha et al., 2014; Das et al., 2015). The CCD comprises 2^n factorial runs with $2n$ axial runs and one central run (n_c). For the reproducibility of the data, center points are used and verified. The following equation helps to design experimental data points.

$$N=2^n+2n+n_c \tag{2.58}$$

where N is the total number of runs.

An empirical-second degree polynomial equation has been used to correlate the responses with input factors as follows (Sahu et al., 2009, Kushwaha et al., 2014):

$$Y=\beta_0+\sum_{i=1}^{n}\beta_i X_j+\sum_{i=1}^{n}\beta_{ii}X_i^{\,2}+\sum_{i=1}^{n}\sum_{j>1}^{n}\beta_{ij}X_iX_j \tag{2.59}$$

Now, Y is the predicted response during experiments, X_i and X_j are independent variables like, various parameters, β_0 refers the constant coefficient, β_i signifies the linear coefficient, β_{ii} is the quadratic coefficient during optimization, and β_{ij} refers the interaction coefficient. To optimize all the independent input variables, Eq. (2.60) has been used through a desirability function (D_i) for three responses.

$$D_i = [\prod_{i=1}^{N} d_i^{r_i}]^{1/\sum r_i} \quad (2.60)$$

Where N is the number of responses during analysis, r_i signifies a particular response among all, d_i refers the partial desirability function for a specific response (Bose and Das, 2015).

Experimental design for alum coagulation study for pretreatment of tea factory waste water:

Response surface optimization technique has been adopted for the designing of the experiments during alum coagulation study for the pretreatment of tea industrial liquid effluent (**Table 2.3**). Four different parameters such as, alum dosage (A_1, 50-300 mg L^{-1}), pH (B_1, 4-10), stirring speed (C_1, 10.47-62.83 rad s^{-1}) and stirring time (D_1, 30-180 min) were considered as the input variables. The desired responses were Percentage removal of total dissolved solids (%, TDS), percentage removal of total suspended solids (%, TSS) and the turbidity (NTU) of the samples.

Table 2.3. Experimental design for the optimization study of alum coagulation process

Run No	Alum dosage (mg L^{-1})	Initial pH	Stirring speed (rad s^{-1})	Stirring time (min)	TSS removal (%)	TDS removal (%)	Turbidity (NTU)
1	175.00	7.00	36.65	105.00	91.2	75	1.19
2	175.00	7.00	36.65	30.00	75	67	1.8
3	300.00	4.00	62.83	180.00	73.44	65	2.8
4	300.00	4.00	62.83	30.00	74.25	63.5	2.55
5	300.00	7.00	36.65	105.00	79.1	70	2.55
6	50.00	10.00	10.47	180.00	58	40	2.95
7	50.00	4.00	62.83	30.00	61.54	45	2.75
8	50.00	4.00	62.83	180.00	63	35	3.05
9	300.00	4.00	10.47	30.00	70.2	62	2.35
10	300.00	4.00	10.47	180.00	77.05	68	2.2
11	175.00	10.00	36.65	105.00	80	62.5	1.23
12	175.00	7.00	36.65	105.00	87.03	76.24	1.1
13	50.00	10.00	62.83	180.00	61.22	33	3.2
14	50.00	7.00	36.65	105.00	67.55	48	2.65
15	300.00	10.00	10.47	30.00	67.5	57.5	2.6
16	175.00	7.00	36.65	180.00	82	75	1.02
17	300.00	10.00	10.47	180.00	72	55	2.25
18	50.00	10.00	62.83	30.00	55	42	3.1
19	175.00	7.00	36.65	105.00	88	73.25	0.84
20	175.00	7.00	10.47	105.00	84.5	73.5	1.5
21	300.00	10.00	62.83	30.00	71.35	60.5	2.75
22	175.00	7.00	36.65	105.00	90.05	77.11	1.02
23	175.00	7.00	36.65	105.00	89.14	76.11	0.5
24	50.00	10.00	10.47	30.00	53	40	2.8
25	175.00	4.00	36.65	105.00	85.5	66	1.48
26	300.00	10.00	62.83	180.00	72	59	2.98
27	50.00	4.00	10.47	180.00	65	42	2.9
28	50.00	4.00	10.47	30.00	58	47	2.4
29	175.00	7.00	62.83	105.00	76	72.1	1.3
30	175.00	7.00	36.65	105.00	87.25	74.21	0.9

Experimental design to optimize the process parameters during treatment of paper industrial effluents:

It is necessary to optimize the process parametric conditions during raw effluent treatment using the spinning basket membrane ultrafiltration.

Design expert software (response surface methodology) 8.0.7.1 was used for the present study. Initially, three parameters, like, TMP drop (A_2: kPa), rotational speed (B_2: rpm) and retentate flow rate (C_2: L min^{-1}) have been considered as input variables based on the previous experiments on the spinning basket module (SBM), whereas, permeate flux (R_1: L m^{-2} h^{-1}), % removal of TDS (R_2: %), and ionic conductivity of collected permeate (R_3: S m^{-1}) were dependent variables. Three inputs were chosen based on our previous work on the spinning basket membrane module.

According to design expert software, the maximum (+) and the minimum (-) level of three parameters, like, TMP drop (kPa), rotational speeds (rad s^{-1}, rpm), and retentate flow rate (L min^{-1}) were 207 and 414 kPa; 100 (10.47 rad s^{-1}) and 700 (73.30 rad s^{-1}) rpm; 1 and 4 L min^{-1}, respectively. Whereas, the molecular cutoff (MWCO) of 50 kDa was fixed during the process optimization study. **Table 2.4** delivers the design of the experiment for the optimization, and the values of the responses. All the experiments were performed according to the statistical design made by the design expert software itself. To optimize all the independent input variables, Eq. (2.60) has been studied through a desirability function (D_i) for three responses using design expert software. A similar observation can be initiated using MWCO membranes, like, 5, 10, 30 kDa.

Table 2.4. Experimental design for optimization of process parameters during treatment of paper industrial effluents

Run No	Factor 1 A_2: TMP drop (kPa)	Factor 2 B_2: Rotational speed (rpm)	Factor 3 C_2: Retentate flow rate (L min^{-1})	Response 1 Permeate flux (L m^{-2} h^{-1})	Response 2 Ionic conductivity (S m^{-1})	Response 3 % removal of TDS
1	414	100	4	52.25	2.1	95
2	310.5	400	2.5	70	0.75	97.5
3	310.5	400	2.5	70	0.75	97.5
4	310.5	400	2.5	70	0.75	97.5
5	207	700	1	58.68	2.0	95.2
6	207	400	2.5	47.35	1.65	95.9
7	207	100	1	36.9	2.4	94
8	310.5	400	1	64.85	1.05	96.65
9	414	700	1	98.85	1.8	95.5
10	310.5	700	2.5	93.31	0.7	97.5
11	414	400	2.5	74.24	0.81	97.2
12	310.5	400	2.5	70	0.75	97.5
13	310.5	400	4	84.23	0.77	97.4
14	310.5	100	2.5	52	1.7	95.8
15	310.5	400	2.5	70	0.75	97.5
16	414	700	4	106.24	0.65	98
17	207	700	4	65.55	1.04	96.8
18	310.5	400	2.5	70	0.75	97.5
19	414	100	1	49.49	2.2	94.7
20	207	100	4	40.5	2.3	94.5

Experimental strategy and statistical investigation to optimize the process parameters for the leaching of polyphenols:

To optimize the leaching parameters, response surface methodology was applied in the present study. According to central composite design (CCD), the faced centered model has been used to optimize the effective leaching parameters with a minimum number of trials (Das et al., 2015). Three process parameters, such as the solid content (g), temperature ($^{\circ}$C) and leaching time (min) have been considered as the input variables. The total polyphenols (mg L^{-1} GAE equivalent) has been chosen as the output response. Design expert software 7.0.1 was used to perform the central composite design. The maximum (+1) and minimum range (-1) of three inputs viz., the solid content (A_3), temperature (B_3) and leaching time (C_3) were 1 and 3 g, 30 and 90°C, 10 and 90 min, respectively. The experiments were

performed according to the statistical design made by the software itself. **Table 2.5** describes the design of the experiment and the values of the responses.

Table 2.5. Experimental design to optimize the total polyphenols leaching

Run No	Factor 1 A_3: Solid weight (g)	Factor 2 B_3: Time (min)	Factor 3 C_3: Temp (˚C)	Response 1 Total polyphenols (mg L^{-1} GAE)
1	1	10	30	254.17
2	3	10	30	586.67
3	1	90	30	435.83
4	3	90	30	795.00
5	1	10	90	310.00
6	3	10	90	560.00
7	1	90	90	585.83
8	3	90	90	1050.00
9	1	50	60	675.00
10	3	50	60	1100.00
11	2	10	60	625.00
12	2	90	60	1166.67
13	2	50	30	772.50
14	2	50	90	1058.33
15	2	50	60	1183.33
16	2	50	60	1225.00
17	2	50	60	1191.67
18	2	50	60	1358.33
19	2	50	60	1216.67
20	2	50	60	1241.67

2.4.5. Artificial neural network design:

An artificial neural network (ANN) is nothing but a theoretical prediction made by a computational approach. This theoretical model performs, like, the real performance of human brain neurons.

Some interconnected signaling elements help to continue the evaluation process. The nature of the flux decline behavior during tea factory wastewater treatment has been analyzed using ANN with experimental data.

Valuable information is released to the external elements through the process elements by the help of the own dynamic state responses. ANN are the combination of multiple nodes. The combined nodes interact with each other to identify the accurate outcomes (Das et al.,

2015; Baguena et al., 2016). To understand the relationship between theoretical and experimental data, two layered feed-forward Levenberg-Marquardt algorithm was studied. To predict the experimental data from the predicted points between independent and dependent parameters, an artificial neural network was applied during leaching of total polyphenols from tea factory solid wastes. Solid content (g) in water, time (min), and temperature ($^{\circ}$C) were put in the input layer of neural network system. Total polyphenols (mg L^{-1} GAE) was put in the output layer.

The experimental data was obtained from the **Table 2.5**. The number of hidden neurons were 10. The all experimental points were divided into the following stages: training: 19, validation: 9 and testing: 9 points. Root mean square errors (RMSE) were calculated to predict the highest regression coefficient (R^2) using MATLABR2015b (licensed version, Indian Institute of Guwahati, India) neural network toolbox (Das et al., 2017).

References:

A. B. Das, V. V. Goud, C. Das, Extraction of phenolic compounds and anthocyanin from black and purple rice bran (*Oryza sativa* L.) using ultrasound: A comparative analysis and phytochemical profiling, Ind. Crop. Prod. 95 (2017) 332-341.

A. Das, A. K. Golder, C. Das, Enhanced extraction of rebaudioside-A: Experimental, response surface optimization and prediction using artificial neural network, Ind. Crop. Prod. 65 (2015) 415-421.

A. Sarkar, D. Sarkar, M. Gupta, C. Bhattacharjee, Recovery of Polyvinyl Alcohol from Desizing Wastewater Using a Novel High-Shear Ultrafiltration Module, Clean – Soil, Air, Water 40 (2012) 830-837.

A. Das, D. Paul, A. K. Golder, C. Das, Separation of Rebaudioside-A from stevia extract: Membrane selection, assessment of permeate quality and fouling behavior in laminar flow regime, Sep. Purif. Technol. 144 (2015) 8-15.

C. Das, P. Patel, S. De, S. DasGupta, Treatment of Tanning effluent using nanofiltration followed by reverse osmosis, Sep. Purif. Technol. 50 (2006) 291-299.

D. T. Velickovic, D. M. Milenovic, M. S. Ristic, V. B. Veljkovic, Kinetics of ultrasonic extraction of extractive substances from garden (*Salvia officinalis* L.) and glutinous (*Salvia glutinosa* L.) sage, Ultrason. Sonochemist. 13 (2006) 150-156.

D. Kushwaha, S. Saha, S. Dutta, Enhanced Biomass Recovery During Phycoremediation of Cr(VI) Using Cyanobacteria and Prospect of Biofuel Production, Ind. Eng. Chem. Res. 53 (2014) 19754-19764.

D. Sarkar, A. Sarkar, A. Roy, C. Bhattacharjee, Performance characterization and design evaluation of spinning basket membrane(SBM) module using computational fluid dynamics (CFD), Sep. Purif. Technol. 94 (2012) 23-33.

E. M. Goslan, S. W. Krasner, M. Bower, S. A. Rocks, P. Holmes, L. S. Levy, S. A. Parsons, A comparison of disinfection by-products found in chlorinated and chloraminated drinking waters in Scotland, Water Res. (2009) 4698-4706.

H. A. H. Oumarou, H. Fauduet, C. Porte, Y. S. Ho, Comparison of Kinetic Models for the Aqueous Solid-Liquid Extraction ofTiliaSapwood in a Continuous Stirred Tank Reactor, Chem. Eng. Comm. 194 (2007) 537-552.

J. Zhishen, T. Mengcheng, W. Jianming, The determination of flavonoid contents in mulberry and their scavenging effects on superoxide radicals, Food Chem. 64 (1999) 555-559.

J. Li, R. D. Sanderson, E. P. Jacobs, Ultrasonic cleaning of nylon microfiltration membranes fouled by Kraft paper mill effluent, J. Membr. Sci. 205 (2002) 247–257.

J. N. Sahu, J. Acharya, B. C. Meikap, Response Surface Modeling and Optimization of Chromium (VI) Removal from Aqueous Solution using Tamarind Wood Activated Carbon in Batch Process, J. Hazard. Mater. 172 (2009) 818-825.

L. M. J. Facundo, J. A. M. Roca, B. C. Uribe, S. A. Blanco, Ultrasonic cleaning of ultrafiltration membranes fouled with BSA solution, Sep. Purif. Technol. 120 (2013) 275-281.

M. C. V. Vela, S. A. Blanco, J. L. Garcia, E. B. Rodriguez, Analysis of membrane pore blocking models applied to the ultrafiltration of PEG, Sep. Purif. Technol. 62 (2008) 489-498.

M. Frappart, M. Jaffrin, L. H. Ding, Reverse osmosis of diluted skim milk: Comparison of results obtained from vibratory and rotating disk modules, Sep. Purif. Technol. 60 (2008) 321–329.

M. R. Rover, R. C. Brown, Quantification of total phenols in bio-oil using the Folin–Ciocalteu Method, J. Anal. Appl. Pyrol. 104 (2013) 366-371.

M. J. C. Baguena, M. C. V. Vela, J. M. G. Zafrilla, S. A. Blanco, J. L. Garcia, D. C. Martinez, Comparison between artificial neural networks and Hermia's models to assess ultrafiltration performance, Sep. Purif. Technol. 170 (2016) 434-444.

N. Li, L. S. Taylor, M. G. Ferruzzi, L. J. Mauer, Kinetic Study of Catechin Stability: Effects of pH, Concentration, and Temperature, J. Agric. Food Chem. 60 (2012) 12531-12539.

P. Sharma, M. Ramchiary, D. Samyor, A. B. Das, Study on the phytochemical properties of pineapple fruit leather processed by extrusion cooking, LWT-Food Sci. Technol. 72 (2016) 534-543.

R. V. S. S. Gottumukkala, N. Nadimpalli, K. Sukala, G. V. Subbaraju, Determination of Catechin and Epicatechin Content in Chocolates by High-Performance Liquid Chromatography, Inter. Scholar. Res. Notice. 2014 (2014) 1-5.

S. Muthukumaran, K. Yang, A. Seuren, S. Kentish, M. Ashokkumar, G. W. Stevens, F. Grieser, The use of ultrasonic cleaning for ultrafiltration membranes in the dairy industry, Sep. Purif. Technol. 39 (2004) 99–107.

S. Muthukumaran, S. Kentish, S. Lalchandani, M. Ashokkumar, R. Mawson, G. W. Stevens, F. Grieser, The optimisation of ultrasonic cleaning procedures for dairy fouled ultrafiltration membranes, Ultrasonics Sonochem. 12 (2005) 29-35.

S. Kitanovic, D. Milenovic, V. B. Veljkovic, Empirical kinetic models for the resinoid extraction from aerial parts of St. John's wort (*Hypericum perforatum* L.), Biochem. Eng. J. 41 (2008) 1-11.

S. Banerjee, S. De, An analytical solution of Sherwood number in a stirred continuous cell during steady state ultrafiltration, J. Mem. Sci. 389 (2012) 188-196.

S. De, Novel Separation Processes (Web) Module 3: Membrane Based Separation Processes. National program on technology enhanced learning (NPTEL), 2012, pp. 30–120 (http://nptel.ac.in/courses/103105060/Sde_pdf/Module-3.pdf) accessed on 13.03.18.

S. Bose, C. Das, Role of Binder and Preparation Pressure in Tubular Ceramic Membrane Processing: Design and Optimization Study Using Response Surface Methodology (RSM), Ind. Eng. Chem. Res. 53 (2014): 12319-12329.

S. Karadirek, N. Kanmaz, Z. Balta, P. Demircivi, A. Uzer, J. Hizal, R. Apak, Determination of total antioxidant capacity of humic acids using CUPRAC, Folin–Ciocalteu, noble metal nanoparticle- and solid–liquid extraction-based methods, Talanta 153 (2016) 120-129.

R. W. Field, D. Wu, J. A. Howell, B. B. Gupta, Critical flux concept for microfiltration fouling, J. Membr. Sci. 100 (1995) 259-272.

R. W. Field, J. J. Wu, Modelling of permeability loss in membrane filtration: Re-examination of fundamental fouling equations and their link to critical flux, Desalination. 283 (2011) 68-74.

V. B. Briao, C. R. G. Tavares, Pore blocking mechanism for the recovery of milk solids from dairy wastewater by ultrafiltration, Braz. J. Chem. Eng. 29 (2012): 393-407.

V. Singh, P. K. Jain, C. Das, Performance of spiral wound ultrafiltration membrane module for with and without permeate recycle: Experimental and theoretical consideration, Desalination 322 (2013) 94-103.

V. Singh, C. Das, Comparison of spiral wound UF membrane performance between turbulent and laminar flow regimes, Desalination 337 (2014) 43-51.

CHAPTER 3

SPINNING BASKET MEMBRANE ULTRAFILTRATION OF HUMIC ACIDS AQUEOUS SOLUTION AND COMPARISON WITH UNSTIRRED BATCH CELL

In this chapter, an unstirred batch ultrafiltration was carried out for the treatment of Humic acids synthetic solution to identify the fouling characteristics. In another study, the performance characteristics of the spinning basket membrane module towards Humic acids ultrafiltration was studied with different membrane basket rotations to minimize the concentration polarization during the ultrafiltration process. Due to the very less study about the treatment of natural organic components using dynamic membrane modules, the spinning basket membrane module was selected for the ultrafiltration of Humic acids solution. Regarding the investigation of internal fouling for this module, modified Hermia's pore-blocking mechanisms were analyzed successfully. About the cleaning process, the membrane module back rotation and the application of ultrasonication have been presented with the fruitful productivities.

The work presented in this chapter is published in the following journals.

***Suman Saha**, Chandan Das, 2018. A lab-scale spinning basket membrane module for the assessment of Humic acids ultrafiltration with effect of sonication on membrane fouling, **Chem. Eng. Comm.** 205: 1457-1498.*

***Suman Saha**, Chandan Das, 2017. Purification of Humic acids contained simulated wastewater using membrane ultrafiltration. **European Water** 58: 33-40.*

***Suman Saha**, Chandan Das, 2015. Analysis of fouling characteristics and flux decline during Humic acids batch ultrafiltration. **J. Chem. Eng. Process Technol.** 6: 252-258.*

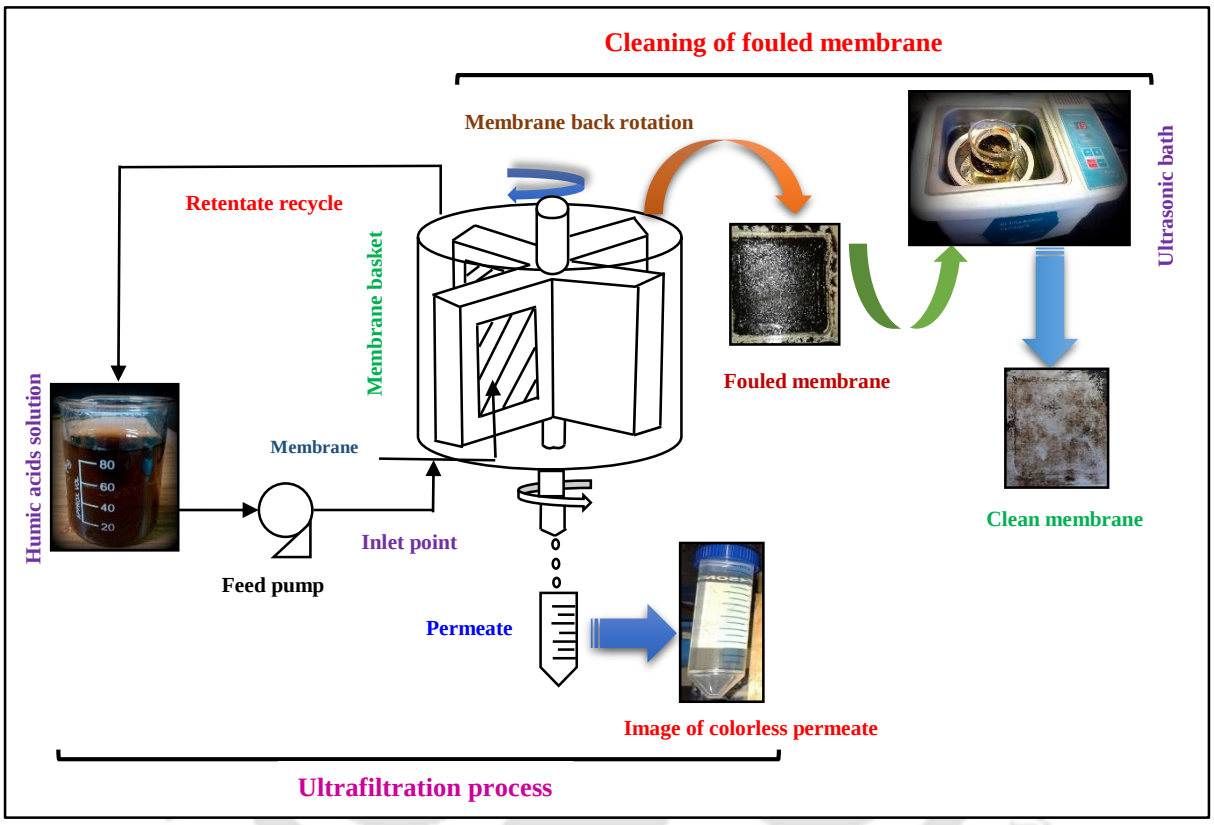

Schematic of lab-scale spinning basket membrane module for the assessment of Humic acids ultrafiltration with effect of sonication on membrane fouling

3.1. Spinning basket membrane ultrafiltration of Humic acids:

The performance characteristic of the spinning basket membrane module during Humic acids ultrafiltration has been studied and discussed at great length. The flux decline behavior was analyzed and compared with an unstirred batch cell module at different operating conditions, such as, applied TMP drops, and initial feed concentration. The process parameters optimization study using response surface methodology has been represented in the next chapter. Here, the effects of different membrane basket rotations, cleaning of fouled membrane, and the power consumption were studied and reported.

3.2. Results and discussion:

3.2.1. Transient flux decline for unstirred batch cell membrane module (U.S.B.M.M.):

Fig. 3.1 displays the variation of Humic acids permeate flux with time at different TMP drops, such as, 207 to 414 kPa in a dead end unstirred filtration set up. The Humic acids permeate flux declines sharply within the 10 min of ultrafiltration process time. Due to an increase in driving force, the flux decline rises with rising TMP drops. For example, it can be observed from **Fig. 3.1** that the variation of flux decline is maximum at 414 kPa pressure. As the TMP drop increases, the deposition of rejected molecules on the membrane surface is increased resulting a faster growth of the concentration boundary layer near the effective membrane surface (Das et al., 2006). This behavior leads to decline the Humic acids permeate flux and gives higher steady flux value.

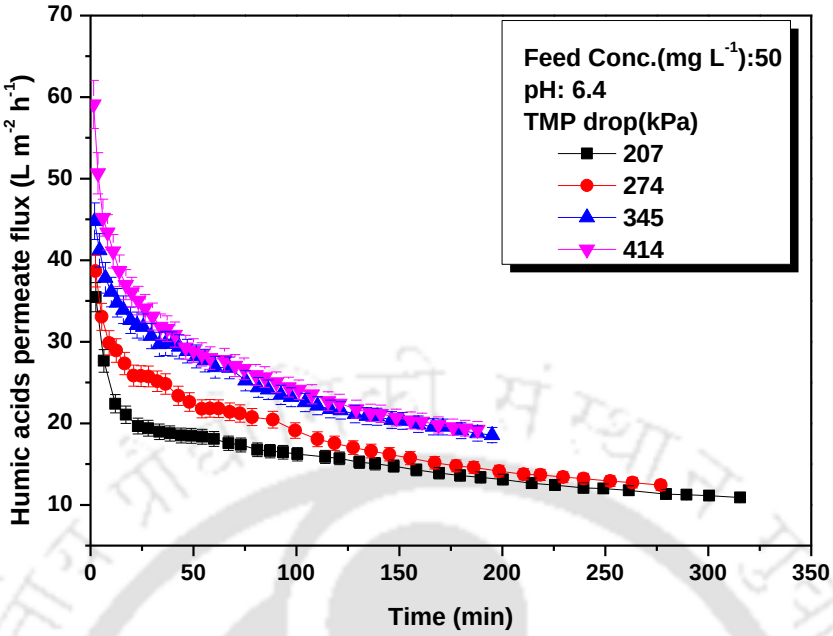

Fig. 3.1. Comparison of permeate flux with respect to time at different operating pressures condition during batch cell operation

Theoretical analysis of permeate flux decline with respect to time and transmembrane pressure drop (ΔP, kPa):

The theoretical approach of the flux decline using artificial neural network (ANN) analysis with respect to time has been shown in the **Fig. 3.2** for the different TMP drops (207, 276, 345 kPa). The comparative study between theoretical and experimental flux decline for the different TMP drops has been analyzed here. The similar kind of observation, like, TMP drop of 345 kPa has been noticed for the TMP drop of 414 kPa during analysis. To analyze the best fitting prediction using an artificial neural network (ANN) model, statistical analysis has been studied with the experimental data point for various TMP drops. The filtration time (min) was taken in the input layer for training. Output layer was the permeate flux (L m^{-2} h^{-1}) for the prediction which was compared with the experimental data. **Table 3.1** presents statistical analysis of variance (ANOVA) for theoretical flux decline behavior during batch ultrafiltration of Humic acids solution. The statistical data describes the error calculation and a significant difference between the experimental and theoretical flux decline for Humic acids ultrafiltration. From the **Table 3.1**, it is clear that the comparative study is significant with 0.99 regression (R^2) for all the TMP

drops. **Figs. 3.3 (a)-(c)** delivers the prediction of theoretical and experimental flux decline behavior using artificial neural network (ANN) for various TMP drops condition. It is observed that all the points are very close to the diagonal line significantly with perfect regression values for all the cases. The high F-value, and low p-value delivers the good model prediction towards the theoretical analysis of Humic acids permeate flux decline (Baguena et al., 2016). At the low TMP drop of 207 kPa, a minimum mean square error of 0.71 is observed than other TMP drops.

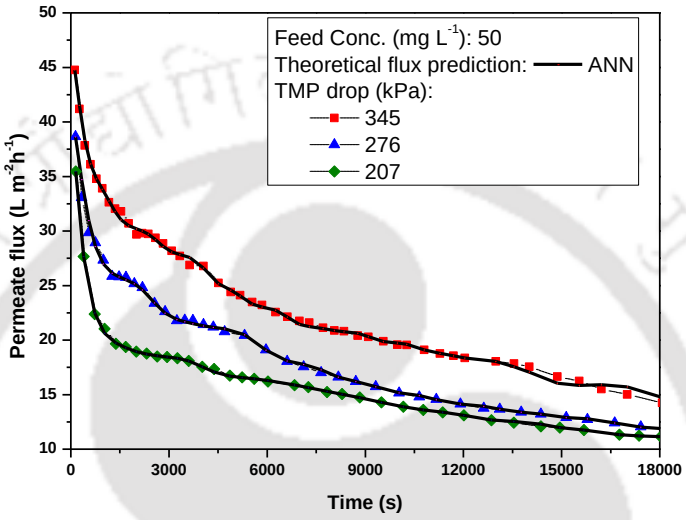

Fig. 3.2. Experimental and ANN predicted transient flux decline behavior with respect to process time for different TMP drops (ΔP , kPa)

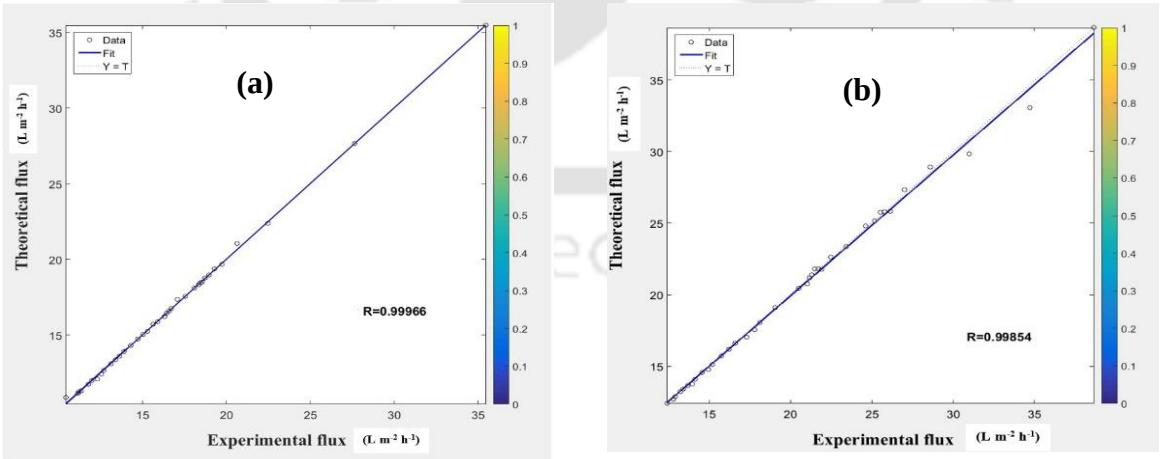

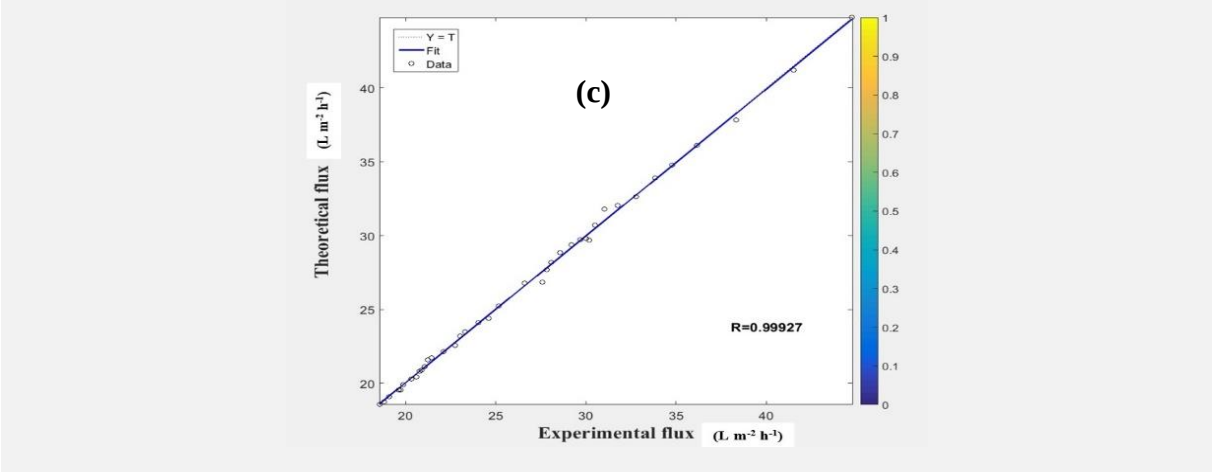

Fig. 3.3. The prediction of theoretical and experimental flux values using ANN analysis at different TMP drops **(a)** 207, **(b)** 276, and **(c)** 345 kPa

Table 3.1. Analysis of variance for theoretical permeate flux at different ΔP, (kPa)

Source ΔP,(kPa)	Sum of square	Degrees of freedom	Mean square error	F-value	p-value	Total error	Regression R^2
207	36.65	52	0.71	4.41	0.0001	8.47	0.99
276	506.63	52	9.74	375.38	0.0001	1.38	0.99
345	1091.34	52	20.98	216	0.0001	5.13	0.99

Effect of feed concentration on permeate flux:

Initial feed concentration of pure Humic acids (HAs) solution was varied as 50, 150 and 250 mg L^{-1} at various transmembrane pressure drops (TMP) conditions (207 and 414 kPa). It is obviously seen from **Figs. 3.4 (a)** and **(b)** that, with rising initial Humic acids (HAs) concentration, permeate flux decreases. One exciting behavior has been witnessed in **Fig. 3.4 (a)** that, with rising feed concentration from 50 to 150 mg L^{-1}, the permeate flux decline is almost equal for the first 50 min. At a low transmembrane pressure (TMP) drop (207 kPa), rejected molecules deposition, near the membrane active surface is very slow initially. Due to the dead end ultrafiltration process, the concentration of rejected particles just nearby the membrane active surface increases gradually, which produces lower permeate flux at the concentration of 150 mg L^{-1} than the concentration of 50 mg L^{-1} after 50 min of ultrafiltration. When the Humic acids feed concentration is maximum of 250 mg L^{-1} (high concentration during the present study), the permeate flux is very lower than other

conditions. The higher feed concentration creates film or gel or cake layer very fast due to the higher retention of Humic acids components. The gel layer becomes thicker one with the process time which gives lower Humic acids (HAs) permeate flux than other conditions, like, 50 and 150 mg L^{-1} feed concentrations. While, the permeate flux decreases quickly for all conditions in the first 25 min for a high TMP drop of 414 kPa. The formation of gel layer is responsible for the rapid decrease in permeate flux. Humic acids (HAs) molecules deposit very fast on the membrane active surface and block the active pores in a short time. As a result, permeate flux decreases with rising initial feed concentration, and reaches its saturated value faster than the lower TPM drop at 207 kPa.

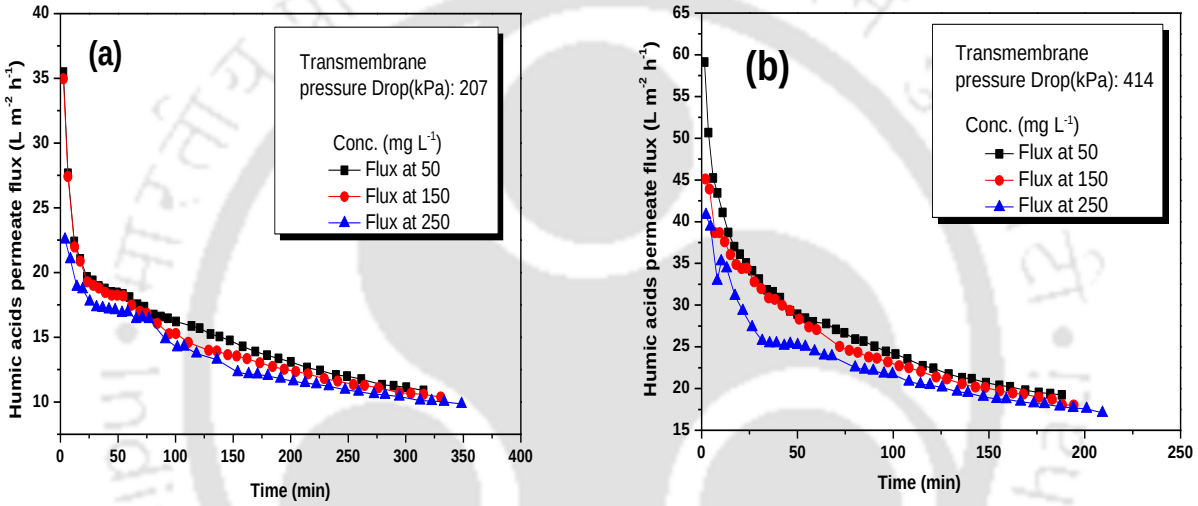

Fig. 3.4. Variation of Humic acids permeate flux at different feed concentration with respect to time at **(a)** 207 and **(b)** 414 kPa TMP drops

3.2.2. Humic acids permeate flux variation with respect to time for shear-enhanced membrane ultrafiltration:

The variation of Humic acids permeate flux at the different initial HAs solution of 50, 150 and 250 mgL^{-1} with 300 rpm (31.41 rad s^{-1}) basket rotation is shown in **Fig. 3.5**. Here, the transient flux displays an initial gradual decay during the process time at a low TMP (207 kPa) drop. Similarly, at a changing of Humic acids concentration, from lower to higher, permeate flux has also been decreased for the same TMP drop of 207 kPa because of the deposition of rejected Humic substances on the effective membrane surfaces. The increase of the effective thickness of the polarized film of the rejected particles on the effective

membrane surface with the increasing TMP drop has been restricted with the help of membrane basket rotation.

In literature, it is clearly observed that above 33% permeate flux has been declined within 50 min after using a vibratory shear-induced membrane ultrafiltration with a high membrane active surface area of 0.05 m^2 to remove natural organic matters from surface water at a high TMP drop of 1000 kPa and high energetic consideration (Petala and Zouboulis, 2006). Whereas, due to the membrane basket rotation, the decline of permeate flux has been restricted within 16% after 100 min. Not only that, a very low permeate flux value with the large membrane effective area of 1.9×10^{-2} m^2 has been reported during high shear skim milk rotating disk ultrafiltration earlier.

Authors have reported near about 30 L m^{-2} h^{-1} or 8.33×10^{-6} m s^{-1} permeate flux was found with a high smooth disk rotation of 300 rpm at 600 kPa TMP drop (Ding et al., 2003). Whereas, for the same rotational speed during this present study, permeate flux value was much higher (67.79 L m^{-2} h^{-1}) than the other modules, like, rotating disk module. Due to the vortex-like circulation between the membrane steel plate and the cylindrical case, the accumulated solutes are easily swept away from the effective membrane surfaces during ultrafiltration (Sarkar et al., 2012). For this reason, the permeate flux decline has been observed very less than rotating disk filtration. Membrane internal pore blocking during filtration is the main reason for initial and average permeate flux decline.

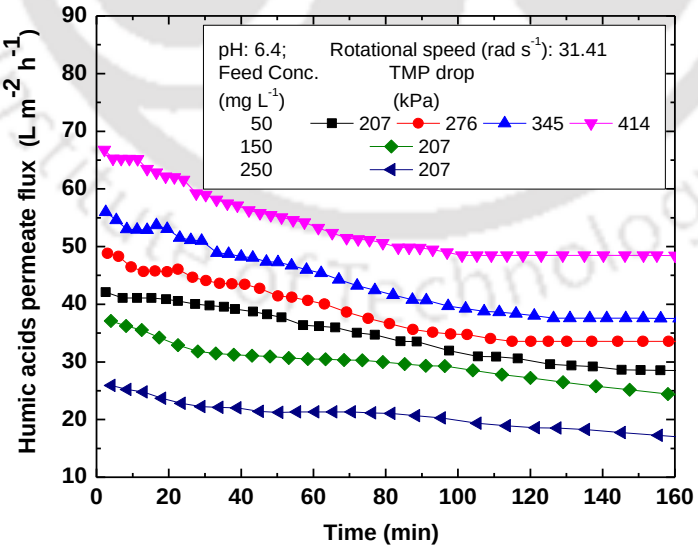

Fig. 3.5. Permeate flux variation with respect to time at various initial feed conditions and TMP drops with fixed rotational speed of 300 rpm (31.41 rad s^{-1})

Effects of rotational speed during separation of Humic acids using SBMM:

For the minimization of the cake layer development during membrane separation, the present filtration work was performed at different rotational speeds (ω, rad s^{-1}). The effects of different rotational speeds (10.47, 20.93, 52.36, and 73.30 rad s^{-1}) on permeate flux have been shown in **Figs. 3.6 (a)-(d)**. The increase of the rotational speed from 10.47 to 20.93 rad s^{-1}, has given the gradual increase of Humic acids permeate flux, while this value raised further increasing of ω at 73.3 rad s^{-1}. It was found that the permeate flux varied with rotational speed. With increasing basket rotation, permeate flux is increased for all the cases as similar as the variation of TMP drop. With the influence of rotation of the membrane basket, the rate of generation of turbulence is raised during ultrafiltration which helps to increase the permeate flux significantly (Sarkar et al., 2012). The deposition rate of rejected molecules on the membrane effective surfaces is very marginal and slow due to the membrane basket created turbulence and shear force. Thus, a higher permeate flux has been observed with the increase of rotation of the membrane basket. High rotation also boosts the permeation of solvent to diminish the mass transfer resistance of polarized film of rejected Humic acids molecules. With continuous rotation of the membrane basket at high speed of 700 rpm, some solute particles are broken down and create small particles in size resulting a severe decline of permeate flux due to internal pore blocking.

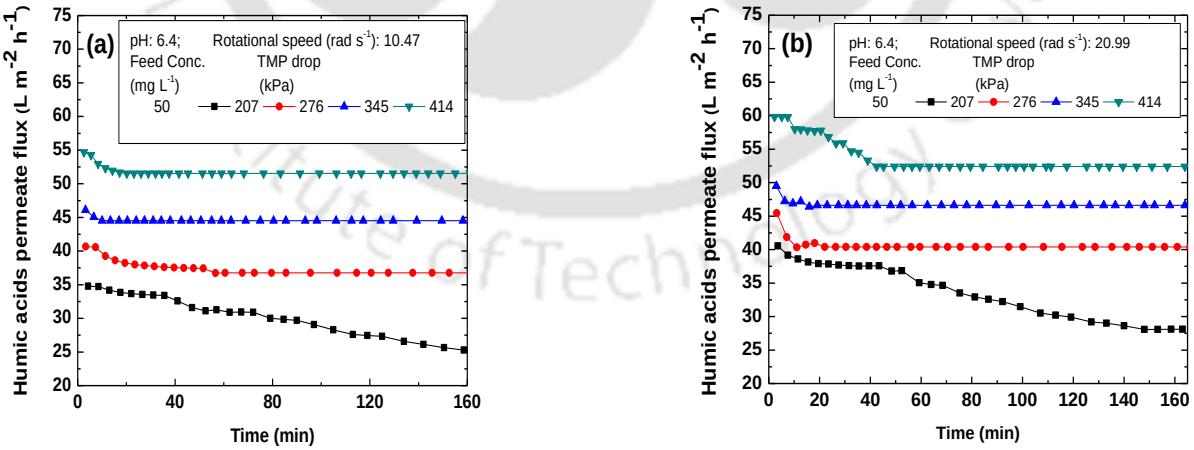

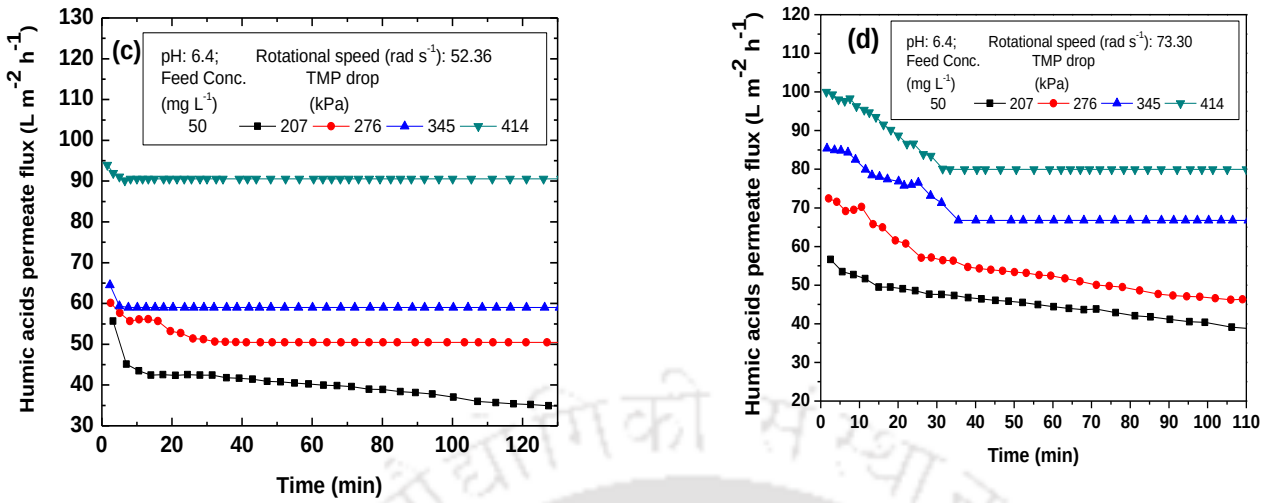

Fig. 3.6. Variation of permeate flux with respect to time at different operating pressures condition with different rotational speeds at **(a)**10.47, **(b)**20.93, **(c)**52.36, and **(d)**73.30 rad s^{-1}.

3.2.3. Variation of observed rejection at different TMP drops during U.S.B.C.M ultrafiltration of Humic acids solution:

The variation of the permeate quality in terms of rejection of Humic acids (HAs) molecules with various TMP drops at different initial feed concentrations is displayed in **Fig. 3.7**. It is evidently observed that with the rising of TMP drops, the quality of permeate in terms of molecules rejection progresses for all the initial feed concentrations. For example, at 50 mg L^{-1} (low feed concentration), with the rising in the TMP drop from 207 to 414 kPa, solute retention also rises from 92.1 to 94.2%. Now, during the concentration of 150 and 250 mg L^{-1}, the rejection results are 91.5 to 95% and 91.3 to 96%, respectively. This can be delivered in terms of the generation of cake layer or gel layer due to concentration polarization during ultrafiltration. At a raised TMP drop, rejected molecules form a polarized film layer which produces extra mass transfer resistance. This resistance behaves like a secondary membrane in a series with the actual membrane (Das et al., 2006). This interesting behavior gives significantly high rejection at high TMP drop, like, 345 and 414 kPa. At a fixed pressure drop of 207 kPa with increasing initial Humic acids (HAs) concentration, rejection reduces. This reverse phenomenon has been happened due to the lower compaction of a gel or cake layer made of rejected solutes which cannot retain small solute particles in size at the high concentration of 150 and 250 mg L^{-1} firstly. As the TMP

drop increases, the formed gel layer also becomes compacted which helps for more rejection of Humic acids molecules.

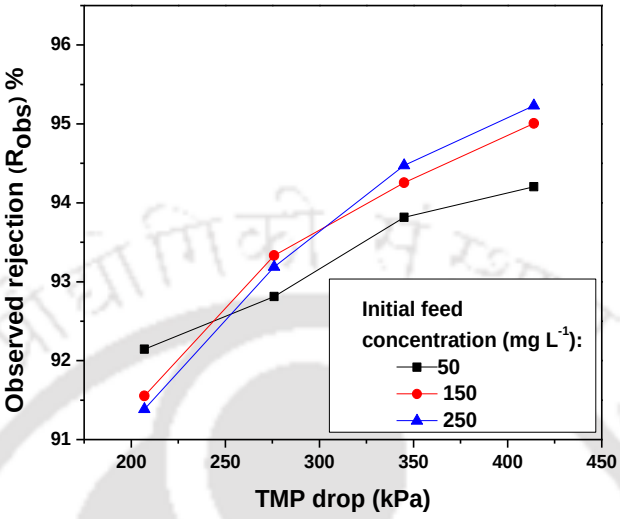

Fig. 3.7. Variation of observed rejection with different TMP drops during Humic acids dead end ultrafiltration

3.2.4. Variation of observed rejection in the presence of rotational speed during SBMM ultrafiltration of HAs solution:

In **Fig. 3.8**, it is found that with the increasing applied pressure drop at a fixed ω, HAs solute particles rejection improves for all the parametric conditions. For example, at 10.47, 20.93, 31.41, 52.36, and 73.30 rad s^{-1} rotational speed, from lower to higher (207 to 414 kPa) TMP drop, rejection of solutes was increased from 92.50 to 95.03, 93 to 95.56, 93.8 to 96, 93.2 to 95.3 and 92.7 to 94.5%, respectively. The rejection of natural organic components, like, Humic acids was already found near about 80% to 92% varying MWCO from 30 to 100 kDa during vibratory shear-induced ultrafiltration at a high pressure of 10 bar or 10^3 kPa. It revealed that the lower fraction of Humic acids molecules was not rejected by the membranes (Petala and Zouboulis, 2006). Whereas, in the present study, with 414 kPa TMP drop above 96% rejection has been experimented. For each TMP drop, solute rejection increases with increasing ω at first then decreases. At a fixed TMP drop of 207 kPa after changing ω from 10.47 to 31.41 rad s^{-1}, solute rejection increases from 92.5 to 93.8%, then decreases to 92.7% when the ω is 73.3 rad s^{-1}. During the continuous rotation

at high speed, some solutes may collide with each other and create small particles in size. At high applied TMP drop, small solute particles can easily appear on the permeate side and give lower rejection suddenly. However, the decrease in solute rejection at the high ω of 52.36 and 73.3 rad s^{-1} was very marginal. As a result, it can be said that the rotational speed has a significant impact on Humic acids rejection during the spinning basket ultrafiltration.

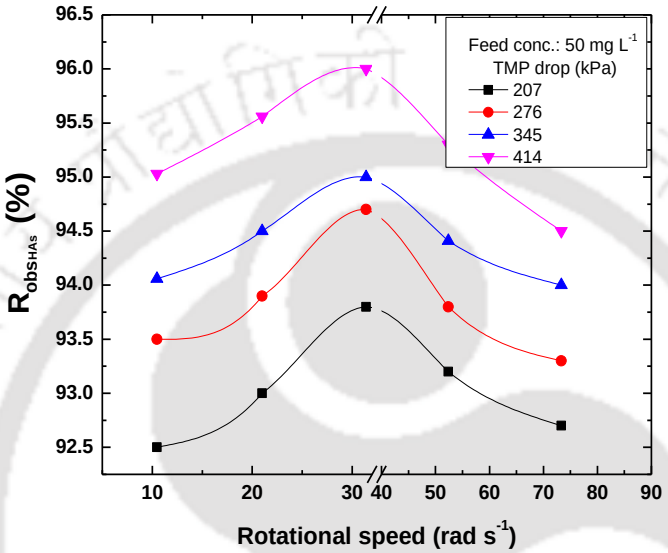

Fig. 3.8. Variation of observed rejection in presence of rotational speed during SBMM ultrafiltration of HAs solution

3.2.5. Variation of VRF with time for unstirred batch cell and spinning basket membrane operation:

The variation of VRF with operating time at different transmembrane pressure (TMP) drops (207, 276, 345, 414 kPa) for batch cell and spinning basket membrane operation have been shown in **Figs. 3.9 (a)** and **(b)**, respectively. Raising of VRF has an important impact on membrane permeation. It has a significant character over membrane performance (Singh et al., 2013). With the increased driving force, permeate rate is boosted producing VRF to raise. During the unstirred batch filtration **(Fig. 3.9 (a))**, a severe alteration in VRF has been observed. At 207 kPa, VRF value is approximately 3.5 which is raised up to 4.5 for the high TMP drop of 414 kPa. An almost similar trend has been found for the TMP drop of 345 and 414 kPa which indicates the comparable effects on membrane performances for both the TMP drops. Whereas, a gradual raising profile of VRF with filtration time has

been noticed in the **Fig. 3.9 (b)**. In the presence of basket rotation, deposition of retained particles on the membrane surfaces has been controlled resulting a long time membrane performance. **Fig. 3.9 (c)** describes the behavior of VRF profile with process time at different membrane basket rotations, like, 10.47, 20.93, 31.41, 52.36, and 73.30 rad s^{-1} at a fixed TMP drop of 414 kPa.

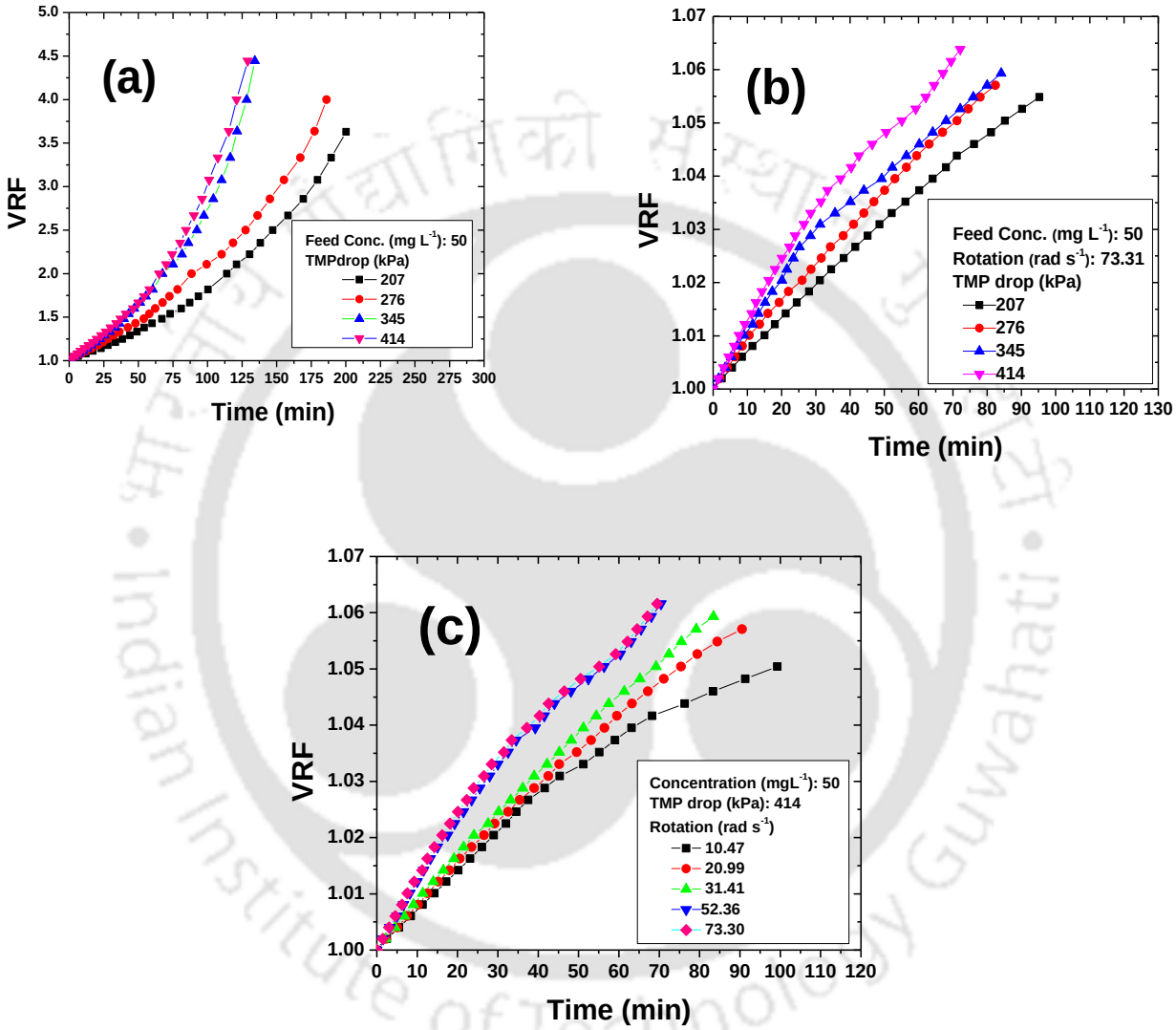

Fig. 3.9. Variation of VRF with process time at different TMP drops during **(a)** batch cell ultrafiltration, **(b)** spinning basket membrane ultrafiltration at constant rotational speed, and **(c)** at different rotational speeds with fixed TMP drop

3.2.6. Application of Hermia's pore blocking model for batch cell ultrafiltration:

In the present work, Hermia's pore blocking model was used to study the fouling characteristics during Humic acids (HAs) dead end ultrafiltration to explain the mechanism of pore clogging with different TMP drops. **Figs. 3.10 (a)-(d)** show the implementation of

Hermia's pore blocking model to recognize the fouling mechanisms, occurring during the Humic acids (HAs) ultrafiltration test. **Fig. 3.10 (a)** describes the fitting of the experimental results to the complete pore blocking model (CPBM). At the high TMP drops of 345 and 414 kPa high differences were obtained between the experimental and predicted flux decline. When the size of the rejected particles is greater than the membrane active pores, complete pore blocking happens (Vela et al., 2008). Rejected particles neither arrive into the membrane active pores nor reach to the permeate side. **Fig. 3.10 (b)** shows the fitting of experimental results to the standard pore blocking model (SPBM). When the size of the solute molecules is lower than of membrane active pores, internal pore blocking happens due to the particles adsorption onto the membrane active pore walls (Vela et al., 2008). SPBM reveals that, solute adsorption was occurred moderately at the low TMP drop of 207 kPa. With the raising of TMP drop, the amount of solute particles adsorption in to the pore walls is increased and caused standard blocking severely.

The theoretical investigation of the experimental permeate flux to intermediate pore blocking model (IPBM) for all parametric conditions have been shown in the **Fig. 3.10 (c)**. When the membrane active pore size is almost similar to the solutes, membrane pores are obstructed just to the arrival of the feed side. This hypothetic phenomenon occurs in an ultrafiltration process resulting intermediate pore clogging (Vela et al., 2008).

When the solute sizes are too much larger than the membrane active pores, a cake layer of rejected solute particles is generated on the membrane effective surface with the filtration time. This type of phenomena is very natural for the unstirred dead end filtration. With the raising of TMP drops, more molecules are rejected by the membrane pores and create a dense cake layer, results a faster decline of permeate flux. **Fig. 3.10 (d)** displays the best fitting of the cake layer formation during the Humic acids ultrafiltration. The predicted R^2 values are very much significant and accurate due to the faster rejected solute deposition on the membrane active surface for all the experimental conditions during the experiment. **Table 3.2** describes the model constants for all types of pore blocking model. It was obtained that the IPBM and CFM revealed the best fitting based on the predicted R^2 values for all the parametric conditions.

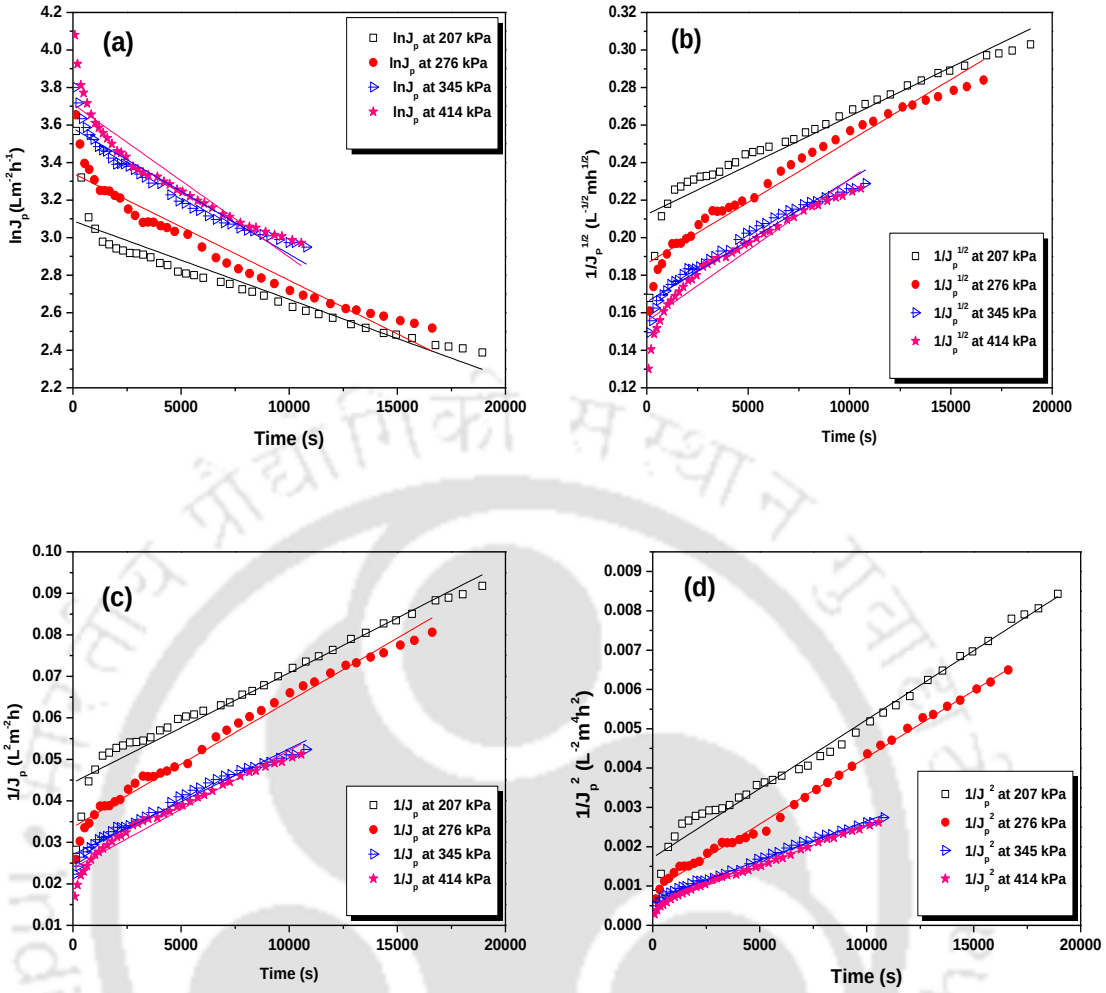

Fig. 3.10. Hermia's pore block models for batch cell filtration (CPBM **(a)**, SPBM **(b)**, IPBM **(c)**, and CFM **(d)**) for 50 kDa membrane cutoff and 50 mg L^{-1} initial feed conditions

Table 3.2. Summary of the model parameters of all pore blocking models for 50 kDa membrane

TMP drop (kPa)	CPBM			SPBM			IPBM			CFM		
	$k_c\times10^5$ (s^{-1})	$J_0\times10^6$ (ms^{-1})	R^2	$k_s\times10^6$ ($m^{-1/2}s^{-1/2}$)	$J_0\times10^6$ (ms^{-1})	R^2	$k_i\times10^6$ (m^{-1})	$J_0\times10^6$ (ms^{-1})	R^2	$k_{gl_{HAs}}\times10^7$ ($m^{-2}s$)	$J_0\times10^6$ (ms^{-1})	R^2
207	4.15	7.45	0.83	5.22	6.18	0.91	2.65	6.27	0.98	3.51	7.37	0.99
276	5.704	8.68	0.91	6.54	8.03	0.95	3.04	7.72	0.98	3.96	9.36	0.99
345	6.706	11.03	0.91	6.51	10.02	0.94	2.55	10.29	0.98	4.21	10.84	0.99
414	8.161	12.56	0.89	7.56	11.56	0.91	2.84	11.72	0.98	4.73	20.99	0.99

3.2.7. Application of modified Hermia's model for the spinning basket membrane ultrafiltration:

Figs. 3.11 (a)–(d) reveal the application of modified Hermia's model during Humic acids ultrafiltration using the spinning basket membrane module (S.B.M.M.). The model curve fitting for the ultrafiltration experimental results to the CPBM has been demonstrated in **Fig. 3.11 (a)** with the following operating conditions: TMP drop of 207 kPa, the initial feed concentration of 50 mg L^{-1} and ω of 10.47, 20.93, 31.41, 52.36 and 73.30 rad s^{-1}.

The complete pore clogging happens due to the presence of large size of particles in the feed solution. The high slope decline has been found at high ω. Continuously increased k_c values have been tabulated in **Table 3.3**.

Whereas, **Fig. 3.11 (b)** illustrates the proper fitting of experimental data to evaluate the standard pore blocking due to the solute particle adsorption. When the continuous solute adsorption onto the membrane pore wall occurs due to the presence of small particles in size, the standard pore blocking model (SPBM) proves the significant model prediction for fouling study. With the raising of rotational speeds of membrane basket, small solute particles blocked the pore walls internally and caused internal clogging. Hence, this model shows significant agreement with the experimental result with 0.99 R^2.

Fig. 3.11 (c) displays the theoretical study of the intermediate pore blocking. The membrane active surfaces cannot completely retain all the solute particles due to the large molecular weight of humic substances. As a result, during continuous filtration, these rejected particles can settle over the other molecules which were already deposited.

The theoretical fitting of the cake layer generation during the SBMM ultrafiltration at various basket rotational speeds (ω, rad s^{-1}) with the constant TMP drop of 207 kPa has been displayed in **Fig. 3.11 (d)**. The predicted R^2 values are not much accurate than others at high membrane basket rotation (52.36 and 73.36 rad s^{-1}) due to restriction over the faster solute deposition on the membrane surfaces. A decreasing order of the cake layer constant for the spinning basket module, $k_{gl_{HAs}}$ has been observed with increasing rotational speed.

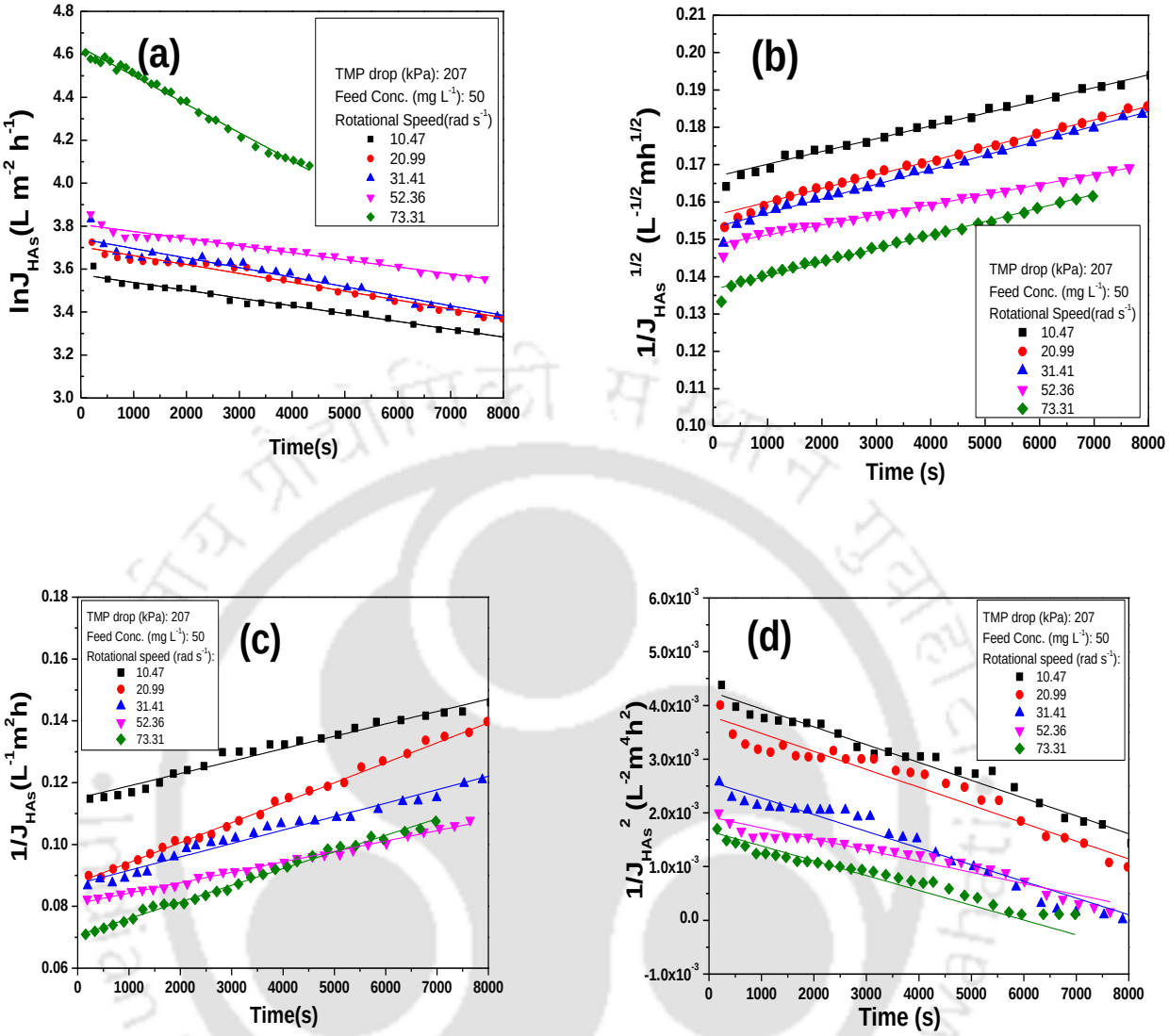

Fig. 3.11. Modified Hermia's pore clogging behavior models fitting curve (CPBM **(a)**, SPBM **(b)**, IPBM **(c)**, and CFM **(d)**) at 50 kDa MWCO

Table 3.3. List of the model parameters of modified Hermia's pore blocking models

ω (rad s^{-1})	CPBM			SPBM			IPBM			CFM		
	$k_c \times 10^5$ (s^{-1})	Residual sum of squares $\times 10^3$	R^2	$k_s \times 10^6$ ($m^{-1/2}s^{-1/2}$)	Residual sum of square $\times 10^5$	R^2	$k_{cf} \times 10^6$ (m^{-1})	Residual sum of square $\times 10^5$	R^2	$k_{glHAs} \times 10^7$ ($m^{-2}s$)	Residual sum of square $\times 10^7$	R^2
10.41	3.61	4.60	0.98	3.35	2.04	0.99	4.02	6.62	0.99	3.34	4.78	0.98
20.93	4.13	7.80	0.97	3.58	6.33	0.99	6.46	2.75	0.99	3.32	10.90	0.95
31.41	4.44	19.70	0.95	3.79	6.58	0.98	7.34	7.76	0.98	2.11	9.11	0.95
52.36	4.54	6.60	0.95	4.61	7.88	0.98	7.76	1.04	0.99	2.07	3.90	0.93
73.30	4.79	7.60	0.97	4.75	8.87	0.98	8.58	2.24	0.99	1.75	7.63	0.92

3.2.8. Variation of total resistance during unstirred batch cell and spinning basket membrane ultrafiltration:

Resistance variation with ultrafiltration process time is also very significant study to check the membrane permeation efficiency during separation (Singh and Das, 2014). During the unstirred batch cell operation, Humic acids (HAs) molecules were adsorbed on the membrane effective surface resulting in enhanced total membrane resistance. The variation of total resistance with operating time for dead end ultrafiltration has been shown in **Fig. 3.12 (a)**. As the TMP drop rises, the development of the concentration boundary layer on the membrane effective surface is increased very fast due to the rapid deposition of retained molecules. Hence the total resistance also increases continuously with raising TMP drop. Whereas, the total resistance difference with process time for the spinning basket membrane module has been discussed in **Fig. 3.12 (b)**. With the increasing TMP drop, $R_{t_{SBM}}$ increases gradually with operating time. For each TMP drop, the resistance profile changes slowly with process time for the influence of basket rotation at 73.30 rad s^{-1}. Due to the generation of shear force and turbulence, the rejected solute particles cannot deposit on the membrane surfaces. This phenomenon restricts the development of resistance rapidly. After one hour operation, a continuous increasing of $R_{t_{SBM}}$ has been reported with the increase of TMP drop due to membrane pore fouling. Beyond 120 min, the variation in resistance profile is negligible and steady values are achieved. At fixed pressure (414 kPa), the influence of different rotational speeds (10.47, 20.93, 31.41, 52.36 and 73.31 rad s^{-1}) on total resistance has been reported in **Fig. 3.12 (c)**. With the increase of basket rotation from 10.47 to 73.30 rad s^{-1} a decreasing order of $R_{t_{SBM}}$ from 4.33×10^{13} to 2.41×10^{13} m^{-1} has been observed in this figure. Increased rotational speed gives an increased dynamic

pressure on membrane surfaces. The combined force, like, applied TMP drop and dynamic pressure can easily restrict the generation of mass transfer resistance of the polarized layer.

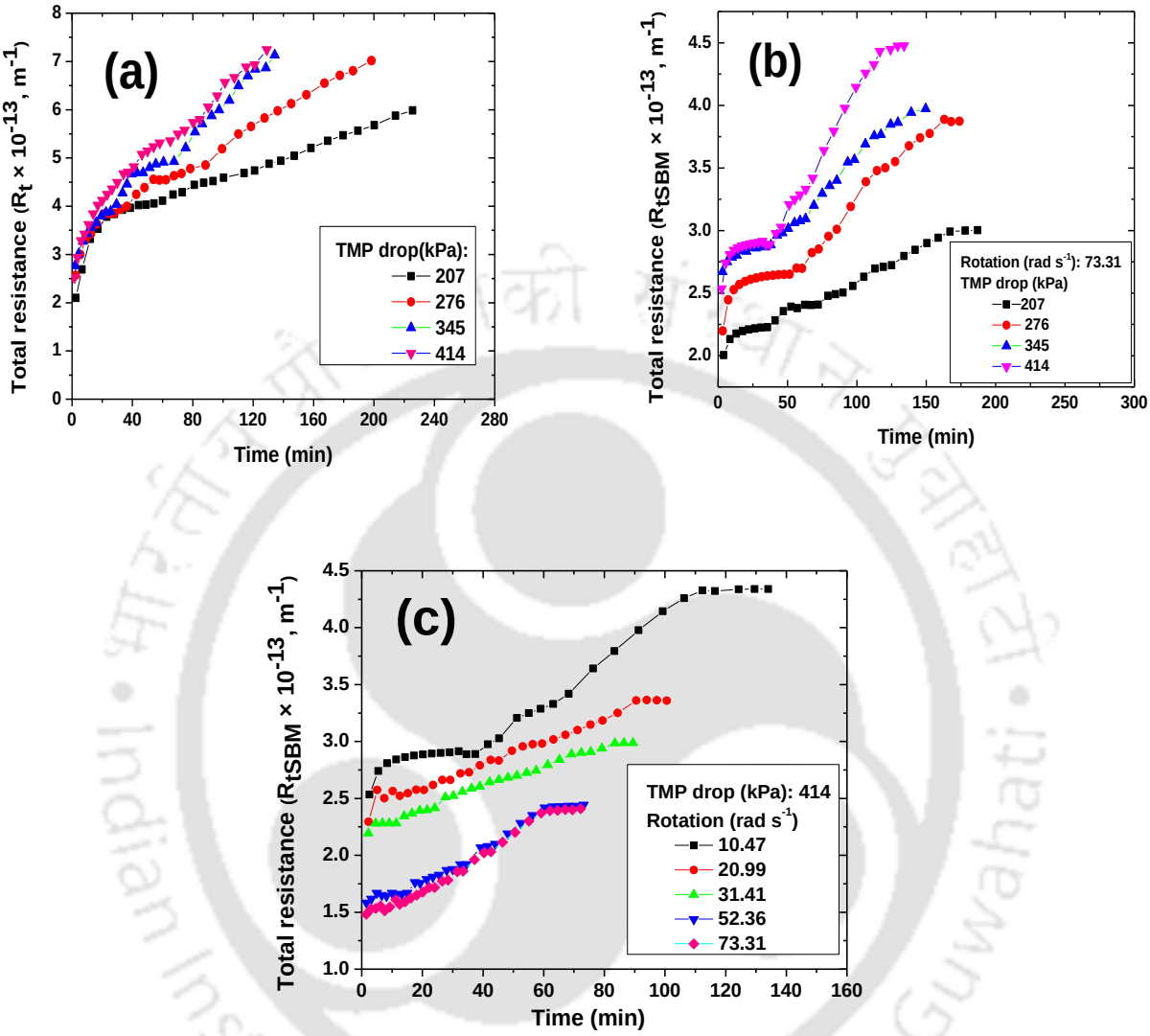

Fig. 3.12. Total resistance variation for **(a)** unstirred batch cell operation, **(b)** spinning basket membrane ultrafiltration at constant rotational speed (73.31 rad s^{-1}) with various TMP drops (207 to 414 kPa), and **(c)** different rotational speeds at fixed TMP drop

3.2.9. The effects of membrane basket back rotation on membrane permeability recovery followed by ultrasonication:

Fig. 3.13 (a) shows the effects of back rotational speed to improve the steady state flux of the fouled membrane at a fixed TMP drop. Membrane basket rotation was varied from -10.47 to -52.36 rad s^{-1}. The negative sign (-) indicates the direction of membrane basket rotation. Due to the local vacuum on the membrane surfaces, after minimizing applied

pressure, the accumulated solutes became disengaged from the membrane surfaces (Sarkar et al., 2012). This phenomenon increased hydraulic permeability. Initial hydraulic permeability and resistance of a compact UF membrane were 6.76×10^{-11} m Pa^{-1} s^{-1} and 1.84×10^{13} m^{-2}, respectively. After the ultrafiltration of HAs of 50 mg L^{-1} solution, the water permeability was decreased to 2.8×10^{-11} m Pa^{-1} s^{-1}. On the other side, hydraulic resistance was increased to 4.08×10^{13} m^{-2}. The cleaning efficiency for the back rotation of the membrane basket was calculated as 47.8%. Hydraulic steady flux was recovered from 32.5 to 36.0 L m^{-2} h^{-1}. **Fig. 3.13 (a)** reveals that beyond 300 rpm (31.41 rad s^{-1}) of rotation, the steady water flux is constant. If rejected solutes block the membrane pore walls or adsorbed on membrane surfaces, the created membrane shear, and turbulence are not enough to eliminate small particles from the membrane pore walls (Sarkar et al., 2012). To remove the irreversible membrane fouling, ultrasonic bath has been introduced in this project instead of the chemical cleaning process.

Fig. 3.13 (b) illustrates the results of the effects of ultrasonication over membrane cleaning. With increasing sonication time, higher hydraulic flux values have been reported. Cleaning efficiency was calculated based on the membrane resistance. It is observed that with increasing sonication time from 5 min to 25 min, cleaning efficiency also increased from 72% to 88%. Whereas, at 15 min of sonication, cleaning efficiency was already obtained over 85%. To obtain the optimum sonication time for maximum cleaning efficiency, this process was carried out up to 25 min.

However, beyond 15 min, the increase of efficiency was almost insignificant. It can be considered as the optimum sonication time to clean the fouled membrane for this study. The recovered permeability was about 5.02×10^{-11} m Pa^{-1} s^{-1}. The compression and expansion cycles which are formed by the transmitting of the ultrasound wave through a liquid medium (mainly DI water) release bubbles to collapse.

The collapsed bubble breaks the interface between solutes (foulant) and membrane. Therefore, the foulant is removed from the membrane pore walls and also from surfaces (Muthukumaran et al., 2004; Li et al., 2002; Facundo et al., 2013). In the present study, the breakage of the membrane surface was not found as the membrane hydraulic permeability value was found to remain almost invariant after the cleaning study.

A similar trend has been reported during the ultrasound clean of the fouled membrane after the cross-flow ultrafiltration of Humic acids (HAs) solution. It is reported that the ultrasound-assisted cleaning is an effective process without damaging the membrane surface during the cross-flow filtration of Humic acids solution (Ng et. al, 2013).

Whereas, the effects of ultrasonication on the cleaning of a ceramic membrane during the treatment of emulsification wastewater has also performed previously. It was observed that the morphology of the fouled membrane was found to be changed in the presence of ultrasound. Not only that, the ultrasonication was not effective to remove the foulant stuck inside the membrane pores (Li et al., 2007).

After the first set of the cleaning process, spinning basket module was set to perform for further treatment of Humic acids solution to analyze the efficiency of the cleaned membrane in the presence of constant rotational speed, initial feed concentration and TMP drop of 10.47 rad s^{-1}, 50 mgL^{-1} and 414 kPa, respectively. The cleaning efficiency after completion of 2nd sets of cleaning-filtration -cleaning process was calculated as 86%.

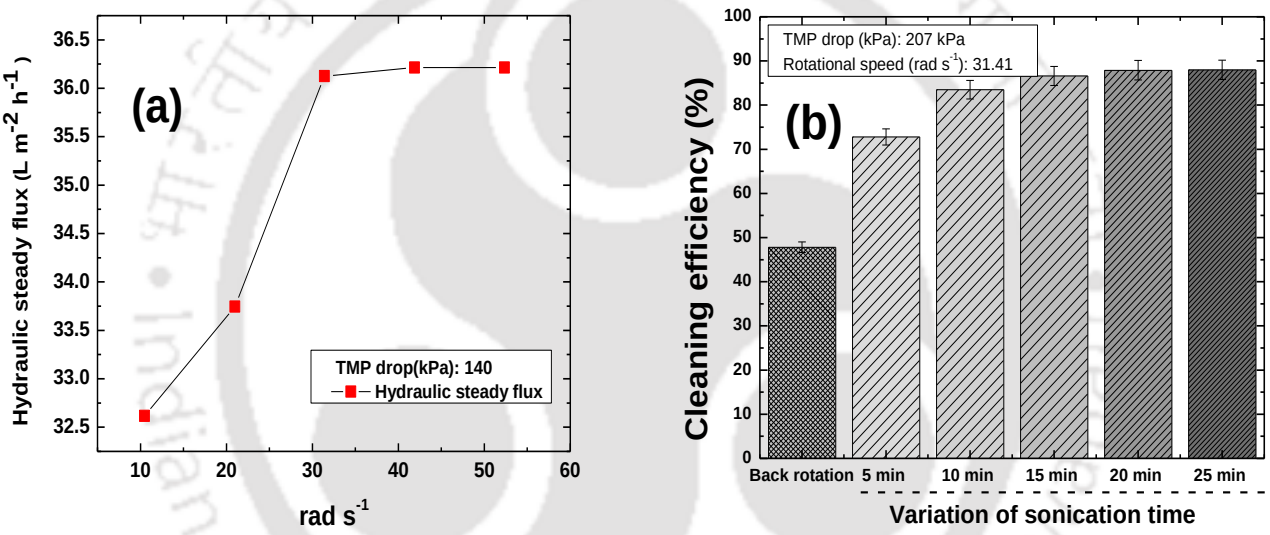

Fig. 3.13. (a) Effects of rotational speed on improvement of steady hydraulic flux during back rotation of spinning basket at fixed TMP drop of 140 kPa and **(b)** variation of cleaning efficiency with membrane basket back rotation and different sonication time

3.2.10. Discussion on the total power requirement during SBM ultrafiltration:

The variation of total electric power (kW) at the different applied TMP drops and rotational speeds has been discussed in **Fig. 3.14**. It clearly says that the total power increases with increasing rotational speed (ω). Whereas, at constant ω, it varies very slowly with applied TMP drops.

The maximum power was reported as 0.32 kW after using maximum TMP drop and ω of 414 kPa and 73.3 rad s^{-1}, respectively. The net power consumption after completing one cycle of the cleaning process was 0.42 kW. Total power consumed during a full cycle (filtration and cleaning of the membrane) was calculated as 0.74 kW. Whereas, extreme power consumption of 0.5 kW was reported during the rotating disk ultrafiltration (Ding et al., 2003). Not only that, near about 18.15 kW maximum power consumption was informed to investigate ionic concentration and COD reduction in dairy process wastewater using high-speed shear-enhanced reverse osmosis process (Frappart et al., 2008).

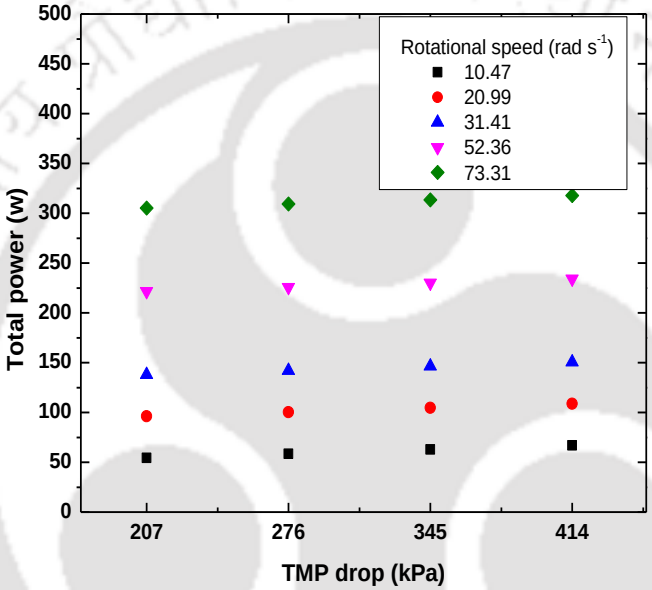

Fig. 3.14. Variation of total power calculation of spinning basket module at different rotational speeds and TMP drop

3.3. Permeate quality analysis for dead end filtration and spinning basket membrane ultrafiltration:

Initial Humic acids concentration in the feed was prepared as 50, 150 and 250 mg L^{-1}. COD of three concentrations were measured as 165, 450 and 659.2 mg L^{-1} respectively. The pH values were 6.4, 5.4 and 5.03 respectively. **Table 3.4** delivers the comparison of quality of the permeate for various transmembrane pressure drops (TMP drops) in terms of final Humic acids (HAs) concentrations, observed rejection (%), ionic conductivity, pH, TDS, and the final COD values through the unstirred batch cell.

It was found in **Table 3.4** that maximum total dissolved solids (TDS) was removed at 414 kPa due to the formation of the cake layer with raised applied transmembrane pressure drop (TMP drop). With the increasing TMP drop from 345 to 414 kPa, the change in ionic concentration was marginal. The rate of reducing of ionic conductivity and TDS is almost linear with rising TMP drop. With the raising of TMP drop, the generation of gel layer on the membrane active surface has been increased. The gel layer delivers an extra mass transfer resistance which increases the retention rate at high TMP drop. It was observed that pH of permeates were improved to 7.25 which become almost constant with transmembrane pressure drops.

On the other side, **Table 3.5** reports the comparison of permeate qualities for various parameters during the spinning basket ultrafiltration. The rotational speed was considered as an important parameter to improve the permeate quality. As a result, the variation of different physicochemical properties in the presence of different membrane basket rotation and TMP drops have been enlisted in the **Table 3.5**.

It was found that the extreme removal of TDS was noticed at the high TMP (414 kPa) drop in the presence of the rotational speed. Whereas, due to the generation of small particles during high rotation, TDS in permeate was increased at the high rotational speed of 73.31 rad s^{-1}. Ionic conductivity was reduced in the presence of rotational speed. With the increasing of rotational speed from 10.47 to 52.36 rad s^{-1}, the rejection rate of solute molecules has been raised thus, the electrical or ionic conductivity is also decreased from the Humic acids solution. It is very vibrant that with the rising of TMP drop the quality of the permeate in terms of removal of TDS and ionic conductivity has been improved.

The pH was changed to 7.5 from its initial value of 6.4. Approximately 90% minimization of Humic acids substances was reported from contaminated water using ferrate (IV) oxidization at various pH levels of 7.1 to 7.8 (Qu et al., 2003). This comparison delivers that the spinning basket membrane filtration has better rejection capacity (94.5%) than other processes.

Table 3.4. Physiochemical properties of permeates at steady state during batch cell filtration

Properties	Conc.: 50 mg L^{-1}				Conc.: 150 mg L^{-1}				Conc.: 250 mg L^{-1}			
	ΔP (kPa)				*ΔP* (kPa)				*ΔP* (kPa)			
	207	276	345	414	207	276	345	414	207	276	345	414
Permeate conc. (mg L^{-1})	3.93	3.56	3.24	2.90	12.50	10.10	8.9	7.50	21.2	17.16	14.8	12.45
Observed rejection (%)	92.1	92.8	93.5	94.2	91.55	93.33	94.25	95.00	91.38	93.18	94.48	95.23
pH	7.34	7.31	7.24	7.21	7.15	7.18	7.20	7.25	7.12	7.25	7.28	7.28
Ionic cond. (Sm^{-1}) ($\times 10^{-2}$)	1.15	1.07	1.03	1.03	1.25	1.20	1.14	1.07	1.28	1.23	1.20	1.18
TDS (mg L^{-1}) ($\times 10^{-3}$)	6.67	6.22	6.01	5.97	7.25	6.96	6.61	6.21	7.42	7.13	6.96	6.84
COD (mg L^{-1})	24.02				25.00				28.00			

Table 3.5. Comparative study of physiochemical characteristics of permeates during spinning basket ultrafiltration of Humic acids

Exp. No	Pressure (kPa)	Rotational speed (rad s^{-1})	Permeate conc. (mg L^{-1})	Observed rejection (%)	pH	Ionic cond. (S m^{-1}) × 10^{-4}	TDS (mg L^{-1}) × 10^{-2}	COD (mg L^{-1})
1	207	10.47	3.70	92.50	7.40	115.2	6.68	24.72*
2		20.93	3.60	93.00	7.41	118.5	6.87	
3		31.41	3.84	93.80	7.47	127.3	7.38	
4		52.36	3.56	93.20	7.45	132.4	7.47	
5		73.30	3.97	92.70	7.46	130.5	7.59	
6	276	10.47	2.95	93.50	7.29	114	6.61	24.72*
7		20.93	3.24	93.90	7.34	120.2	6.97	
8		31.41	3.28	94.70	7.23	122.6	7.11	
9		52.36	3.44	93.80	7.41	126.5	7.33	
10		73.30	3.89	93.30	7.46	130.6	7.57	
11	345	10.47	2.71	94.06	7.27	122.7	7.11	24.72*
12		20.93	2.83	94.50	7.25	118	6.84	
13		31.41	2.87	95.00	7.22	126.6	7.34	
14		52.36	3.4	94.41	7.41	128.3	7.44	
15		73.30	3.81	94.00	7.45	137	7.94	
16	414	10.47	2.05	95.03	7.22	116.8	6.77	24.72*
17		20.93	2.47	95.56	7.21	116.8	6.77	
18		31.41	2.63	96.00	7.21	125	7.25	
19		52.36	3.44	95.30	7.41	131.6	7.63	
20		73.30	3.85	94.50	7.45	131.9	7.65	

***Note:** Due to the presence of membrane basket rotation, a significant amount of removal of Humic acids has been obtained during the ultrafiltration process which reveals the similar result for the COD (mg L^{-1}) for all the cases.*

3.4. Summary of the chapter:

In the present work, Humic acids water solution was successfully treated using the spinning basket membrane and the unstirred batch cell module at various operating conditions.

- The transmembrane pressure (TMP) drop was an important and significant parameter for the dead end filtration to discover the Humic acids (HAs) permeate flux decline nature. Transient flux decline behavior was studied and compared successfully with the theoretical study using artificial neural network (ANN) system.
- Hermia's pore blocking model was studied to analyze the membrane active pore blocking mechanisms for dead end ultrafiltration. According to the results, it can be considered that the best fits to experimental data are found perfect for the CFM and IPBM for all the parameter conditions which indicates the severe fouling during the Humic acids batch ultrafiltration process.
- Maximum rejection was found at the high applied transmembrane pressure drop of 414 kPa. Whereas, VRF values are higher due to high fouling on the membrane surface for batch cell filtration.
- On the other side, permeate flux decreasing according to process time was peripheral in the presence of rotational speed during spinning basket membrane ultrafiltration. However, an initial decline of Humic acids flux was noticed because of the membrane effective surface pore-clogging.
- Modified Hermia's pore blocking mechanism was applied to analyze the internal pore-clogging behavior.
- Maximum Humic acids rejection was found at a high TMP (414 kPa) drop and the low rotational speed of 31.41 rad s^{-1}. A reduced membrane resistance has been observed with increasing rotation.
- Spinning basket membrane back rotation with distilled water was not sufficient technology to eliminate the rejected solute particles from the active membrane surfaces as well as membrane pore walls. Maximum cleaning effectiveness of 88% was found with ultrasound application.
- Based on the rotational speed, observed solute rejection, and permeate quality, the spinning basket membrane ultrafiltration of Humic acids aqueous solution has been adopted as the valuable and effective mode of separation.

References:

A. Sarkar, D. Sarkar, M. Gupta, C. Bhattacharjee, Recovery of Polyvinyl Alcohol from Desizing Wastewater Using a Novel High-Shear Ultrafiltration Module, Clean-Soil Air, Water 40 (2012) 830-837.

C. Das, P. Patel, S. De, S. Dasgupta, Treatment of Tanning effluent using nanofiltration followed by reverse osmosis, Sep. Purif. Technol. 50 (2006) 291-299.

D. Sarkar, A. Sarkar, A Roy, C. Bhattacharjee, Performance characterization and design evaluation of spinning basket membrane (SBM) module using computational fluid dynamics (CFD), Sep. Purif. Technol. 94 (2012) 23-33.

I. Galambos, G. Vatai, E.B. Molnar, Membrane screening for Humic substances removal, Desalination 162 (2004) 111-116.

J. Li, R. D. Sanderson, E. P. Jacobs, Ultrasonic cleaning of nylon microfiltration membranes fouled by Kraft paper mill effluent, J. Membr. Sci. 205 (2002) 247–257.

J. H. Qu, H. J. Liu, S. X. Liu, P. J. Lei, Reduction of fulvic acid in drinking water by ferrate, J. Environ. Eng. ASCE. 129 (2003) 17-24.

K. K. Ng, C. J. Wu, H. L. Yang, S. C. Panchangam, Y. C. Lin, P. K. A. Hong, C. H. Wu, C. F. Lin, Effect of ultrasound on membrane filtration and cleaning operations, Sep. Sci. Technol. 48 (2013) 215-222.

L. H. Ding, O. Akoum, A. Abraham, M. A. Jaffrin, High Shear Skim Milk Ultrafiltration Using Rotating Disk Filtration Systems, Bioeng. Food Natur. Prod. (AIChE J.) 49 (2003) 2433-2441.

L. M. J. Facundo, J. A. M. Roca, B. C. Uribe, S. A. Blanco, Ultrasonic cleaning of ultrafiltration membranes fouled with BSA solution, Sep. Purif. Technol. 120 (2013) 275-281.

M. D. Petala, A.I. Zouboulis, Vibratory shear enhanced processing membrane filtration applied for the removal of natural organic matter from surface waters, J. Membr. Sci. 269 (2006)1-14..

M. C. V. Vela, S. A. Blanco, J. L. Garcia, E. B. Rodriguez, Analysis of membrane pore blocking models applied to the ultrafiltration of PEG, Sep. Purif. Technol. 62 (2008) 489-498.

M. Frappart, M. Jaffrin, L. H. Ding, Reverse osmosis of diluted skim milk: Comparison of results obtained from vibratory and rotating disk modules, Sep. Purif. Technol. 60 (2008) 321–329.

M. J. C. Baguena, M. C. V. Vela, J. M. G. Zafrilla, S. A. Blanco, J. L. Garcia, D. C. Martinez, Comparison between artificial neural networks and Hermia's models to assess ultrafiltration performance, Sep. Purif. Technol. 170 (2016) 434-444.

S. Li, X. Weihong, X. Nanping, Effect of Ultrasound on the treatment of emulsification wastewater by ceramic membranes, Chin. J. Chem. Eng., 15 (2007) 855-860.

S. Muthukumaran, K. Yang, A. Seuren, S. Kentish, M. Ashokkumar, G. W. Stevens, F. Grieser, The use of ultrasonic cleaning for ultrafiltration membranes in the dairy industry, Sep. Purif. Technol. 39 (2004) 99–107.

V. Singh, P. K. Jain, C. Das, Performance of spiral wound ultrafiltration membrane module for with and without permeate recycle: Experimental and theoretical consideration, Desalination 322 (2013) 94-103.

V. Singh, C. Das, Comparison of spiral wound UF membrane performance between turbulent and laminar flow regimes, Desalination 337 (2014) 43-51.

CHAPTER 4

SPINNING BASKET MEMBRANE ULTRAFILTRATION OF PAPER INDUSTRY AND TEA FACTORY WASTE EFFLUENTS: EXPERIMENTAL AND THEORETICAL ASPECTS

In this chapter, detailed explanations are described for the treatment of paper and tea industrial effluents using the spinning basket membrane ultrafiltration. To improve the performances of membranes, pretreatment of wastewater was done for the removal of suspended particles present in the effluents using vacuum filtration for paper industry wastewater, and alum coagulation for tea factory effluent. The spinning basket membrane module was employed using different molecular weight cutoff (MWCO) membranes, various membrane basket rotations, and the different transmembrane pressure drops. Modified Hermia's pore blocking methods were studied to analyze the internal pore blocking mechanisms during real industrial effluent treatment. Response surface methodology was performed to optimize the process parametric conditions and to figure out the combined effects of different parameters on the permeate flux and dissolved solids removal. The analysis of rejected materials found from paper industrial waste effluent was studied using different analytical techniques, such as Fourier Transform Infrared Spectra, energy dispersive X-ray spectra, thermal gravimetric analysis, etc.

The work presented in this chapter is published in the following journal.

***Suman Saha**, Chandan Das, 2017. Spinning basket membrane ultrafiltration of paper industry waste effluent: Experimental and theoretical aspects. **J. Environ. Chem. Eng.** 5 4583-4593.*

***Suman Saha**, Rijumoni Boro, Chandan Das, "Treatment of tea factory effluent in a coagulation-ultrafiltration integrated hybrid process", **Clean Soil Air Water** (Under review).*

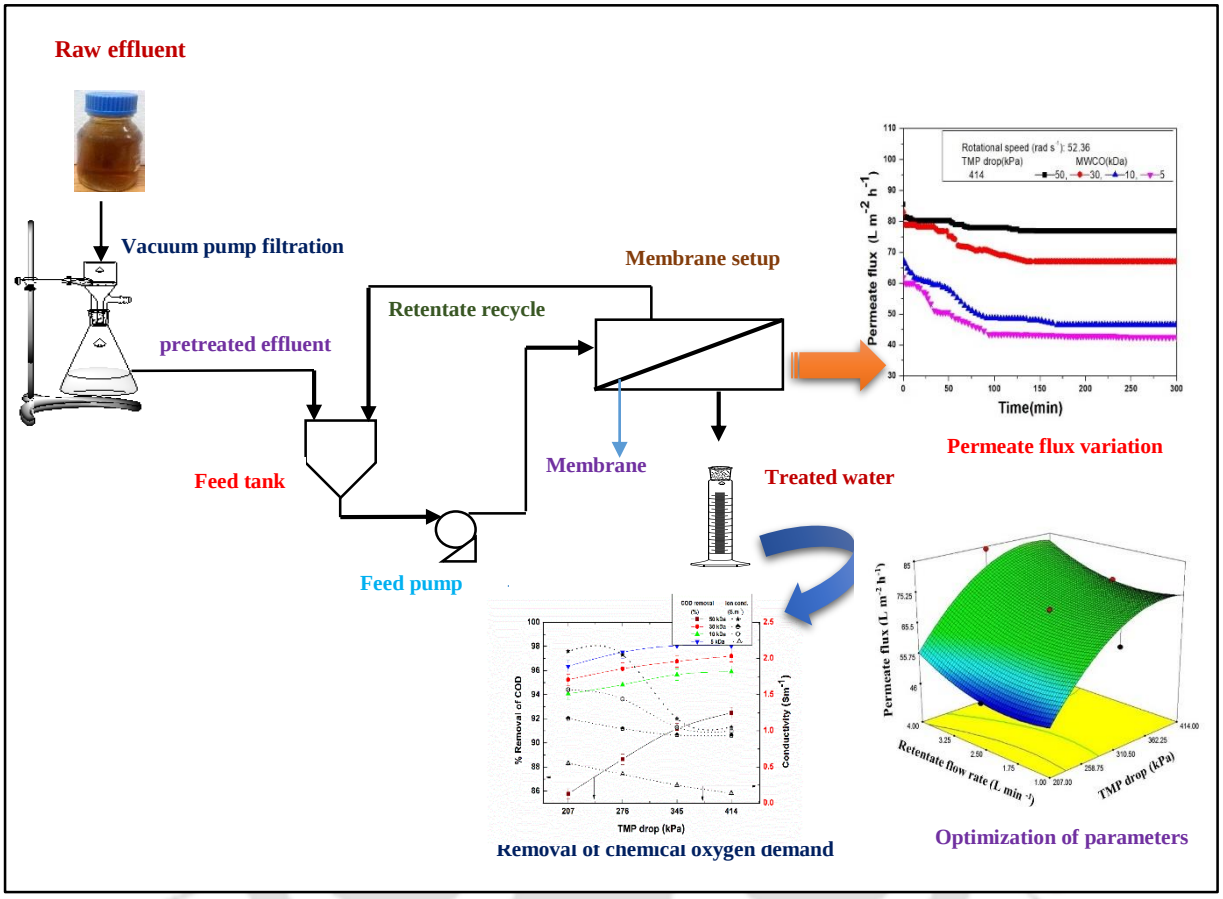

Spinning basket membrane ultrafiltration of paper industry waste effluent: Experimental and theoretical aspects

4.1. Treatment of paper and tea industry wastewater using membrane ultrafiltration:

The main objective of the ultrafiltration process is to describe the permeate flux decline behavior using four various molecular weight cutoff (MWCO) membranes, such as, 5, 10, 30 and 50 kDa at various process conditions, like, applied transmembrane pressure (TMP) drops (207 to 414 kPa), and spinning basket rotations (10.47 to 73.30 rad s^{-1}) for the treatment of real effluents collected from two different industries, such as paper and pulp industry and tea processing factory. The process parameters, like, applied TMP drops, rotational speeds, and retentate flow rate were optimized using the design expert software. The overview of the rotational diffusion model is studied and compared with other diffusion models to evaluate the module performance. This study, however, evidences that for a continuous filtration process, the utilization of newly shear-enhanced spinning basket membrane module for industrial effluent treatment can be performed successfully with the low power consumption than other existing dynamic filtration processes.

4.2. Results and discussion:

4.2.1. Analysis of paper industry raw and pretreated effluent (after vacuum filtration):

The pretreatment of paper industry raw effluent was performed by vacuum filtration 0.45 μm filter paper. the main target was to remove the total suspended solids (TSS) materials from the raw wastewater. Hence, the TSS was removed by 77% using this preliminary process. The pretreatment of raw effluent helps to perform membrane ultrafiltration with fruitful output. **Table 4.1** describes the comparative study of physicochemical properties of raw effluent with vacuum filtration.

Table 4.1. Comparison of physicochemical properties of paper industry waste effluents before and after pretreatment

Properties	Raw effluent	After vacuum filtration (0.45μm)
pH	10.40	9.02
TSS (mg L^{-1})	1594	360
TDS (mg L^{-1})	4007	3199
Ionic conductivity (S m^{-1})	4.80	4.57
Clarity (*T*, %)	60.26	68.23
COD (mg L^{-1})	8470	6430
BOD (mg L^{-1})	4450	2150
Sodium (mg L^{-1})	117	113
Potassium (mg L^{-1})	107	105
Zinc (mg L^{-1})	59.4	59.4
Iron (mg L^{-1})	42	32.4
Magnesium (mg L^{-1})	1.7	1.7
Nickel (mg L^{-1})	2.4	2.4
Copper (mg L^{-1})	1.03	1.03
Manganese (mg L^{-1})	8.33	8.33

4.2.2. Analysis of variance (ANOVA) and response surface for the coagulation study of tea industry wastewater:

The optimum coagulation conditions, like, alum dosage (*A*, mg L^{-1}), pH (*B*,), stirring speed (*C*, rpm, rad s^{-1}) and stirring time (*D*, min) are determined by the regression models and good prediction towards percentage (%) removal of TSS, TDS and minimization of turbidity from the effluent. The response surface methodology helps to reveal the experimental results to different model terms that can display the good dependency of responses based on the perfect statistical analysis. In the present optimization study, no transformation is applied to confirm the suggested quadratic models for all respected responses. Eqs. (4.1-4.3) show the best fit quadratic models for the percentage removal (%) of TSS (X_1); TDS (X_2) and minimization of turbidity (X_3, NTU) from the wastewater, respectively.

Percentage removal of TSS (%) model:

$$X_1 = 86.33 + 6.37 \times A_1 - 2.11 \times B_1 + 0.14 \times C_1 + 2.10 \times D_1 + 0.51 \times A_1 \times B_1 - 0.15 \times A_1 \times C_1 - 0.53 \times A_1 \times D_1 + 0.44 \times B_1 \times C_1 + 0.12 \times B_1 \times D_1 - 0.99 \times C_1 \times D_1 - 10.59 \times A_1^2 - 1.17 \times B_1^2 - 3.67 \times C_1^2 - 5.42 \times D_1^2 \quad (4.1)$$

Percentage removal of TDS (%) model:

$$X_2 = 73.94 + 10.47 \times A_1 - 2.44 \times B_1 - 0.55 \times C_1 - 0.69 \times D_1 - 0.78 \times A_1 \times B_1 + 1.22 \times A_1 \times C_1 + 1.72 \times A_1 \times D_1 + 0.78 \times B_1 \times C_1 - 0.34 \times B_1 \times D_1 - 1.09 \times C_1 \times D_1 - 13.56 \times A_1^2 - 8.31 \times B_1^2 + 0.24 \times C_1^2 - 1.56 \times D_1^2 \quad (4.2)$$

Turbidity (NTU) model:

$$X_3 = 1.39 - 0.49 \times A_1 + 0.092 \times B_1 - 0.064 \times C_1 - 0.16 \times D_1 + 0.12 \times A_1 \times B_1 - 3.13 \times 10^{-3} \times A_1 \times C_1 + 0.022 \times A_1 \times D_1 + 0.19 \times B_1 \times C_1 - 0.034 \times B_1 \times D_1 + 0.047 \times C_1 \times D_1 + 0.14 \times A_1^2 + 0.66 \times B_1^2 - 0.14 \times C_1^2 - 0.24 \times D_1^2 \quad (4.3)$$

Table 4.2 describes the statistical analysis of all the regression parameters. The high F-value with low p-value describes that the model is significant for each response. The low p-value of less than 0.0001 implies that the quadratic model terms are highly significant towards optimization study. The coefficient of determination (R^2) signifies that all the model terms are perfect to optimize the process parameters. The adjusted R^2 reveals reasonable agreement with predicted one. The good adequate precisions for all the cases reveal that all the models can be used to navigate the design planetary. The models statistical standard deviation, the pure error and Lack-of fit values have been tabulated in the **Table A2** in the appendix which implies that the experiments were studied very accurately. These values are analyzed using response surface methodology. The insignificant Lack-of-fit test indicates that all the models have significant quadratic relations between the process parameters and the responses. The percentage removal (%) of TSS and TDS are mostly dependent on the alum dosage (A, mg L^{-1}), pH (B) and stirring speed (C, rpm). The turbidity is mainly influenced by the alum dosage (A, mg L^{-1}). The optimum coagulation conditions are as following: alum dosage: "200.26 mg L^{-1}"; pH: "6.1"; stirring speed: "29.11 rad s^{-1} (278 rpm)"; stirring time: "115 min". The predicted theoretical values of percentage removal of TSS, TDS and the minimized turbidity (NTU) are 87.5%, 76% and 1.08 NTU, respectively.

Table 4.2. Analysis of variance (ANOVA) results for response parameters

Responses	Model F value	p- value Prob>F	R^2	Adjusted R^2	Predicted R^2	Adequate Precision	Mean square	Residual
TSS (%)	23.86	<0.0001	0.96	0.92	0.89	15.45	249.32	158.22
TDS (%)	48.56	<0.0001	0.98	0.96	0.90	20.33	394.24	137.50
Turbidity (NTU)	20.82	<0.0001	0.92	0.90	0.89	20.12	55.82	1.47

Conjugate effects of alum dosage, stirring time, pH and stirring speed on TSS removal:

The conjugate effects of alum dosage, pH, stirring time and speed has been observed in the **Figs. 4.1 (a)-(d)**. **Fig. 4.1 (a)** reveals that with the increasing alum dosage from 50 to 200.26 mg L^{-1} and at a low stirring speed of 100 rpm, the rate of removal of TSS is also increasing progressively from 65 to 79%. Beyond 200.26 mg L^{-1}, the removal efficiency has been deteriorated. With the increasing alum dosage, the positively charged elements in the wastewater also increase which helps to aggregate the small floccs into the large one resulting rapid sedimentation and the high elimination of TSS. Whereas, at an over dosage of alum concentration, the high concentration of a positively charged ion prevents the segregation of the flocks which has been found in this figure also. The particle size analysis of the effluent before and after alum coagulation has been shown in **Fig. A2** in the appendix. The cumulative diameter of the particles present in the effluent has been reduced from 2132.0 to 1547.1 nm. After a certain point, the rate of removal of TSS has been decreased with the increasing alum dosage from 200.26 to 300 mg L^{-1}. The same trend has been found in the **Fig. 4.1 (b)**. Whereas, in Fig. **Fig. 4.1 (c)**, the removal rate increases at neutral pH. The high-speed rotation with the maximum stirring time (**Fig. 4.1 (d)**) results in the deterioration of the generation of flocculants during the coagulation process.

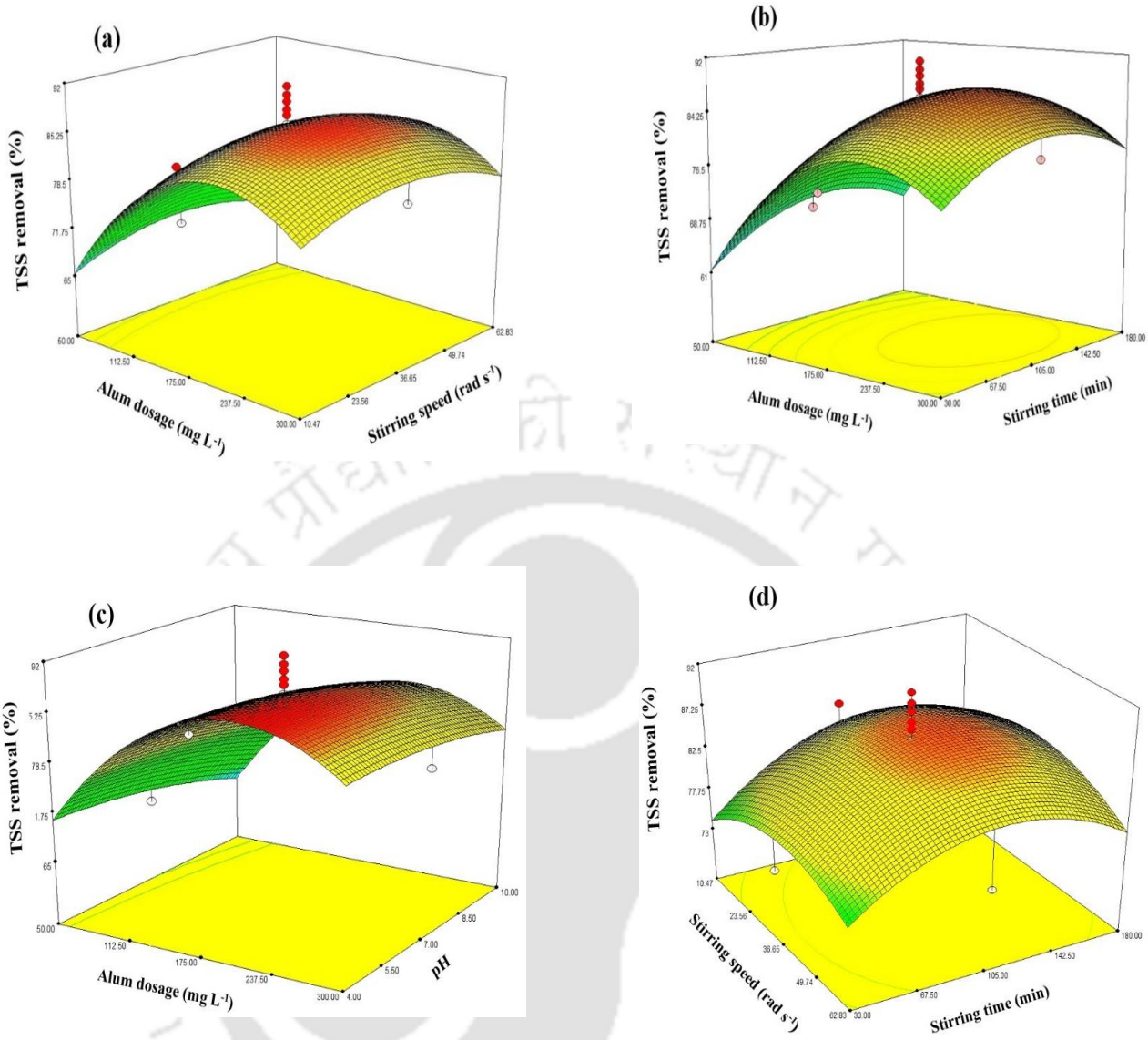

Fig. 4.1. Quadratic effects of **(a)** alum dosage (mg L^{-1}) and stirring speed (rad s^{-1}), **(b)** alum dosage (mg L^{-1}) and stirring time (min), **(c)** alum dosage (mg L^{-1}) and pH, **(d)** stirring speed (rad s^{-1}) and stirring time (min) on percentage removal (%) of TSS from effluent

Effects of input parameters on the removal efficiency of total dissolved solids (TDS):

The significant effects of different parameters on the removal of TDS have been displayed in the **Figs. 4.2 (a)-(d)**. The quadratic effects of alum dosage with stirring speed have been discussed in **Fig. 4.2 (a)** and **(b)**. To determine the different alum dosages on the removal of dissolved organic materials, alum dosage was varied from 50 to 300 mg L^{-1}. From this

figure, it is noticed that the removal efficiency of TDS is a function of variation of alum dosage. It is directly proportional to the increasing of alum ion dosage at a certain point of 200.26 mg L^{-1}. The negatively charged ion present in the effluent becomes neutralized with the increasing alum dosage which results in the good removal of organic pollutants. An increasing in aluminum ion beyond 200.26 mg L^{-1} results negative improvement on the removal efficiency due to the charge reversible for excess alum dosage. **Fig. 4.2 (c)** demonstrates a good efficiency of the removal of TDS with the increasing alum dosage at neutral pH. The tea effluent mainly contains more amount of hydrolyzed phenolic compounds (Yadav and Kalaiyarasi, 2015; Chen et al., 2015). The maximum removal of TDS has been observed at pH 6.1 with 200.26 mg L^{-1} alum dosage. This optimal pH condition is very close enough to the initial pH of tea effluent. It is clear to conclude that the coagulation process gives better performance at pH near to neutral due to the better adsorption of the charged organic compounds onto the alum surface than high pH. It is justified that the pre-treatment of tea effluent can be performed without adjusting the initial pH condition which is economical and environmentally beneficial. In **Fig. 4.2 (d)** shows the linear effects of stirring time (min) on the removal of TDS at a constant stirring speed of 36.65 rad s^{-1}. On the other side stirring speed gives steady effect over the TDS removal.

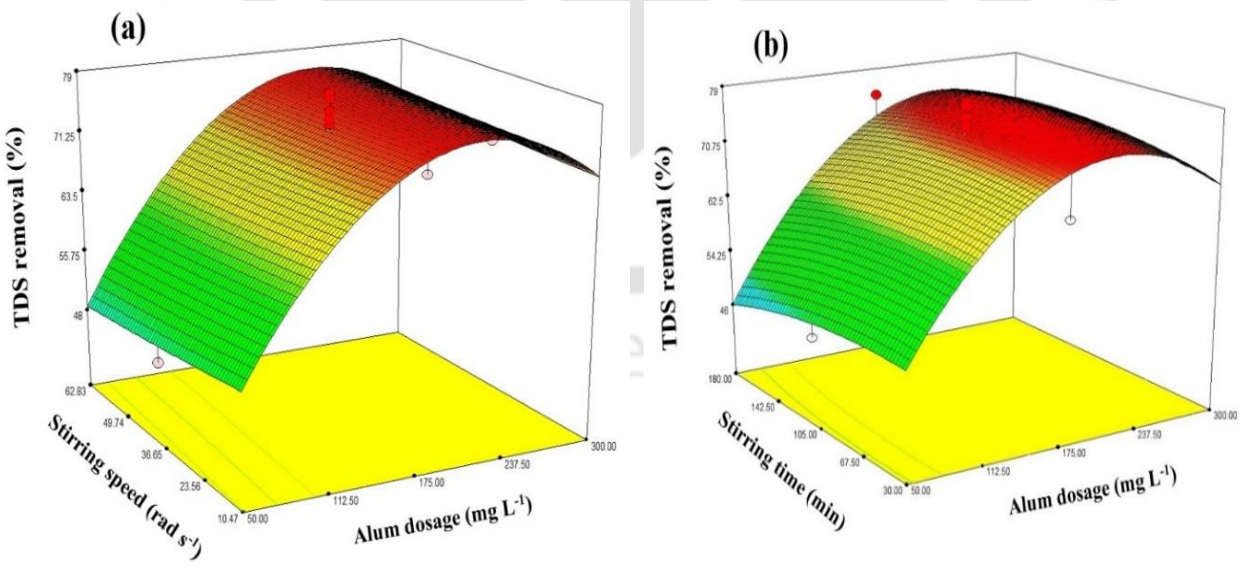

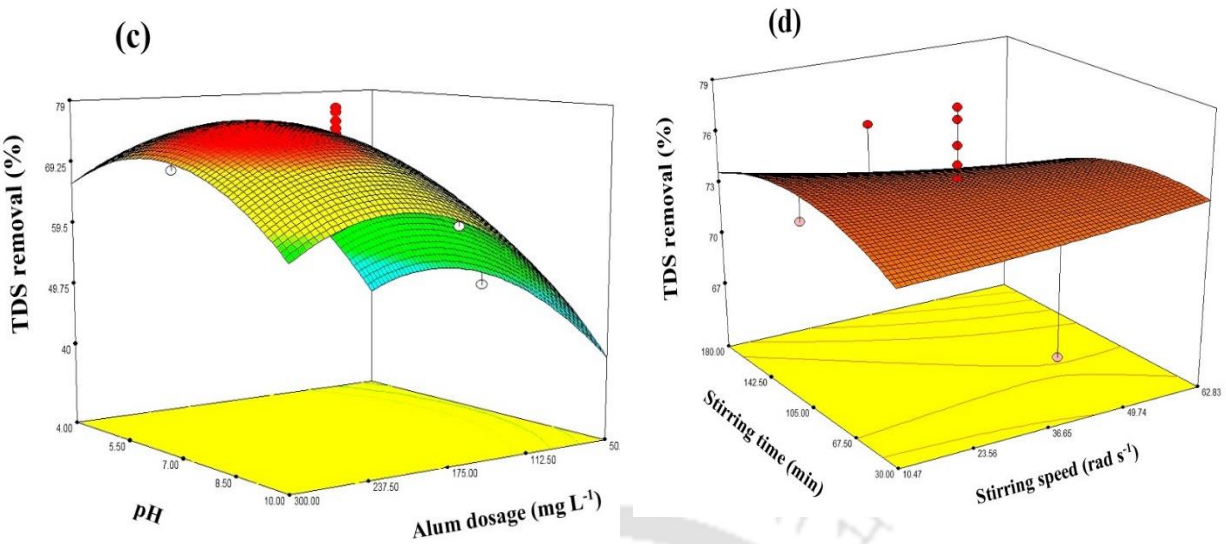

Fig. 4.2. Conjugate effects of **(a)** alum dosage (mg L^{-1}) and stirring speed (rad s^{-1}), **(b)** alum dosage (mg L^{-1}) and stirring time (min), **(c)** alum dosage (mg L^{-1}) and pH, **(d)** stirring speed (rad s^{-1}) and stirring time (min) on percentage removal (%) of TDS from effluent

Quadratic behavior of input parameters on turbidity removal from wastewater:

The effect of alum dosage on pre-treatment of tea factory effluent has been explored in terms of the reduction of turbidity (NTU) of the effluent. **Figs. 4.3 (a)-(d)** reveal the nature of the removal of turbidity at the different operating condition. The turbidity reduction profiles at different alum dosages are presented in **Figs. 4.3 (a)-(c)**. From these figures, it is evident that with the increasing alum ion, the turbidity of the effluent has been decreased gradually up to an optimum limit of the alum dosage of 200.26 mg L^{-1}. The reverse trend of the increasing of turbidity of effluent after 200.26 mg L^{-1} signifies the deterioration of treated water quality due to the high alum dosage. With the high amount of positively charged materials, the repulsive forces between the positive and negatively charged particles prevent the coagulation of organic matters resulting in the high turbidity of the water (Yadav and Kalaiyarasi, 2015). From the **Fig. 4.3 (d)**, it is found that at moderate stirring speed is a favorable criterion to generate flocks during coagulation with the process time. The optimal stirring speed of 29.11 rad s^{-1} helps to stable the flocks during pre-treatment of tea factory effluent using different alum dosages.

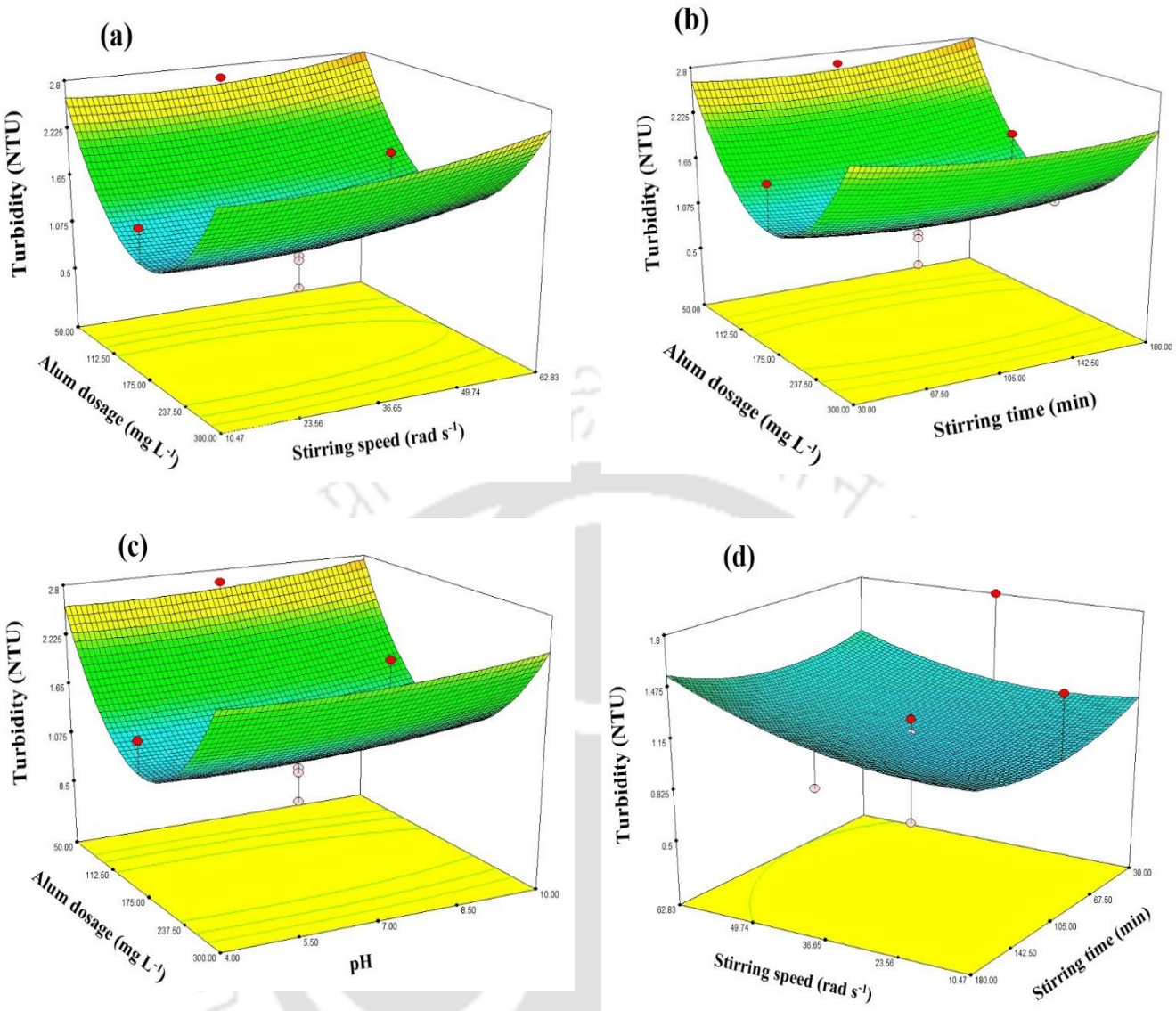

Fig. 4.3. Quadratic effects of **(a)** alum dosage (mg L^{-1}) and stirring speed (rad s^{-1}), **(b)** alum dosage (mg L^{-1}) and stirring time (min), **(c)** alum dosage (mg L^{-1}) and pH, **(d)** stirring speed (rad s^{-1}) and stirring time (min) on minimization of turbidity (NTU)

4.2.3. Variation of permeate flux with time during treatment of industrial effluent:

Figs. 4.4 (a) and **(b)** represent the permeate flux variation at a low TMP drop (ΔP, kPa) of 207 kPa and at a high TMP drop (ΔP, kPa) of 414 kPa, respectively for the various molecular weight cutoff (MWCO) membranes. With rising MWCO from 5 to 50 kDa, the permeate flux rises for all the TMP drop conditions (ΔP, kPa). The transient flux shows a preliminary steady decay across the filtration time at TMP drop (ΔP, kPa) of 414 kPa after using 5 and 10 kDa membranes. In the current study, the osmotic pressure effect is surely

irrelevant as the pulp and paper mill effluent comprises generally high molecular weight polydispersed natural organic materials (Shao et al., 2011). As a result, the permeate flux decline during the low MWCO membranes from its initial point happens due to the membrane active pore blocking during ultrafiltration. Whereas, the increase of the formation of cake layer on the membrane effective surfaces has been controlled in the presence of various membrane basket rotational speeds. In literature, minimum amount of permeate flux of 30 L m^{-2} h^{-1} with a large membrane effective area of 1.9 m^2 has been described with disk rotation of 52.36 rad s^{-1} at 600 kPa during high shear skim milk ultrafiltration earlier (Ding et al., 2003). Whereas, in the current study, in the presence of rotational speed, a higher amount of permeate flux value was achieved due to the less generation of cake layer on the membrane effective surfaces than rotating disk filtration.

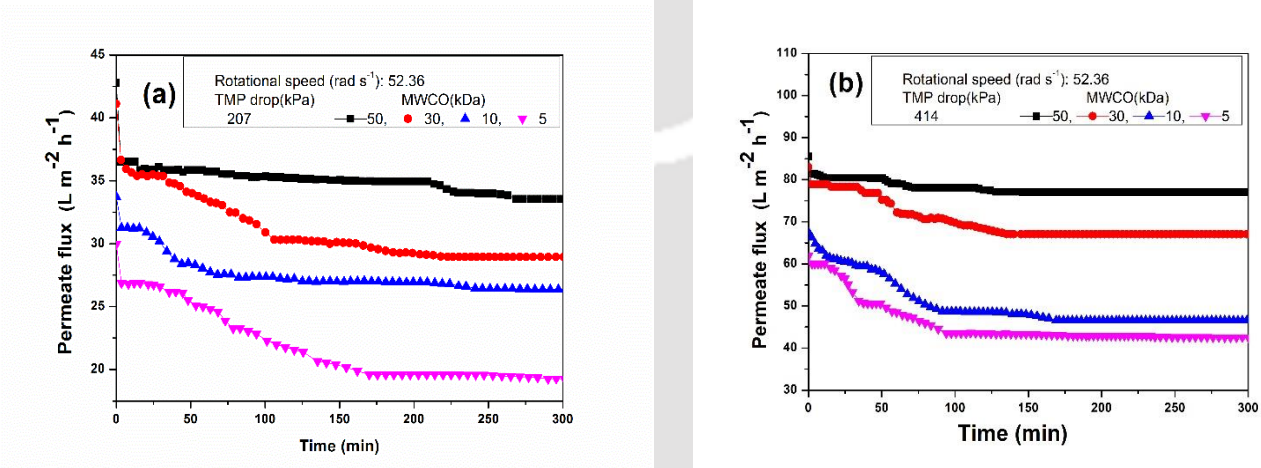

Fig. 4.4. Variation of permeate flux with respect to time at **(a)** 207 kPa and **(b)** 414 kPa for various MWCO membrane with fixed rotational speed of 52.36 rad s^{-1}

4.2.4. Analysis of permeate flux decline based on theoretical approach during the final treatment of tea factory wastewater:

TMP drops, various MWCO and a high rotational speed of membrane basket play a significant role to analyze permeate flux decline nature. **Fig. 4.5** shows the evaluation of permeate flux over ultrafiltration time for each MWCO membrane in the presence of high rotational speed. The permeate flux increases with the increasing MWCO from 5 to 50 kDa. For the same TMP drop with different MWCO, it is clear that the continuous decline of

permeate flux has been occurred at 5 and 10 kDa due to the complete pore blockage during the low MWCO membrane.

The steady state permeate flux was obtained very fast for 50 kDa membrane than others. This nature happens due to the internal pore blocking phenomena for high MWCO membrane in the presence of high membrane basket rotation of 73.36 rad s^{-1}. In the present study, a vortex-like circulation due to the membrane arm rotation reduces the deposition of rejected solutes on the active membrane surfaces. As a result, concentration polarization is insignificant due to the rotation (Sarkar et al., 2012). The adsorption of small solutes in to the membrane pore walls must be the dominating nature to decline the permeate flux for high MWCO membranes (30 and 50 kDa).

The nature of the flux decline can also be observed during theoretical model analysis using ANN with good regression (R^2) values throughout the ultrafiltration process time for all the cases. The ANN model prediction is represented in the same figure with the straight line. To avoid the complexity, one intermediate layer has been studied during the theoretical prediction of permeate flux decline (Baguena et al., 2016). A statistical analysis of variance has been tabulated in the **Table 4.3** to identify the best model prediction using ANN. The high F-value with very low p-value for each case indicates that the theoretical prediction for the design variables are adequate. Only 0.76% mean square error has been found with perfect regression for the MWCO membrane of 50 kDa. Not only that, the low p-value also indicates that the model is statistically significant.

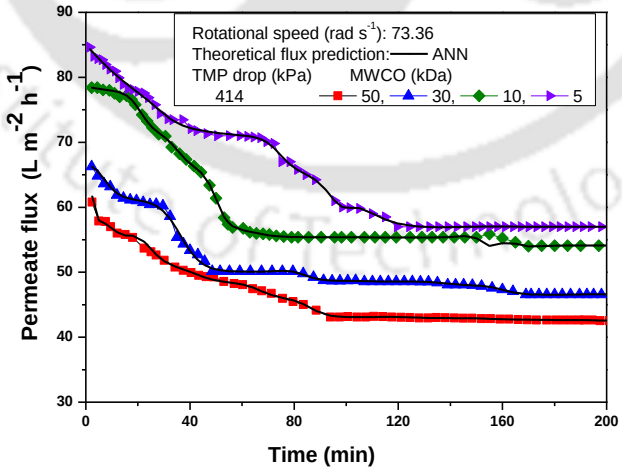

Fig. 4.5. Variation of permeate flux with respect to time for various MWCO membrane with fixed rotational speed of 73.36 rad s^{-1}

Table 4.3. Analysis of variance for permeate flux

MWCO (kDa)	Sum of square	Degrees of freedom	Mean square error (MSE)	F-value	p-value	Total error	Regression R^2
5	50.6	52	0.03	375.38	0.0004	0.508	0.99
10	36.65	52	0.16	249.5	0.0005	0.74	0.99
30	10.94	52	0.10	216.1	0.0002	0.54	0.99
50	39.77	52	0.002	324.58	0.0002	0.12	0.99

4.2.5. Analysis of permeate flux decline using modified Hermia's irreversible pore clogging method:

Figs. 4.6 (a)-(d) reveal the basics of pore blocking mechanisms as well as cake layer formation using various MWCO membranes with a fixed TMP drop (ΔP, kPa) and basket rotational speed. The curve fitting for the experimental data to the complete pore blocking model (CPBM) has been demonstrated in **Fig. 4.6 (a)**. The final k_c values of the complete pore blocking model (CPBM) have been listed in **Table 4.4**. High slope decay has been found at high for the 5 and 10 kDa membranes. Whereas, for high MWCO membranes, like, 30 and 50 kDa membranes, the slope decline behavior is marginal than others. **Fig. 4.6 (b)** illustrates the good model fitting of experimental data to the standard pore blocking mechanisms (SPBM) due to the continuous solute adsorption on the membrane active surfaces. The SPBM shows good agreement with experimental results with 0.97 R^2 for 5, 10 and 30 kDa MWCO membranes. **Fig. 4.6 (c)** delivers the theoretical analysis of the experimental data to the intermediate pore blocking mechanisms (IPBM) for different MWCO membranes. As shown in **Fig. 4.6**, the IPBM fits the experimental results at a very early stage of filtration. This mechanism shows that SPBM as well as IPBM are mainly the dominating factor during the present study (Vela et al., 2008). **Fig. 4.6 (d)** shows the fitting of the cake layer model (CFM) during spinning basket membrane ultrafiltration for various MWCO membranes at constant membrane basket rotational speeds (ω, rad s^{-1}) and TMP drop of 414 kPa. The predicted R^2 values with experiments are not accurate for all the MWCO membranes due to control over the faster deposition of rejected molecules on the membrane surfaces.

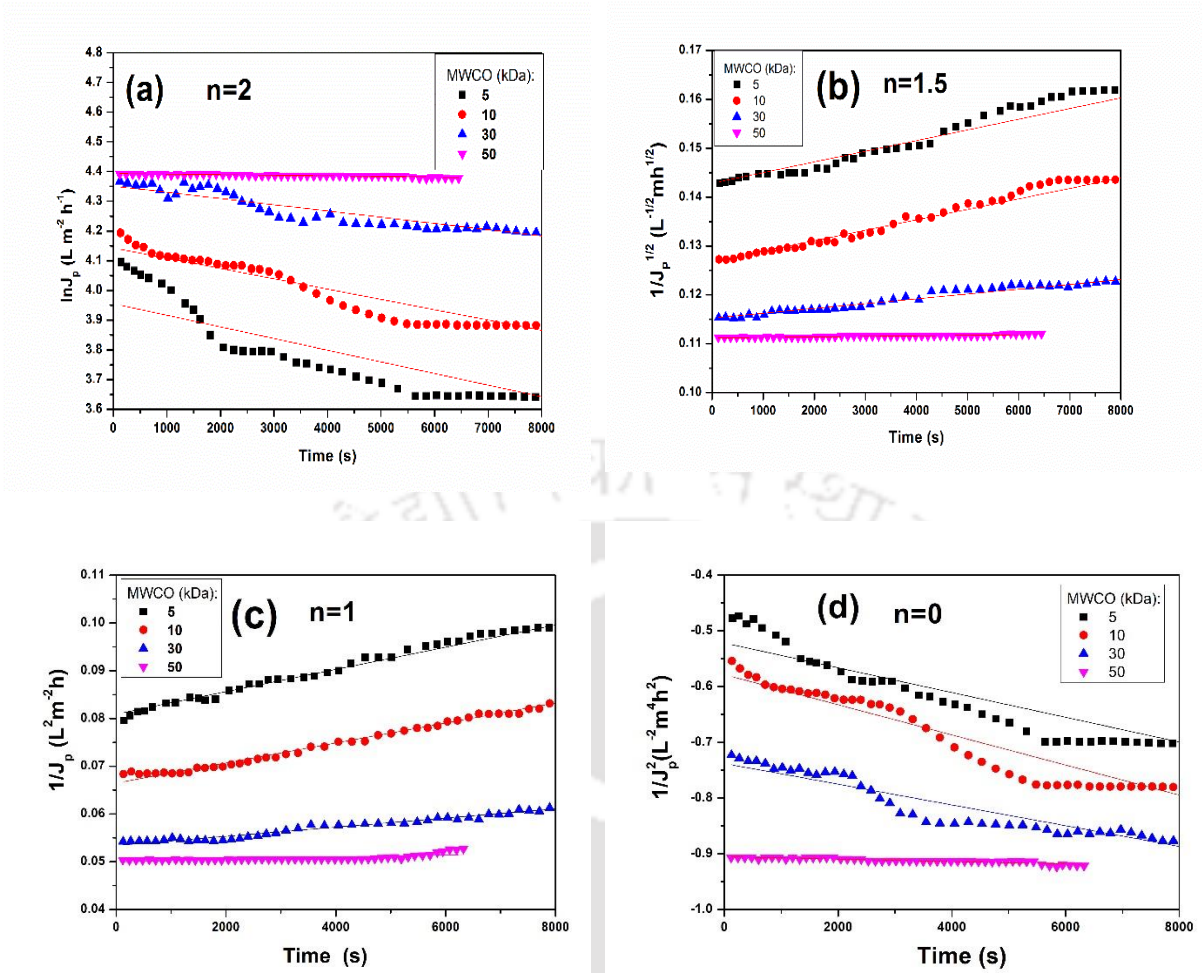

Fig. 4.6. Linearized fitness plots for Hermia's pore block models (CPBM **(a)**, SPBM **(b)**, IPBM **(c)**, and CFM **(d)**) for different MWCO at constant rotational speed and TMP drop of 52.36 rad s^{-1} and 207 kPa, respectively

Table 4.4. Summary of the model parameters of all pore blocking models during ultrafiltration of paper industry effluent using various MWCO membranes at constant rotational speed and TMP drop of 52.36 rad s^{-1} and 207 kPa respectively

MWCO (kDa)	CPBM			SPBM			IPBM			CFM		
	$k_f \times 10^5$ (s^{-1})	Residual sum of squares	R^2	$k_s \times 10^6$ ($m^{-1/2}\ s^{-1/2}$)	Residual sum of square $\times 10^5$	R^2	$k_i \times 10^6$ (m^{-1})	Residual sum of square $\times 10^5$	R^2	$k_{cl} \times 10^7$ ($m^{-2}s$)	Residual sum of square	R^2
5	3.91	0.25	0.87	2.18	18.3	0.97	2.33	2.85	0.99	2.21	0.043	0.85
10	3.47	0.06	0.91	2.13	5.87	0.97	2.09	1.59	0.99	2.7	0.029	0.91
30	2.09	0.02	0.89	0.97	1.38	0.97	0.96	0.97	0.98	1.86	0.014	0.91
50	2.01	0.001	0.83	0.12	0.05	0.90	0.24	0.53	0.95	0.22	0.0002	0.82

The mechanism of permeate flux decline during tea factory effluent treatment using modified Hermia's pore blocking method:

The permeate flux decline behavior at high speed rotation (73.34 rad s^{-1}) and a high TMP drop (414 kPa) was analyzed using modified Hermia's pore clogging methodology. **Figs. 4.7 (a)-(d)** display various reversible and irreversible pore blocking nature using different MWCO membranes with high TMP drop and rotational speed. The curve fitting for the experimental data to the CPBM has been displayed in **Fig. 4.7 (a)**. The final k_c values for all the fouling models have been presented in **Table 4.5**. The regression (R^2) coefficients for all the cases has been enlisted in the **Table 4.6**. At a close observation, it is found that the membrane pores are blocked completely for the very beginning of the filtration. The good R^2 values for the low MWCO membranes (5 and 10 kDa) reveal that the permeate flux declines gradually for the low MWCO due to the complete pore clogging nature at the initial stage of filtration. The theoretical pore clogging prediction for CPBM is not significant at the final stage of the filtration due to the high speed rotation. Still, a gradually decreasing of the permeate flux value has been found with the filtration time due to the irreversible internal pore blocking behavior. From the **Fig. 4.7 (b)**, it is found that the standard pore blocking mechanism signifies the perfect model fitting at the initial stage of filtration. Whereas, intermediate model estimates (**Fig. 4.7 (c)**) the decline of the permeate flux with the significant model fitting at the final stage of filtration due to the severe solute adsorption in to the membrane active pore walls. According to the maximum value of R^2, it can be revealed that the standard pore blocking mechanism dominates the nature of the permeate flux decline at the beginning of the filtration. Whereas, internal pore clogging performance reveals its leading nature at the later stage of the ultrafiltration process. **Fig. 4.7 (d)** displays the fitting of the cake layer formation for different MWCO membranes at a high basket rotation of 73.36 rad s^{-1} and TMP drop of 414 kPa. The predicted R^2 values with experiments are not significant for all the MWCO membranes due to control over the faster deposition of rejected molecules on the membrane surfaces.

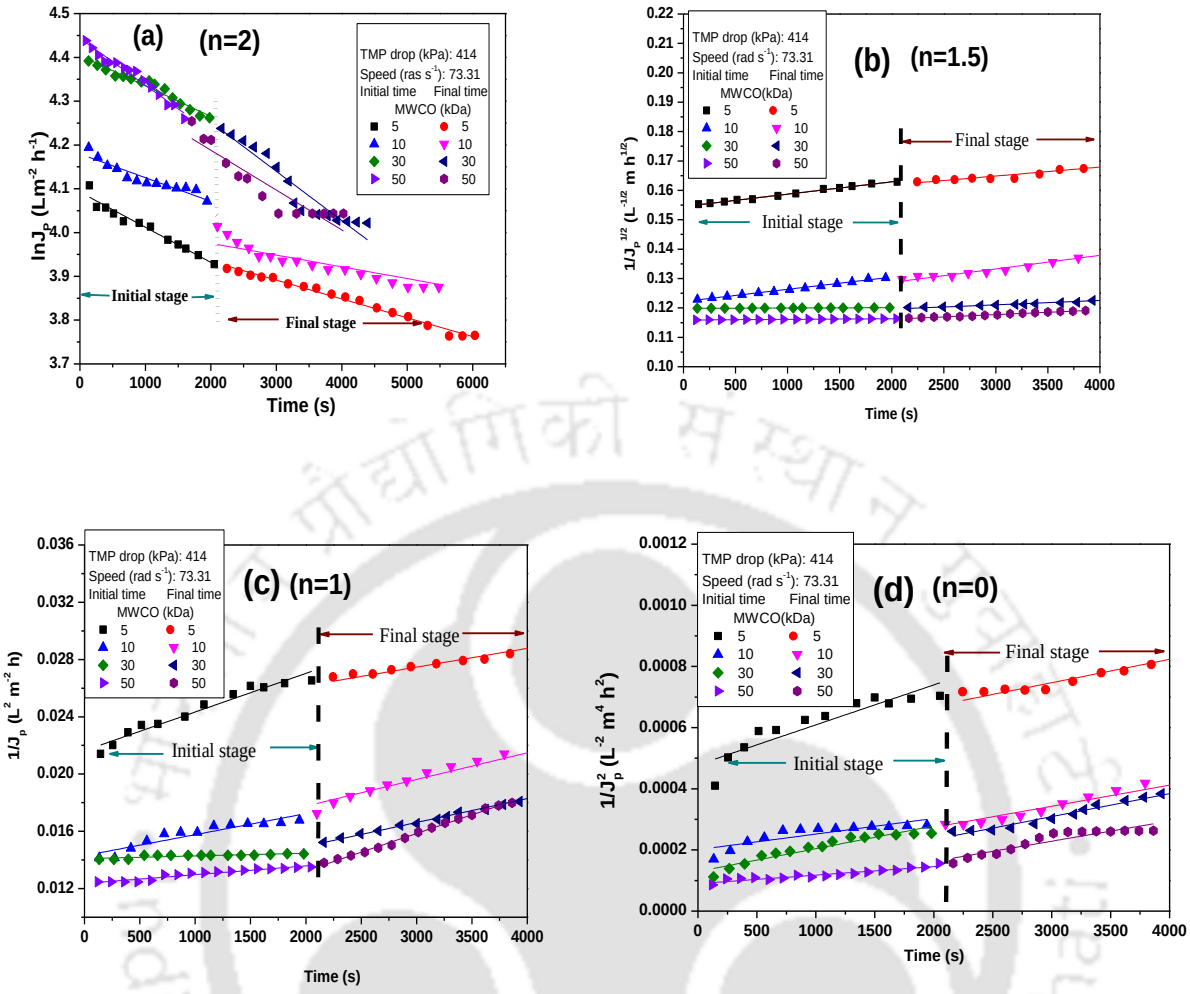

Fig. 4.7. Modified Hermia's pore blocking model fitness during treatment of tea factory wastewater (CPBM **(a)**, SPBM **(b)**, IPBM **(c)**, and CFM **(d)**) for different MWCO at constant rotational speed and TMP drop of 73.34 rad s^{-1} and 414 kPa, respectively

Table 4.5. Summary of the model parameters of all pore blocking models using various MWCO membranes at constant rotational speed and TMP drop of 73.36 rad s^{-1} and 414 kPa, respectively

MWCO (kDa)	CPBM		SPBM		IPBM		CFM	
	$k_f \times 10^5$ (s^{-1})	Residual sum of square $\times 10^3$	$k_s \times 10^6$ ($m^{-1/2}$ $s^{-1/2}$))	Residual sum of square $\times 10^7$	$k_{cf} \times 10^6$ (m^{-1})	Residual sum of square $\times 10^6$	$k_{cl} \times 10^7$ ($m^{-2}s$)	Residual sum of square $\times 10^8$
5	8.03	1.23	1.66	3.98	1.06	1.54	1.31	1.49
10	5.41	1.48	1.57	4.09	1.04	1.29	0.58	0.39
30	6.95	0.98	2.38	0.007	1.09	0.076	0.81	0.59
50	10.07	1.02	3.73	0.02	1.20	0.163	0.56	0.23

Table 4.6. Summary of the regression (R^2) coefficients of all pore blocking models

MWCO (kDa)	CPBM		SPBM		IPBM		CFM	
	Initial stage	Final stage	Initial stage	Final stage	Initial stage	Final stage	Initial stage	Final stage
5	0.95	0.98	0.99	0.97	0.92	0.98	0.82	0.97
10	0.88	0.92	0.99	0.96	0.90	0.98	0.71	0.94
30	0.95	0.90	0.99	0.95	0.90	0.99	0.83	0.97
50	0.97	0.85	0.99	0.95	0.92	0.99	0.88	0.85

4.2.6. Variation of observed rejection with rotational speed for MWCO membranes:

To evaluate the influence of rotational speed on solute rejection during paper industry effluent treatment, the experiment was carried out at different arm rotation (ω) as 10.47, 31.41, 52.36 and 73.30 rad s^{-1}. The results have been displayed in **Fig. 4.8 (a)**. In **Fig. A1** in the appendix, it is clearly observed that with the increasing pressure drop at a fixed ω (52.36 rad s^{-1}), solute particle rejection improves in terms of COD removal for all the different MWCO. Natural organic substances found from paper industrial effluents are the mixture of high and low molecular weight organic compounds. The contribution of the smaller particles gives lower rejection during high MWCO membrane ultrafiltration, like, 50 kDa. However, with the increasing TMP drop from 207 to 414 kPa during ultrafiltration, conductivity decreases from 2.1 to 1.05 S m^{-1}. Whereas, the initial ionic conductivity of the feed stream was 4.57 S m^{-1}. On the other side, the impact of the rotational speed on the removal of polyphenols from the pre-treated effluent has been demonstrated in the **Fig. 4.8 (b)**. Two different types of rejection stages have been observed by the varying arm rotation from 10.47 to 73.30 rad s^{-1}. With the increasing membrane basket rotation from 10.47 to 52.36 rad s^{-1}, the removal of polyphenols increases for all the MWCO membranes and TMP drops. Due to the high-speed rotation, some solutes may collide with other particles and creates very small particles in size. These small particles contribute a little decline of the rejection curve at the high rotation of the membrane basket. This criterion has been shown as the saturation stage of the solute rejection in the following figure. It is clear that optimal rotational speed can be chosen as 52.36 rad s^{-1} for the rejection of solute particles for all the parametric conditions. Based on the published information, it is revealed that near about 82% COD removal was achieved using consecutive aerobic and anaerobic bioreactor to treat pulp and paper mill effluent (Singh and Thakur, 2006). On the other side, 80-85% COD removal was reported using polyethersulfone/ functionalized multi-walled carbon nanotubes based nanocomposite membranes for the treatment of paper mill effluent

(Saranya et al., 2014). In the present study almost 98% removal of COD was observed in the presence of rotational speed of 52.36 rad s^{-1}. Whereas, 91% removal of materials was reported using the electrochemical process to treat tea factory effluent (Justin et al. 2009). However, only 78% removal of organic components in terms of chemical oxygen demand was obtained during polyaluminum ferric chloride coagulation-ceramic membrane ultrafiltration of tea industry wastewater (Chen et al., 2015). In the presence of rotational speed, the induced shear rate forces the particles away from the membrane active side to the feed side. As a result, an increasing rejection kinetics has been found with the increasing of TMP drop in the presence of membrane basket rotation.

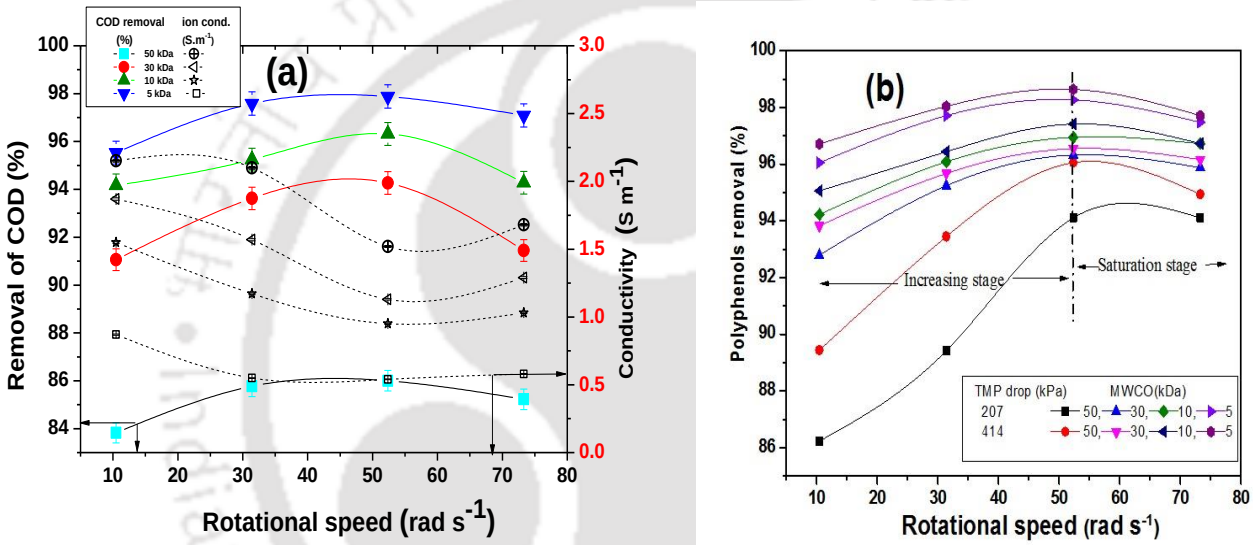

Fig. 4.8. Variation of observed rejection based on **(a)** COD removal during paper industry wastewater treatment and the **(b)** percentage removal of polyphenols from tea factory effluent for different MWCO membranes with respect to different rotational speeds

4.2.7. Variation of J_{exp} with J_{cal} using different diffusion models for shear-induced filtration:

Three diffusion models, namely, rotational diffusion, shear-induced diffusion, and Brownian diffusion models are analyzed and represented in **Fig. 4.9**. J_{exp}/ J_{cal} for rotational and shear-induced diffusion are very close to the diagonal line due to the high solute-solute transmission in the presence of continuous membrane basket rotation. During rotational diffusion, the ratio of the experimental and calculated permeate flux values are in the range

of 0.99 to 1.05 for each TMP drop. The statistical analysis for the experimental and calculated permeate flux reveals the significant model term with high correlation coefficient (R^2) values of 0.98 and 0.99 for the rotational and shear-induced diffusion model, respectively. The low residual sum of square of 1.63 and 3.07 for the rotational and shear-induced diffusion model, respectively conferred that these two models were suitable in the present study. Whereas, a comparatively high residual sum of square (11.64) and the low R^2 (0.80) reveals the insignificant model prediction for the Brownian diffusion model. With continuous rotation, some small particles can appear in permeate sides through shear-induced diffusion. The share-induced and the rotational diffusion models are related to the spinning basket membrane rotation. These models correspond to random contact between two particles in the present of rotational speed which intensify random displacement of the particles within feed stream as well as on the membrane surface. This phenomenon has been observed during the treatment of the industrial effluents using spinning basket membrane module. Whereas, Brownian diffusion model describes the diffusional restriction made by accumulation of soluble molecules near the membrane surface. Brownian diffusion model provides a significant transport mechanism for the considerable small particles present in the solution. The particle size analysis of the sample has been shown in **Fig. A3** in the appendix. The standard error analysis is presented in the **Table A3** in the appendix. The cumulative diameter of the particles present in the effluent has been reduced from 3469.2 to 647.7 nm. The size of the particles is found greater than 0.1 μm. From literature, it is clear that Brownian diffusion coefficient is inversely proportional to particle size (Singh and Das, 2014). Thus, the predicted permeate flux using Brownian diffusion model deviates more from the experimental permeate flux values.

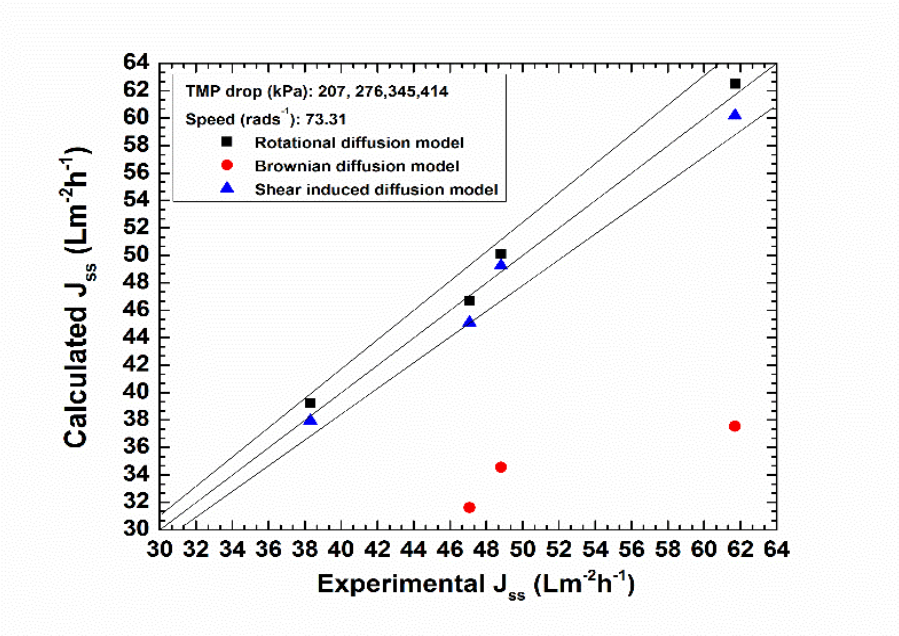

Fig. 4.9. Variation of J_{exp} with J_{cal} using rotational, shear-induced and Brownian diffusion models for high rotational speed of 73.31 rad s^{-1}

4.2.8. Optimization study of permeate flux variation and permeate quality:

According to design expert software, the regression analysis has been employed to fit the responses. As suggested by the said software, no transformation was applied for this study. Quadratic models have been recommended to analyze the data for three responses. Eqs. (4.4-4.6) represent the final regression function to estimate the permeate flux (L m^{-2} h^{-1}), the ionic conductivity of collected permeate (S m^{-1}) and % removal of TDS (%), respectively. The coded factors are described below:

Permeate flux model (L m^{-2} h^{-1}) model:

$$R_1 = 69.98 + 13.21\times A_2 + 20.07\times B_2 + 4.00\times C_2 + 7.07\times(A_2\times B_2) - 4.00\times10^{-3}\times(A_2\times C_2) + 0.99\times(B_2\times C_2) - 9.14\times A_2^{\,2} - 1.88\times B_2^{\,2} + 4.60\times C_2^{\,2} \quad (4.4)$$

Ionic conductivity decreasing (S m^{-1}) model:

$$R_2 = 76.00\times10^{-3} - 18.00\times10^{-3}\times A_2 - 45.00\times10^{-3}\times B_2 - 26.00\times10^{-3}\times C_2 - 2.38\times10^{-3}\times(A_2\times B_2) - 2.38\times10^{-3}\times(A_2\times C_2) - 24.00\times10^{-3}\times(B_2\times C_2) + 46.00\times10^{-3}\times A_2^{\,2} + 46.00\times10^{-3}\times B_2^{\,2} + 14.00\times10^{-3}\times C_2^{\,2} \quad (4.5)$$

Percentage removal of TDS (%) model:

$$R_3 = 97.47 + 0.40\times A_2 + 0.90\times B_2 + 0.56\times C_2 + 0.04\times(A_2\times B_2) + 0.09\times(A_2\times C_2) + 0.41\times(B_2\times C_2) - 0.86\times A_2^{\,2} - 0.76\times B_2^{\,2} - 0.39\times C_2^{\,2} \quad (4.6)$$

The relationship between the independent and dependent parameters was developed with the help of a quadratic polynomial second order model which are represented in Eq. (4.4)

to Eq. (4.6). These equations reveal the presence of the quadratic effects of the independent variable on the dependent one. As a result, it is appropriate to name the effects as quadratic effects. Analysis of variances for all the three responses has been displayed in the **Table 4.7**. A higher value of R^2 is always favorable. The measurement of the signal to noise ratio has been decided by adequate precision and a value greater than 4 is desired. The high correlation values refer good fitting of experimental data to suggest a simulated equation based model.

Design Expert Software has been performed to optimize all three responses during treatment of waste effluent. According to the software, the analyzed optimum condition is as follows: TMP drop: "350.61 kPa"; rotational speed: "600 rpm (62.83 rad s^{-1})"; retentate flow rate: "2 L min^{-1}". The predicted values of permeate flux, ionic conductivity and percentage removal of TDS are 87.9 L m^{-2} h^{-1}, 0.81 S m^{-1}, and 97.42 %, respectively. The three-dimensional desirability function diagram of the optimized condition is shown in **Fig. A4** in the appendix.

Table 4.7. Analysis of variance (ANOVA) results for response parameters

Response	Model F value	Prob >F	R^2	Adjusted R^2	Predicted R^2	Adequate Precision
Permeate flux (L m^{-2} h^{-1})	49.95	<0.0001	0.98	0.96	0.89	27.36
Ionic conductivity (S m^{-1})	46.47	<0.0001	0.98	0.96	0.81	18.61
Removal of TDS (%)	76.41	<0.0001	0.99	0.97	0.81	25.48

4.2.9. Combined effects of TMP drop, rotational speed, and retentate flow rate on permeate flux:

Figs. 4.10 (a), **(b)**, and **(c)** represent the three-dimensional response surface analyzed diagram of the combined effect of (a) TMP drop and rotational speed, (b) TMP drop and retentate flow rate, (c) rotational speed and retentate flow rate, respectively. From **Fig. 4.10 (a)**, it is clear that at constant retentate flow rate, with an increase of rotational speed from 100 to 700 rpm (10.47 to 73.30 rad s^{-1}), permeate flux value increases when TMP drops was fixed. The maximum permeate flux has been found for the maximum rotational speed of 700 rpm (73.31 rad s^{-1}) with 414 kPa TMP drop. With increasing rotational speed, permeate flux has been increased during SBMM ultrafiltration. In **Fig. 4.10 (b)**, with the increase of retentate flow rate from 1 to 4 Lmin^{-1} at a constant rotational speed of 400 rpm

(41.89 rad s^{-1}), permeate flux value increases from 46 to 55.75 L m^{-2} h^{-1} when the TMP drop is 207 kPa. While during the high TMP drop of 414 kPa, the rate of increment of permeate flux value is nominal (70 to 85.5 L m^{-2} h^{-1}). The less interactive effects of the retentate flow rate with TMP drop and rotational speed have been noticed on the increment of permeate flux during the SBMM ultrafiltration process.

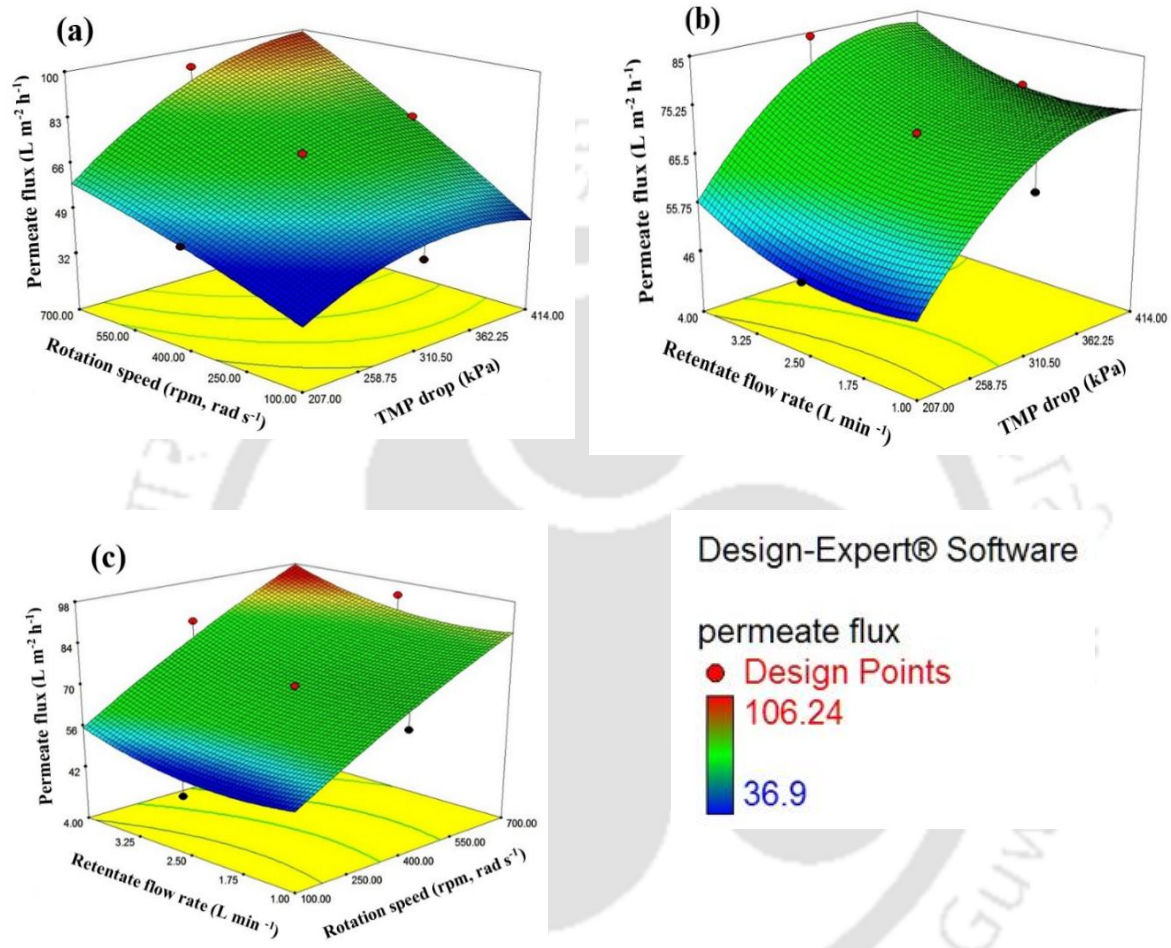

Fig. 4.10. Combined effects of **(a)** TMP drop and rotational speed at constant retentate flow rate of 2.50 L min^{-1}, **(b)** TMP drop and retentate flow rate at constant rotational speed of 400 rpm (41.89 rad s^{-1}), **(c)** rotational speed and retentate flow rate at constant TMP drop of 310 kPa on the permeate flux

4.2.10. Quadratic effects of TMP drop, rotational speed, and retentate flow rate on ionic conductivity for collected permeate:

Fig. 4.11 (a) reveals the impact of TMP drop and rotational speed on the decreasing of ionic conductivity in permeate. At a constant retentate flow rate of 2.50 L min^{-1}, with increasing basket rotation speed from 100 to 400 rpm (10.47 to 41.89 rad s^{-1}), ionic

conductivities of collected permeate decreases from 0.185 to 0.165 S m^{-1}. When the rotation is high (700 rpm or 73.31 rad s^{-1}), the value of ionic conductivity again increases due to the small particle diffusion. The same trend has been found with increasing TMP drop from 207 to 414 kPa. The combined impact of TMP drop and retentate flow rate with fixed rotational speed has been displayed in **Fig. 4.11 (b)**. In **Fig. 4.11 (c)**, with the constant TMP drop of 310 kPa, the decreasing rate of ionic conductivity is high after changing rotational speed from 100 to 700 rpm (10.47 to 73.30 rad s^{-1}). Whereas, the marginal effect has been observed during changing the retentate flow rate from 1 to 4 L min^{-1}.

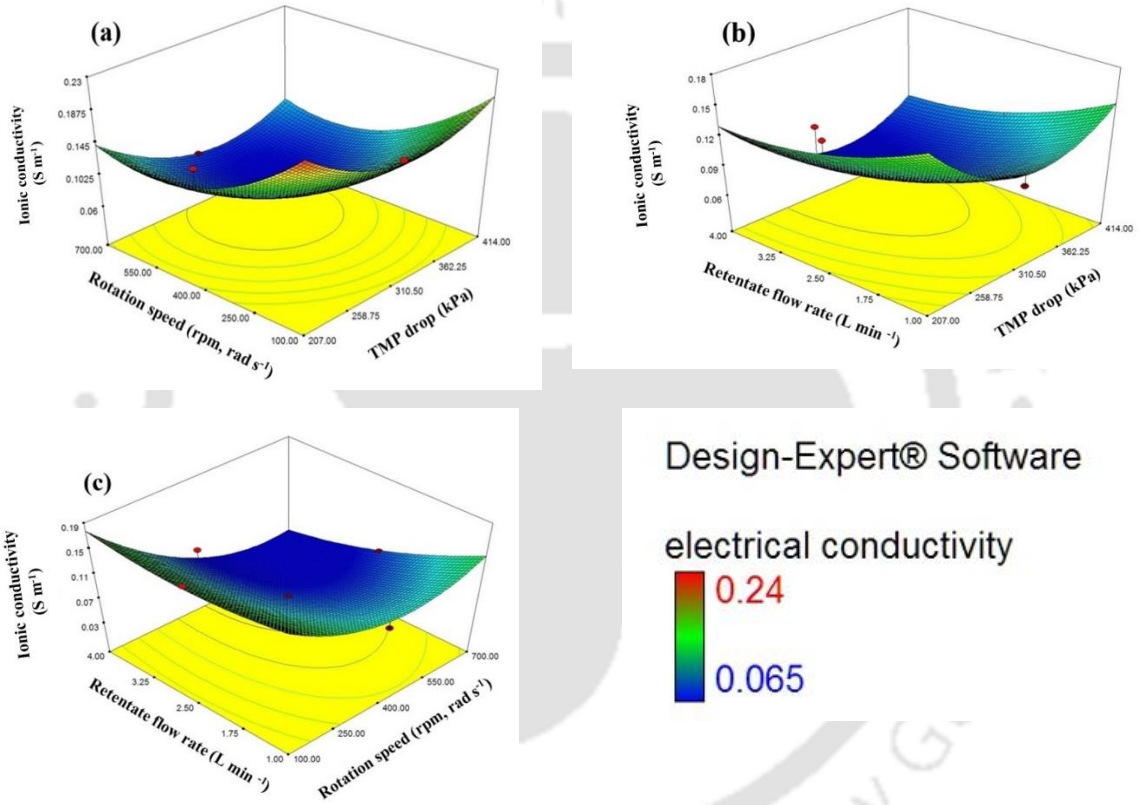

Fig. 4.11. Combined effects of **(a)** TMP drop and rotational speed at constant retentate flow rate of 2.50 L min^{-1}, **(b)** TMP drop and retentate flow rate at constant rotational speed of 400 rpm (41.89 rad s^{-1}), **(c)** rotational speed and retentate flow rate at constant TMP drop of 310 kPa on the ionic conductivity of collected permeate

4.2.11. Analysis of quadratic effects of TMP drop, rotational speed, and retentate flow rate on percentage removal of TDS from permeate:

The relationship between input parameters (TMP drop, rotational speed, and retentate flow rate) and the desired response, such as, percentage removal of TDS from collected permeates are represented in **Fig. 4.12**, based on mathematical analysis of the experimental

data. The nonlinear effect has been observed. High percentage removal of TDS is obtained with the increasing rotational speed of membrane basket. It is also observed from **Fig. 4.12 (a)** that after a certain point, with the increase of rotation, TDS removal decreases. This phenomenon occurs due to the high collision of particles in the presence of high rotation. **Fig. 4.12 (b)** and **(c)** represent the three-dimensional response surface diagram of the combined effect of TMP drop with retentate flow rate and rotational speed with retentate flow rate, respectively. When the rotational speed is constant in Fig. 8b, the removal rate of TDS is almost linear with the changing retentate flow rate at low TMP drop of 207 kPa.

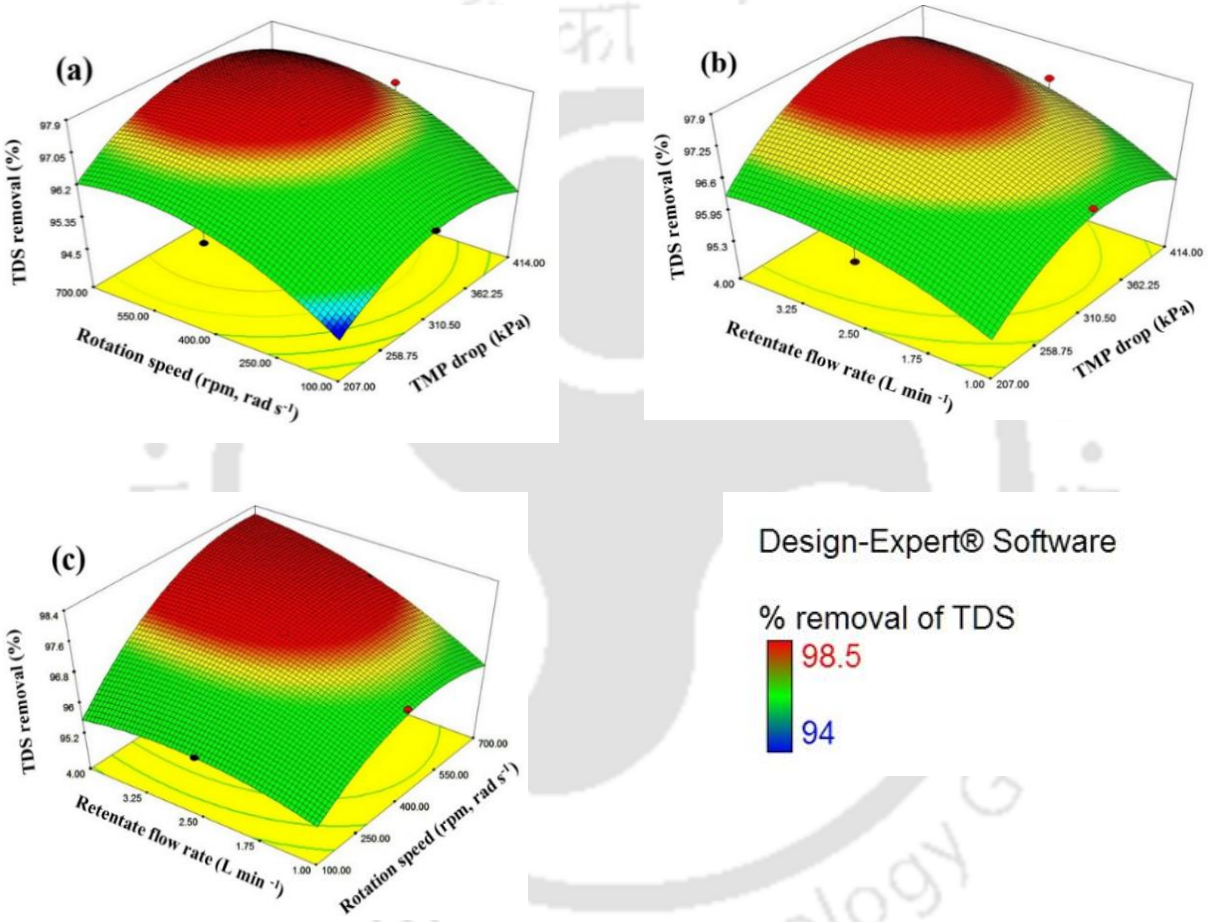

Fig. 4.12. Combined effects of **(a)** TMP drop and Rotational speed at constant retentate flow rate of 2.50 L min^{-1}, **(b)** TMP drop and retentate flow rate at constant rotational speed of 400 rpm (41.89 rad s^{-1}), **(c)** rotational speed and retentate flow rate at constant TMP drop of 310 kPa on the percentage (%) removal of TDS from collected permeate

4.2.12. Study on total power consumption:

For the evaluation of the shear-induced module, it is necessary to calculate the energy consumption during filtration. The total power requirement has been calculated by energy consumed per unit volume. The maximum power supply was found as 0.32 kW after

applying maximum TMP drop and ω of 414 kPa and 73.3 rad s^{-1}, respectively. Whereas, maximum power consumption of 0.5 kW was reported during treatment of high shear skim milk using rotating disk filtration (Ding et al., 2003). Though the dynamically induced membrane filtration consumes high energy with increasing shear rate, comparatively low consumption of power has been found during SBMM ultrafiltration.

4.3. Characterization of rejected materials of paper industry wastewater using different techniques:

The characterization of dissolved organic materials found in paper industry wastewater was done after collecting the rejected components of ultrafiltration based on different techniques, like, Fourier Transform Infrared (FTIR), energy dispersive X-ray spectra, thermo gravimetric analysis. **Fig. 4.13** represents the FTIR analysis of natural materials during treatment of paper mill effluent. The wide adsorption band at 3200-3400 cm^{-1} indicates the presence of intermolecular O-H stretching in the materials (Zhang et al., 2011). The sharp peaks at 2870 and 2955 cm^{-1} are on behalf of the asymmetric and symmetric stretching of aliphatic (-C-H) groups, respectively. The strength of these peaks reveal that the paper mill effluent comprises more aliphatic compounds (Li et al., 2011). Two different peaks around 3209 and 3385 cm^{-1} show the presence of phenolic compounds (O-H stretching) and amides groups (N-H stretching), respectively. The sharp peak around 2390 cm^{-1} gives the indication of the C=O group. The asymmetric stretching of unsaturated carbons (C=C=C) occurs around 1806 cm^{-1} which indicates that the natural compounds found in paper mill wastewater contains unsaturated carbon components. The unsaturated carbons are the result of the degradation of lignin compounds. The peaks around 1630–1660 cm^{-1} are the responsible for the substituted or unsubstituted stretching of amide groups (C=O), and the -NH deformation occurs at 1510-1560 cm^{-1} (Xiaoli et al., 2007). The peak at 1587 cm^{-1} indicates the presence of aromatics (C-H stretching). The strong peaks at 1395 and1412 cm^{-1} are attributed to the stretching of COO^{-1} asymmetric stretching and aromatic C=C vibrations, respectively (Li et al., 2011). The peak around 1240 cm^{-1} indicates the presence of carboxylic acids (C-O stretching), alcohols (OH deformation), esters, and ethers groups (Xiaoli et al., 2007; Zhang et al., 2011). Another peak around 1012 cm^{-1}indicates the strong presence of the cyclic ether group. The bands appeared at 468-627, 720, 872 cm^{-1} can be attributed to halide groups, alkenes (=C-H bending) and N-

H bending of amines groups, respectively. Among all, some major groups are displayed in the **Table 4.8**.

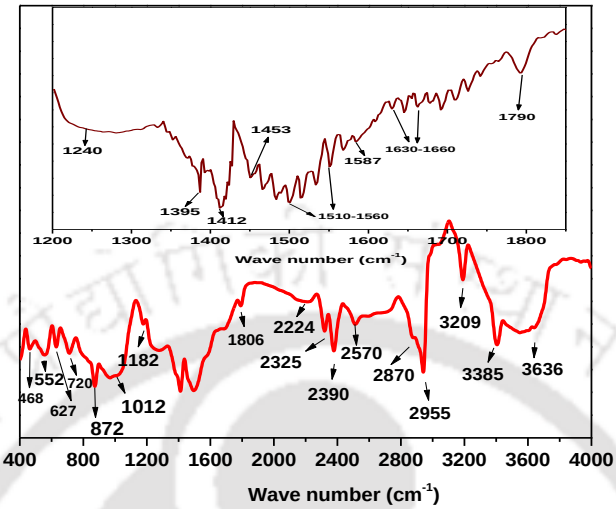

Fig. 4.13. Fourier Transform Infrared (FTIR) spectra of rejected materials of spinning basket membrane ultrafiltration of paper industry effluent

Table 4.8. Functional groups identification in FTIR spectra

Groups	Peak position (cm^{-1})	Source of bond
-C-H (aliphatic)	2870-2955	Alkanes
-N-H stretching	3385	Amides
O-H stretching	3209, 3636	Phenolic compounds, Intermolecular H_2O
C=O bend	2325-2390	Ketones
C=C=C	1806	Unsaturated carbons
-C-H	1587	Aromatics
C=O	1630-1660	Unsubstituted stretching of amide groups carbon
C=C	1412	Aromatic carbon
COO^{-1} asymmetric stretching	1395	Carboxyl group
O-H	1240	Alcohol, esters
N-H bending	872	Amines
=C-H	720	Alkenes

The morphology structure and the variation of the elemental composition of rejected materials are shown in the **Fig. 4.14 (a)** and **(b)**, respectively using an Energy-dispersive X-ray spectroscopic(EDX). The various metal compounds, like, zinc, sodium, manganese, iron, potassium etc. with different weight percentages have been detected in the organic

mixture separated from paper industrial effluent. Apart from metals, nitrogen, sulphur, chlorinated compounds are also present in this complex mixture. The maximum weight percentages of carbon and oxygen are specified that this organic mixture has a significant amount of carbon source which can be compared to humic like materials.

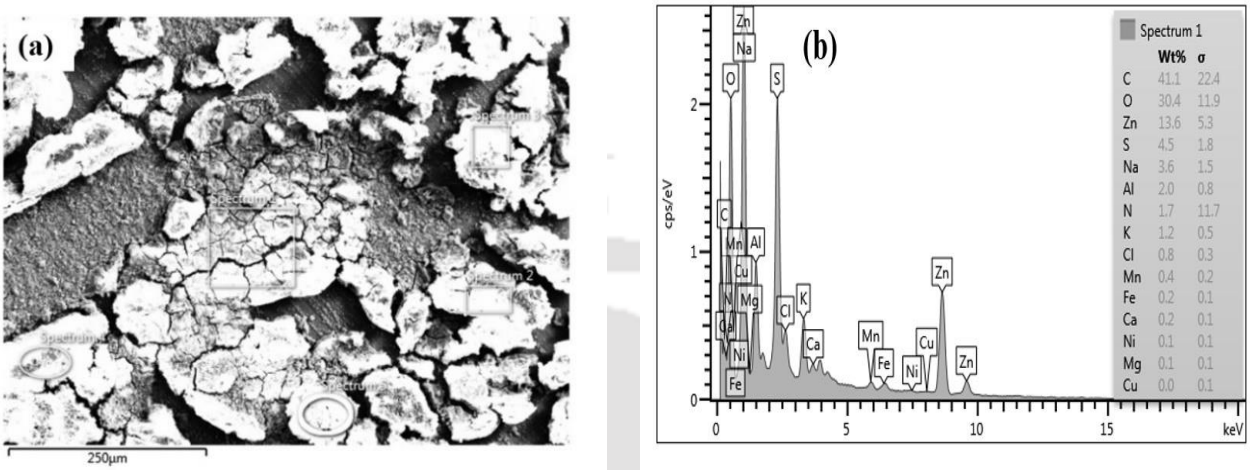

Fig. 4.14. EDX analysis of rejected materials of spinning basket membrane ultrafiltration of paper industry effluent, **(a)** morphology and **(b)** variation of the elemental composition

Fig. 4.15 displays the thermal gravimetric (TG) and the corresponding differential thermo gravimetric (DTG) analysis of rejected materials during ultrafiltration of paper industry waste effluents. The continuous decreasing curve reveals the thermal degradation of various organic compounds present in rejected materials. The first mass loss after 50°C and up to 110°C for the evaporation of water molecules present in the organic materials. The next steady weight loss has been appeared from 110 to 400°C due to the degradation of carboxyl groups, carbonyl compounds, alcoholic groups, and also aliphatic components. These complex materials After 400°C, the mass losses of this organic compounds were happened near 450°C for the degradation of nitrogen containing compounds (Zhang et al., 2011). The degradation of long chain hydrocarbons was occurred after 400°C and it continued up to 500°C. However, according to previous literature, due to the continuous raising of temperature, the condensation of the long aliphatic component was happened which can form an aromatic structure during the thermal degradation of these complex materials (Zhang et al., 2011). As a result, after 500°C, the rate of degradation was found slow due to the formation of cyclic compounds. These materials were degraded after 600°C. The thermal degradation analysis confirms that there were a huge number of long chain

hydrocarbons and nitrogen containing components present in the paper industry waste effluents which has been removed using ultrafiltration (Li et al., 2011).

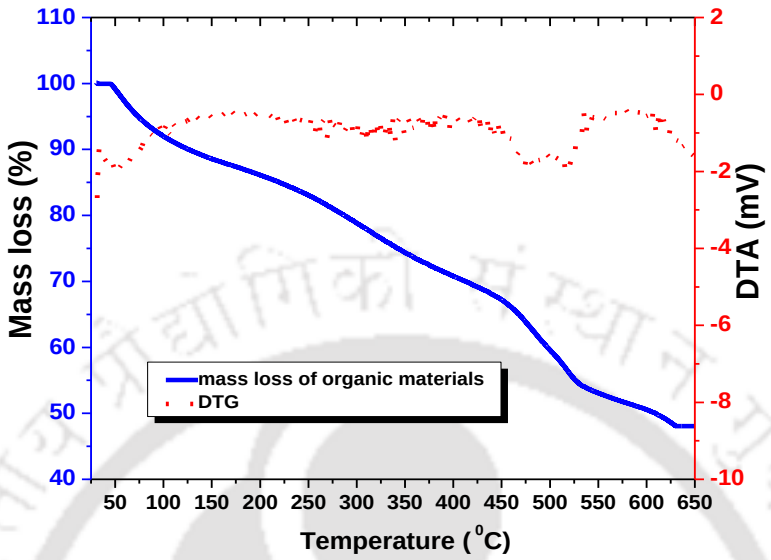

Fig. 4.15. Variation of mass loss from thermal gravimetric analysis (TGA) of rejected materials during spinning basket membrane ultrafiltration of paper industry effluent

4.4. Permeate quality analysis after the treatment of paper and tea factory effluents:

The comparison of permeate qualities after spinning basket ultrafiltration of paper and tea industry wastewater for different MWCOs and rotational speeds have been displayed in terms of pH, TDS (mg L^{-1}), COD removal (%), ionic conductivity (S m^{-1}), final BOD concentration (mg L^{-1}), % of clarity, Turbidity (NTU), final ion concentrations in the **Table 4.9** and **Table 4.10**, respectively. With an increase in rotation, permeate quality in terms of COD removal, decreasing of metal ion concentration improves for both the cases. Ion conductivity also decreases significantly with increasing TMP drops. TDS is also removed due to the good rejection of solutes in the presence of shear-induced force. It is listed that the pH of permeate has been changed to 7.45 after treatment of paper industrial effluent which become invariant with the pressure drop and rotational speed for all cases. The variation of pH for the tea factory wastewater treatment was also marginal. It is obvious that the rotational speed was an important parameter to improve permeate quality for both the effluents.

Table 4.9. Comparison of physiochemical properties of permeates at steady state shear-enhanced ultrafiltration

Speed (rad s^{-1})	MWCO (kDa)	pH	Ionic cond. (S m^{-1})	TDS (mg L^{-1})	COD removal (%)	Turbidity (NTU)	Clarity (*T*, %)	Sodium (mg L^{-1})	Potassium (mg L^{-1})	Zinc (mg L^{-1})	Iron (mg L^{-1})	Magnesium (mg L^{-1})	Nickel (mg L^{-1})	Copper (mg L^{-1})	Manganese (mg L^{-1})	BOD removal (%)
10.47		7.40	0.87	4.5	95.92	2.05	85.31	1.22	1.80	1.30	13.24	0.07	0.50	0.20	3.45	96.74
31.41	5	7.40	0.55	2.25	97.25	2.63	87.70	1.21	1.25	1.30	13.15	0.07	0.50	0.20	3.22	97.60
52.36		7.45	0.54	2.25	97.58	2.44	91.46	1.41	1.36	1.45	13.15	0.07	0.50	0.20	3.25	97.60
73.30		7.45	0.58	3.5	97.08	3.85	93.22	1.45	1.40	1.50	13.15	0.07	0.50	0.20	3.25	97.60
10.47		7.41	0.16	8.5	94.17	5.71	84.11	27.27	22.7	4.16	15.23	1.25	0.50	0.25	3.95	93.76
31.41	10	7.40	0.12	6.85	95.24	4.87	86.39	17.22	20.6	3.83	14.45	1.25	0.50	0.25	3.95	94.55
52.36		7.35	0.95	5.44	96.32	4.40	89.12	16.41	8.30	2.51	14.05	1.25	0.50	0.20	3.95	96.01
73.30		7.31	1.03	6.54	94.28	4.81	90.22	15.45	2.14	2.56	14.05	1.25	0.50	0.20	3.88	95.50
10.47		7.41	1.87	8.25	91.05	5.95	84.14	13.04	12.55	16.12	27.10	1.25	1.35	0.25	5.08	89.45
31.41	30	7.40	1.57	7.25	93.31	5.28	86.50	10.11	8.50	10.10	24.52	1.25	1.35	0.25	5.05	92.00
52.36		7.35	1.13	6.04	93.77	4.44	89.89	7.41	6.50	8.54	24.47	1.25	1.35	0.25	5.05	94.01
73.30		7.31	1.29	6.5	91.44	4.89	91.36	6.46	4.60	5.48	23.33	1.25	1.35	0.25	5.05	92.80
10.47		8.49	2.15	14.5	83.82	10.70	81.47	34.00	30.00	20.07	31.11	1.50	1.50	0.30	6.35	82.01
31.41	50	8.47	2.10	10.35	85.76	8.84	85.11	27.00	30.5	12.05	27.12	1.50	1.50	0.30	6.30	87.00
52.36		8.45	1.52	9.07	86.00	8.56	87.70	13.00	15.15	11.30	25.45	1.50	1.50	0.30	6.30	89.00
73.30		8.46	1.68	9.85	85.22	9.97	89.53	13.00	15.10	10.30	25.22	1.50	1.50	0.30	6.30	88.50

Table 4.10. Physio-chemical properties of permeates at steady state spinning basket membrane ultrafiltration of tea factory wastewater

Speed (rad s^{-1})	MWCO	pH	Ionic cond. (S m^{-1})	TDS (mg L^{-1})	COD (mg L^{-1})	Turbidity (NTU)	Clarity (%)	Sodium (mg L^{-1})	Iron (mg L^{-1})
10.47	5	6.90	1.17	2.8	40	1.02	85.5	2.5	0.47
31.41		6.80	1.03	2.5	35	0.96	88.70	2	0.45
52.36		6.90	0.75	2.07	30	0.95	94.46	1.4	0.40
73.30		6.80	1.0	2.1	38	0.98	91.72	1.6	0.45
10.47	10	7.01	1.74	4.5	47	1.05	85.11	6.02	0.55
31.41		7.01	1.07	4.07	41.5	1.00	87.48	5.5	0.51
52.36		7.05	0.9	3.28	40	0.98	92.02	2.8	0.51
73.30		7.01	1.01	5.54	45.71	1.02	88.12	3.2	0.54
10.47	30	7.10	1.77	9.05	152.55	1.05	83.04	7.05	1.1
31.41		7.10	1.54	8.55	70	1.03	88.70	6.22	1.05
52.36		7.10	0.79	7.90	60	1.00	90.55	4.12	0.70
73.30		7.10	1.07	8.05	62.25	1.05	88.37	4.75	0.95
10.47	50	7.25	1.9	28.5	170	1.07	82.57	8.5	1.44
31.41		7.25	1.55	20.35	132	1.05	86.01	7.22	1.32
52.36		7.25	1.07	15.07	117.4	1.05	86.70	5.5	1.01
73.30		7.25	1.11	17.5	120	1.07	85.04	6.95	1.06

4.5. Summary of the chapter:

Utilization of shear-enhanced spinning basket membrane module for the treatment of paper and tea industry effluents is an effective process towards water sustainability. The coagulation-ultrafiltration system can be used as a cost efficient process to treat tea factory effluent.

- In the present study, use of vacuum filtration and the commercial alum as an effective coagulant reagent was successfully discussed for the pre-treatment purposes.
- Among 5, 10, 30 and 50 kDa MWCO membranes, maximum permeate flux was obtained for 50 kDa MWCO membrane for both the cases.
- High rotation of spinning basket helps to increase membrane shear rate which enhances the solvent permeation to reduce the mass transfer resistance of the polarized layer of rejected solutes.
- Due to high generation of turbulence at a high rotation of 52.36 and 73.30 rad s^{-1}, the deposition of rejected particles on membrane surfaces is very less which results in a minimum resistance at these rotational speeds.
- Maximum rejection of 98% was observed on the basis of COD removal at high applied pressure of 414 kPa with low rotational speed, and 5 kDa MWCO membrane during the paper industry wastewater treatment. On the other side, significant removal of total

polyphenolic compounds was achieved from the tea factory wastewater with increasing membrane basket rotation from 10.47 to 52.36 rad s^{-1}.

- Due to the continuous basket rotation, particles can appear in the permeate side through shear-induced and rotational diffusions. Thus, the rotational and shear-induced model prediction reveal good model fitting towards spinning basket membrane ultrafiltration.
- RSM has been applied to optimize the permeate flux and permeate quality. Optimum permeate quality has been obtained when initial TMP drop, rotational speed and retentate flow rate were 350.61 kPa, 600 rpm (62.83 rad s^{-1}) and 2 L min^{-1}, respectively.
- At the cost of very low energy consumption, good rejection was obtained during spinning basket membrane ultrafiltration compared to the other existing shear-enhanced filtration.

References:

B. Chen, X. Xiong, Z. Yao, N. Yin, Z. X. Low, Z. Zhong, Integrated membrane process for wastewater treatment from production of instant tea powders, Desalination 355 (2015) 147-154.

C. Xiaoli, T. Shimaoka, C. Xiaoyan, G. Qiang, Z. Youcai, Spectroscopic studies of the progress of humification processes in humic substances extracted from refuse in a landfill, Chemosphere 69 (2007) 1446-1453.

D. Sarkar, A. Sarkar, A. Roy, C. Bhattacharjee, Performance characterization and design evaluation of spinning basket membrane(SBM) module using computational fluid dynamics (CFD), Sep. Purif. Technol. 94 (2012) 23-33.

J. Shao, J. Hou, H. Song, Comparison of humic acid rejection and flux decline during filtration with negatively charged and uncharged ultrafiltration membranes, Water Res. 45 (2011) 473-482.

L. H. Ding, O. Akoum, A. Abraham, M. Y. Jaffrin, High Shear Skim Milk Ultrafiltration Using Rotating Disk Filtration Systems, AIChE J. 49 (2003) 2433-2441.

M. C. V. Vela, S. A. Blanco, J. L. Garcia, E. B. Rodriguez, Analysis of membrane pore blocking models applied to the ultrafiltration of PEG, Sep. Purif. Technol. 62 (2008) 489-498.

M. Justin, S. Fred, E. Lazarus, K. John, Electrochemical treatment of a Kenyan tea factory wastewater, J. agric. pure appl. sci. technol. 2 (2009) 68-75.

M. J. C. Baguena, M. C. V. Vela, J. M. G. Zafrilla, S. A. Blanco, J. L. Garcia, D. C. Martinez, Comparison between artificial neural networks and Hermia's models to assess ultrafiltration performance, Sep. Purif. Technol. 170 (2016) 434-444.

P. Singh, I. S. Thakur, Colour removal of anaerobically treated pulp and paper mill effluent by microorganisms in two steps bioreactor, Bioresour. Technol. 97 (2006): 218-223.

R. Saranya, G. Arthanareeswaran, D.D. Dionysiou, Treatment of paper mill effluent using Polyethersulfone /functionalized multiwalled carbon nanotubes based nanocomposite membranes, Chem. Eng. J. 236 (2014) 369-377.

S. K. Yadav, R Kalaiyarasi, Feasibility analysis of industrial symbiosis between cement industry and tea industry, Inter. J. Environ. 4 (2015) 20-34.

V. Singh, C. Das, Comparison of spiral wound UF membrane performance between turbulent and laminar flow regimes, Desalination. 337 (2014) 43-51.

X. Li, M. Xing, J. Yang, Z. Huang, Compositional and functional features of humic acid-like fractions from vermicomposting of sewage sludge and cow dung, J. Hazard. Mater. 185 (2011) 740-748.

Y. Zhang, J. Du, F. Zhang, Y. Yu, J. Zhang, Chemical characterization of humic substances isolated from mangrove swamp sediments: The Qinglan area of Hainan Island, China, Est. Coast. Shelf Sci. 93 (2011) 220-227.

CHAPTER 5

RECOVERY OF TOTAL POLYPHENOLS FROM TEA FACTORY SOLID WASTE MATERIALS USING A HYBRID PROCESS OF LEACHING-MEMBRANE ULTRAFILTRATION

In this chapter, leaching of total polyphenols from tea factory solid waste, collected from M/s. Sindhu Tea Pvt. Ltd., Golaghat, Assam, India, was carried out using five solvents, namely, ethanol, methanol, acetone ethyl acetate and de-ionized water at different times and solid waste. A wide range of leaching temperature was also explored while de-ionized water was used as a green solvent. Optimum leaching of total polyphenols has been achieved applying response surface methodology. The different kinetic models were analyzed and compared to obtain the leaching and diffusion rate. Finally, the spinning basket membrane ultrafiltration was performed to recover and concentrate the leached polyphenols. Simultaneously, the recovery of the green solvent such as, water has also been successfully carried out using the ultrafiltration process.

The work presented in this chapter is communicated in the following journal.

***Suman Saha**, Chandan Das, Utilization of Tea Factory Solid Waste towards Polyphenols extraction: Optimization Study and Kinetic Model Analysis, **Asia-Pacific J. Chem. Eng.** (under review).*

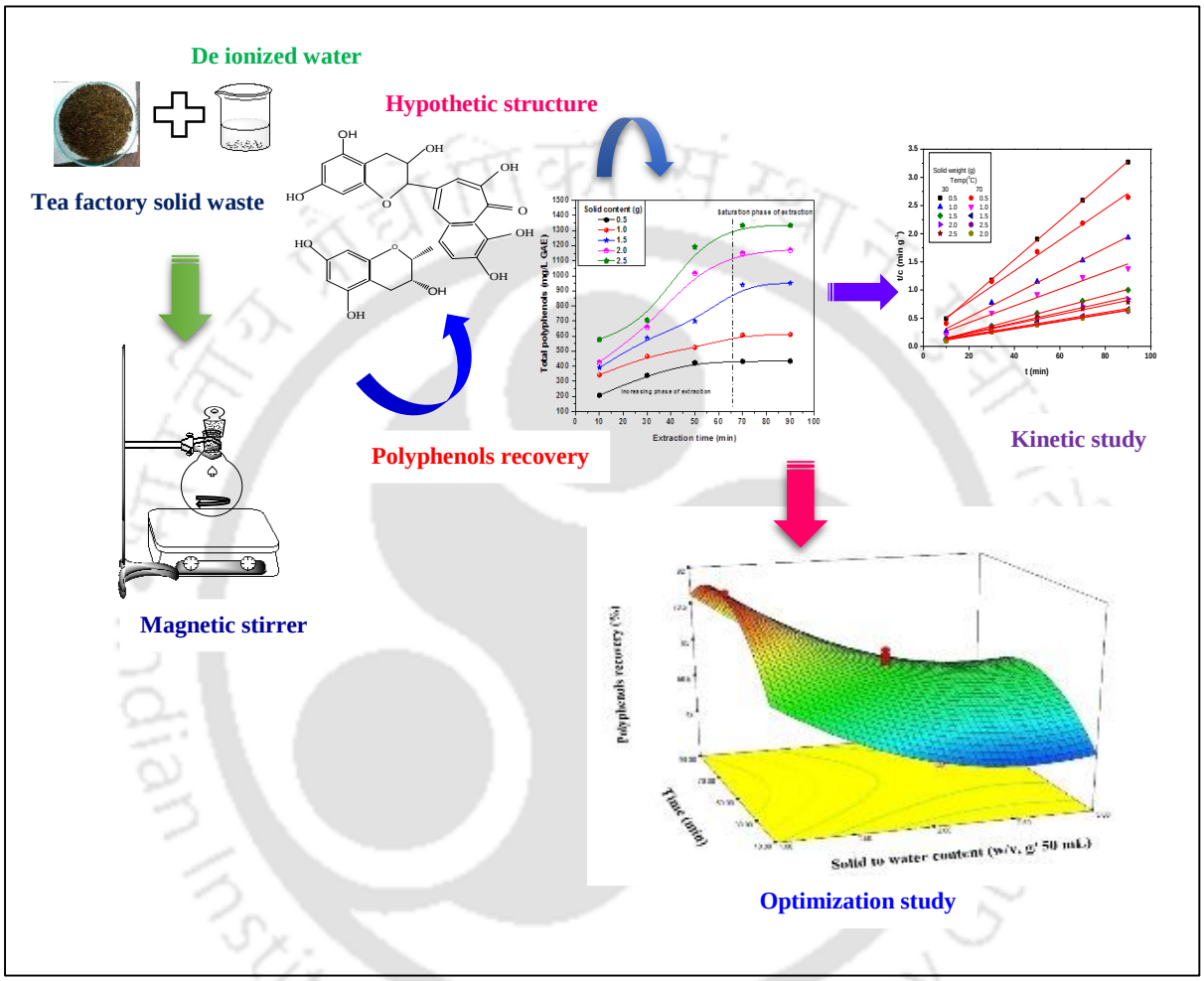

Schematic diagram of leaching of total polyphenols from tea factory solid wastes

5.1. Utilization of tea factory generated solid wastes towards polyphenols recovery using leaching-membrane ultrafiltration:

The effective utilization of the industry generated residues for various purposes, like, biofuel generation, phenolic components leaching etc. rather than such pollution creating activities is a major concern towards solid wastes management. Tea industrial solid wastes are the potential source of the phenolic compound, which can be recovered through ecofriendly water leaching and membrane ultrafiltration techniques. This chapter focused on the use of renewable, reasonable leaching of polyphenols compounds from tea factory solid wastes materials using batch leaching process. Five solvents, namely, ethanol, methanol, acetone, ethyl acetate and de-ionized water, were used to extract the maximum total polyphenols from tea factory solid waste. The influence of temperature (30-90°C) during water leaching of total polyphenols was also explored. The effects of different solid waste content in water (0.5 to 2.5 g) at a various contact time of 10 to 90 min on the leaching of polyphenols from tea factory solid waste were verified. To optimize the leaching parameters such as solid content (g), leaching process time (min) and temperature ($^{\circ}$C), response surface methodology (RSM) were studied to achieve the optimum leaching of total polyphenols. The leaching and diffusion rate were determined and compared using different rate kinetic models, like, pseudo first order, second order, the Elovich rate kinetic models, the unsteady diffusion, the film theory, and the Ponomaryov equation. Finally, spinning basket membrane ultrafiltration was performed to concentrate the total phenolic content and recover the green solvent such as, water after leaching.

5.2. Results and discussion:

5.2.1. The effects of solvent concentration on the leaching of total polyphenols:

The effects of five different solvents, namely, methanol, ethanol, acetone, ethyl acetate on the leaching of polyphenols are shown in **Fig. 5.1**. It is clearly observed from **Fig. 5.1. (a)** that leaching increases with solvent concentrations up to solvent to water ratio of 4:1 (vol: vol). It is reported in the literature that the polyphenols such as, catechins, flavonoids, phenolic acids found from plant pigments are easily soluble in water and different organic solvents, like, methanol, ethanol, acetone. However, the nature of the solubility depends on the source of the polyphenols (Jun et al., 2009). The solvent and water mixture intensifies the leaching efficiency by increasing total phenolic components. The further increase in solvent concentration for ethanol and acetone from 3:2 to 4:1 (vol: vol) the leaching of total

polyphenols was almost constant. Whereas, it is also shown in Fig. 1a that ethanol gives the maximum leaching of total polyphenols among five solvents. During the leaching of secondary plant compounds namely, phenolic substances, ethanol and water mixture reveals the significant leaching efficiency due to the high solubility of phenolic compounds in the ethanol water liquid phase **(**Das et al., 2017). The leaching efficiency of pure water with various temperature is shown in **Fig. 5.1. (b)**. It is noticed that with the increasing leaching temperature from 30 to 70° C, the leaching of total polyphenols increases for all the solid contents. The diffusivity of the phenolic compounds in the solid waste and its miscibility with the water increases with leaching temperature. With increasing temperature from 30 to 70°C diffusion occurs through denatured cell walls. The high amount of diffusion of phenolic compounds occurs with the change of solid content from low to high due to the high penetration of water into the solid waste cell wall with rising temperature. The viscosity of the solvent also reduces at a raised temperature causing easier dispersion of solvent into the interstices of the solid waste (Das et al., 2015). At 70°C, the recovery reaches its saturation point. It is also observed that polyphenols recovery by ethanol to water ratio of 3:2 (vol: vol) is comparable to pure water at 70°C. Hence, pure water at 70°C is taken as the solvent for leaching of polyphenols from solid tea waste.

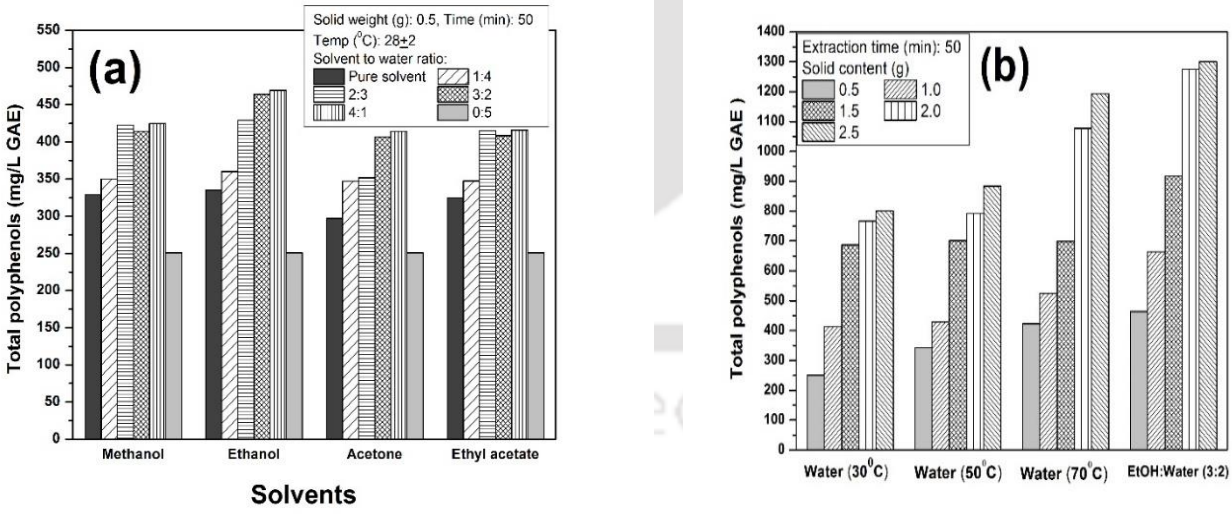

Fig. 5.1. (a) The effect of various solvents on the leaching of total polyphenols from tea factory solid waste at constant leaching time (50 min), temperature (28±2°C), and solid weight (0.5 g), **(b)** the comparative study between the ethanol-water mixture (28±2°C) and the de-ionized water (30-70°C) on the total polyphenols leaching

5.2.2. Effects of solid content with respect to time on the kinetics of total polyphenols leaching:

Fig. 5.2 describes the dependency of tea factory solid waste content on the leaching of total polyphenols with respect to time. This figure reveals the linear variation of the rate of leaching of polyphenols with time, irrespective of solid content in water. Two different phases of leaching are noticed in this figure. Firstly, the leaching efficiency is found to increase with process time. A linear variation occurs up to 70 min. The phenolic compounds are found less in water at the beginning of leaching. With increasing process time, the amount of extractive compounds rises in the water. Diffusional leaching happens with leaching process time signifying the rising of polyphenols content into the water The intact mass transfer resistance comprises in the solid phase of leaching which infers the higher diffusion of polyphenols with leaching progress time. A similar type of observation was found by the other researchers (Das et al., 2015; Das et al., 2017; Pol et al., 2007). For the second phase, beyond 70 min, the leaching of total polyphenols extents its saturation or equilibrium state as the slower leaching hinders the leaching of total polyphenols. The overall leaching process has been hampered due to the collective accumulation of polyphenols resulting lower leaching efficiency beyond the saturation time. Thus, after 70 min of process time, the recovery of phenolic compounds has been found almost constant for all cases. It is clear that the optimum process time for the leaching of polyphenols from solid waste has been observed from 60 to 70 min.

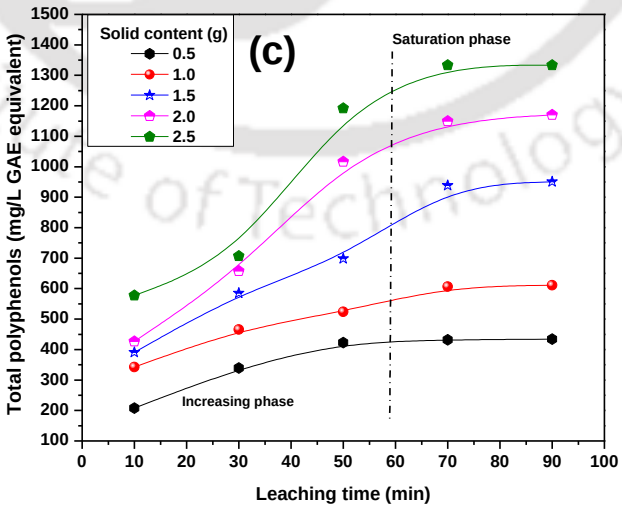

Fig. 5.2. Variation of the total polyphenols leaching with the progress of contact time at different solid tea waste content (temperature 70°C, stirring speed 500 rpm).

5.2.3. Optimization of leaching of total polyphenols and study on statistical analysis using response surface methodology (RSM):

Response surface methodology (RSM) has been used to investigate the interaction effect during polyphenols leaching in between input and output variables. As advised by the said software, no transformation was applied.

The quadratic model has been suggested to analyze the output variable such as leaching total polyphenols. Eq. (5.1) represents the final regression function to estimate the recovery of phenolic components.

$$R_4 = 1196.23 + 160.70 \times A_3 + 197.63 \times B_3 + 108.59 \times C_3 + 90.05 \times (A_3 \times B_3) + 58.75 \times (A_3 \times C_3) + 53.55 \times (B_3 \times C_3) - 287.67 \times A_3^2 - 116.83 \times B_3^2 - 244.75 \times C_3^2 \quad (5.1)$$

Variance analysis has been performed to identify and verify the statistically significant terms. Analysis of variances for the response has been displayed in **Table 5.1.** A favorable high value of R^2 (0.97) has been observed.

The calculation of the signal to noise ratio has been selected by measuring adequate precision and a value greater than 4 is accepted. The high correlation values refer good fitting of leaching data to suggest a replicated equation based model. The high *F*-value with low *p*-value signifies the quadratic model equation for the leaching of phenolic compounds for different process parameters. The non-significant lack of fit term denotes that the leaching of total polyphenols was carried out specifically. All parameters show the important significant model term to obtain a higher amount of polyphenols from tea factory solid waste materials. Nonetheless, there is a clear effect of individual parameters on the recovery of phenolic compounds.

Table 5.1. Statistical parameters of RSM predicted model equation for total polyphenols leaching using ANOVA

Source	Sum of square	df	Mean square	F-value	P-value prob>F	
Model	2.16×10^{6}	9	2.41×10^{5}	20.58	<0.0001	Significant
A_3 (Solid content)	3.35×10^{5}	1	3.35×10^{5}	28.64	<0.0003	
B_3 (Time)	2.88×10^{5}	1	2.88×10^{5}	24.62	0.0006	
C_3 (Temp)	5.18×10^{4}	1	5.18×10^{4}	4.43	0.0616	
A_3B_3	7250.09	1	7250.09	0.62	0.4495	
A_3C_3	63.25	1	63.25	5.41×10^{-3}	0.9428	
B_3C_3	1.76×10^{4}	1	1.76×10^{4}	1.51	0.2475	
A_3^2	1.36×10^{5}	1	1.36×10^{5}	11.68	0.0066	
B_3^2	1.26×10^{5}	1	1.26×10^{5}	10.82	0.0082	
C_3^2	1.01×10^{5}	1	1.01×10^{5}	8.93	0.0136	
Residual	1.17×10^{5}	10	1.17×10^{4}	-	-	
Lack of fit	9.68×10^{4}	5	1.94×10^{4}	4.79	0.0554	Not significant
Pure error	2.02×10^{4}	5	4046.30	-	-	
Cor total	2.29×10^{6}	19	-	-	-	
Std. Dev.						108.19
Mean						869.58
C.V.%						12.44
PRESS						6.59×10^{5}
R^2						0.97
Adjusted R^2						0.94
Predicted R^2						0.85
Adequate Precision						12.77

5.2.4. Combined effects of leaching time and solid waste content on polyphenols leaching:

Fig. 5.3 represents the three-dimensional response surface analyzed diagram of the combined effect of leaching time and solid waste content on total polyphenols leaching. Extracted amount increases with increasing leaching time at constant solid waste content. For example, at a fixed solid content of 1.0 g in 50 mL water, the extracted is near about 425 mg L^{-1} GAE when the process time is 10 min. With increasing leaching time from 10 to 70 min, the amount of total polyphenols also increases up to 700 mg L^{-1} GAE. Whereas,

the recovery reaches its saturation position after 70 min. However, leaching of total polyphenols increases with the increasing solid content up to 2.5 g, then decreases. The leaching efficiency is hindered due to the high collective accumulation of polyphenols in water at high solid waste content. A low concentration gradient of polyphenols between solid waste and water results a drop in total polyphenols leaching beyond 2.5 g of solid waste content.

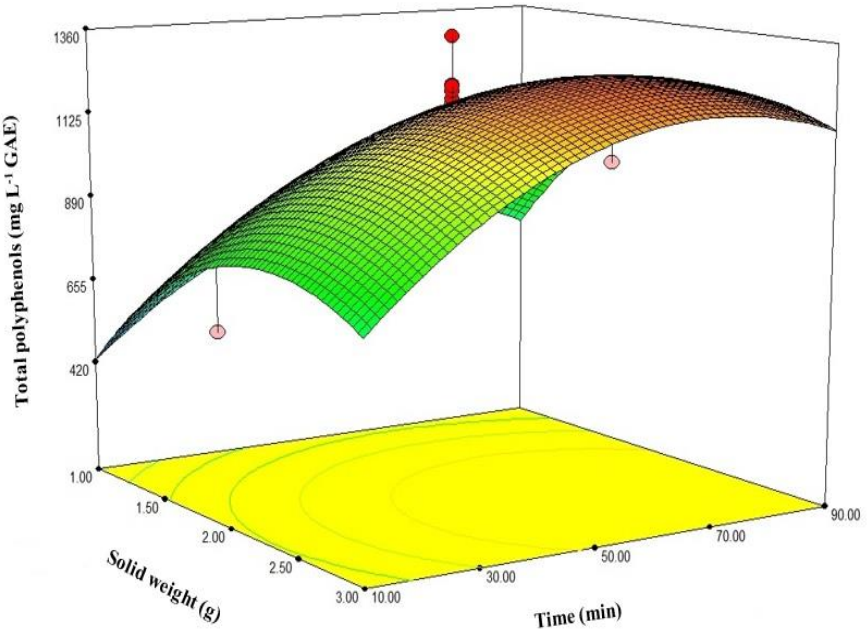

Fig. 5.3. The combined effects of leaching time (min) and solid weight content (g) at a constant temperature of 60˚C on the leaching of total polyphenols.

5.2.5. Role of leaching temperature and solid content on leaching of polyphenols:

The quadratic impact of leaching temperature and solid waste on the leaching of total polyphenols has been presented in **Fig. 5.4**. The leaching temperature has a strong effect on value aided polyphenols recovery from tea factory solid waste. Keeping time and solid content constant at 50 min and 1.0 g respectively, with increasing temperature from 30˚C to 75˚C, leaching of total polyphenols increases from 510 to above 800 mg L^{-1} GAE. The diffusivity and as well as the solubility of the phenolic compounds increases with leaching temperature. The low viscosity of the water at high elevated temperature helps to penetrate the water into the interstices of the solid waste very easily which produces more leaching

of phenolic compounds. Beyond 75°C, recovery decreases due to the decomposition of polyphenols. It is elucidated that the optimum temperature for the leaching of total polyphenols can be found from 60 to 75°C. The reverse trend of the recovery of phenolic compounds has been observed with the increasing solid content from 2.5 to 3.0 g. Solvent volatility is also an important reason for this low recovery.

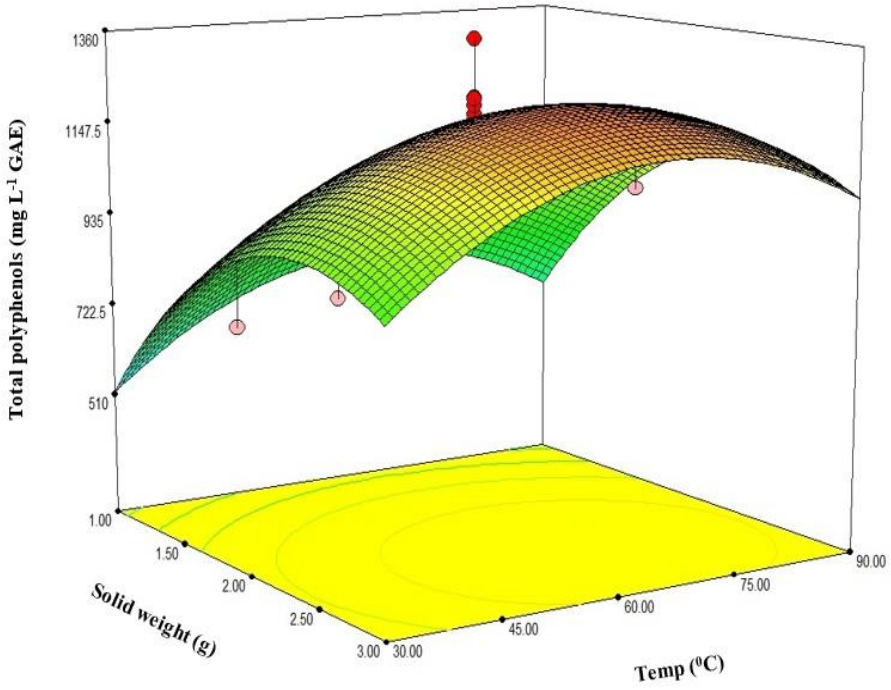

Fig. 5.4. The combined effects of leaching temperature (°C) and solid weight content (g) at a constant time of 50 min on the leaching of total polyphenols.

5.2.6. Effects of temperature and time on leaching of polyphenols:

The conjugate effects of temperature and time on total polyphenols leaching are displayed in **Fig. 5.5.** At constant solid content and temperature of 1.55 g and 30°C, respectively, with increasing leaching time from 10 to 75 min recovery increases linearly. During the progress of the leaching process, components come into the water and recovery is observed to increase. The leaching of any material from solid particle depends on the distribution mechanisms of the solute in this solid matrix. Due to the uneven spreading of phenolic compounds within the water insoluble fiber complex of tea solid waste, solute material gradually dissolves and diffuses throughout the leaching process time. Sometimes water

also diffuses in the reverse direction resulting in a slight drop in the leaching rate beyond 75 min of process time. On the other side, with the increasing leaching temperature beyond 75°C, degradation of polyphenols results in the lower leaching yield. The drop of leaching efficiency has been noticed at high temperature due to the volatility of solvent or the thermal impact on residual solid materials.

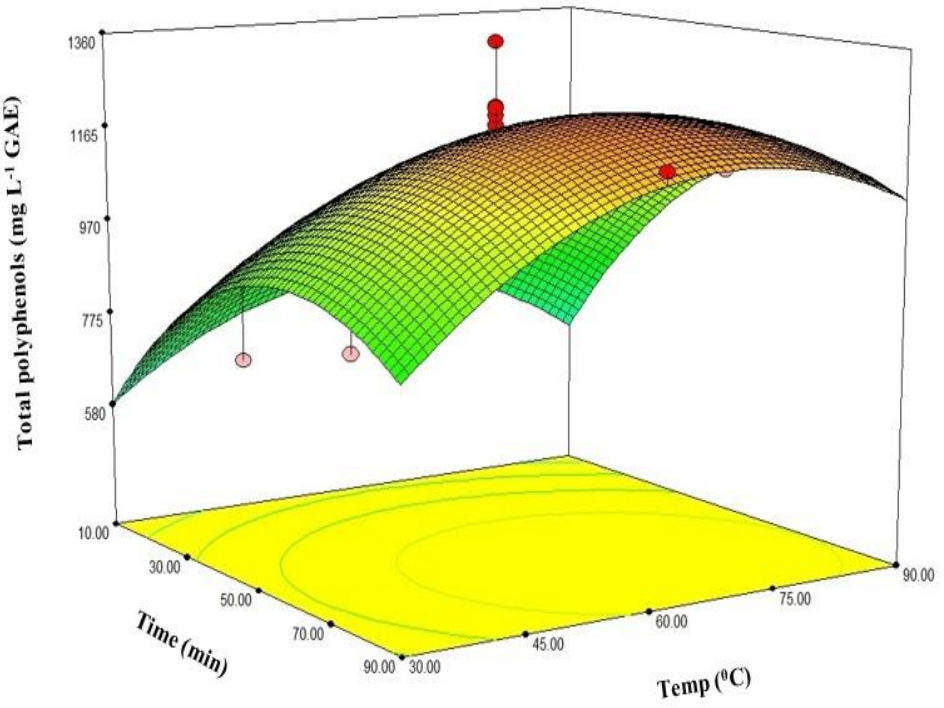

Fig. 5.5. The combined effects of leaching time (min) and temperature (°C) at a constant solid content of 1.55 g on total polyphenols leaching.

5.2.7. Model identification based on statistical analysis:

In order to certify any mathematical model, the identification of arbitrariness and changeability are essential constituents of any regression model. Residual plot analysis helps to categorize the validity of any model. The graphical presentation of residual analysis of response surface method for total polyphenols is shown in **Fig. 5.6. (a)**.

This figure represents the validation of the fitting of analyzed data for the leaching of phenolic compounds with statistical conventions and the standard deviations (SD) between the actual and predicted response for all parameters. This graphical representation confirms that the residual points fall very close to the standard straight line revealing the normal

distribution of output points during recovery of total polyphenols with significant experimental results.

The residual versus predicted response is presented in the **Fig. 5.6. (b)**. **Fig. 5.6. (c)** shows the comparison between actual values and predicted values for total polyphenols leaching. It is clear that the distribution of all design points for the total polyphenols leaching is along with the diagonal line revealing the perfect model fitting to optimize the process parameters during treatment of tea factory solid waste towards total polyphenols leaching.

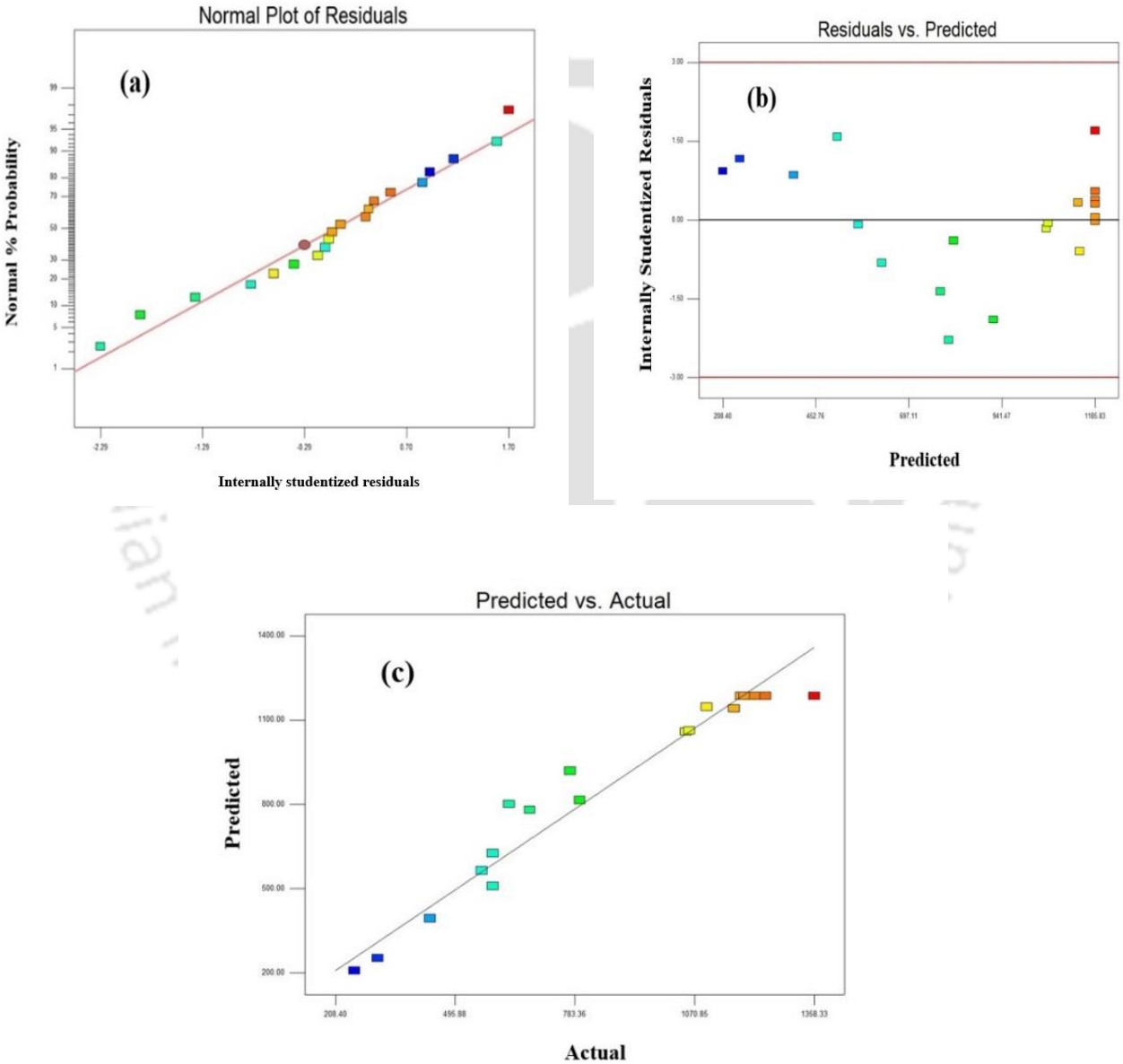

Fig. 5.6. (a) Normal probability plot for residual, **(b)** plot between residual and predicted response, **(c)** plot for predicted vs actual values for total polyphenols recovery.

5.2.8. Optimization study to extract total polyphenols:

The optimum parametric conditions for the optimum recovery of total polyphenols predicted from response surface methodology with a maximum and minimum limit of input parameters has been justified with the desirability function. The desirability of this model is 0.9. **Fig. A5** in the Appendix reveals the desirability plot between solid content (g) and leaching time (min) to optimize phenolic compounds recovery. The analyzed optimum parametric condition is as follows: solid content (g): "2.45 g"; leaching time (min): "68.06 min"; leaching temperature (°C): "67.33°C". The predicted value of total polyphenols is 1270.34 mg L^{-1} GAE. Furthermore, the leaching experiment is implemented to recover phenolic compounds on the basis of above said optimized parametric conditions to determine the error between the theoretical and experimental value. The extracted amount has been found near about 1222.5 mg L^{-1} GAE. It reveals that only 3.7% error (Error, %= (theoretical value- experimental value) /theoretical value×100) has been accounted between theoretical and experimental prediction which is quite significant. On the other side, total flavonoids in terms of quercetin and the total epigallocatechin have been found as 370 mg L^{-1} quercetin equivalent and 285 mg L^{-1}, respectively.

5.2.9. Comparison between RSM and ANN models:

The response surface methodology data was used to develop ANN model for total phenolic content measurement. The model performance was obtained using coefficient of regression (R^2). It was obtained that the ANN model with significant R^2 of 0.97 can be predicted the experimental data and the coefficient of regression (R^2) was higher than response surface methodology. **Fig. 5.7** represents the comparison between experimental data, and ANN model predicted outcome. The **Table A4** in the appendix section represents the error calculation of RSM and ANN models.

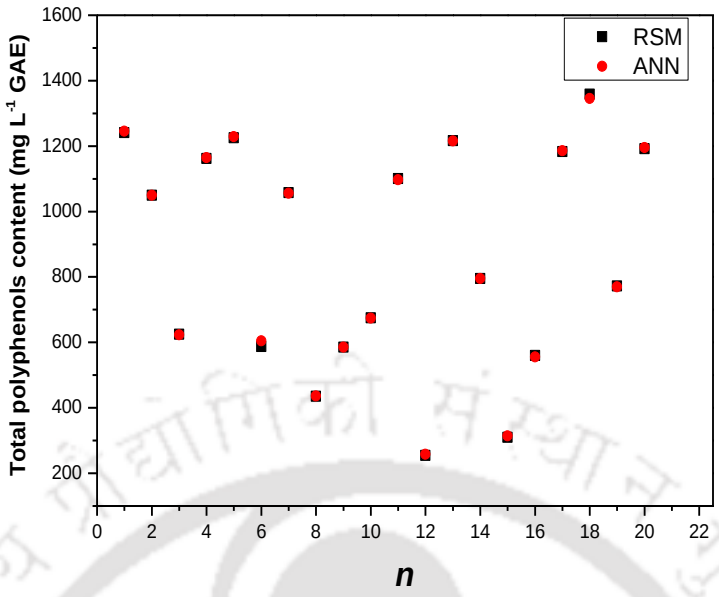

Fig. 5.7. Comparisons between ANN and RSM model for total polyphenols (mg L^{-1} GAE) leaching from tea factory solid wastes

5.3. Kinetic models analysis:

5.3.1. Determination of leaching kinetic model for the leaching of total polyphenols:

Fig. 5.8 (a) reveals the linear fitness of pseudo first-order kinetics according to the experimental data. From this figure, it is observed that the linearization is better at the low leaching temperature (50°C) than higher temperature (70°C). With increasing temperature from 50 to 70°C, a very low coefficient of R^2 has been found (**Table 5.2**). It reveals that optimum leaching temperature can be found between 50 and 70°C. A maximum amount of polyphenols is dissolved and extracted very fast when the temperature is at 50°C during the leaching. **Fig. 5.8 (b)** represents the pseudo second-order kinetics. From this linearized plot, it is clear that the leaching of polyphenols reaches its equilibrium or saturation point very fast with the increasing solid content from 0.5 to 2.5 g as the slop has been decreased by the high amount of solid content in water for each temperature.

Thus, a decreased rate constant has been observed (**Table 5.2**) with increasing solid content in water. To find a correlation between the experimental and theoretical data, the Elovich kinetic model has been discussed in the **Fig. 5.8 (c)**. The kinetic constants, α (L mg^{-1}) and ζ (mg L^{-1} min^{-1}) for the Elovich model are presented in the **Table 5.2**.

It is observed that the coefficient of determination is reasonably high for low solid content such as 0.5 to 1.5 g solid in water indicating faster leaching. However, the Elovich kinetic model signifies the better prediction than first-order kinetics. The pseudo second-order presents the high R^2 value to predict the accurate physicochemical process.

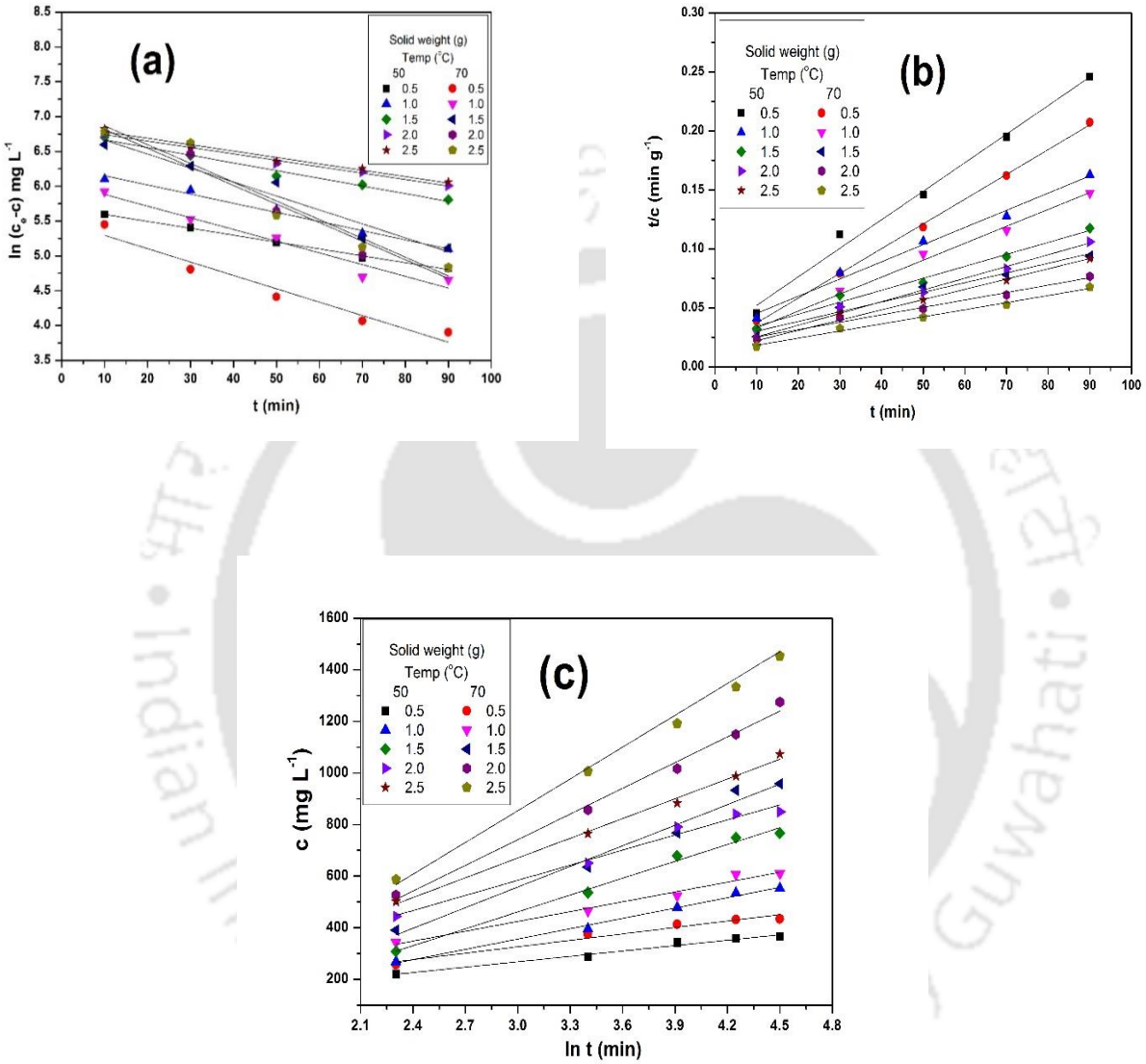

Fig. 5.8. Influence of different solid waste and temperature on the kinetics of the total polyphenols leaching from tea factory waste **(a)** pseudo first-order model, **(b)** pseudo second-order model, and **(c)** the Elovich leaching models (solid content: 0.5-2.5 g, Temp: 50 and 70°C, stirring speed: 500 rpm).

Table 5.2. Values of the linearized rate constant for the pseudo first order, second order, and the Elovich models

Solid weight (g)	pseudo first-order		pseudo second-order		Elovich model		
	$k_1 \times 10^2$	R^2	$k_2 \times 10^5$	R^2	$\alpha \times 10^3$	ζ	R^2
Temp. 50°C							
0.5	2.27	0.99	21.1	0.99	14.3	163.48	0.98
1.0	3.03	0.98	6.95	0.99	7.49	96.03	0.98
1.5	2.54	0.98	4.21	0.98	5.11	90.17	0.98
2.0	2.12	0.98	6.47	0.98	4.58	93.21	0.98
2.5	2.11	0.98	5.64	0.98	3.91	75.37	0.99
Temp 70°C							
0.5	4.41	0.94	27.3	0.99	12.01	209.07	0.96
1.0	3.87	0.94	11.2	0.99	7.87	179.08	0.97
1.5	4.62	0.93	3.07	0.97	3.75	163.56	0.97
2.0	6.15	0.96	2.08	0.98	3.09	154.05	0.98
2.5	6.20	0.94	2.96	0.99	2.43	107.68	0.98

5.3.2. Analysis of various diffusion models during total polyphenols leaching:

The unsteady diffusion model has been presented in the **Fig. 5.9 (a)**. The diffusion rate constant is increasing at first with the increasing of solid content from 0.5 to 2.0 g, then decreases at the high solid content of 2.5 g. This observation reveals that the optimum solid content can be found between 2.0 to 2.5 g of solid waste in 50 mL of water. Due to the increase of substantial diffusion resistance, the overall leaching process has been hindered at the high amount of solid content in water.

The same trend has been observed for the film theory kinetic model which has been shown in the **Fig. 5.9 (b)**. On the other side, the Ponomaryov kinetic model (**Fig. 5.9 (c)**) reveals the good model prediction for all the parametric conditions with respect to the significant regression coefficient (R^2) which has been tabulated in the **Table 5.3**. As the entire mass transfer resistance involves in the solid phase of leaching the higher diffusion occurs with the low amount of solid content in water (0.5 to 2.0 g).

Table 5.3 presents the values of all parameters of all kinetic models. Independently of the solid waste content, the model based on film theory predicts the highest diffusion rate, while the Ponomaryov model reveals the good correlation coefficient (R^2).

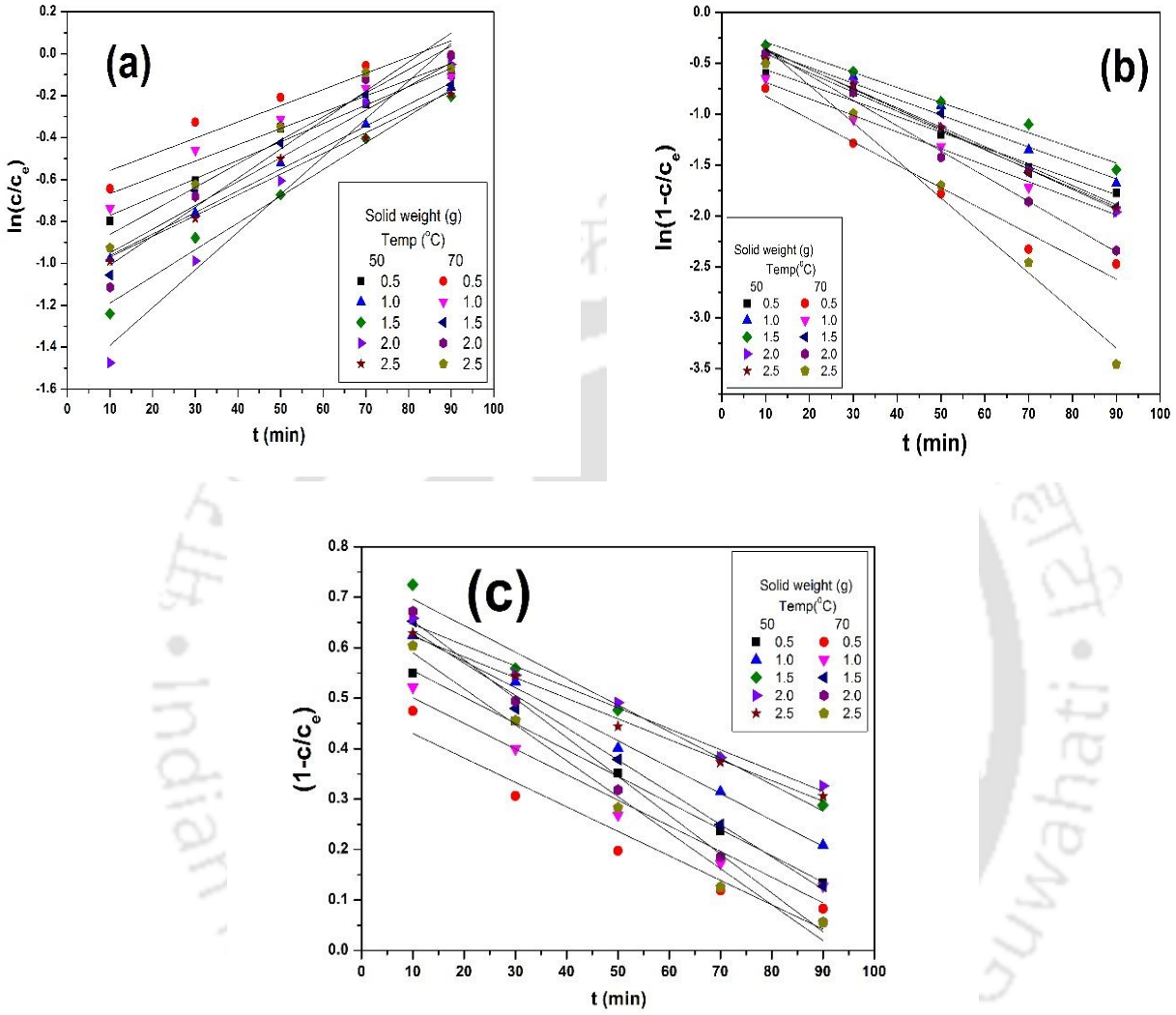

Fig. 5.9. Variation of different diffusion kinetics models for the leaching of total polyphenols from tea factory solid waste **(a)** unsteady diffusion model, **(b)** the model based on film theory analysis, and **(c)** Ponomaryov's kinetic model at various parametric conditions (solid content: 0.5-2.5 g, Temp: 50 and 70°C, stirring speed: 500 rpm).

Table 5.3. Values of the linearized parameters for the unsteady diffusion, film theory, and the Ponomaryov models

Solid weight (g)	unsteady diffusion			film theory model			Ponomaryov model		
	a_0	$k_3\times10^3$	R^2	a_1	$k_4\times10^3$	R^2	a_2	$k_5\times10^3$	R^2
	Temp 50°C								
0.5	0.58	8.77	0.98	0.33	15.99	0.98	0.61	5.24	0.99
1.0	0.66	10.30	0.99	0.20	15.66	0.98	0.68	5.25	0.99
1.5	0.73	12.75	0.99	0.13	14.84	0.98	0.79	5.25	0.98
2.0	0.79	18.00	0.98	0.15	19.71	0.99	0.89	4.14	0.98
2.5	0.66	9.88	0.98	0.19	18.89	0.98	0.66	4.08	0.99
	Temp 70°C								
0.5	0.47	7.73	0.90	0.45	22.47	0.96	0.48	4.85	0.98
1.0	0.53	7.76	0.93	0.41	16.31	0.99	0.55	5.08	0.97
1.5	0.65	11.35	0.92	0.16	19.07	0.98	0.70	6.97	0.99
2.0	0.68	13.84	0.94	0.11	24.81	0.99	0.73	7.7	0.98
2.5	0.62	11.24	0.93	0.02	36.88	0.98	0.65	7.13	0.98

5.3.3. Prediction of empirical model kinetics for the aqueous leaching of total polyphenols:

Four empirical diffusion models namely, parabolic diffusion, power law, hyperbolic diffusion and the Weibull's equation were analyzed during leaching of total polyphenols from the tea factory solid waste using simple aqueous solvent at different parametric conditions. **Figs. 5.10 (a)-(d)** represent linearized forms of parabolic diffusion, power law, hyperbolic diffusion and the Weibull's equation, respectively.

From the **Table 5.4**, it is observed that with increasing solid content leaching coefficient (a_3, min^{-1}) decreases gradually for the parabolic diffusion. A high initial slope has already been found from the **Fig. 5.10 (a)** revealing good leaching of polyphenols followed by the uniform diffusion as the values of the rate of diffusion are almost equal. The parabolic diffusion reveals that the plant particles are isotropic in nature. A good model prediction during the power law model with the increasing leaching exponent signifies that the uniform leaching occurs with the increasing solid content, from 0.5 to 2.0 g. Beyond 2.0 g solid in 50 mL water, the value of leaching coefficient decreases which signifies the optimum solid content between 2.0 to 2.5 g. The leaching also varies significantly with respect to time. Whereas, the good model prediction for hyperbolic and the Weibull's

empirical model reveals that the diffusion of polyphenols occurs only towards the outer surface of solid particles (Kitanovic et al., 2008). Nonetheless, the model based on parabolic diffusion predicts the significant leaching coefficient (a_3, $min^{-0.5}$), while, the Weibull's model gives the highest diffusion coefficient (a_9, min^{a_8}) for all the operating conditions.

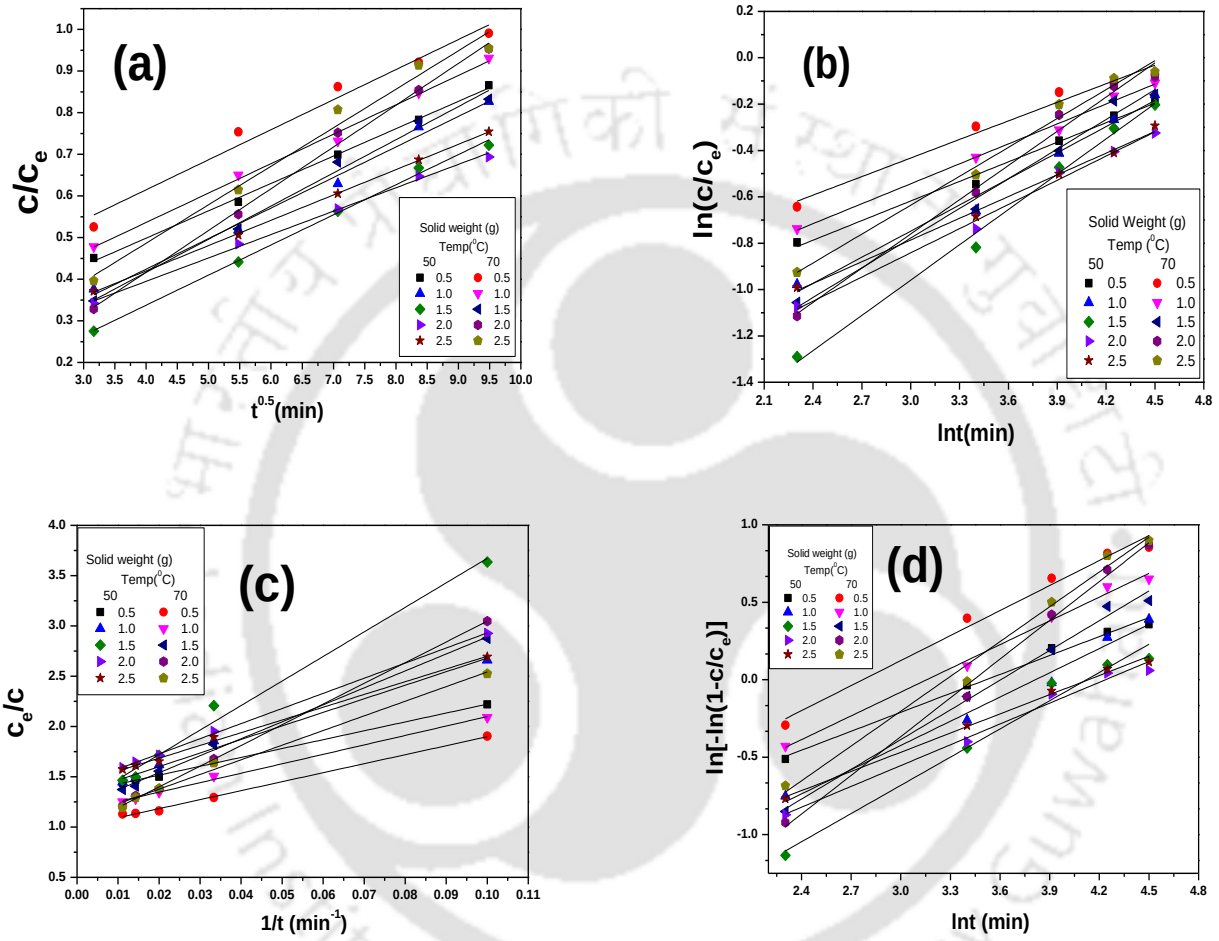

Fig. 5.10. Linearized plot for different empirical models for the diffusion of total polyphenols in to the aqueous state **(a)** parabolic diffusion, **(b)** power law, **(c)** hyperbolic diffusion, and **(d)** Weibull's empirical model at various operating conditions (solid content: 0.5-2.5 g, Temp: 50 and 70°C, stirring speed: 500 rpm).

Table 5.4. Values of the linearized leaching coefficients and diffusion rate constants for the parabolic, power law, hyperbolic, and the Weibull's empirical models

Solid weight (g)	Parabolic model			Power law model			Hyperbolic model			Weibull's model		
	a_3	$a_4 \times 10^2$	R^2	a_5	n	R^2	a_6	a_7	R^2	a_8	a_9	R^2
Temp 50˚C												
0.5	0.24	6.58	0.99	0.23	0.28	0.98	0.11	0.15	0.99	0.41	4.19	0.98
1.0	0.13	7.44	0.99	0.15	0.38	0.98	0.07	0.10	0.99	0.52	7.30	0.98
1.5	0.05	7.24	0.99	0.08	0.51	0.99	0.04	0.05	0.98	0.61	12.23	0.99
2.0	0.17	5.62	0.99	0.15	0.55	0.99	0.07	0.09	0.98	0.65	16.58	0.98
2.5	0.18	6.08	0.99	0.18	0.31	0.99	0.08	0.11	0.99	0.41	5.51	0.99
Temp 70˚C												
0.5	0.33	7.22	0.97	0.29	0.27	0.97	0.11	0.11	0.99	0.54	4.45	0.99
1.0	0.25	7.07	0.99	0.25	0.29	0.99	0.11	0.12	0.99	0.61	5.02	0.99
1.5	0.10	7.97	0.99	0.13	0.43	0.98	0.06	0.07	0.98	0.64	10.04	0.99
2.0	0.02	10.03	0.99	0.11	0.49	0.98	0.05	0.05	0.99	0.83	17.64	0.99
2.5	0.12	10.01	0.98	0.15	0.42	0.98	0.07	0.07	0.99	0.75	11.60	0.98

5.4. Analysis of permeate flux decline during spinning basket ultrafiltration:

Fig. 5.11 shows the evaluation of the permeate flux over ultrafiltration time for each MWCO membrane in the presence of high rotational speed of 52.36 $rads^{-1}$. The permeate flux increases with the changing of TMP drops from 207 to 414 kPa. The permeate flux decline has been restricted within 5 min (250 s) of filtration. The steady state permeate flux was obtained very fast for 207 kPa. This nature ensues due to the internal pore blocking phenomena for the low TMP drop. In the present study, a vortex-like circulation due to the membrane arm rotation reduces the deposition of rejected solutes on the active membrane surfaces. As a result, concentration polarization is insignificant due to the rotation. The adsorption of small solutes in to the membrane pore walls must be the dominating nature to decline the permeate flux for high TMP drop in the beginning of this process.

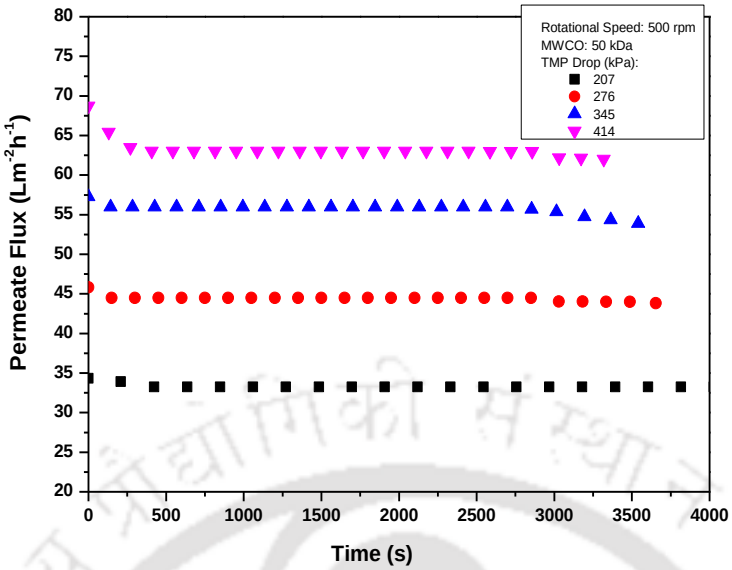

Fig. 5.11. Variation of permeate flux with respect to time during total polyphenols recovery using various MWCO membranes with fixed rotational speed of 52.36 rad s^{-1}

5.4.1. Impact of rotational speed and TMP drop on the total polyphenols concentration and the green solvent recovery:

The impact of different rotation of the membrane basket (10.47 and 52.31 rad s^{-1}) on the recovery of water has been analyzed based on the clarity test (**Fig. 5.12 (a)**). Similarly, **Fig. 5.12 (b)** reveals the influence of different parametric conditions on the concentration of total polyphenols based on observed rejection (%, R_0). The clarity of feed and all permeate samples were examined as % $T = 100 \times 10^{-Abs}$ with 660 nm (*Abs* is determined as optical absorbance) wave length using UV-vis spectrometer, (Make: M/s. Thermo Fisher Scientific, India; Model: UV 2300). The different MWCO membranes help to concentrate the total polyphenols and simultaneously the used water has been recovered during membrane ultrafiltration. With the increasing TMP drop from 207 to 414 kPa the clarity of permeated water is increased for both the MWCO membranes. The clarity of the feed sample was calculated as 61.38%. Whereas, the maximum clarity (91.2% approximate) of recovered water has been achieved using 30 kDa MWCO membrane at high speed rotation of 52.31 rad s^{-1} and TMP drop of 414 kPa as the maximum total polyphenols rejection has been occurred at this particular parametric condition. In the presence of rotational speed,

the induced shear rate forces the particles away from the membrane active side to the feed side resulting in a rising clarity of recovered water with the increasing of TMP drop in the presence of membrane basket rotation. The influence of rotational speed and TMP drop to concentrate the total polyphenols in a lab-scale membrane module after leaching has been demonstrated in the **Fig. 5.12 (c)**.

This figure shows the variation of the total polyphenols content in feed, retentate and permeate samples during the spinning basket membrane ultrafiltration. The volume of the feed was about to 15 L and the total polyphenols content in the feed solution was 18.34 g. In specific, the minimum concentration of phenolic components was measured in the permeate where total polyphenols were actually low due to the rejection of higher molecular weight polyphenols. Whereas, the highest value was obtained in the retentate portion because of the concentration of total polyphenols. With the changing of TMP drop from 207 to 414 kPa, the concentration of polyphenols also rises in the retentate side for all the parametric conditions. Due to the lower fraction of the phenolic components present in the feed samples which was not retained by the membrane has been appeared in the permeate side. The antioxidant activity of the phenolic components was determined using the indices of the reduction technique of the radical scavenging activity (%) of 1,1-diphenyl-2-picryl-hydrazyl free radical (DPPH°). The scavenging activity was calculated as, free radical scavenging (%)= $[(A_r – A_c / A_c) \times 100]$, whereas, A_r is the absorbance of the reactional mixture of free radical is and concentrated phenolic compounds and A_c is the absorbance of control solution (A_c) (Sharma et al., 2016).

Fig. 5.12 (d) displays the free radical scavenging activity of total polyphenolic compounds concentrated by ultrafiltration at different rotational speed (10.47 and 52.31 rad s^{-1}) and MWCOs (30 and 50 kDa). It is clear from this figure that free radical scavenging activity intensely depends on the concentration of the total polyphenols. With increasing rotational speed and TMP drop the concentration becomes higher, as a result the lower the reduction of the absorbance of DPPH° has been occurred and the higher the percentage of its reduction is observed.

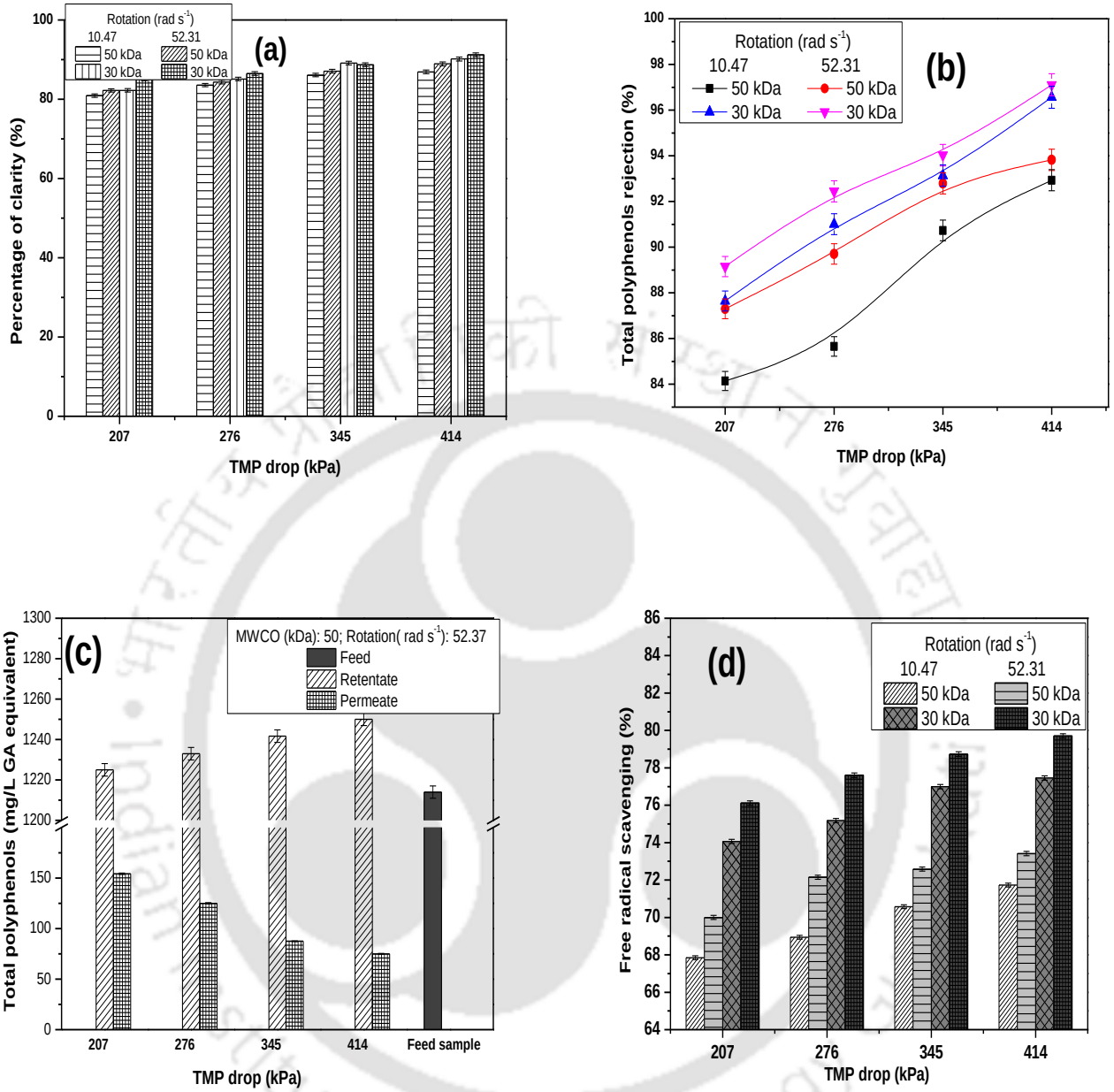

Fig. 5.12. The impact of different rotation of membrane basket (10.47 and 52.31 rad s^{-1}) and MWCO membranes **(a)** on the recovery of water based on clarity, **(b)** total polyphenols rejection, **(c)** the impact of TMP drop (207 to 414 kPa) and rotation (52.31 rad s^{-1}) on the concentration variation of the total polyphenols, and **(d)** the free radical scavenging activity of total polyphenolic compounds concentrated by ultrafiltration at different rotational speed (10.47 and 52.31 rad s^{-1}) and MWCOs (30 and 50 kDa).

5.4.2. Degradation study of concentrated samples:

The degradation of total polyphenols content in the stored samples has been analyzed using a first order kinetic model (Eq. 5.2). The concentrated samples were stored in the refrigerator under 4°C (Ozkan et al., 2005).

$$\frac{dC^{'}}{C^{'}} = -k^{'}dt \tag{5.2}$$

$$\ln\left(\frac{C^{'}}{C_0}\right) = -k^{'}t \tag{5.3}$$

$$t_{1/2} = \frac{0.6932}{k^{'}} \tag{5.4}$$

It is assumed that total polyphenols degradation was occurred with respect to storage time. Where C_0 was the initial concentration of total polyphenols after membrane ultrafiltration and $C^{'}$ is the concentration value according to storage time (t, min) incubation (Ozkan et al., 2005). The effects of various MWCO membranes (50 and 30 kDa) and TMP drops (207 to 414 kPa) on the recovery of total polyphenols during storage time was studied and displayed in **Fig. 5.13**. At high MWCO of 50 kDa and a low TMP drop of 207 kPa, the total polyphenols showed the highest sensitivity for the degradation as indicated by the maximum reaction rate constant (k') and lowest half-life ($t_{1/2}$) values (**Table 5.5**). With the raising of TMP drops the half-life degradation has been increased due to the high concentration of phenolic compounds was found at high TMP drops. Whereas, at low MWCO of 30 kDa shows the significant stability of total polyphenols based on the highest half-life ($t_{1/2}$) values because of the slow degradation of phenolic components. The lowest stability of total polyphenols was observed at MWCO of 50 kDa and TMP drop of 207 kPa due to the low purification of phenolic components. The concentration of phenolic components decreased significantly with storage time (days). Many factors are responsible for the degradation of phenolic compounds including, purification conditions, storage temperature, oxidation, pH variation etc. The loss of total polyphenols is happened due to the oxidation. With the increasing TMP drop at a low MWCO membrane of 30 kDa, the total polyphenols concentration was also increased resulting low oxidation tendency than other conditions. As a result, the degradation rate was also found low for this condition.

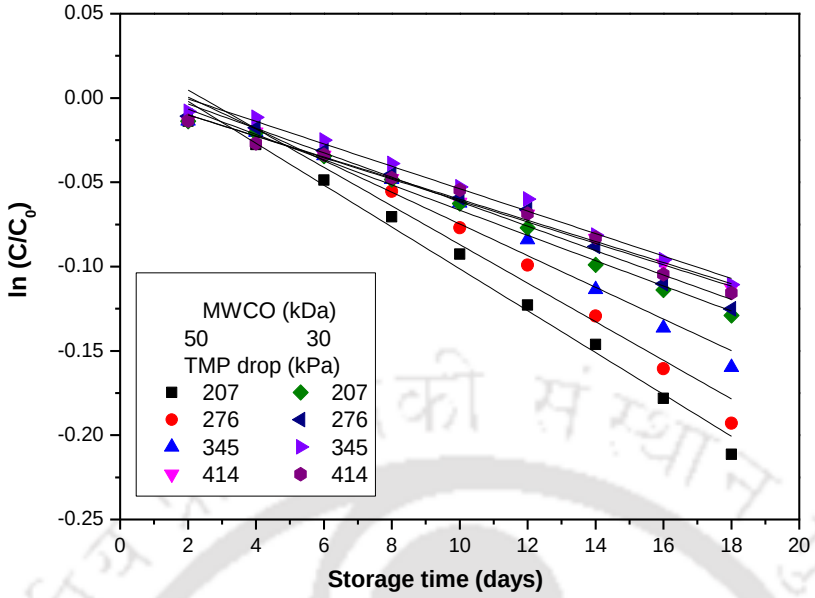

Fig. 5.13. Degradation kinetics of total polyphenols for different MWCO membranes of 50 and 30 kDa and TMP drops (207 to 414 kPa) with respect to storage time

Table 5.5. Effects of MWCO and TMP drops on the degradation of total polyphenols

MWCO (kDa)	TMP drop (kPa)	$-k' \times 10^3$ (day^{-1})	$t_{1/2}$ (days)	R^2
50	207	12.41	55.85	0.98
	276	11.45	60.54	0.96
	345	9.40	73.74	0.96
	414	6.40	108.31	0.99
30	207	7.49	92.55	0.98
	276	7.25	95.61	0.98
	345	6.65	104.24	0.98
	414	6.35	109.16	0.98

5.5. Summary of the chapter:

In the present study, tea factory solid waste was utilized to recover valuable organic products, namely, polyphenols using five different solvents (ethanol, methanol, acetone, ethyl acetate and de-ionized water). The solid waste content in water, as well as leaching

time and temperature, were important parameters to achieve maximum leaching of total polyphenols for a particular condition. The major findings are pointed out as follows

- Among the different organic solvents (methanol, ethanol, acetone and ethyl acetate), ethanol-water mixture was the most efficient solvent mixture to recover polyphenols. However, de-ionized water leaching of polyphenols at approximately, 70°C was also verified to be as significant as regularly used solvents. Based on the cost effective and green solvent leaching, de-ionized water has been selected to optimize the process parameters in the present study.
- With the increasing leaching temperature from 50 to 70°C, total polyphenols leaching was also increased due to the high amount of phenolic compounds diffusion. Beyond 70°C, the leaching yield reached the equilibrium state as the decomposition of polyphenols started.
- To optimize the leaching process parameters, response surface methodology was studied using central composite design. The optimum leaching of total polyphenols of 1270.34 mg L^{-1} GAE has been obtained when solid waste content in 50 mL water (g), time (min) and temperature (°C) were 2.45 g, 68.06 min, and 67.33°C, respectively.
- Among all the leaching kinetics, such as pseudo first order, second order, and the Elovich kinetics, the pseudo second order kinetic predicts the highest regression correlation (R^2) to recover the total polyphenols from the tea industry solid waste materials.
- Whereas, the model based on film theory reveals the significant diffusion rate, while the Ponomaryov model reveals the good correlation coefficient (R^2) due to the slower diffusion of solid waste extracted polyphenols.
- On the other side, it is clear that the spinning basket module seems to be a valid approach for the recovery of total polyphenols after hot water leaching from the tea factory solid waste. The concentrated phenolic materials can be considered a source of antioxidant compounds. The degradation study reveals that the total phenolic components degrade linearly with time.

References:

A. Das, A. K. Golder, C. Das, Enhanced extraction of Rebaudioside-A: Experimental, response surface optimization and prediction using artificial neural network, Ind. Crop. Prod. 65 (2015) 415-421.

A. B. Das, V. V. Goud, C. Das, extraction of phenolic compounds and anthocyanin from black and purple rice bran (*Oryza sativa* L.) using ultrasound: A comparative analysis and phytochemical profiling. Ind. Crops Prod. 95 (2017) 332-341.

B. B. Uzun, E. A.Varol, F. Ates, N. Ozbay, A. E. Putun, Synthetic fuel production from tea waste: Characterisation of bio-oil and bio-char, Fuel 89 (2010) 176-184.

G. S. Dhillon, S. Kaur, S. K. Brar, Perspective of apple processing wastes as low-cost substrates for bioproduction of high value products: A review, Renew. Sustain. Energy Rev. 27 (2013) 789-805.

E. Malkoc, Y. Nuhoglu, Investigations of nickel(II) removal from aqueous solutions using tea factory waste, J. Hazard. Mater. B127 (2005) 120-128.

E. Malkoc, Y. Nuhoglu, Fixed bed studies for the sorption of chromium(VI) onto tea factory waste, Chem. Eng. Sci. 61 (2006) 4363-4372.

J. Pol, E. V. Ostra, P. Karasek, M. Roth, K. Benesova, P. Kotlarikova, J. Caslavsky, Comparison of two different solvents employed for pressurised fluid extraction of stevioside from *Stevia rebaudiana*: methanol versus water, Anal. Bioanal. Chem. 388 (2007) 1847-1857.

M. Ozkan, A. Yemeicioglu, B. Cemeroglu, Degradation of various fruit juice anthocyanins by hydrogen peroxide, Food Res. Inter. 38 (2005) 1015-1021.

P. Sharma, M. Ramchiary, D. Samyor, A. B. Das, Study on the phytochemical properties of pineapple fruit leather processed by extrusion cooking, LWT-Food Sci. Technol. 72 (2016) 534-543.

S. Kitanovic, D. Milenovic, V. B. Veljkovic, Empirical kinetic models for the resinoid extraction from aerial parts of St. John's wort (*Hypericum perforatum* L.), Biochem. Eng. J. 41 (2008) 1-11.

S. Maiti, G. Gallastegui, G. Suresh, S. J. Sarma, S. K. Brar, P. Drogui, Y. L. Bihan, G. Buelna, M. Verma, C. R. Soccol, Hydrolytic pre-treatment methods for enhanced biobutanol production from agro-industrial wastes, Bioresour. Technol. 249 (2018) 673-683.

X. Jun, S. Deji, Z. Shou, L. Bingbing, L. Ye, Z. Rui, Characterization of polyphenols from green tea leaves using a high hydrostatic pressure extraction, Inter. J. Pharma. 382 (2009) 139-143.

CHAPTER 6

OVERALL CONCLUSIONS AND PERSPECTIVE OF FUTURE DIRECTIONS

6.1. Overall conclusions

The different treatment processes such as membrane ultrafiltration, alum coagulation, extraction were attempted to treat Humic acids like natural organic materials and various industrial effluents (paper and tea factory wastes) in this thesis successfully. Spinning basket membrane module was performed for the ultrafiltration process.

- The ultrafiltration of Humic acids solution using spinning basket membrane module was performed successfully. The feasibility assessment of Humic acids ultrafiltration was also achieved by dead-end mode ultrafiltration where the TMP drop was an important parameter to explore the permeate flux decline nature. The transient flux decline behavior during ultrafiltration process time was evaluated and equated with the theoretical approach using artificial neural network (ANN) analysis. The cake layer formation and pore blocking mechanisms were confirmed using Hermia's pore blocking model for dead-end ultrafiltration.

- In the presence of membrane basket rotational speed, the permeate flux decline was found to be marginal due to the less concentration polarization. During filtration, an initial decline of permeate flux was observed due to the severe pore-clogging. The irreversible pore blocking behavior was studied using Modified Hermia's pore blocking mechanism. For the observed rejection, Maximum solute rejection was noticed at a high TMP (414 kPa) drop and low rotational speed of 31.41 rad s^{-1}. A reduced membrane resistance has been observed with increasing membrane basket rotation. Regarding cleaning of the fouled membrane, maximum cleaning efficiency of 88% was obtained with ultrasound application than simple membrane basket back rotation. Based on the membrane basket rotation, energy consumption, and permeate quality, the ultrafiltration of Humic acids aqueous solution using spinning basket membrane process is implemented as the appreciated and operative mode of separation.

- Utilization of spinning basket membrane module for the treatment of paper and tea industry waste effluents is a significant process to control the water pollution. To reduce the total suspended solids from the industrial effluents, the vacuum filtration for the paper industrial wastewater and the alum coagulation using commercial alum as an effective coagulant reagent during tea factory effluents pretreatment were successfully performed in the present study. During final treatment such as spinning basket membrane ultrafiltration, maximum permeate flux was obtained for 50 kDa MWCO membrane for both the cases among 5, 10, 30 and 50 kDa MWCO membranes. Whereas, 5 kDa MWCO membrane gives higher rejection of solutes than others. High rotational speed helps to raise the membrane shear rate which enriches the solvent permeation reducing the mass transfer resistance of the polarized layer of retained solutes. Due to the high turbulence at 52.36 and 73.30 rad s^{-1}, the deposition of rejected solute molecules on membrane effective surfaces is marginal which results in a less membrane resistance for both effluent treatments. The module performance was evaluated using three different diffusion models such as Brownian, rotational and shear-induced model.

- Response surface methodology helps to optimize the process parameters successfully. The optimum permeate quality during industrial effluent treatment was found when the TMP drop, membrane basket rotation and retentate flow rate were 350.61 kPa, 600 rpm (62.83 rad s^{-1}) and 2 L min^{-1}, respectively.

- Towards recovery of value added products from solid wastes, tea factory waste was used to extract total polyphenols using five different solvents (ethanol, methanol, acetone, ethyl acetate and de-ionized water). Among the different organic solvents (methanol, ethanol, acetone and ethyl acetate), ethanol-water mixture was the most effective solvent mixture to extract total polyphenols. Whereas, de-ionized water extraction of polyphenols at approximately, 70°C was also verified to be as efficient and significant like ethanol. The selection of solvent for the further study was based on the cost effectiveness. As a result, de-ionized water was chosen as a green solvent to optimize the process parameters in the present study. extraction temperature played an important role during recovery of total polyphenols from solid wastes.

- With raising the extraction temperature from 50 to 70°C, the phenolic components extraction increased due to the high amount of phenolic compounds diffusion. Whereas, beyond the high temperature of 70°C, the recovery of polyphenols extended its equilibrium position due to the decomposition of polyphenols. Response surface methodology was studied to find out the optimum process parametric conditions for the extraction of total polyphenols. The optimum extraction of total polyphenols of 1270.34 mg L^{-1} GAE has been obtained with the optimized parameters such as, solid waste content in 50 mL water (g), time (min) and temperature (°C) were 2.45 g, 68.06 min, and 67.33°C, respectively. During the kinetic evaluation of extraction, the pseudo second order kinetic was found to be perfect according to the highest regression correlation (R^2). Whereas, the theoretical diffusion rate was significant for the model based on film theory.

- After extraction of total polyphenols under different parametric conditions, membrane ultrafiltration was carried out successfully to concentrate the phenolic compounds and recover the green solvent such as water. It was clear that the spinning basket module seems to be a valid and efficient approach to concentrate the total polyphenols after hot water extraction from the tea factory solid waste. The concentrated phenolic materials can be considered as a source of antioxidant compounds. On the other side, the degradation study reveals that the total phenolic components degrade linearly with time.

6.2. Perspective of future directions

- Scaling up of newly designed spinning basket membrane module for the large scale continuous operation
- Treatment of other different industrial waste effluents such as, oily wastewater, municipal and domestic sewage etc. filtration to identify the behavior of concentration polarization
- Comparative study of spinning basket ultrafiltration with spiral wound module and cross flow filtration
- Commercialized application of alum coagulation followed by membrane ultrafiltration of tea industry effluents in a continuous mode
- Application of extracted and concentrated phenolic compounds found from tea factory solid wastes in the field of corrosion inhibition, pharmaceuticals, and natural dye preparation etc.

Appendix:

Table A1. Conversion of rpm to rad s^{-1}

rpm	rad s^{-1}
100	10.47
200	20.93
300	31.41
500	52.36
600	62.83
700	73.30

Note: 1 rpm= $2\pi/60$ rad s^{-1}

Table A2. Theoretical error prediction using RSM for the alum coagulation study of tea factory wastewater

Responses	Model standard deviation	Pure error	Lack of fit	Comment
TSS (%)	3.25	18.10	0.074	not significant
TDS (%)	3.03	18.80	0.109	
Turbidity (NTU)	0.31	0.3	0.237	

Table A3. Analysis of error for the three diffusion models during ultrafiltration of paper industry wastewater

Diffusion models	Residual sum of squares $RSS = \sum_{i=1}^{n}(y_i - f(x_i))^2$	Standard error $\sigma = \sqrt{\frac{\sum(\bar{y}-y)^2}{n-2}}$	Mean square error (MSE) $MSE = \frac{1}{n}\sum_{i=1}^{n}(y_i - \bar{y}_i)^2$
Rotational	1.63	0.054	0.82
Shear induced	3.08	0.074	1.54
Brownian	11.64	0.144	5.82

Table A4. Theoretical error prediction between RSM data and ANN data for the extraction of total polyphenols from tea factory solid wastes

RSM data	ANN data	Error
1241	1245.79	-4.79
1050	1050.08	-0.08
625	623.08	1.91
1162.22	1165.00	-2.78
1225	1228.79	-3.79
587	604.55	-17.55
1057.33	1056.15	1.17
435.67	435.89	-0.22
585.5	585.07	0.43
675	674.05	0.94
1100.25	1097.45	2.79
254.16	258.35	-4.19
1216.67	1215.79	0.87
795	795.01	-0.01
310	313.93	-3.93
560	555.78	4.21
1183.33	1185.79	-2.46
1358.33	1345.79	12.53
772.25	769.68	2.56
1191.67	1195.79	-4.12

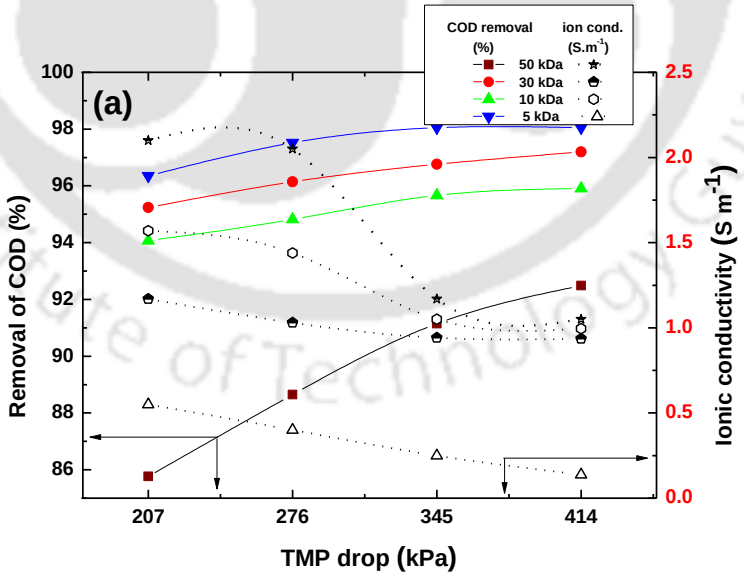

Fig. A1 Variation of observed rejection for different MWCO membranes with respect to TMP drops

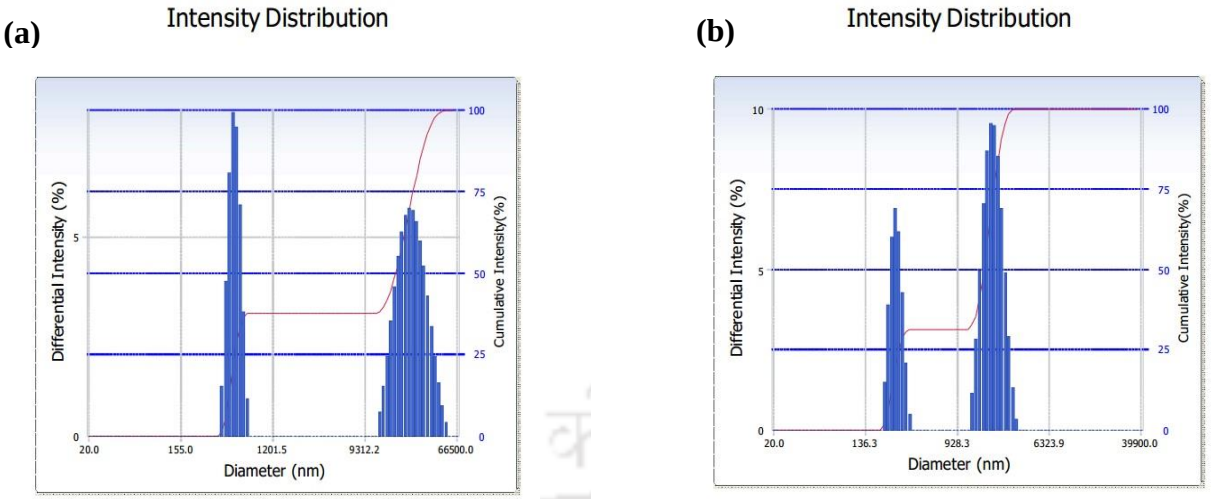

Fig. A2 Particle size distribution (a) before alum pre-treatment; (b) after alum pre-treatment

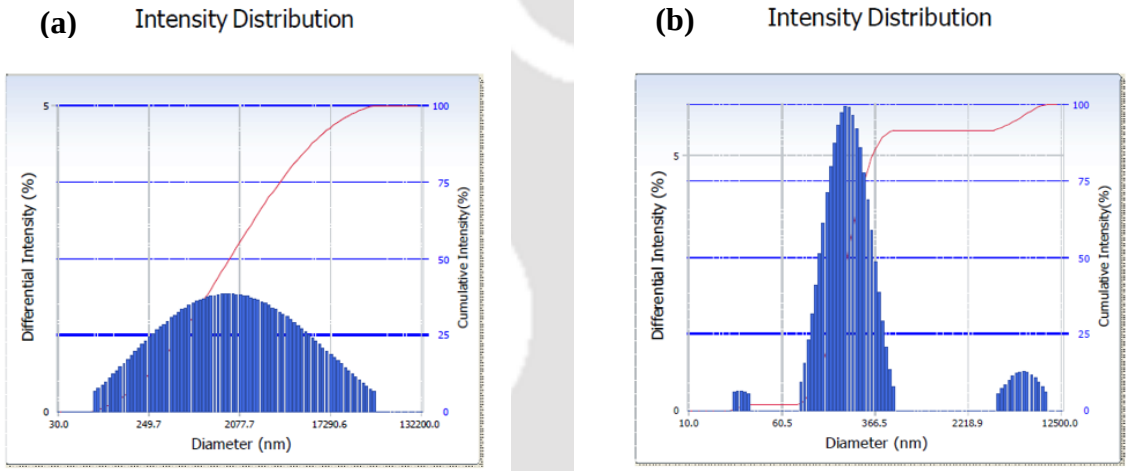

Fig. A3 Particle size distribution (a) at the beginning of the treatment; (b) during spinning basket membrane ultrafiltration in the presence of rotational speed of 73.31 rad s^{-1}

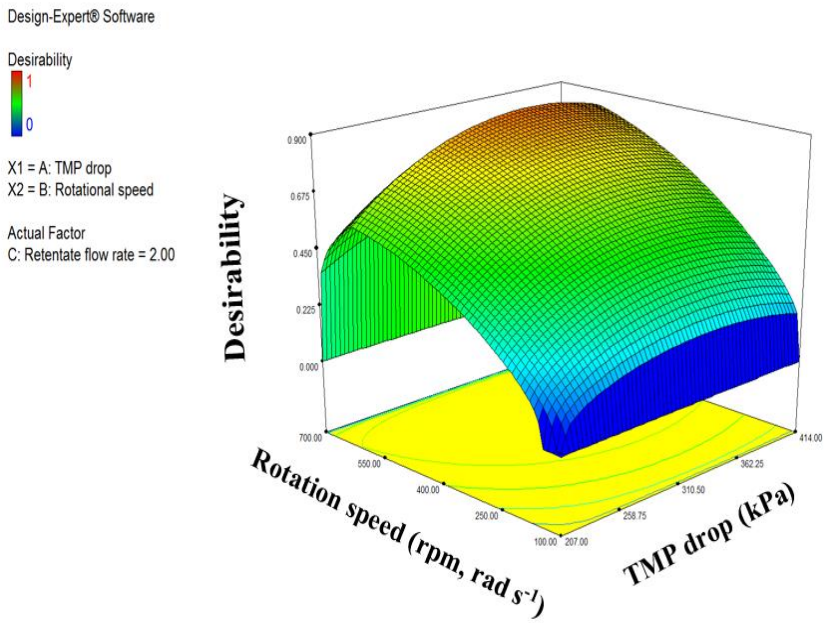

Fig. A4 Three dimensional diagram of desirability function with respect to rotational speed and TMP drop for all three responses at fixed retentate flow rate of 2 L min^{-1}

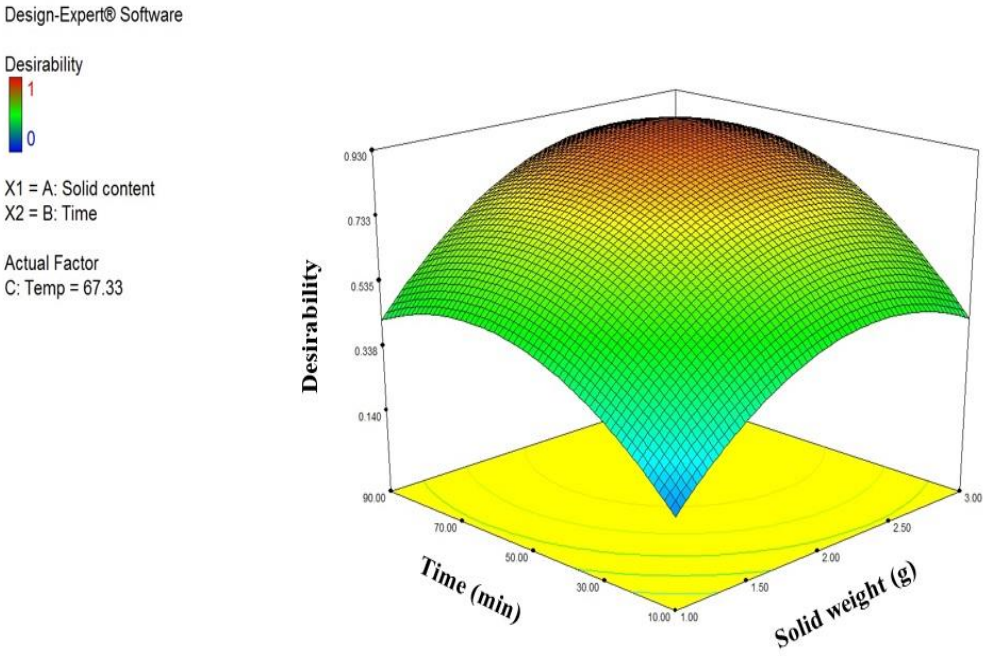

Fig. A5 Three dimensional diagram of desirability function with respect to leaching time and solid to water content to optimize the leaching of polyphenols

Research output

Published Journal Papers:

- **Suman Saha**, Chandan Das, A lab-scale spinning basket membrane module for the assessment of Humic acids ultrafiltration with effect of sonication on membrane fouling, **Chem. Eng. Comm.** 205 (2018) 1457-1498.
- **Suman Saha**, Chandan Das. Purification of Humic acids contained simulated wastewater using membrane ultrafiltration. **European Water** 58 (2017) 33-40.
- **Suman Saha**, Chandan Das. Spinning basket membrane ultrafiltration of paper industry waste effluent: Experimental and theoretical aspects. **J. Environ. Chem. Eng.** 5 (2017) 4583-4593.
- **Suman Saha**, Chandan Das. Analysis of fouling characteristics and flux decline during Humic acids batch ultrafiltration. **J. Chem. Eng. Process Technol**.; 6 (2015) 252-258.

Communicated Papers:

- **Suman Saha**, Chandan Das, Utilization of Tea Factory Solid Waste towards Polyphenols Extraction: Optimization Study and Kinetic Model Analysis, **Asia-Pacific J. Chem. Eng.** (under review).
- **Suman Saha**, Rijumoni Boro, Chandan Das, "Treatment of tea factory effluent in a coagulation-ultrafiltration integrated hybrid process", **Clean Soil Air Water** (Under review).

Conferences:

- **Suman Saha**, Rijumoni Boro and Chandan Das " Treatment of tea factory effluent in a coagulation-ultrafiltration integrated hybrid process", International Conference on Water Resources Management, 11-12th January, 2018, CSIR-Central Glass & Ceramic Research Institute (CSIR-CGCRI) Kolkata.
- **Suman Saha** and C. Das "Effects of rotational speed and membrane molecular weight cut-off on Humic acids ultrafiltration using spinning basket module" in Indian Chemical Engineering Congress (CHEMCON-2015), 27-30th December, 2015, IIT Guwahati, India.
- Rijumoni Boro, **Suman Saha** and C. Das "Oily waste water treatment using different technologies" in Indian Chemical Engineering Congress (CHEMCON-2015), 27-30th December, 2015, IIT Guwahati, India.
- **Suman Saha** and Chandan Das "Recovery of poly-functional polymers using membrane ultrafiltration", REFLUX 2.0, Annual Chemical Engineering Symposium, 29-30th March 2014, Indian Institute of Technology Guwahati, Assam, India.

- Sujoy Bose, **Suman Saha** and Chandan Das "Investigation of morphological and mechanical behaviour of a ceramic membrane based on different parameters", in International Conference on "Membranes and Applications" (ICMA 2013), 22-23th November, 2013, CSIR-Central Glass & Ceramic Research Institute (CSIR-CGCRI) Kolkata.